The Dissertation Committee for Rachel Veronica Simon Wallace Certifies that this is the approved version of the following Dissertation:

A new close mammal relative and the origin and evolution of the mammalian central nervous system

Committee:

Timothy Rowe, Supervisor

Christopher J. Bell

Richard A. Ketcham

Chris Kirk

Matthew W. Colbert

A new close mammal relative and the origin and evolution of the mammalian central nervous system

by

Rachel Veronica Simon Wallace

Dissertation

Presented to the Faculty of the Graduate School of

The University of Texas at Austin

in Partial Fulfillment

of the Requirements

for the Degree of

Doctor of Philosophy

The University of Texas at Austin

May 2018

Dedication

This dissertation is dedicated to my mom and dad, for encouraging me through my entire educational journey; to my husband, for motivating me to never give up and to push for success; and to my daughter, Beatrix, for giving me a new perspective of my life.

Acknowledgements

I would like to thank my advisor, Dr. Timothy Rowe, for sharing all of his wisdom with me for the past eight years. I am also thankful to Dr. Rowe for all of his patients. The hours of conversation we have had together have opened my eyes to evolutionary and developmental anatomy.

I would like to thank my committee, Drs. Chris Bell, Rich Ketcham, Chris Kirk, and Matt Colbert, for setting time aside to read my dissertation and provide valuable feedback. I feel fortunate to have worked with such a harmonious and insightful committee. I thank my committee for the valuable discussions I have had with each of them on an individual basis throughout the years.

The Jackson School has provided numerous, invaluable resources to me. Thank you for supporting me with TA opportunities that have shown me how much I value teaching. I also want to thank the Lundelius Grant for Student Research in Vertebrate Paleontology as a helpful source of financial support during those long summers when TA-ships are dry. And of course, I am thankful to Drs. Jessie Maisano and Matt Colbert (also a committee member) for all of their assistance with CT data acquisition in The University of Texas High-Resolution X-ray Computed Tomography Facility.

The struggles through graduate school would not be possible without social support. For that, I thank UT Paleo graduate students for insightful conversations and emotional support. It is always nice to know you are not alone! And above all, no greater support has come from anyone than from my husband, Gerard Wallace (soon to be Dr. Wallace), and our beautiful, funny little girl, Beatrix.

Thank you, everyone, for making this all possible.

Abstract

A new close mammal relative and the origin and evolution of the mammalian central nervous system

Rachel Veronica Simon Wallace, Ph.D.

The University of Texas at Austin, 2018

Supervisor: Timothy B. Rowe

Mammals are distinguished by the presences of the cerebral neocortex, and dentary-squamosal jaw joint, among other traits. These traits likely evolved outside of Mammalia, in Mammaliaformes. Recent fossil discoveries from South America elucidate the evolution of the brain in taxa outside of Mammaliaformes. A new skull of a close mammal relative, *Pseudotherium argentinus,* from the Late Triassic Ischigualasto Formation in Argentina was scanned at The University of Texas High-Resolution X-ray Computed Tomography (CT) Facility. CT data reveal a unique combination of ancestral and derived characters. Phylogenetic analysis supports a sister-taxon relationship between *Pseudotherium* and the derived Tritylodontidae. An endocast reconstruction further supports a derived phylogenetic position among cynodonts. A comparison of the *Pseudotherium* endocast with other cynodont endocasts suggests that the cerebral hemispheres enlarged in probainognathian cynodonts, while the total endocranial volume remained relatively constant until the origin of Mammaliaformes. This expansion is also present in the foramen magnum. Encephalization volume and skull length were compared with foramen magnum size in extinct and extant cynodonts, birds, and lizards. Endocranial volume and foramen magnum size, and foramen magnum size and skull length, are correlated following a 3/2 power

law. Therefore, foramen magnum size can be used to predict endocranial volume for fossils. Regression analyses show foramen magnum size is significantly increased in Mammaliaformes. This change reflects an increase in medulla oblongata size and supports a concerted model of brain evolution outside of Mammalia. Because the increase in medullary size coincides with the origin of the neocortex, I hypothesize that the mammalian pyramidal tract originated in Mammaliaformes. The hypotheses from this dissertation are testable given recent fossil discoveries. However, morphological data of those specimens are not readily available. Morphological descriptions in this dissertation are accompanied by detailed figures, and the data will be digitally archived and made publically available on DigiMorph.org. The intent is to model a communication and data-sharing standard to be implemented in all future fossil discoveries.

Table of Contents

Chapter 1: First record of a basal mammaliamorph from the Carnian-Norian Ischigualasto Formation of Argentina[1]

INTRODUCTION

One of the major transformations in vertebrate evolution occurred in a series of events leading up to the origin of crown Mammalia (Rowe, 1988). The transformation, which occurred by or before the Middle Jurassic, took place as several pulses of expansion of the relative size of the brain (encephalization) and the emergence of the uniquely mammalian neocortex (Rowe et al, 2011). This was probably driven in part by a ten-fold duplication in olfactory receptor genes that induced hypertrophy of the olfactory bulbs and olfactory (pyriform) cortex, as well as the cerebellum and brainstem. In their epigenetic responsiveness to the neurosensory system, the skull, craniovertebral joint and neck were profoundly modified (Rowe, 1996a, b; Rowe and Shepherd, 2016; Shepherd and Rowe, 2017; Rowe, 2017). The famous shift in position and function of mammalian auditory ossicles were also part this transition. From their primitive position on the lower jaw and dual function in feeding and audition, the auditory ossicles became detached from the jaw and decoupled from feeding to take their characteristic mammalian position suspended beneath the otic capsule and functioned solely in hearing. Controversy surrounds whether this was a unique transition (Rowe, 1996 a, b; 2017), or one that occurred multiple times via different mechanisms (e.g., Luo, 2007; Wang, et al., 2001). Also involved in the mammalian transition was the evolution of endothermy, lactation, parental care, and prolonged activity (Kemp, 2005; Kielan-Jaworowska et al., 2004). A suite of other skeletal modifications include: formation and lengthening of the secondary palate, an occlusal dentition with roots deeply implanted by a periodontal ligament, ossification of the alisphenoid, and the double occipital condyle. These and other features may be related to the integration of orthonasal olfaction, retronasal olfaction, taste, and somatosensation from the teeth and tongue, into a larger

[1] Authors: R. Wallace, R. Martinez, and T.B. Rowe. R. Wallace wrote the paper, made the figures, and conducted the phylogenetic analyses. R. Martinez discovered the fossil and contributed to the Geological Setting section. T. Rowe contributed to the background of mammalian evolution, assisted with figures, and provided some additional anatomical observation.

sensory system that has been termed ‘ortho-retronasal olfaction,’ which may have played a role in mammalian cortical evolution (Rowe and Shepherd, 2016; Rowe, 2017).

While the fossil record provides a fairly dense taxonomic sample of stem-mammals, another well-known feature of this record is that the closest extinct relatives of Mammalia among Cynodontia were small, and many taxa are known only from isolated teeth (Lillegraven et al., 1979; Kielan-Jaworowska et al., 2004). Most of the Late Triassic and Jurassic non-mammalian cynodonts occupy the two smallest orders of vertebrate size magnitude, and it was not until the Cenozoic that the independent evolution of large body size began to characterize various mammalian clades (Kemp, 1982, 2005).

One of the key nodes on the mammalian stem is Mammaliaformes, the clade originating in the last common ancestor shared by (crown) Mammalia and the Late Triassic *Morganucodon oehleri* (Kemp, 1983; Rowe, 1988, 1993). Most of the osteological features that currently diagnose Mammaliaformes are understood as marking the onset of encephalization, and the evidence now available suggests that at least a small neocortex had differentiated in the dorsal cortex of the telencephalon (Rowe et al, 2011; Rowe and Shepherd, 2016). Integumentary evidence from the remarkably preserved Early Jurassic Chinese fossil *Castorocauda* (Ji et al., 2006) suggests that a pelt of modern aspect, with guard hairs and velus underfur, was present at or very shortly after the origin of Mammaliaformes, but prior to the origin of Mammalia itself. Interdependencies discovered in the ontogeny of living mammals demonstrate that the development of innervated hair follicles induces somatosensory maps on the neofortex. The presence of guard hairs in an early mammaliaforms suggests that at least a small neocrotex had differentiated, and within it a primary somatosensory field (Rowe et al, 2011; Rowe and Shepherd, 2016). The origin of Mammaliaformes thus involved a marked pulse in encephalization in which the brain and skull began to look and function more like those of living mammals than to more primitive cynodonts of the Early and Middle Triassic, most of which retained a narrow, tubular forbrain brains and relatively small olfactory bulbs.

Mammaliamorpha (Rowe, 1988) is a more inclusive clade which stems from the last common ancestor shared by Mammalia and the extinct clade Tritylodontidae. Mammaliamorpha is strongly diagnosed by many features of the skull and postcranial skeleton (Kemp, 1983; Rowe, 1988, 1993; 2017). But the many characters which offer strength to the diagnosis may simply

mark the long expanse of missing fossil record that pre-dates the origin of Mammaliamorpha. In other words, with new discoveries of more-basal Triassic fossils we should expect that at least some of the diagnostic features of mammaliamorphs will prove to have wider, more inclusive distributions along the mammaliamortph stem. A number of features of the new taxon described here demonstrate this point.

The origin of Mammaliamorpha is coming into sharper focus with recent discoveries of new Late Triassic and Early Jurassic cynodont fossils that clearly possess complex assemblages of derived features that were passed on to crown mammals. These fossils suggest a modest global diversification of small cynodonts whose members lie just within Mammaliamorpha, or just outside on its stem. Untangling these relationships is critical to fully understanding the evolutionary sequence of transformations involved in mammalian origins. As described below, subtle skeletal features suggest that the origin of Mammaliamorpha involved neurosensory modifications that occuirred earlier than previously known, setting a stage for the more profound neurosensory transformations seen in early members of Mammaliaformes, and later in the origin of Mammalia (Rowe et al, 2011).

The comparative framework for evaluating the new taxon involves a number of Triassic and Jurassic fossils that, according to current hypotheses, lie just inside of or slightly outside of Mammaliamorpha. We informally refer to them as the 'taxa of interest' because they have the most direct bearing on understanding the phylogenetic position of *Pseudotherium*. These cynodonts occupied the two smallest orders of vertebrate size magnitudes, and they are known mostly from partial skulls and partial post-cranial skeletons. Owing to their small size, however, these fossils have proven difficult to prepare and to study in detail using conventional methods. This material is also scattered across widely separated museum collections and few researchers have had the opportunity to study all the relevant material first-hand. The literature is variable in its depth of description and in its quality of illustration. As a result, a measure of uncertainty surrounds anatomical interpretations of the specimens as well as their phylogenetic relatiosnhips. Uncertainty also attends the precise sequence of events that culminated in the origin of Mammalia, and this in turn has fueled controversy over which characters transforming over pan-mammalian history were affected by homoplasy.

The ‘taxa of interest’ include the well-known Late Triassic to Middle JurassicTritylodontidae which is the plesiomorphic sister taxon to all other mammaliamorphs (Rowe, 1988; 1993). Also of interest are the taxa referred to Brasilodontidae. This is a problematic taxon of questionable monophyly, based on several small, incomplete specimens. They include *Brasilodon quadrangularis*, *Brasilitherium riograndensis*, *Minicynodon maieri*, and *Protheriodon estudianti*, from the Middle and Late Triassic of Brazil and Argentina; and *Panchetocynodon damodarensi* from the Early Triassic of India (Bonaparte, 2013; Bonaparte et al., 2013). Bonaparte (2013) considered Brasilodontidae to be monophyletic and to be the sister taxon to Mammaliaformes (his Mammalia), but his taxon sampling omitted Tritylodontidae, leaving his results equivocal with respect to membership in Mammaliamorpha. Analyses by Luo (2007), scoring only *Brasilitherium*, and Liu and Olson (2010), scoring *Brasilodon*, and considering *Brasilitherium* as its junior synonym, found them to lie within Mammaliamorpha, but outside of Mammaliaformes. Abdala (2007) found the group to be paraphyletic, with *Brasilitherium* as a sister taxon to Mammaliaformes, and *Brasilodon* as the sister taxon to Mammaliamorpha + *Pachygenelus* (representing Tritheledontidae, below).

Additional taxa of interest are the Late Triassic to Early Jurassic species referred to Tritheledontidae (=Ictidosauria Broom 1929, 1932; =Diarthrognathidae, *sensu* Haughton and Brink, 1954), another group of uncertain monophyly. From the Late Triassic of Argentina, the best known include *Riograndia guaibensis* and *Chaliminia musteloides*, and possibly also *Irajatherium hernandezi*. Also included are *Elliotherium kersteni*, from the Late Triassic of South Africa, and *Pachygenelus monus* and *Tritheledon riconoi* from the Early Jurassic of South Africa. Fragmentary specimens from other parts of the world have been referred to Ttritheledontidae (see reviews by Martinelli et al, 2005, Martinelli and Rougier, 2007; Sidor and Hancox. 2006).

Recent reviews of Tritheledontidae have all found weak support for its monophyly (Martinelli et al, 2005, 2017; Martinelli and Rougier, 2007; Sidor and Hancox. 2006). All of the known specimens are very small and incomplete, and the few known postcranial elements are largely undescribed. The name has been used for different sets of taxa by different authors, and the phylogenetic results of different studies are difficult to compare owing to different taxon sampling. With that caveat, some authors infer Tritheledontidae to lie within Mammaliamorpha

(e.g., Bonaparte et al., 2005; Hopson and Barghusen, 1986; Hopson and Kitching, 2001; Rubidge and Sidor, 2001; Luo, 2007; Luo et al., 2015), while others have placed it just outside (e.g., Rowe, 1993; Martinez et al., 1996; Abdala, 2007; Martinelli, 2017). Lucas and Luo (1993) obtained both results, with Tritheledontidae just inside or just outside of Mammaliamorpha. Sidor and Hancox (2006) and Martinelli and Rougier (2007) addressed relationships among tritheledontids but neither study included Tritylodontidae, hence their results are uninformative with respect to its inclusion in Mammaliamorpha. Liu and Olsen (2010) inferred tritheledontids to be paraphyletic, with *Pachygenelus monus* and *Riograndia guaibensis* as successive outgroups to Mammaliamorpha.

Here, we describe a new fossil cynodont from the early Late Triassic Ischigualasto Formation of Argentina using micro-computed tomography (μCT) of an isolated skull. Computed tomography (CT) and μCT have advanced steadily in versatility and resolution over the last three decades (Rowe et al., 1995, 1997; Ketcham and Carlson, 2001; Carlson et al., 2003; Rowe et al., 2016; Davis et al., 2017) and they have now been used to scan a few of the more important fossils from the mammalian stem, as well as many extinct and extant crown mammals (e.g., Rowe et al., 2005, 2011; Rodriguez et al., 2013; Ruf et al, 2014). The specimen scanned well, showing marked X-ray contrast between matrix and bone that permitted digital preparation of features that would not have been possible using conventional mechanical preparation. As a result, the scans show details of both external and internal anatomy that were not readily observable through visual inspection of the specimen itself. In addition, the scans enabled careful inspection of sutural relationships between bones that resulted in a number of unexpected findings, for example that *Pseudotherium* retains a large prefrontal bone and a vestigial postorbital bone. From the scans we also generated a number of animations of serial sections in all three orthogonal planes and enlarged 3D printouts that augmented our ability to understand the anatomy of the new taxon.

We also approximated its relationships using a recently published data matrix designed to resolve relationships among non-mammalian cynodonts (Liu and Olsen, 2010; modified by Martinelli et al., 2016, 2017). We note that very little of the new anatomical detail revealed by the CT scans is reflected in this matrix, and that a broader comparative sample of CT scan data of relevant fossils needs to be made available before it will be useful or informative to build a more

comprehensive matrix that reflects this new source of information on evolutionary variation in stem-mammals. For example the scans showed extensive pneumaticity around the braincase in the new taxon, which we provisionally consider autapomorphic of *Pseudotherium*, but without CT scans the condition in the other taxa of interest cannot be determined.

GEOLOGICAL AND PALEONTOLOGICAL SETTINGS

The holotype of the new taxon (PVSJ 882) was found in 2006 by RNM during a field trip to the Ischigualasto Formation carried out by the Instituto y Museo de Ciencias Naturales of the Universidad Nacional de San Juan. This nonmarine unit crops out in northwestern Argentina and forms part of the Ischigualasto-Villa Union Basin (Fig. 1.1). The Ischigualasto Formation comprises a sequence of fluvial channel sandstones with well-drained floodplain sandstones and mudstones. Interlayered volcanic ash layers above the base and below the top of the formation provide chronostratigraphic control and have yielded ages of 231.4 ± 0.3 Ma and 225.9 ± 0.9 Ma (Rogers et al., 1993; Martínez et al., 2011).

The Ischigualasto Formation is divided into four members (Currie et al., 2009): the La Peña (from the base to 40 m), the Cancha de Bochas (40 to 180 m), the Valle de la Luna (180 to 650 m) and the Quebrada de la Sal (650 to 700 m) members (Fig. 1.1). The La Peña Member consists of multi-story channel sandstones and conglomerates covered by poorly-drained floodplain mudstones. The Cancha de Bochas Member is composed of thick, well-drained floodplain mudstones interbedded with high-sinuosity channel sandstones. The Valle de la Luna Member is mostly characterized by amalgamated high-sinuosity channels, abandoned channels and marsh deposits. Finally, the Quebrada de la Sal Member consists of tabular fluvial deposits.

The Ischigualasto Formation is divided from base to top into three abundance-based biozones (Martínez et al., 2011): the *Scaphonyx-Exaeretodon-Herrerasaurus* biozone; the *Exaeretodon* biozone; and the *Jachaleria* biozone. The *Scaphonyx-Exaeretodon-Herrerasaurus* biozone is characterized by a predominance of the rhynchosaur *Scaphonyx*, the cynodont *Exaeretodon*, and the dinosaur *Herrerasaurus*, but also includes the majority of known fossils and the highest taxonomic diversity. The *Exaeretodon* biozone is characterized by low diversity and high relative abundance of the cynodont *Exaeretodon*. The *Jachaleria* biozone is almost devoid of vertebrate fossils except for scarce specimens of the dicynodont *Jachaleria*.

The new specimen was found at the Valle Pintado locality, which is located in the upper levels of the La Peña Member and in the lower portion of the *Scaphonyx-Exaeretodon-Herrerasaurus* biozone. The material was found in a fossiliferous layer 40 m above the base of the Formation. To date, this is one of the most fossiliferous horizons known in the Ischigualasto Formation. Diverse and abundant fauna were recovered from the same level, including several specimens of the theropod dinosaur *Herrerasaurus*, the type specimen of the basal sauropodomorph dinosaur *Panphagia*, the only known specimen of lagerpetid dinosauromorph (Martínez et al., 2012), plus various carnivorous and herbivorous cynodonts, rynchosaurs, and pseudosuchian archosaurs.

MATERIALS AND METHODS

Computed tomography

Much of the superficial surface of the skull was exposed through manual preparation. Anatomical investigation of the interior utilize micro-computed tomography (µCT) (Rowe et al., 1997; Ketcham and Carlson, 2001; Carlson et al, 2003; Rowe et al., 2016), and from these scans 3D printouts of enlarged models of the specimen were made to augment and extend observation of its surficial anatomy. This approach complements earlier analyses using µCT to study various regions of the closely related brasilodont *Brasilitherium riograndensis* (Rodrigues et al., 2013, 2014; Ruf et al., 2014), the tritheledont *Riograndia guaibensis* (Rodriguez et al., 2018). The specimen scanned extremely well thanks to a marked X-ray contrast between fossil bone and matrix.

The holotype of *Pseudotherium* (PVSJ 882) was scanned by Dr. Jessie Maisano at the University of Texas High-resolution X-ray Computed Tomography Facility (http://www.ctlab.geo.utexas.edu) on November 11, 2013, using its Xradia microXCT 400 Scanner. Owing to the length of the specimen (69 mm), it was scanned in two parts, each of which consisted of a single rotation using cone-beam data acquisition, and the two halves were stitched together using an Xradia software plugin application. The entire dataset was reconstructed as a total of 1733 coronal CT slices exported as 16bit TIFF files that measure 1024 x 1008 pixels. Voxels are cubic and measure 44.21 microns along each orthogonal axis.

Scanning parameters are as follows: Xradia 0.7X objective, 110kV, 10W, 2s acquisition time, detector 50.5 mm, source -96.8 mm, XYZ [-2096, 39633, -111], camera bin 1, angles ±180, 1081 views, 1 mm CaF_2 filter, dithering. End reference (60 frames, 1.5s each). Reconstructed with center shift -6.5, beam hardening 0.1, theta 0, byte scaling [-20, 500], binning 1, recon filter smooth (kernel size = 0.5).

The CT data were processed using VGStudio MAX version 2.1 software to generate 3D volumetric renderings to produce supplemental animations of the skull rotating about each orthogonal axis, and movies through slice stacks. Volumetric models were generated using the HQ Scatter algorithm unless otherwise noted. Isosurface renderings are more ubiquitous in the literature, but they only present a thresholded surface of a scanned item which reduced their anatomical informativeness compared to volumetric reconstructions (Ketcham and Carlson, 2001). Because the fossil bone in the new taxon is significantly more attenuating to X-rays than the surrounding matrix, a histogram adjustment was applied to digitally render matrix voxels as transparent in some of the illustrations below (e.g., Fig. 1.2), enabling visualization of bones completely encased by matrix. Still images were exported from VGStudio, cropped in Adobe Photoshop®, and labeled in Adobe Illustrator®. Figure 2 illustrates the difference in information conveyed between a volume rendering of the new taxon that has was digitally filtered (prepared), and an isosurface rendering. Although the isosurface rendering appears sharper and less cloudy, the high-quality scatter volume rendering reveals more fractures and sutures. Fractures and sutures are even clearer with Phong volume rendering, though they may be a distraction from other anatomical features. Grayscale histogram-based digital preparation was able to expose deep elements, such as the orbitosphenoid, and although some elements, such as the occipital condyles (Fig. 2C and D), appear to have been lost after digital preparation, examination of the specimen reveals that the cortical bone of the occipital condyles was eroded away, reconstructed, leaving only spongy bone remains. Cross sectional slices (Fig. 1.2E and F) illustrate how little fossil bone

is lost in the digital preparation threshold selected for these CT images of *Pseudotherium* and even thin, wispy elements can be seen in the nasopharyngeal and endocranial areas.

Institutional abbreviations

PVSJ, Instituto y Museo de Ciencias Naturales, San Juan 5400, Argentina; **UFRGS-PV**, Setor de Paleovertebrados, Instituto de Geosciencias, Universidade Federal do Rio Grande do Sul, Porto Alegre, Brazil.

Nomenclature

We follow the nomenclatural recommendations based on the Phylocode that are discussed at length elsewhere (Gauthier et al., 1988; Rowe, 1988; Rowe and Gauthier, 1992; de Queiroz and Gauthier, 1992; de Queiroz, 1994; Cantino and de Queiroz, 2000) and employ taxonomic names that are detailed in *Phylonyms, the Companion Volume to the Phylocode* (Cantino et al., *in press*). The name Mammalia is used in reference to the crown clade (Rowe, 1988, *in press* A). The name Mammaliaformes (Rowe, 1988) is used in reference to the clade stemming from the last common ancestor shared by Mammalia and *Morganucodon oehleri* (Rowe, *in press* B), while the name Mammaliamorpha (Rowe, 1988) is used in reference to a slightly more inclusive clade stemming from the last common ancestor shared by Mammalia and *Tritylodon longaevus* (Rowe, 1988, *in press* C). Herein we use the name Probainognathia in reference to the clade stemming from the last common ancestor of Mammalia and *Probainognathus jenseni* (Romer, 1970).

Supplemental data

Supplemental data will be made available on www.DigiMorph.org. The include the original CT dataset, serial section movies, 3D movies in X- Y- and Z- axis rotation; serial sdection movies in coronal, sagittal, and horizontal slice planes; and an STL file of the holotype.

RESULTS

Systematic paleontology

Therapsida Broom, 1905

Cyndontia Owen, 1861

Probainognathia Hopson, 1990

Pseudotherium gen. nov.

Etymology: *Pseudo* (L.) for false, plus Greek *therios* (G.) for wild beast, a mammal

Type and only known species: *Pseudotherium argentinus* sp. nov.

Diagnosis: As for the species.

***argentinus*, sp. nov.**

Etymology: Species name, *argentinus*, in reference to its provenance.

Holotype: Instituto y Museo de Ciencias Naturales, San Juan 5400, Argentina, PVSJ 882 (Figs 2 - 30), an isolated skull that is missing the mandibles, most of the premaxillae, zygomatic arches, and quadrates. One incomplete stapes and one quadratojugal are preserved. The specimen is relatively three-dimensional, although there is evidence that the facial portion is slightly dorsoventrally crushed. The skull is long and narrow, with distinct sagittal and lambdoidal crests that overhang the slanting occiput. The left side of the skull is more distorted than the right, with the apical end of the canine crown leaning medially and some of the orbital and braincase elements displaced or missing. The snout is constricted both dorsoventrally and mediolaterally behind the long canines. It has nine sectorial postcanines that are relatively small with simple blunt, rounded cusps, and the secondary palate extends slightly posterior to the maxillary tooth row

Type Locality. Valle Pintado in Ischigualasto Provincial Park, San Juan Province, Argentina (S 30° 08' 14", W 67° 52' 39"). The single known specimen was discovered 40 m above the base of the Ischigualasto Formation, in the upper portion of the La Peña Member (sensu Currie et al., 2009) and lower portion of the *Scaphonyx-Exaeretodon-Herrerasaurus* biozone. The holotype (PVSJ 882) was found intermixed with the holotype (PVSJ 874) of the basal sauropodomorph *Panphagia protos* (Martínez and Alcober, 2009) and an unnamed lagerpetid dinosauromorph (PVSJ 883; Martínez et al., 2012).

Age. Late Carnian on the basis of a radioisotopic date near the base of the Ischigualasto Formation in the vicinity of the type locality (Rogers et al., 1993). This date was recently recalibrated to 231.4 ± 0.3 Ma (Martínez et al., 2011).

Diagnosis: *Pseudotherium argentinus* is a probainognathian cynodont possessing the following combination of features: the lacrimal contributes extensively to the floor of orbit; the frontal has a long orbital process that contacts a very short orbital process of the palatine near the floor of the orbit; the orbital process of the palatine is low and contributes little to the orbital wall; the prefrontal is large and exposed mostly inside the nasopharyngeal cavity; a vestige of the postorbital bone is preserved behind the orbit, but lacks an ossified postorbital bar; the interpterygoid vacuities remained open throughout life; laterally flaring parasphenoid alae intersect at an obtuse angle between their contacts with the petrosal promontorium; there is a longitudinal ventral process on basisphenoid; the lambdoidal crest strongly overlaps the occipital plate; CT scans show a high degree of pneumatization around the braincase in the parietal, petrosal, squamosal, basioccipital, basisphenoid, supraoccipital, and exoccipital; the vertical margin of the petrosal (prootic) lateral flange is notched; the upper canines are long, laterally compressed and non-serrated with a ridge on both their labial and lingual surfaces; there are nine upper postcanine teeth with the first postcanine consisting of a single cusp, while blunt, indistinct cusps form the crowns of the remaining postcanines. Lastly, *Pseudotherium argentinus* is larger than most of the other 'taxa of interest' mentioned above, measuring 69 mm minimum length, not including the missing premaxillae.

Maturity at time of death: A number of features suggest that the holotype was approaching full skeletal maturity at time of death. The sagittal and lamdoidal crests are very well developed; the orbit is relatively small compared to other skull proportions; the prootic and opisthotic are fused to form the petrosal; and extensive fusion has occurred between the basioccipital and exoccipitals, and between the tabular, supraoccipital, and interparietal. Additionally, a short diastema between the canine and the first postcanine suggests that a tooth had been shed and not replaced. There are also irregular wear facets on all of the postcanine tooth crowns. The only suggestions of immaturity include the presence of a pair of small un-erupted replacement postcanine crowns situated at the base of the right and left fouth postcanine roots, visible in the CT scans, and possibly the presence of an interpterygoid vacuity.

Description of the skull

Premaxilla

The premaxillae are almost entirely missing in the holotype of *Pseudotherium*. All that remains are short fragments of the posterior extremities of the right and left medial palatine (palatal) processes, which are visible in CT sections between the incisive fossae (paracanine fossae) for the lower canines. As in *Brasilitherium* (Ruf et al., 2014: Fig. 1.3D) the medial margin of each has a dorsally directed process suggesting that the premaxillae abutted but did not fuse on the midline. As preserved, they are slightly separated in both *Pseudotherium* and *Brasilitherium*, but in life the premaxillae probably met on the midline behind the sphenopalatine fissure. Compared to *Brasilitherium* the medial palatine process in *Pseudotherium* is very thin and delicately built. Underlying the premaxillary palatine process is the medial palatine (palatal) process of the maxilla (Fig. 1.4). The snout is too incomplete to determine whether the posterior border of the sphenopalatine fissure was formed by the premaxillae, maxillae, or both.

Septomaxilla

The facial process of the septomaxilla forms the ventrolateral border of the naris, and the transverse shelf or footplate forms its floor. The facial process extends from the naris posteriorly to wedge between the nasal and the maxilla, tapering to a point immediately anterior to the canine root. A septomaxillary canal traverses the length of the footplate (Fig. 1.5). The posterior opening of the canal is roughly level with the anterior end of the vomer in coronal section. The canal opens anterolaterally and, posteriorly, its lateral enclosure is completed by the facial process of the maxilla. The canal probably conveyed the nasolacrimal duct forwards to its anterior terminus in the floor of the narial cupola, near the presumed position of the aperture of the vomeronasal organ (Rowe et al., 2005; Ruf et al., 2014, figs. 3B, 8). These anatomical relations represent the ancestral condition for probainognathian cynodonts.

Maxilla

The maxilla comprises much of the lateral surface of the snout, forming the lateral wall of the nasopharyngeal passage and the anterior half of the secondary palate. It contacts the septomaxilla and premaxilla anteriorly, the nasal dorsally and medially, and the palatine,

prefrontal, and lacrimal posteriorly. It supports the vomer for a short distance, but internal damage to the snout complicates interpretation of the relations of these two bones. The facial process of the maxilla extends from anterior to the canine, where it contributes to a precanine diastema, to the level of the orbit, and it reaches its greatest height above the upper canine root, where the nasals only narrowly separate the right and left maxillae on the dorsal midline. Dorsoventral postmortem compression of the rostrum has caused the canine roots to rupture and weather through the maxilla.

The maxillary palatal process extends anterior to the upper canine and encircles much of the incisive (paracanine) fossa, which accommodated the lower canine tip when the jaws were closed (Figs 3, 4). The secondary palate is long and ends 3-4 mm posterior to the distal-most tooth. The maxilla forms the anterior half of the secondary palate, its contribution ending posteriorly at the level of the fifth postcanine tooth where it contacts the palatal process of the palatine. Behind this point, the maxilla forms the root of the zygomatic arch and contacts the lacrimal along the anterior rim of the orbit. The maxilla also extends beneath the orbit as a bony shelf. In a highly unusual (apomorphic) relationship, however, the lacrimal expands over the orbital floor, covering the maxilla and largely excluding its participation in the orbital floor or in the border of the subtemporal fenestra (Fig. 1.6).

The maxillary canal courses the entire length of the facial process and, in life, transmitted the maxillary branch of the trigeminal nerve, innervating the upper dentition, and conveying cutaneous branches from the surface of the snout (Fig. 1.7). The canal opens through the anterior floor of the orbit, and then runs above the postcanine tooth roots. It exits externally via three foramina on either side of the face that are bilaterally symmetrical in size and position (Fig. 1.6). The smallest and most anterior foramen is positioned behind the canine root. Two other foramina are aligned dorsoventrally and are positioned over the diastema. The foramina positions and the branching pattern of their associated canals are similar to the pattern reconstructed for *Ecteninion* (Benoit et al., 2016). If that reconstruction is accurate, the dorsal foramen and the small anterior foramen in *Pseudotherium* contained the internal nasal nerve, while the ventral foramen contained the superior labial nerve. The largest foramen on the lateral facial process is positioned anterior to the root of the zygomatic arch above the roots of postcanine teeth 5 and 6. It is the exit to a canal that has an independent origin from the maxillary canal. According to Benoit et

al., (2016) it contained the caudal alveolar ramus of the maxillary nerve. This arrangement of maxillary foramina is similar to *Brasilodon* (Bonaparte et al., 2005) and *Brasilitherium* (Ruf et al., 2014), and at least some tritylodontids (Sues, 1986). It reflects a reduction in number from the multiple cutaneous foramina present in cynodonts plesiomorphically (Estes, 1961; Rowe et al., 1995), and a stabilization of their numbers and position on the face.

Jugal

Very little of the jugal is preserved in the holotype of *Pseudotherium*, save for a sliver of bone wedged between the maxilla and the lacrimal at the root of the zygomatic arch. The root of the zygomatic arch is largely formed by the maxilla. However, the jugal probably contributed to its dorsal portion as suggested by a deep groove between the maxilla and the lacrimal just posteromedial to the jugal fragment.

Nasal

The nasal forms the dorsal margin of the naris and the roof of the nasopharyngeal passageway. It contacts the facial process of the septomaxilla, and it passes along the length of the maxillary facial process where the two bones share a beveled scarf contact that lacks complex interdigitation. The nasal has a short contact with the prefrontal, and meets the lacrimal just anterior to the orbital rim. The nasal is constricted on the snout by the maxilla between the roots of the canine, and it then expands posteriorly where it achieves its greatest width at the front of the orbit where the maxilla, perfrontal, and lacrimal are in contact. The internasal sutural boundary has shallow interdigitations along their sutural boundary. The nasal tapers to a thin plate at its rear extremity, where it overlaps the frontal. A nutrient canal runs through the nasal roof at its posterior end.

Vomer and possible ethmoid ossifications

CT scans of *Pseudotherium* show thin, wispy elements in the nasal cavity that may reflect the early evolutionary onset of ossification of the nasal capsule (Fig. 1.8). They are comparable to those illustrated for *Brasilitherium* (Ruf et al., 2014), but the interpretation of these elements in both *Pseudotherium* and *Brasilitherium* is complicated by fragmentation of other bony

elements into the lumen of the nasopharyngeal passageway, a lack of bilateral symmetry, and mottling of the matrix that fills the passageway. The vomer is broken and detached from the maxilla, and these fragmentary bony structures may simply be exfoliated from the inner surface of the maxilla. Extensive ossification of the nasal capsule is apomorphic of crown Mammalia (Rowe, 1988; Rowe, et al., 2005), and no unequivocal intermediate ossifications have been reported in any other fossils. Because the phylogenetic positions of *Pseudotherium* and *Brasilitherium* are not far outside of crown Mammalia, these peculiar structures warrant further discussion.

The earlier CT study of *Brasilitherium* interpreted the elements as a partially ossified nasoturbinal and first ethmoid turbinal, and reported that the posterodorsal end of the nasal septum was partially ossified to form a mesethmoid, all of which support olfactory epithelium in mammals (Ruf et al., 2014). In *Pseudotherium*, one of the ossified elements lies in the general location of the mammalian maxilloturbinal. It is most clearly visible on the left side as a C-shaped structure of very thin bone, but it preserves no bony attachment to the maxilla, floating freely inside the matrix of the nose. A similar free-floating structure is illustrated in *Brasilitherium* in a similar position (Ruf, et al., 2014).

These structures are exceedingly small compared to even the smallest turbinals known in mammals, and it is instructive to examine them in light of the pattern in which turbinals develop in mammalian ontogeny, as they become the supporting skeleton of the olfactory epithelium (reviewed in Rowe, et al., 2005; Rowe and Shepherd, 2016). The olfactory epithelium begins its development on the inner walls of the cartilaginous embryonic nasal capsule, as olfactory receptor genes are expressed. In mammals the nasal capsule becomes extensively ossified and within it grows an elaborate labyrinth of thin bony struts known as “ethmoid turbinals” (or turbinates). Epithelial growth quickly exceeds the surface area of the nasal capsule walls, causing it to fold into the lumen of the capsule. Each epithelial fold is supported by a transient cartilage that grows apically into the fold from the nasal capsule wall, but at no time is there an extensive, stand-alone cartilaginous skeleton (as is the case in some birds). The growing cartilage is quickly replaced by rigid perichondral bone that forms the mature ethmoid turbinals. Growth of the olfactory epithelium and its turbinals begins adjacent to the main olfactory bulb and proceeds rostrally. As they grow, the turbinals widen rostrally, branching and interleaving in intricate

patterns that eventually occupy a large volume of the nasal space. The mature olfactory epithelium is confined to the dorsal and caudal regions of the nasal chamber, where the turbinals sequester numerous pockets and recesses into which odorant molecules volatilize. The turbinals subdivide the nasal chamber, maintain spatial integrity of its epithelia, and the spatial zonation of olfactory receptors. The number of functional olfactory receptor genes correlates most strongly with mature olfactory epithelial surface area (Garrett and Steiper, 2014). The ossification of ethmoid turbinals in the ancestral mammal supported the expansion of the surface area of its olfactory epithelium by an order of magnitude over nasal chambers lacking such structures (Rowe et al., 2005).

Additionally, the vomer in both *Pseudotherium* and *Brasilitherium* is plesiomorphic in being Y-shaped with a long vertical stem that is at least half the height of the nasopharyngeal cavity (Fig. 1.9), restricting olfactory space to the dorsal half of the nasopharyngeal chamber. This is the same condition found in *Thrinaxodon* (Fourie, 1974; Rowe et al., 1995). The groove in the top of the Y-shaped vomer supported the cartilaginous internasal septum (Crompton et al., 2017), which ossifies in Mammalia to become the mesethmoid (Rowe, et al., 2005). In mammalian development, the internasal septum ossifies to form a tall mesethmoid and the 'stem' of the vomer is reduced or absent. The mammalian vomer is now V-shaped, and the ossified mesethmoid rises above it nearly the entire height of the nasopharyngeal passage (Rowe et al., 2005; Rowe, 2017).

CT scans of two tritylodont specimens reportedly preserve slight ossification of the rear part of the nasal capsule (Kielan-Jaworowska et al., 2004). However, a lack of contrast between bone and matrix in these specimens leaves interpretation of the CT data equivocal. No similar structures have been observed in CT scans of taxa more closely related to mammals, including *Morganucodon* and *Hadrocodium* (Rowe et al, 2011) and our unpublished datasets for other tritylodonts. Moreover, if not simply artifacts, a strict interpretation based on phylogenetic analysis (below) resolves these structures as synapomorphies that link *Pseudotherium* and *Brasilitherium*, to the exclusion of all other taxa of interest to this analysis. The evidence that these small bones represent enhancement of the olfactory system is enticing, but not decisive and underscores the desirability of CT scanning more of these small Mammaliamorph specimens.

The vomer in *Pseudotherium* has drifted from its rostral articulation atop the palatal processes of the maxillae and palatines. The posterior end of the vomer is visible in ventral view where it forms a triangular plate in the roof of the choana. It tapers posteriorly to a median point, bordered by the pterygoid. The vomer forms the anterior end of a ventral midline ridge on the primary palate that begins at the choana and extends onto the pterygoids, and it may have been continuous with a keel on the basisphenoid that extends onto the basioccipital. The midline keel may have been the site of attachment for the median raphe of the pharyngeal constrictors (Sues, 1986) and the posterior pterygoid muscle (Barghusen, 1986). The vomer apparently diminishes in height anteriorly, and it becomes C-shaped on either side where it wrapped around the vomeronasal organ (Fig. 1.4).

Lacrimal

The lacrimal contributes broadly to the orbital wall and floor and forms the anterior orbital rim (Figs 3, 6). Its long facial process is exposed for a short distance on the lateral side of the snout in front of the orbit, but its rostral extremity continues anteriorly, concealed laterally beneath the facial process of the maxilla. In this region, the lacrimal forms part of the wall of the nasopharyngeal cavity. The lacrimal is pierced by two lacrimal foramina, probably for the ducts of the lacrimal and Harderian glands (Rowe et al., 2005), that open along the anterior rim of the orbit. Passing forward they become confluent and merge into a single canal that is enclosed for a short distance by the lacrimal facial process, before emptying into the nasopharyngeal cavity.

The structure of the lacrimal in the orbital wall and floor is quite unusual. The lacrimal contacts the nasal and prefrontal anteromedially above the orbit. The orbital plate of the lacrimal is a thick bone that overlies and conceals a broad ventral sheet-like expansion of the prefrontal. The orbital process of the lacrimal forms almost the entirety of the anteromedial wall of the orbit, meeting a very short process of the palatine near the floor of the orbit, and a long process of the frontal that completes the posterior margin of the orbital wall. The lacrimal forms most of the floor of the orbit, covering most of the maxilla and largely excluding it from participation in the orbit.

Palatine

The palatine forms the posterior half of the secondary palate, the rear walls of the nasopharyngeal passage, the anterolateral end of the primary palate, and makes a minor contribution to the ventral wall of the orbit (Figs. 3, 6). Its palatal process contacts the maxilla anteriorly, while its dorsal plate contacts the vomer medially, and the pterygoid posteriorly. The lateral margin of the dorsal plate extends far posteriorly, forming a ridge that outlines the lateral margin of the primary palate. This lateral ridge is illustrated in *Brasilitherium* (Bonaparte, 2013) and is similar to the palatal ridges in *Morganucodon* (Kermack et al., 1981) and tritylodontids (Sues, 1986).

The orbital process of the palatine (also referred to as the dorsal, or ascending, process of the palatine) is short, rising just above the lateral flange of the pterygoid when the specimen is viewed laterally. The short orbital process is wedged between the lacrimal anteriorly and the frontal posteriorly, and it forms the ventral-most portion of the orbital wall. The orbital process of *Pseudotherium* is shorter than in other probainognathian cynodonts. The orbital process of other taxa of interest is taller (dorsoventrally) than it is long (anteroposteriorly), and it forms the posteroventral border of the orbital wall in *Ecteninion* (Martinez et al., 1996), *Prozostrodon* (Bonaparte and Barberena, 2001), *Riograndia* (Soares et al., 2011), *Brasilitherium* (Bonaparte et al., 2013), and *Morganucodon* (Kermack et al., 1981).

The orbital process of the palatine in *Kayentatherium* is illustrated as a low structure, as in *Pseudotherium.* However, unlike *Pseudotherium*, the orbital process of *Kyentatherium* is also long, extending to the alisphenoid (eptipterygoid, Sues, 1986: fig. 5). In all of the taxa mentioned above, the orbital process of the palatine contacts the frontal dorsally, the lacrimal anteriorly, and the orbitosphenoid posteriorly. However, the orbital region is reportedly damaged in many specimens as a result of mechanical prepartion, and therefore difficult to interpret with certainty. Owing to the high, medial position of the orbitosphenoid in *Pseudotherium*, it can be stated with confidence that the palatine did not contact the orbitosphenoid. The orbital process of the palatine in *Pseudotherium* is shorter dorsoventrally than in any other non-mammalian cynodont.

Two or three foramina are associated with each palatine; the greater palatine foramen at its anterior border with the palatal process of the maxilla, and one to two foramina for the lesser

palatine nerve on the lateral margin of the palatine where the palatal process and the dorsal plate connect.

Pterygoid

Although broken and with displaced parts, the pterygoid is fairly complete preserving the three processes found in other non-mammalian cynodonts: the anterior (palatal) process, the transverse process (lateral flange), and the quadrate process. Its pattern of troughs and ridges (Figs. 1.10, 1.11) resembles the pterygoid of other probainognathans including *Morganucodon* (Kermack et al., 1981), *Kayentatherium* (Sues, 1986), *Sinoconodon* (Crompton and Sun, 1985; Crompton and Luo, 1993), *Brasilitherium* (Bonaparte et al., 2013), and *Riograndia* (Soares et al., 2011). This pattern may also be present in *Pachygenelus* (Bonaparte et al., 2013) but as yet it is unknown in *Brasilodon*.

The horizontally oriented anterior process of the pterygoid forms the rear end of the primary palate. The lateral edges of the primary palate are defined by a ridge formed by the palatine and pterygoid. This lateral ridge deepens posteriorly and it likely formed the ventromedial process of the pterygoid as in *Brasilitherium* (Bonaparte, 2013). Barghusen (1986) called these 'choanal crests' and maintained that they indicate the presence of a soft palate that was a direct continuation of the osseous secondary palate. He summarized older literature (Broom, 1936; Crompton, 1955; Tatarinov, 1963) in arguing that the ridges themselves suggest the attachment of soft tissue, that a deep channel for the air passage is positioned dorsal to the crests, and that the choanal crests are continuous with the bony secondary palate.

Where the left and right pterygoids meet in the roof of the choana is a well-developed median keel that passes forward onto the vomer and ends near the front of the choana. This keel is unlike anything known in extant mammals. The keel does not extend into the nasopharyngeal passage as a bony structure, as in *Kayentatherium* (Sues, 1986) and *Morganucodon* (Kermack et al., 1981), but it may have continued anteriorly as a cartilaginous nasal septum dividing the nasopharyngeal passage (Crompton et al., 2017).

At the posterior end of the lateral ridge of the pterygoid is the root of the transverse process (lateral flange). The root of the transverse process projects anteriorly and contacts the posterolateral-most corner of the palatine. In lateral view, the lateral flange deepens posteriorly

and is deepest is where the so-called ‘pterygoid wing’ (Bonaparte, 2013) would have projected ventrally had it not broken off postmortem. The pterygoid wing borders a posteriorly facing concavity on the transverse process that may have served as the origin for the the posterior division of the pterygoid musculature (Bonaparte et al., 2013). Similar concavities are described in *Brasilitherium* (Bonaparte et al., 2013), the tritylodontid *Kayentatherium* (Sues, 1986), and the mammaliaform *Megazostrodon* (Rowe, 1986). The severely reduced pterygoid transverse processes in crown mammals complicates their interpretation with respect to muscle attachments in non-mammalian cynodonts.

Where the transverse process meets the lateral ridge, the pterygoid continues posteriorly where it outlines open interpterygoid vacuities. The interpterygoid vacuities are generally thought to be open in early ontogeny of basal cynodonts, and to close at maturity (Martinelli and Rougier 2007). Closure of the interpterygoid vacuities is associated with maturity in *Thrinaxodon*, galesaurids, *Diademodon*, basal probainognathians, and basal mammaliaforms, and they remain open in juveniles of some of those taxa (Martinelli and Rougier, 2007). Interpterygoid vacuities have been described among juvenile tritylodontids as well as “randomly in some [seemingly] adult specimens” (Martinelli and Rougier, 2007). Open interpterygoid vacuities are described in arguably mature specimens of *Brasilodon*, *Brasilitherium*, and in tritheledontids where the mesocranial region is preserved (Bonaparte et al., 2005; Martinelli and Rougier, 2007). Considering the many features suggesting that the holotype of *Pseudotherium argentinus* was approaching full skeletal maturation at time of death (above), it apparently shares with these taxa the condition of interpterygoid vacuities that remain open throughout life.

The pterygoid is overlapped by the alisphenoid dorsolaterally (Fig. 1.11). The pterygoid ends medially where it sutures to the robust basipterygoid process of the basisphenoid (Fig. 1.24). The quadrate ramus (process) of the pterygoid projects posterolaterally to where it is appressed to the ventromedial surface of the quadrate ramus of the alisphenoid. It ends where the quadrate ramus of the alisphenoid contacts the lateral flange of the petrosal.

Prefrontal

The prefrontal is reportedly absent in all of the various specimens referred to as brasilodontids and tritheledontids (e.g., Bonaparte 2013; Bonaparte et al., 2003, 2005, 2013;

Martinelli and Rougier, 2007) and in *Therioherpeton* (Bonaparte and Barberina, 2001). However in *Prozostrodon brasiliensis*, although the postorbital arch is absent, remnants of the prefrontal and postorbital bones persist in their plesiomorphic position in the orbital margin (Figs 3, 12). The contact between prefrontal and postorbital that is plesiomorphic for Cynodontia (Rowe et al., 1995) is interrupted in *Prozostrodon* by a lateral process of the frontal, which also participates in the orbital rim (Bonaparte and Barberina, 2001).

Pseudotherium preserves a condition similar to *Prozostrodon* in which the postorbital arch was not simply broken away but was probably absent as an ossified bar in life, and the prefrontal and postorbital persist in the orbital margin, along with a short process of the frontal. Externally the prefrontal is positioned in its primitive position on the anterodorsal corner of the orbit, lying between the lacrimal anteriorly, the frontal posteriorly, the nasal anteromedially, and the parietal posteriorly. CT data reveal that the prefrontal is far more extensive than can be observed on the surface of the skull and that it forms an unusually broad flat plate that extends into the inner surface of the snout, internal to the lacrimal. Its anterior extremity is almost at the level of the lacrimal.

The prefrontal was also tentatively identified in *Brasilitherium*, occupying the same position on the dorsolateral edge of the orbital rim as in *Pseudotherium* (Ruf et al., 2014: fig. 4a). Its external sutural relationships are difficult to observe in the published 3D surface rendering of *Brasilitherium*; a volume rendering would likely show the sutures more clearly. The prefrontal is unequivocally absent in tritylodonts and other members of Mammaliamorpha (Rowe, 1988, 1993; Gauthier et al., 1988). Although we follow published accounts in our scored matrix, it is clear that CT scans are needed to confirm its absence in titheledonts and *Therioherpeton*.

Postorbital

Both zygoma are broken in *Pseudotherium*, but the skull roof is sufficiently well-preserved to show the persistence of a vestigial postorbital bone. The preserved zygoma of *Brasilitherium* indicates that the postorbital arch was not ossified (Ruf et al., 2014: Fig. 2a), as is likely the case in *Pseudotherium*. The postorbital bone is seen as a small flat plate appressed against the lateral surface of the frontal behind the orbit. Cross sections show a sliver of frontal wedged between the putative postorbital and the parietal, confirming that the element is distinct

(Fig. 1.12). This suggests that evolutionary modification of the orbital boundary occurred in at least two steps. First came the loss of an ossified postorbital arch, and only later did the postorbital and prefrontal bones to fail to ossify entirely, in a condition diagnostic of Mammaliamorpha, or perhaps Mammaliamorpha + Tritheledontidae (Rowe, 1988, 1993).

Frontal

The frontal forms the dorsal margin of the orbit. A hooked, fingerlike orbital process projects ventrally and forms the posterior margin of the orbital wall. Posterior to it is a large orbital fissure. The orbital process of the frontal contacts the orbital process of the palatine deep in the ventromedial part of the orbit. In lateral view, the frontal is overlapped anteriorly in the orbit by the lacrimal, and anterodorsally by the prefrontal. Posteriorly, a small portion of the alisphenoid overlaps the frontal. In dorsal view the frontal is overlapped anteriorly by the nasals, and posteriorly by the parietals. A supraorbital foramen is positioned between the frontal, tapering nasal processes, and the prefrontal. This foramen has also been identified in *Brasilitherium* (Bonaparte et al., 2013) and in *Riograndia* (Soares, 2004; Soares et al., 2011) and may have transmitted a cutaneous branch of the opthalmic nerve.

A study of *Brasilitherium* based on μCT (Rodrigues et al., 2014; Fig. 1.3) suggested that the frontal enclosed an enlarged olfactory bulb compared to more basal cynodonts, and on this basis speculated that *Brasilitherium* represented an increase in olfactory performance compared to non-mammaliaform cynodonts. However, coronal CT scans through the frontal of *Pseudotherium* show a comparable curvature of the frontal over the top of the olfactory bulb, and its superior preservation shows that the plesiomorphic orbitosphenoid also occupied part of this space beneath the frontal (Fig. 1.13). The geometry of the space enclosed between the alisphenoids in *Brasilitherium* and *Pseudotherium* reveals a very minor apparent increase in relative size of the olfactory (piriform) cortex compared to more basal cynodonts. Ontogenetic interdependencies observed in the development of living mammals indicate that increases in olfactory bulb volume induce enlargement of the olfactory cortex (Rowe and Shepherd, 2016; Rowe 2017). This correlated expansion suggests only minor improvement in olfactory capabilities in these taxa. There is no clear evidence that the mature telencephalon had yet differentiated into neocortex and olfactory cortex in either *Brasilitherium* or *Pseudotherium*,

emphasizing their general plesiomorphic organization compared to members of Mammaliaformes (Rowe et al, 2011; Rowe and Shepherd, 2016; Rowe, 2017).

Parietal

The parietals are largely confined to the intertemporal girder, forming the roof over a narrow endocranial cavity, and presenting an extremely long attachment area for the temporalis musculature. There is no pineal foramen, nor is there any hint of an impression on the undersurface of the parietals indicating the persistence of a pineal eye beneath the skull roof. The parietal's anterior extent is notable, overlapping the frontal dorsolaterally and terminating as a thin process that almost reaches the nasal. The anterior process of the parietal overlaps the rear part of the prefrontal. The left and right parietals meet on the midline and fuse posteriorly above the alisphenoid and prootic, where they form a tall sagittal crest that protrudes posteriorly beyond the level of the occipital condyles. The sagittal crest is posteriolaterally continuous with the lambdoidal crest and the supraoccipital. Where the base of the fused parietals forms the roof of the endocranial cavity, CT scans indicate that they enclose an extensive network of hollow cavities (Fig. 1.14). Much like the condition in *Brasilitherium* (Bonaparte, 2013) and mammaliamorphs (Rowe, 1988, 1993) the lateral flange of the prootic is tall and has extensive lateral overlap onto the lateral face of the parietal. The rear edge of the alisphenoid also overlaps the lateral surface of the parietal.

Squamosal

The squamosal extends from its medial contact with the parietal at the base of the sagittal crest laterally over the supraoccipital and petrosal to form the face of the prominent lambdoidal crest. The temporal processes are incomplete in *Pseudotherium*, more so for the left than the right side. A shallow V-shaped notch separates the temporal process of the squamosal from the lambdoidal crest. Below its parietal contact, the squamosal contacts the anterior lamina of the petrosal in the medial wall of the temporal fenestra. Descending from the root of the temporal process is a deep flange (Fig. 1.15). Cutting into the flange are two deep notches, separated by a hook-shaped squamosal septum. The lateral notch held the quadratojugal, while the dorsal plate of the quadrate was wedged into the medial notch (Luo and Crompton, 1994), however neither

the quadrate nor quadratojugal is preserved in articulation. Medial to the quadrate, the squamosal abuts against the paroccipital process. It does not completely cover the paroccipital process and it is likely that this failure of complete coverage permitted the paroccipital process to contact the quadrate. This organization of the squamosal flange is similar to *Brasilitherium* (Bonaparte, et al., 2013) and many basal mammaliamorphs (Rowe, 1988, 1993).

Quadratojugal

The quadratojugal is the smallest bone in the skull. The left quadratojugal is preserved embedded in the base of the squamosal flange, where it occupies the quadratojugal notch (Fig. 1.16). This position of a tiny splint-like quadratojugal bone embedded in its own notch in the ventrum of the descending flange of the squamosal is the plesiomorphic condition as reported in *Kayentatherium* and other cynodonts (Sues, 1986: 232, Fig. 1; Luo and Crompton, 1994).

The presence of a quadratojugal in its own notch distinct from the quadrate notch is apomorphic to eutheriodonts (Therocephalia + Cynodontia) (Rowe, 1986, 1988). The quadratojugal is unknown in tritheledonts owing to non-preservation. Although unknown in *Morganucodon*, its presence is indicated by a clearly defined quadratojugal facet in its primitive position on the front of the lateral flange of the quadrate (Kermack et al., 1981; Rowe, 1986).

Luo (2011) argued that the quadratojugal was lost in tritheledontids and Mammaliaformes, and that it re-evolved in *Brasilitherium*, based in part on the phylogenetic hypothesis that tritylodontids represent a basal radiation of herbivorous cynodonts (Luo, 2011). Luo also reconstructed the middle ear of *Brasilitherium* with the quadrate and quadratojugal wedged together into a single notch (Luo, 2007, 2011; Rodrigues et al., 2013). In *Pseudotherium*, two depressions adjacent to the paroccipital process can be seen within the quadrate notch, but there is no doubt that it retains the plesiomorphic condition of a quadratojugal having its own notch separate from the quadrate. The craniomandibular joint and middle ear regions in *Brasilitherium* may be more similar to *Pseudotherium* than suggested by prior reconstructions of *Brasilitherium*. In any event, the phylogeny recovered in this analysis (below) supports the interpretation that little variation affected the shape and attachment of the quadratojugal in

cynodont evolution, until the quadratojugal was ultimately lost in the last common ancestor of Mammalia (Rowe, 1986, 1988, 1993).

Quadrate

The quadrate is not preserved in *Pseudotherium*, but the notch for the insertion of its dorsal plate is incised into the ventral edge of the squamosal. The quadrate of *Brasilitherium* has been described as being very similar to *Morganucodon* in structure (Bonaparte et al., 2013), having a stapedial process that overlaps the anterior process of the paroccipital process (Bonaparte et al., 2013.; Luo and Crompton, 1994). Because the squamosal flange closely resembles *Brasilitherium*, the quadrate of *Pseudotherium* may have been similar to *Brasilitherium*.

Stapes

An incompletely preserved right stapes (Fig. 1.17) was broadly perforated, with separate anterior and posterior crua. Part of its footplate is wedged deeply into the fenestra ovalis, and its anterior crus projects about half the distance between the fenestra ovalis and the paroccipital process. Missing are the distal end of the anterior crus, most of the posterior crus, and the 'head' of the stapes that articulated with the quadrate. The footplate is "C"-shaped as preserved. It is likely that half of the footplate is missing and the "C" shape is the result of breakage along a central concavity such as described for *Morganucodon* (Kermack et al., 1981) and *Brasilitherium* (Rodrigues et al., 2013).

Petrosal

The prootic and opisthotic are fused to form the petrosal (periotic). A line resembling a suture between the crista interfenestralis and the paroccipital process is the clearest superficial indication that the prootic and opisthotic were at one time distinct. However, CT cross sections of that region reveal no trace of a suture and show that the prootic and opisthotic are coossified. For descriptive purposes, the prootic portion of the petrosal will be referred to simply as the prootic.

The prootic encloses the otic capsule and forms the posterolateral portion of the braincase. The membranous anterior lamina projects forward to contact the rear edge of the alisphenoid. The anterior lamina is separated from the alisphenoid by two foramina for the maxillary (V_2) and mandibular (V_3) branches of the trigeminal nerve. The prootic flares laterally, forming a broad anterior lamina that slopes almost vertically at its lateral-most edge (Fig. 1.18). It sits atop and abuts the quadrate ramus of the alisphenoid. The lateral flange is perforated by a vascular foramen, probably for the vena cava lateralis (Rougier et al., 1992), located posterior to the V_3 foramen. Posterior to the V_3 foramen is a small nutrient foramen similar to *Kayentatherium* and *Morganucodon* (Kermack et al., 1981; Sues, 1986). Directly lateral to the vascular foramen is a unique notch into the vertical margin of the prootic lateral flange that is not directly comparable with other cynodonts that may have housed the lateral head vein.

Posterior to the notch is the pterygoparoccipital foramen. It is almost entirely enclosed by the lateral flange anteriorly and the paroccipital process posteriorly. The squamosal overlaps the paroccipital process dorsolaterally so that it may be considered to contribute to the partial enclosure of the foramen. In *Kayentatherium* (Sues, 1986) and *Morganucodon* (Kermack et al., 1981) the pterygoparoccipital foramen is open laterally, a derived condition compared to the completely enclosed foramen present in more basal eucynodonts. While the pterygoparoccipital foramen of *Pseudotherium* is nearly entirely enclosed by the prootic and squamosal, the lateral flange and squamosal do not actually contact one another (Fig. 1.19).

An external ascending groove rises dorsally from each pterygoparoccipital foramen and cuts between the prootic and the squamosal. Within the groove, and posterodorsal to the pterygoparoccipital foramen, is the entrance to the posttemporal canal, through which passed the arteria diploëtica magna (Rougier et al., 1992). The superior ramus of the stapedial artery fit within the ascending groove and entered inside of skull through a dorsal foramen, identified as the diploëtic foramen in *Brasilitherium* (Bonaparte et al., 2013: fig. 1).

The petrosal encapsulates the inner ear and is perforated by several foramina. It contacts the squamosal laterally, the exoccipital posteromedially, and the basioccipital anteromedially. The prootic canal is positioned posterior to the lateral flange vascular foramen, near the fenestra ovalis. The perilymphatic foramen, and the jugular and hypoglossal foramina share a common pit but are otherwise distinct. The jugular and hypoglossal foramina are posteromedial to the

perilymphatic foramen and lie close together, but remain separate. The pars cochlearis is completely ossified within the petrosal and exposed ventrally, giving *Pseudotherium* a slightly convex promontorium (Fig. 1.20). A promontorium is derived among eucynodonts. It is present in Mammaliaformes (Luo et al., 1995), in the non-mammaliaform cynodont *Brasilitherium* (Rodrigues et al., 2013).

The cochlea (Fig. 1.21) is medially in-turned and is broadest posteriorly near the vestibule and narrows anteriorly towards its apex. Relative to the cochlea of more basal cynodonts including *Probainognathus* (see Luo, 2001: fig. 4), the cochlea of *Pseudotherium* is elongate, more comparable to *Brasilitherium* (Rodrigues et al., 2013) and other basal mammaliamorphs (Luo, 2001; Luo et al., 2016). The posterior vestibule bears a large anterior semicircular canal (SCC), a smaller posterior SCC, and a lateral SCC that is similar in size to the posterior. The anterior and posterior SCCs share a long common crus. Even the posterior and lateral SCCs appear to share a short common crus, which is swollen to accommodate the ampulla of the posterior SCC. The ampullae of the anterior and lateral SCCs meet laterally on the dorsum of the vestibule.

The internal auditory meatus is closed by a medial wall, which is pierced by four foramina to the inner ear (Fig. 1.21A). Three are anteroventral to the subarcuate fossa. The anterior-most foramen is small and likely transmitted the facial nerve (VII). The facial nerve passed over the cochlea and exited the petrosal at the posterior end of the cavum epiptericum. The two more posterior foramina transmitted the cochlear and vestibular branches of the vestibulocochlear nerve (VIII). The wider of the two foramina opens at the neck of the cochlea, anterior to the vestibule, and transmited the cochlear nerve. The smaller and more dorsal of the two foramina enters the vestibule just ventral to the ampulla for the anterior SCC and transmitted the vestibular nerve. Although the presence of a walled internal auditory meatus, with separated foramina for VII and VIII is described as an apomorphy of Mammaliamorpha (Kemp, 1983, Rowe, 1988), it was more recently scored as present in *Pachygenelus monas* (Martinelli et al., 2017). The fourth foramen is positioned ventral and slightly anterior to the subarcuate fossa. A digital endocast of the inner ear shows that this foramen marks the entrance to a short canal entering the vestibule immediately anterior to the base of the common crus, which is the position for the vestibular aqueduct in mammals (Luo, 2001).

The paroccipital process is bifurcated laterally into two distinct processes, as in other basal mammaliamorphs (Rowe, 1986, Fig. 34; 1988, 1993). The posterior process protrudes ventrally. It is overlapped posteriorly at its base by a small process of the tabular. In ventral view, a small emargination between the posterior and anterior processes of the paroccipital process probably represents the homolog of the fossa for the stapedial muscle in therian mammals. The petrosal contacts the squamosal near quadrate notch. The larger anterior process of the paroccipital process is elongate, its lateral surface is partially in contact with the squamosal (Fig. 1.22). The anterior process of the paroccipital process made contact with the quadrate (Sues, 1986), while the posterior process probably contacted the hyoid (Rowe, 1986, Fig. 34; 1988).

Orbitosphenoid

The µCT of the holotype are especially useful in visualizing the orbitosphenoid. In *Pseudotherium* the orbitosphenoid is ossified and positioned in its plesiomorphic position (Romer, 1956) just beneath the skull roof where it forms the primary walls of the endocranial cavity (Fig. 1.23). This is similar to the configuration illustrated in *Probainognathus* (Martinelli and Rougier, 2007; Crompton et al., 2017). In lateral view, it is just visible through the dorsum of the orbital fissure but is otherwise covered by the orbital process of the frontal. Although the orbitosphenoid is broken and shifted slightly out of anatomical position, its general shape is recognizable. It spans most of the length of the orbital fissure. In cross section, the orbitosphenoid is a rounded L- shape. The ventral legs of each "L" contact one another at the midline to form a U-shaped cross-section. Descending from this is a vertical median stem, identified in *Probainognathus* as the presphenoid by Crompton et al., (2017). The optic foramen opens through the orbitosphenoid's lateral surface. Unlike *Probainognathus*, in which the right and left optic foramina are confluent (Crompton, et al., 2017), they remain separate in *Pseudotherium* and penetrate the lateral orbitosphenoid wall near its center.

Alisphenoid

The alisphenoid forms the posterior margin of the orbital fissure. Dorsally, the tall alisphenoid overlaps the ventral edges of the frontal and parietal. The posterodorsal corner of the

alisphenoid is overlapped by the anterior lamina of the prootic (petrosal). In basal cynodonts, the orbital fissure is a broad space between the orbital wall and alisphenoid. In tritylodontids and mammaliaforms, an ossified lateral wall that largely closes the orbital fissure is formed by contributions from the alisphenoid, orbitosphenoid, frontal, and in some taxa the palatine (Sues, 1986; Soares et al., 2011). *Pseudotherium* is plesiomorphic in having a widely open orbital fissure.

A posteriorly directed process of the alisphenoid contacts the anterior margin of the prootic, separating the foramina for the maxillary and mandibular branches of the trigeminal nerve. The anterior margin of the alisphenoid is broken dorsally where it would have contacted the frontal. The pterygoid process of the alisphenoid overlies the lateral surface of the pterygoid adjacent to the border of the interpterygoid vacuity. Posteroventrally, the quadrate ramus of the alisphenoid makes contact with the lateral flange of the prootic. Its ventromedial surface is underlapped by the quadrate ramus of the pterygoid. Together with the quadrate ramus of the pterygoid, these two processes form the lateral boundary of the large cavum epiptericum (Fig. 1.3).

Basisphenoid and parasphenoid

The endochondral basisphenoid and membranous (dermal) parasphenoid are fused into the parabasisphenoid complex, but the boundaries of the two components can be discerned. The basisphenod portion consists of a triangular, robust basipterygoid processe that contacts the pterygoid, a narrow central portion that is pierced by the carotid foramina and underlies the sella turcica and the pituitary fossa, and a broad posterior end that contacts the basioccipital posteromedially and the petrosal posterolaterally.

The parasphenoid consists of a long, anteriorly projecting rostrum that is “V”-shaped in cross section. In *Pseudotherium*, the short rostrum of the parasphenoid tilts dorsally towards the endocranial cavity where it passes above the interpterygoid vacuites. In life, it likely divided the interpterygoid vacuity and contacted the pterygoids where they form the primary palate. The ventral keel on the parasphenoid rostrum may have been continuous with the midventral keel on the primary palate and extended into the nasopharyngeal cavity in continuity with the cartilaginous nasal septum.

Behind the rostrum are the parasphenoid wings or alae, which flare laterally and underlap the ventral surface of the basisphenoid. The parasphenoid ala terminates at the anterior end of the pars cochlearis and does not participate in the border of fenestra vestibuli.

A median keel runs anteriorly from the basioccipital to the basisphenoid and along the ventral surface of the parasphenoid rostrum. Where the parasphenoid alae converge at the carotid foramina, the median keel deepens and forms a small crest (Fig. 1.24). Although a similar crest was described as an autapomorphy of *Brasilitherium* (Bonaparte et al., 2013), it may althernatively (in conjunction with several other poorly documented features – see Discussion), be a synapomorphy with *Pseudotherium*.

A well-developed parasphenoid ala is potential mammaliamorph synapomorphy that is lacking in *Probainognathus* but reportedly present and fused to the petrosal in tritylodontids such as *Yunnanodon* (Luo, 2001: Fig. 1b) and *Kayentatherium* (Sues, 1986). In Mammaliaformes the wings are absent as discrete structures, and they are reduced or absent in the stem-mammaliaforms *Adelobasileus* (Lucas and Luo, 1993) and *Sinoconodon* (Luo et al., 2001). Reduction and loss of the papasphenoid alae is associated with elongation of the cochlea and its housing within an expanded bony promontorium (Luo et al., 1995). *Pseudotherium* and tritylodontids differ in that the parasphenoid ala extensively underlaps the entire cochlear promontorium in tritylodontids while in *Pseudotherium* it terminates beneath the promontorium apex (Fig. 1.11). *Pseudotherium* resembles *Brasilitherium* in that the promontorium is only partially covered by the parasphenoid ala (basisphenoid wing; Rodrigues et al., 2013). The condition in *Pachygenelus monus* and *Riograndia guaibensis* are unknown.

Basioccipital

Although the basioccipital appears fused with the petrosal and exoccipitals, its borders are sufficiently distinct to warrant a separate discussion from the occiput as a whole. The basioccipital forms the posteroventral portion of the braincase and the ventral rim of the foramen magnum. A ventromedial keel arises anterior to the foramen magnum and spans the length of the basioccipital. Two deep pits occur on either side of a keel on the anterior end of the basioccipital. They may have served as the insertion for the anterior rectus capitis muscles (Sues, 1986). Paired foramina are situated posteriorly and lateral to the perilymphatic foramina, as illustrated in

Morganucodon (Kermack et al., 1981: figs. 98 and 100). Both foramina represent partitioning of the embryonic metotic fissure, which lies between the developing otic capsule and basioccipital, and transmitted the vagus nerve (cranial nerve X) and jugular vein (van Bemmelen, 1901). In mammals, the metotic fissure closes and becomes partitioned in different ways and degrees, such that a single foramen may transmit both structures, or the fissure may be partly or completely divided (de Beer, 1937) as it is in *Pseudotherium*.

The CT scans show the structure of the occipital condyles to be problematic. As in cynodonts ancestrally, the occipital condyle is paired (Rowe, 2017), and in *Pseudotherium* the two condyles resemble the condition in *Thrinaxodon* (Rowe et al., 1995) in which each is a small knob placed at the ventrolateral edge of the foramen magnum (Fig. 1.25).

The basioccipital and basisphenoid are separated on the midline by a distinct gap. This feature is present in *Thrinaxodon* and other cynodonts and is referred to as an "unossified zone" presumably filled by cartilage (Estes, 1961). In *Pseudotherium*, however, volume rendering of the skull reveals that the gap is partially bridged by a ventral median process of the basioccipital. This narrow finger-like process extends forward beneath the basisphenoid, crossing the unossified zone. This process seems unique to *Pseudotherium*. However it is only visible in the volume rendering (Fig. 1.25A); a surface rendering (Fig. 1.25B) fails to distinguish these structures and produces a basioccipital-basisphenoid contact that resembles drawings of *Brasilitherium*, where the unossified zone and median bridge may be covered by residual matrix.

Occiput

The occiput is broader than it is tall. Most of the individual bones in *Pseudotherium* are coossified and their boundaries indistinct, hence the occiput is described here as a single unit. It is partially roofed by the broad lambdoidal crests that rise dorsomedially and meet at a point with the overhanging sagittal crest. A short occipital crest runs vertically below the apex of the sagittal crest. The lateral margins of the supraoccipital are faintly visible, as well as the sutures between the basioccipital and the exoccipitals in the ventral margin of the foramen magnum. The supraoccipital, exoccipitals, and basioccipital comprise the dorsal, lateral, and ventral borders of the foramen magnum, respectively. In ventral view, the hypoglossal (XII) foramen pierces the exoccipital anterior to the condyle.

The tabular forms the lateral surface of the occiput and surrounds the posttemporal fenestra, which probably conveyed the lateral head vein (Rougier, et al., 1992). Its medial boundaries are not superficially observable, but are evident in cross section. The tabular contacts the postparietal dorsally, the supraoccipital dorsomedially, the exoccipital ventromedially, the petrosal ventrally and anteriorly, and the squamosal laterally. The posttemporal fenestrae are low and centered between the foramen magnum and the lateral margins of the occiput. Ventral to each is a horizontal ledge that ends laterally in a process which overlaps the the posterior process of the paroccipital process. There are four depressions on the occiput: two dorsomedial depressions on either side of the supraoccipital, and two ventrolateral depressions between the posttemporal fenestrae and the foramen magnum. These represent insertions of cervical musculature that elevates the head.

The dentition

Because the premaxillae and lower jaw of *Pseudotherium* are not preserved, the form and number of incisors are unknown. The upper canines are long and curved. The canines were displaced postmortem, and the fossil is distorted on its left side, further displacing the left canine. As a result, the long roots of the canines appear to erupt through the overlying maxilla where their roots are broken and eroded. The crown morphology of the canines is distinctive, being buccolingually compressed, and with ridges running nearly the length of the crown on both labial and lingual surfaces (Fig. 1.26). This is an autapomorphic feature of *Pseudotherium*. The relative size and shape of the canines *Pseudotherium* most closely resemble those of *Prozostrodon* which are also relatively long and bear a sulcus on their labial surface (Bonaparte and Barberena, 2001: Fig. 1.11). The canine crowns in *Brasilodon quadrangularis* and *Brasilitherium riograndensis* have not been described in detail. The canines of *Brasilodon* are described as transversely flat with a sulcus running dorsoventrally along the anterolateral surface, similar to *Prozostrodon* (Bonaparte et al., 2003). The canines of *Pseudotherium* and are longer and more curved than those of *Brasilodon* (see Bonaparte et al., 2005: fig. 4). The complete canine crown is lacking in *Brasilitherium riograndensis*, precluding their comparison to *Pseudotherium*.

The roof of the palate is marked by deep paracanine fossae anteriomedial to the canines that would have received what must have been long lower canines when the jaws were closed. A

small diastema separates the canines from the postcanines. If replacement in *Pseudotherium* was like that of other cynodonts, the presence of a diastema suggests that at least one postcanine tooth had been shed and went unreplaced (Luo and Crompton, 2004). There are nine postcanines in the maxilla (Fig. 1.27). The upper tooth row is complete on the left side of the skull, whereas postcanine (PC) 6 and PC9 are absent on the right. Crown complexity increases with each successively distal postcanine, with the exception of the ultimate postcanine, which is somewhat simpler in shape than the penultimate postcanine. All postcanines, except the first, have wear facets that mostly affect the main cusp (A) and are not similarly developed in all teeth. There is less wear in the smaller teeth (Fig. 1.27A). The facets are flat with surfaces medioventrally oriented. PC1 is the simplest in form and its crown has a single cusp. The crown of PC2 comprises a large main cusp and one small distal cusp. Crowns of PC3 – PC6 comprise a relatively large central cusp A and mesial and distal cusps, B and C, respectively. The crowns of PC7 – PC8 are the most ornamented of the postcanines. They are unusual in that the position of their accessory cusps subtly differs between the left and right side. The left PC7 has two small buccal accessory cusps on the mesial and distal sides of cusp C. The more mesial buccal accessory cusp is small enough that it is hardly observable. The right PC7 also has two accessory cusps near cusp C, however, they are more distally positioned, with the more mesial accessory cusp positioned distobuccal to cusp C, and the second accessory cusp positioned immediately distal to cusp C so it is in alignment with the three main cusps. Being the penultimate postcanine, PC8 (Fig. 1.28) has the most ornamentation, comprising three buccal accessory cusps distally. Of the distal accessory cusps for PC8, two are buccal to cusp C (cusps D and E) while the third is immediately distal to cusp C (cusp F). Only the left PC9 is preserved. Three main cusps are distinguishable, and though the shape of the crown resembles PC7 in occlusal view, no distal accessory cusps are visible. It is difficult to determine if PC9 lacks accessory cusps or if the accessory cusps were worn away.

The last four postcanines (PC6 – PC8) differ from the preceding postcanines in orientation within the maxilla. While the first five postcanines are oriented mesiodistally along the length of the snout, the last four postcanines are oriented with their mesial end directed lingually and their distal end directed buccally.

The roots of PC3 – PC9 are incompletely divided and form a figure eight in cross section. The pulp cavity of the postcanines is buccolingually compressed but undivided throughout its length (Fig. 1.27B). On the left, PC4, PC7, and PC9 are higher in the maxilla than the other postcanines in the tooth row. On the right, PC4 and PC7 have shorter crown height, and PC6 and PC9 are absent. There are no replacement teeth in the maxillae, except at the base of the roots of both PC4s (Fig. 1.29).

Postcanine orientation and root constriction

The extreme reductions of upper postcanine size and crown complexity are autapomorphic in *Pseudotherium*, but they resemble the postcanines of other eucynodonts in both orientation and root structure. The more distal upper postcanines (PC6-PC9) are mesiolingually in-turned so that the distal end of one postcanine is actually buccal to the mesial end of the proceeding tooth. Mesiolingually oriented upper postcanine crowns, termed "imbricating" by previous authors (e.g., Rowe, 1993), has been described and/or illustrated for *Lumkuia fuzzi* (Hopson and Kitching, 2001), *Ecteninion lunensis* (Martinez et al., 1996), *Therioherpeton cargnini* (Bonaparte and Barberena, 1975, 2001), *Pachyenelus monus* (Martinelli and Rougier, 2007), *Riograndia guaibensis* (Bonaparte et al., 2001; Soares et al., 2011), *Chaliminia musteloides* (Martinelli and Rougier, 2007), *Diarthrognathus broomi* (Martinelli and Rougier, 2007), *Tritheledon ricoini* (Broom, 1912; Martinelli and Rougier, 2007), *Brasilodon quadrangularis* (Bonaparte et al., 2003: fig. 8b); and *Brasilitherium riograndensis* (Bonaparte et al., 2003: Fig. 14c). The lower postcanines of *Brasilitherium riograndensis* are also imbricated (Bonaparte et al., 2003: fig. 16b). This extensive list suggests that the mesiolingual orientation of the postcanines is apomorphic of probainognathian cynodonts, or perhaps a more inclusive clade.

The incompletely divided roots in *Pseudotherium* are of particular interest since Mammaliamorpha is diagnosed by teeth with completely divided roots (Rowe, 1988, 1993; 2017). As with postcanine orientation, incompletely divided roots have been documented in numerous other probainognathian taxa. These include *Microconodon tenuirostris* (Sues, 2001), *Therioherpeton cargnini* (Bonaparte and Barberena, 1975, 2001), *Prozostrodon brasiliensis* (Bonaparte and Barberena, 2001), *Pachygenelus monus* (Shubin et al., 1991), *Riograndia guaibensis* (Soares et al., 2011), *Irajatherium hernendezi* (Martinelli et al., 2005),

Botucaraitherium belarminoi (Soares et al., 2014), *Brasilodon quadrangularis* (Bonaparte et al., 2003, 2005), and *Brasilitherium riograndensis* (Bonaparte et al., 2003, 2005, 2013). Though the postcanine roots of *Pseudotherium* are constricted, the dental canal for the nerve roots and dental pulp is not divided. Unfortunately not all of the dental canals of eucynodonts with incipiently divided postcanine roots have been described and/or illustrated, an observation that generally requires CT scanning or broken cross-sections of the roots. The dental canals of *Brasilitherium* (Bonaparte et al., 2005) and *Botucaraitherium* (Soares et al., 2014) were reported as divided (although the canals within each lobe of the root appear connected for some teeth, e.g., Soares et al., 2014: fig. 3b), which differs from *Pseudotherium*.

The distribution of crown orientation and root character states among probainognathians are summarized in Table 1.1. The important point is that the two characters are independent from one another. It is possible to have mesiolingually oriented crowns with single, non-constricted roots; conversely, it is possible to have incompletely divided roots of postcanines that are not in-turned. Of the taxa where the postcanine orientation and root shape are both known, in-turned crowns and constricted roots occur in two thirds of those taxa.

DICUSSION

Phylogenetic analysis

We conducted a phylogenetic analysis to estimate the relationship of *Pseudotherium* to other probainognathian cynodonts. We modified a morphological character matrix for cynodonts that was initially assembled by Liu and Olsen (2010), with subsequent modifications to character definitions and character state assignments by Soares et al. (2014) and Martinelli et al. (2016, 2017). This is the most current matrix for the taxa of interest here, and its use enables the most direct comparisons to recenty published results. Our character list and modifications of previous versions of the matrix are presented in Appendix 1.A.

Three taxa were added to the Martinelli et al. (2017) matrix. *Pseudotherium* was added and scored based on observations from CT data, from 3D printouts, and from the specimen itself. *Brasilodon* and *Brasilitherium* were synonymized in the Liu and Olsen (2010) matrix, but a subsequent detailed description of a relatively complete skull of *Brasilitherium* supports two

distinct genera (Bonaparte et al., 2013). *Brasilodon* and *Brasilitherium* were scored as separate taxa in the analyses by Soares et al. (2014) and by Martinelli et al. (2016, 2017). We accept this conclusion and include *Brasilitherium* and *Brasilodon* as separate taxa. Because the monophyly and membership of 'Brasilodontidae' is controversial, *Botucaraitherium* (Soares, et al., 2014), a possible brasilodontid, is also included in the analysis.

The final matrix has 34 taxa and 145 morphological cranial, dental, and postcranial characters (Table 1.2). Of these, 119 are cranial and 16 are postcranial. Taxa range from 14% to 99% complete (based on 145 scorable characters), with an average completeness score of 75% (Table 1.3). The matrix was analyzed in PAUP* 4b10 (Swofford, 2003) using the parsimony algorithm. A heuristic search was performed for 1000 replicates (random addition sequence) with TBR (tree bisection and reconnection) branch swapping. Multistate characters were unordered, and 'inapplicable' characters were treated as missing data. Character state distributions are reported below using the DELTRANS optimization (Appendix 1.B). The parsimony analysis resulted in eight most parsimonious trees (MPTs) consisting of 443 steps, with a consistency index (CI) of 0.4695, and a retention index (RI) of 0.7814.

Bremer support values, also known as Decay Indices, were calculated by a series of manual PAUP converse constraint analyses. Whereas the expected average Decay Index (tree length divided by number of internodes; Zander, 2004) for internodes under this matrix and tree topology is 17, most of the internodes had decay indices of less than five, and the Consistency Index (CI) is 0.47, indicating a high degree of homoplasy with this tree topology. The low Consistency Index is partly a result of homoplasy distributed across the non-probainognathian part of the tree, but most of the individual characters supporting relationships among probainognathians also have CIs of less than 1.

A strict consensus of eight most parsimonious trees (Fig. 1.30) consistently places *Pseudotherium* within Probainognathia. The analysis also reveals that the greatest phylogenetic ambiguity lies in the relationships among non-probainognathian cynodonts, but discussion of those issues is beyond the scope of the present analysis.

Within probainognathians, our analysis had several interesting results. First, there is weak support for a clade that includes *Pachygenelus* and *Riograndia*, and we provisionally restrict the name Tritheledontidae to that clade. It is diagnosed by reduction in numbers and size of the

incisors and canine, and loss of the paracanine fossa (Appendix 1.B). *Therioherpetron*, which is widly considered a tritheledontid (Soares et al., 2011) falls outside that clade. The node containing *Therioherpeton* and mammaliamorphs is weakly supported, with a Decay Index of 1. *Therioherpeton* is only 35% complete, while *Riograndia* is 74% complete and *Pachygenelus* is 93% complete. The sister taxon to this clade (Mammaliamorpha + Tritheledontidae + *Therioherpetron*) is *Prozostrodon*, which is only 46% complete. The incompleteness of *Therioherpetron* and *Prozostrodon* lack postcranial remains, and their crania are not thoroughly described. *Therioherpetron* and *Prozostrodon* thus complicates the diagnosis of Mammaliamorpha. All of the taxa just mentioned are known from specimens that include cranial remains, however, and could potentially contribute far more information to the analysis if they were CT scanned.

Secondly, the analysis found no support for a monophyletic Brasilodontidae, even though character data that was not incorporated into the matrix offers support for a sister taxa relationships between *Pseudotherium* and *Brasilotherium* (below). It did recover a topology in which *Sinoconodon* followed by *Adelobasileus* were consecutive sister taxa to Mammaliaformes. This clade (Mammaliaformes + *Sinocondon* + *Adelobasileus*) was grouped in an unresolved polytomy with *Brasilodon* and *Brasilitherium*. Lying outside this polytomy is *Botucaraitherium*, in a weakly supported node with a Decay Index of 1.

Thirdly, the analysis consistently found a well-supported monophyletic Tritylodontidae (Decay Index ≥ 5). *Pseudotherium* was consistently resolved within Mammaliamorpha, as the sister taxon to Tritylodontidae. Four unambiguous synapomorphies support this phylogenetic position, but the Decay Index for this node is 2. Two of its supporting characters represent character state reversals, and the other two were found to be homoplastic within Mammaliamorpha.

The most parsimonious trees support the monophyly of Mammaliamorpha, based on six unambiguous synapomorphies, none of which represent homoplasy or character state reversals. Whereas the monophyly of Mammaliamorpha was strongly supported by this and other analyses (e.g., Gauthier et al., 1988; Rowe, 1988, 1993; Luo et al., 2015), the larger hierarchy of character distributions beyond the variation captured in the Martinelli et al. (2017) data matrix leaves a

measure of doubt about the overall strength of support for considering *Pseudotherium* as either the sister taxon to tritylodonts or as a member of Mammaliamorpha.

Additional phylogenetic context

Owing to the low Decay Index and low Consistency Index found in our analysis, and because of the effects of character incompleteness, it is important to look beyond the data matrix to additional information in the literature on cynodont skeletal evolution, as well as unpublished CT scans of relevant taxa to assess the phylogenetic position of *Pseudotherium*. Once a broader comparative sample of CT scans is more fully evaluated and published, we expect that an entirely new and much more informative matrix can be developed that will offer more stable resolution and support for the placement of *Pseudotherium* and other probainognathian taxa.

We also note that *Pseudotherium* and the other taxa of interest display a special kind of transitional mammalian characters. These are features such as the complex pattern of pterygopalatine troughs and ridges around the choana or the bifurcation of the paroccipital process, that are seen in the earliest fossil members of crown Mammalia, but that are subsequently so entirely transformed that nothing quite like them is found in extant mammals. Indeed, some of the differences in conceptualization of characters and character states found among the different data matrices that have been compiled over the last three decades for the Late Triassic cynodonts is related to there being no clear modern anatomical analogs. A better anatomical interpretation of these features will undoubtedly clarify the precise sequence of events that led up to the origin of Mammalia.

Some of these characters summarized below suggest that *Pseudotherium* lies either just outside of Mammaliamorpha or just inside, in an unresolved position at the base of Mammaliamorpha (instead of being the sister taxon to tritylodontids). In addition, several characters suggest that *Pseudotherium* forms a clade with *Brasilitherium* that lies just inside or just outside of Mammaliamorpha, and provide weak support for a monophyletic, but less inclusive Brasilodontidae.

Mammaliamorph characters that are lacking in *Pseudotherium*

Although our formal analysis found *Pseudotherium* to lie within Mammaliamorpha, we note that it lacks a number of features that have been considered diagnostic of Mammaliamorpha in other analyses (e.g., Kemp, 1983; Gauthier et al., 1988; Rowe, 1988, 1993; Kielan-Jaworowska et al., 2004; Luo 2007; Luo et al., 2015). These include several diagnostic derived character states that are present in Tritylodontiae and basal Mammaliaformes, but which are lacking in *Pseudotherium*. For example, *Pseudotherium* retains vestigial prefrontal and postorbital bones, which are entirely absent within Mammaliamorpha (Rowe, 1988, 1993, 2017). In the palate, *Pseudotherium* lacks the forwards extension of the ventral pterygoid keel onto the vomer, as is seen in tritylodontids (Sues, 1986) and in *Morganucodon* (Kermack et al., 1981) and other mammaliaforms. Also lacking in *Pseudotherium* are fully divided postcanine tooth roots, another condition generally considered diagnostic of Mammaliamorpha. Additionally, *Pseudotherium* has an ossified medial orbital wall (as in mammaliamorphs), but this wall fails to extend posteriorly to enclose the orbital fissure behind the orbit. The orbital fissure in basal Mammaliamorpha is almost completely closed by the orbitosphenoid and alisphenoid (Rowe, 1988; Crompton et al., 2017). *Pseudotherium* also lacks a floor beneath the cavum epiptericum (which held the trigeminal ganglion), which is at least partially present in tritylodontids, and fully present in Mammaliaformes (Rowe 1988, 1993).

Additional characters *Pseudotherium* shares with Mammaliamorpha

The above plesiomorphies notwithstanding, *Pseudotherium* shares a number of derived character states widely recognized as diagnostic of Mammaliamorpha (e.g., Gauthier et al., 1988; Rowe, 1988, 1993; Kielan-Jaworowska et al., 2004; Luo 2007; Luo et al., 2015). The presence of such features in *Pseudotherium* may indicate that these character states are more widely distributed than previously believed, that they may be homoplastic, or that their distribution is equivocal because of incompleteness of some of the other relevant taxa. In several cases, these features can only be identified with certainty from CT scans.

Probably the most significant resemblance *Pseudotherium* shares with mammaliamorphs is in its cranial endocast (Wallace et al., in prep.), in which the cerebral hemisphers form tall, elongated domes separated by a deep interhemispheric sulcus. Comparable endocasts are now

known in tritylodontids (Wallace et al., in prep.) and *Brasilitherium* (Rodrigues et al., 2015). *Pseudotherium* shares with Mammaliamorpha ossification of the orbital wall (anterior portion of the orbital fissure), in which sheets of bone from the frontal and palatine join to provide a solid orbital wall (although it fails to fully close the orbital fissure behind the orbit). The taxa that are sometimes grouped together as tritheledontids (*Therioherpeton*, *Pachygenelus*, *Riograndia*) preserve a more plesiomorphic condition in which both the orbital wall and orbital fissure remain broadly open. *Pseudotherium* also shares with mammaliamorphs the loss of an intact postorbital arch that separates the orbit from the temporal fenestra (although *Pseudotherium* retains a vestigial postorbital bone).

As in mammaliamorphs, *Pseudotheriuim* has a secondary palate that extends to the back of the tooth row. The arrangement of bones surrounding the choana takes on a distinct configuration in which parabasisphenoid and pterygoid no longer form a single continuous ventral parasagittal ridge, and instead form parallel parasagittal ridges (pterygopalatine ridges) separated by a shallow trough which may mark the passage of the auditory (eustacean) tube from the nasopharynx to the middle ear (Barghusen, 1986). Broad parasphenoid alae are also present in *Pseudotherium* and in basal mammaliamorphs. The condition of these characters in tritheledontids has not been reported, but should be observable in CT scans.

In the otic region, the internal auditory meatus is walled medially with separate foramina for the vestibular and cochlear nerves, and the cochlea is slightly elongated, much like the condition in tritylodontids and *Morganucodon* (Kielan-Jaworowska et al., 2004). A walled internal auditory meatus was scored as present in *Pachygenelus monas* (Martinelli et al., 2017), but we have not been able to confirm this and the geometry of its cochlea has not been described. Adjacent to the otic capsule, the prootic, alisphenoid, and quadrate ramus of the pterygoid join to form a laterally directed flange near the rear edge of the trigeminal foramen, and the paroccipital process is directed laterally (instead of ventrolaterally) and is bifurcated distally, with one distal process forming a separate condyle for a kinetic articulation with the quadrate, and the other apparently articulating with the hyoid. The basicranium is also broadly expanded to widely separate the pterygoid transverse processes. As in *Kayentatherium* (Sues, 1986) and *Morganucodon* (Kermack et al., 1981) the pterygoparoccipital foramen is open laterally, a derived condition compared to the completely enclosed foramen found in more basal cynodonts.

Comparison to 'brasilodontids'

Pseudotherium shares several derived similarities to *Brasilitherium*, and possibly also to *Brasilodon*. *Pseudotherium* resembles *Brasilitherium* in that the promontorium is only partially covered by the parasphenoid ala (= basisphenoid wing; Rodrigues et al., 2013). Both *Pseudotherium* and *Brasilitherium* have a crest between the promontorium and the trough on the prootic, and both taxa have a distinct and gracile crista interfenestralis. A median keel runs anteriorly from the basioccipital to the basisphenoid and along the ventral surface of the parasphenoid rostrum. Where the parasphenoid alae converge at the carotid foramina, the median keel deepens and forms a small crest (Fig. 1.24). Such a crest has only been described in *Brasilitherium* and was thought to be autapomorphic for that taxon (Bonaparte et al., 2013).

Brasilitherium and *Pseudotherium* also have a ventral process on the basisphenoid, a feature of the basisphenoid that is also described for *Brasilodon* (Bonaparte et al., 2005: 27, Fig. 1). The process in *Brasilodon* continues posteriorly as a low crest bordered by two longitudinal depressions. *Pseudotherium* also has a ventral process of the basisphenoid that continues as a crest that is bordered by depressions. *Brasilitherium* and *Pseudotherium* are the only known taxa to retain prefrontal and postorbital bones, while lacking a complete postorbital arch. Both taxa have nine postcanine teeth with reduced crowns with indistinct cusps. Finally, the thin, wispy C-shaped ossifications in the nasal capsule in *Pseudotherium* and *Brasilitherium* may be ambiguous in terms of their identity and function, but their position and form are similar. Given this mosaic of features, there is reason to continue to test whether or not some or all of the taxa variously assigned to 'Brasilodontidae' indeed form a clade, and whether any of these taxa lie inside or just outside of Mammaliamorpha.

CONCLUSIONS

The discovery of *Pseudotherium argentinus* underscores the diversity of very small cynodonts in the mid- to Late Triassic and highlights the acquisition of growing numbers of mammalian features as a distinctive feature of this radiation. Although the phylogenetic position of *Pseudotherium* is not fully resolved, it shares with the other 'taxa of interest' a number of novelties that link it closey to the origin and early diversification of Mammaliamorpha. Current evidence suggests that the evolution of endothermy, lactation, parental care, prolonged activity,

and the beginnings of encephalization were the products of this segment of history, and that it played out in miniaturized cynodonts (Kemp, 2005; Kielan-Jaworowska et al., 2004; Rowe and Shepherd, 2016; Rowe, 2017). The current uncertainty on phylogenetic relationships among those taxa that have been referred to as tritheledontids and brasilodontids is based in part on incompleteness, and also on differing strategies for sampling taxa for analysis. It seems clear that resolving this phylogenetic knot will more precisely elucidate the sequence of events culminating in the origin of Mammalia, and that CT may be a key technology in providing character evidence for this phylogeny.

The taxa of interest described above retain relatively much smaller brains than found in *Morganucodon* and other mammaliaforms. However, *Pseudotherium* and *Brasilitherium* provide evidence of a slight pulse in encephalization that preceded the much more marked encephalization pulse expressed in the last common ancestor of Mammaliaformes (Rowe et al, 2011; Wallace et al., in prep.). In this respect *Pseudotherium* is further from Mammaliaformes than other Late Triassic and Early Jurassic fossils such as *Adelobasileus* and *Sinoconodon* that present a more advanced degrees of encephalization. Aspects of the nose, palate, dentition, the circumorbital configuration, and in elongation of the cochlea also take on a new measure of resemblance to mammals.

We find a weak signal that diagnoses a monophyletic tritheledontidae that includes *Pachygenelus* and *Riograndia*. A weak signal also links *Pseudotherium* and *Brasilitherium*, and with less confidence *Brasilodon*, in a monophyletic Brasilodontidae. While the available evidence seems favors excluding *Therioherpeton*, *Pachygenelus*, and *Riograndia* from Mammaliamorpha, it is less clear whether *Pseudotherium* and *Brasilitherium* lie just within or just outside of that clade. The slight increase in EQ in *Pseudotherium* and *Brasilitherium* compared to tritylodonts and tritheledonts may indicate that brasilidontids lie within Mammaliamorpha, where they would represent the most basal members of the mammaliaform stem. As the specimens upon which these taxa are based are CT scanned, and as the scans are made available to the larger community, we expect improved phylogenetic resolution of this radiation of small cynodonts.

Table 1: Postcanine morphology in derived Probainognathians.

Taxon	**Postcanine crowns oriented anterolingual-posterobuccal**	**Incompletely divided roots**	**Citations**
Lumkuia fuzzi	yes	?	Hopson and Kitching, 2001
Ectenion lunensis	yes	?	Martinez et al., 1996
Microconodon tenuirostris	?	yes	Sues, 2001
Therioherpeton cargnini	yes	yes	Bonaparte and Barberena, 1975, 2001
Prozostrodon brasiliensis	?	yes	Bonaparte and Barberena, 2001
Pachygenelus monus	yes	yes	Shubin et al., 1991; Martinelli and Rougier, 2007
Riograndia guaibensis	yes	yes	Bonaparte et al., 2001; Soares et al., 2011
Irajatherium hernandezi	?	yes	Martinelli et al., 2005
Chaliminia musteloides	yes	No – single, unconstricted root	Martinelli and Rougier, 2007
Diarthrognathus broomi	yes	?	Martinelli and Rougier, 2007
Tritheledon ricoini	yes	No – single, unconstricted root	Broom, 1912; Martinelli and Rougier, 2007
Botucaraitherium belarminoi	no	yes	Soares et al., 2014
Brasilodon quadrangularis	yes	yes	Bonaparte et al., 2005
Brasilitherium riograndensis	yes	yes	Bonaparte et al., 2005, 2013
Pseudotherium argentinus	yes	yes	Wallace et al., 2017

Table 1.2: Character matrix.

Distribution of the character-states for the characters listed in Appendix 1.A I among 34 taxa considered in this analysis. A=0&1, B=1&2, a=0/1, b=1/2. ?=unknown,
dash=inapplicable

Procynosuchus delaharpeae	0000000100	0000000000	0000000000	0000000000	0000000000	0000000000	0001A00000	0000000000	0000000100	000000010	010000000-	-00-000000	0000000-00	000000000	00000
Galesaurus planiceps	0100000000	0000000010	0000100001	1000000000	0000000000	0000000000	0000000000	0000000100	0010000000	0001100100	000010000-	-00-100000	0001100???	?00??0??00	00000
Thrinaxodon liorhinus	01A0000000	0000000000	0000000000	1110000000	0000000000	0000000000	0000000000	0010010100	0010000011	0001100000	010000000-	-00-100000	0001100-00	000000000	?0000
Platycraniellus elegans	0110000000	0000000011	0000000001	0110000000	??00000000	?000000000	0000000000	101??10100	0?1010?0??	0001?0?100	000000000-	-0?-0?000?	??????????	??????????	?????
Cynognathus crateronotus	0000000000	0000001021	0021100000	1110000101	1100010100	?000000000	0000100000	1110010110	1120101112	0001101000	100010000-	-00-100100	0000111000	0001100000	00000
Diademodon tetragonus	A000000000	0000001022	0121110001	1110000001	1100010100	000000A000	0000000000	0010010111	1120101112	1131101000	1200100010	0100?00010	0001111000	0001100000	00000
Trirachodon berryi	11100100A0	0000001121	0111110100	1110100201	1100010100	0000021000	0000000011	0111020110	1110101112	1131101000	1211100020	1101001101?	??01111000	000????000	00000
Sinognathus gracilis	1020?10010	0000??1101	0011110?1?	1?1010?001	1000010100	???????000	00?000?011	0111020110	1110101???	1131200000	02?0?00?20	1100?0201?	??????????	??????????	?????
Langbergia modisei	0010000000	0000000121	0111110100	1110100001	1000010?0	?000?21??0	0000000001?	0?11????10	1110101112	1131101000	1200100020	1101001101?	????1?????	??????????	?????
Pascualgnathus polanskii	1020?10010	0000001122	0121110111?	1110100001	??000101?0	???0?22?000	00???0?0??	????????A0	?120101???	1132100000	02bb000-11	0100-12010	???1101??0	000??10000	00000
Luangwa drysdalli	??00?1000?	0000010121	001111????	1110?00001	???0010100	0000?2??00	000???0???	????????10	1120101???	1131101000	12bb000-20	2100-12010	???1101100	00???11000	00000
Massetognathus pascuali	0111110010	0000001101	0111110112	1110200001	0000010100	0000121100	0000000011	0111020110	11B01011??	1131102111	0211000-22	2100-12010	0000101101	000??11000	00000
Exaeretodon argentinus	0011111010	0000111121	0121110112	11101A0001	0?00010100	0100021100	0000000?1	01????0110	1121101???	1132100101	021b000-12	0100-12210	0000001101	0011111000	00000
Scalenodon angustifrons	??10?1?000	0000??1101	012111????	?1101?0??1	??00010100	?000021100	0000?000??	0?????0?a0	?12??011??	1131101000	12bb000-20	2100-1201?	??????????	??????????	?????
"Scalenodon" hirschoni	???0010???	??001?11??	???1110112	11101?0?0?	0??00?????	???????1?0	00?0?????1	??1?0?0?a?	?1???011??	1132210010	02bb000-22	2100-1201?	??????????	??????????	?????
Chiniquodon theotonicus	1110101010	0000101011	000001011B	1111211001	1000010100	0000010000	000000000?1	?01???1110	1120101112	0001100000	000010000-	-00-100000	??00001101	0001110000	?0000
Lumkuia fuzzi	??10001010	00000?0000	0000010?12	0110100101	0100010010	?000000100	0000000000	0010000110	1120100012	0001100000	000010000-	-00-10000?	????001???	?????????0	?????
Ectenion lunensis	001??00210	0000200000	0000000?1a	1110000201	1100010100	?100010100	0000000011	0011021110	1100101???	0001100000	1a0010000-	-00-?00000	???1??110?	?0?????0??	?????
Probainognathus jenseni	0110100210	0000100101	1000010112	1111101001	1100010000	0000110000	0000000011	0011021110	2100101112	0001100000	000000000-	-00-101100	00?0001107	??0??11000	?0000
Prozostrodon brasiliensis	21?010?2??	??0121?1??	???????112	?1111?1???	??????????	??????????	??????????	??????????	?030111???	0010000000	111000000-	-00-001000	???000????	?0???11111	10000
Therioherpeton cargnini	?????01111	0112?2?100	??0??????2	?11111????	??????????	??????????	??????????	??????????	??????????	00????????	?0?000?00-	-00-?00000	??1?00????	?0???11111	10011
Riograndia guaibaensis	2013101211	011221?10?	1000001112	0111111011	0001020000	?000010200	0010001121	102?13???0	0030111???	0012110011	00b000000-	-00-10100?	??????????	??????????	?????
Pachygenelus monus	2013101211	0112212100	1000000112	0111211011	0001020000	1000010200	00101??121	1022131320	2030111112	0012210010	001000010-	-00-002001	???0001111	101??11111	11111
Pseudotherium argentinus	?010?00111	01011?2?00?	???0?00?12	0111111?0	000103?011	1000?21211	?11??110??	????????00	0?????????	?01???00??	00000?10-	?00-??10??	??????????	??????????	?????
Botucaraitherium belarminoi	?????0????	??????????	??????????	??????????	??????????	??????????	??????????	??????????	?0???11???	?01??????0	01?001110-	-01-00??0?	??????????	??????????	?????
Brasilodon quardangularis	a000?01211	0112212000	1000?00?12	0111111211	0001021001	?0?1122207	0111101121	1022131320	?030111???	0011100001	011001110-	-01-001aa?	?????0111?	?11????????	?????
Brasilitherium riograndensis	0000?01211	0112212000	1000000?12	0111110211	0001021011	?011122207	?111?01121	1022131320	1030111???	0010110001	011001110-	-01-001a1?	??????????	?11????????	?1111
Tritylodon longaevus	102-111111	0112211102	0011110112	1110211211	0000110110	1101021211	1101101031	1022031202	0031111???	1132210-22	-222-21-2-	1100-03221	??????210?	?????1????	?1111
Oligokyphus major	b??-1111?1	0112???102	010110?1?2	?1??21????	????110?10	1101022211	1101100031	0022031202	0031111???	1132110-22	-222-21-2-	1100-03221	11100?2101	111??11211	11111
Bienotherium yunnanense	102-111111	0112211?2	01?1110112	1110211211	0000110110	110?02?011	11?110?031	??22131?02	0031111???	1132110-22	-222-21-2-	1100-03221	??????210?	?11???????1	11111
Kayentatherium wellesi	102-11111?	0112211102	0111111112	0110211211	0000110110	1101021211	11?110?031	1022131202	0031111112	1132110-22	-222-21-2-	1100-0322?	1110002101	1?11111212	?1111
Adelobasileus cromptoni	???????011	11?2??????	??????????	0?????211	0001021011	?211122100	00101110??	??????????	??????????	??????????	??????????	??????????	??????????	??????????	?????
Sinoconodon rigneyi	0002?01011	1112212000	1000?01?12	1111211211	0011031011	?211122210	11101010??	??????0?30	2030111222	2001000001	001001110-	-00-10101?	??????????	??????????	?????
Morganucodon oehleri	0?02?01011	1112212000	2?00001111	1111211211	0011032011	1211122201	1111111121	1022132430	2030111212	2221000001	011001110-	-01-001011	1111001111	111??11211	11111

Table 1.3: Completeness of taxa analyzed.

1. *Morganucodon oehleri* missing 7/145 = 95 % complete
2. *Sinoconodon rigneyi* missing 46/145 = 68 % complete
3. *Adelobasileus cromptoni* missing 111/145 = 23% complete
4. *Kayentatherium wellesi* missing 13/145 = 91% complete
5. *Bienotherium yunnanense* missing 32/145 = 78% complete
6. *Oligokyphus major* missing 33/145 = 77% complete
7. *Tritylodon longaevus* missing 25/145 = 83% complete
8. *Brasilitherium riograndensis* missing 31/145 = 79% complete
9. *Brasilodon quardangularis* missing 32/145 = 78% complete
10. *Botucaraitherium belarminoi* missing 125/145 = 14% complete
11. *Pseudotherium argentinus* missing 75/145 = 48% complete
12. *Pachygenelus monus* missing 10/145 = 93% complete
13. *Riograndia guaibaensis* missing 38/145 = 74% complete
14. *Therioherpeton cargnini* missing 94/145 = 35% complete
15. *Prozostrodon brasiliensis* missing 78/145 = 46 % complete
16. *Probainognathus jenseni* missing 10/145 = 93% complete
17. *Ecteninion lunensis* missing 29/145 = 80% complete
18. *Lumkuia fuzzi* missing 30/145 = 79 % complete
19. *Chiniquodon theotonicus* missing 11/145 = 92% complete
20. *"Scalenodon" hirschoni* missing 78/145 = 46% complete
21. *Scalenodon angustifrons* missing 59/145 = 59% complete
22. *Exaeretodon argentinus* missing 10/145 = 93% complete
23. *Massetognathus pascuali* missing 6/145 = 96% complete
24. *Luangwa drysdalli* missing 39/145 = 73% complete
25. *Pascualgnathus polanskii* missing 34/145 = 77% complete
26. *Langbergia modisei* missing 36/145 = 75 % complete
27. *Sinognathus gracilis* missing 48/145 = 67 % complete
28. *Trirachodon berryi* missing 7/145 = 95% complete
29. *Diademodon tetragonus* missing 1/145 = 99% complete
30. *Cynognathus crateronotus* missing 4/145 = 97% complete
31. *Platycraniellus elegans* missing 40/145 = 72% complete
32. *Thrinaxodon liorhinus* missing 4/145 = 97% complete
33. *Galesaurus planiceps* missing 12/145 = 92% complete
34. *Procynosuchus delaharpeae* missing 4/145 = 97% complete

Average = 75% complete

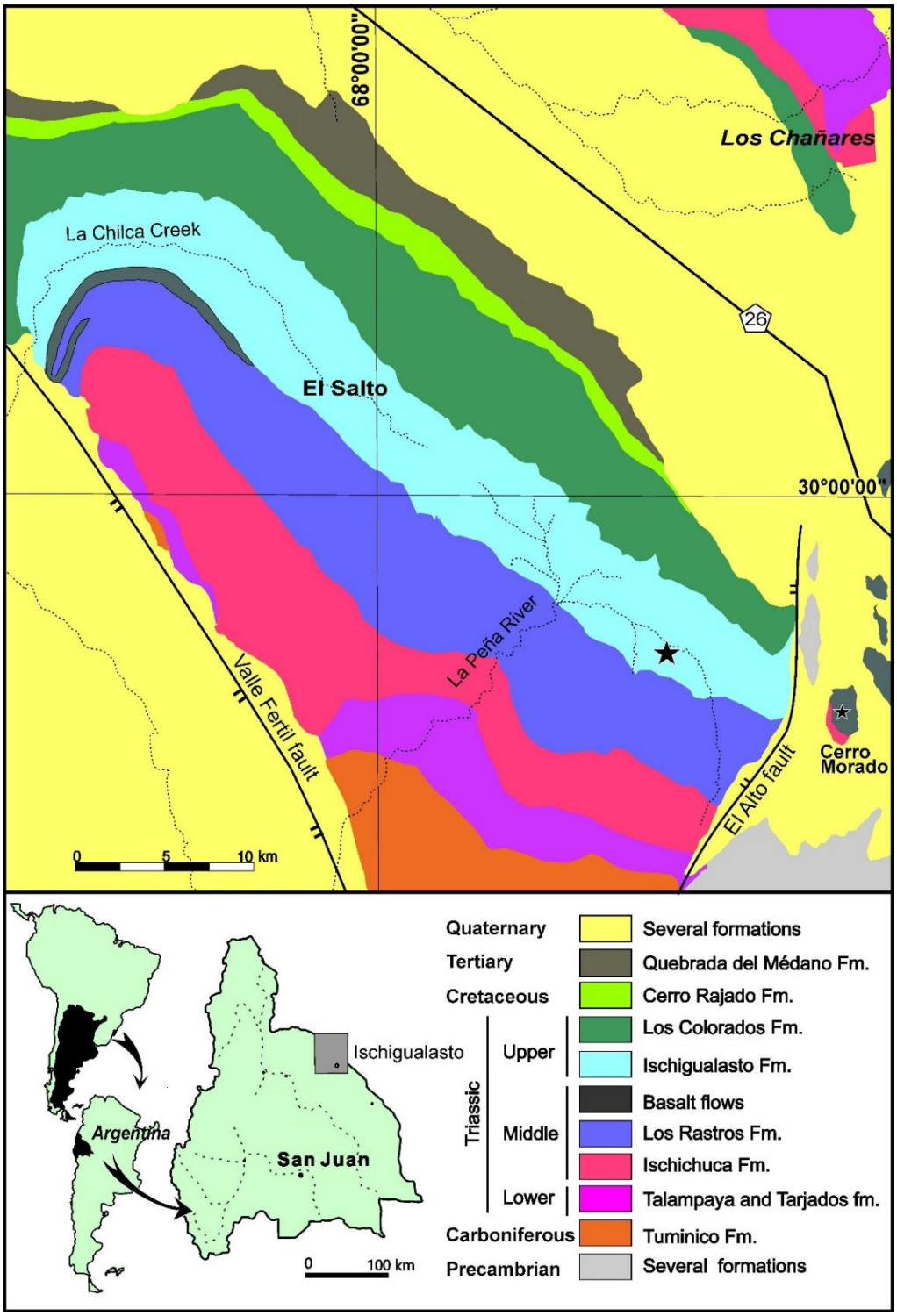

Figure 1.1: Geographic and geologic maps of the southern portion of the Ischigualasto-Villa Unión Basin (modified from Martínez et al., 2012).

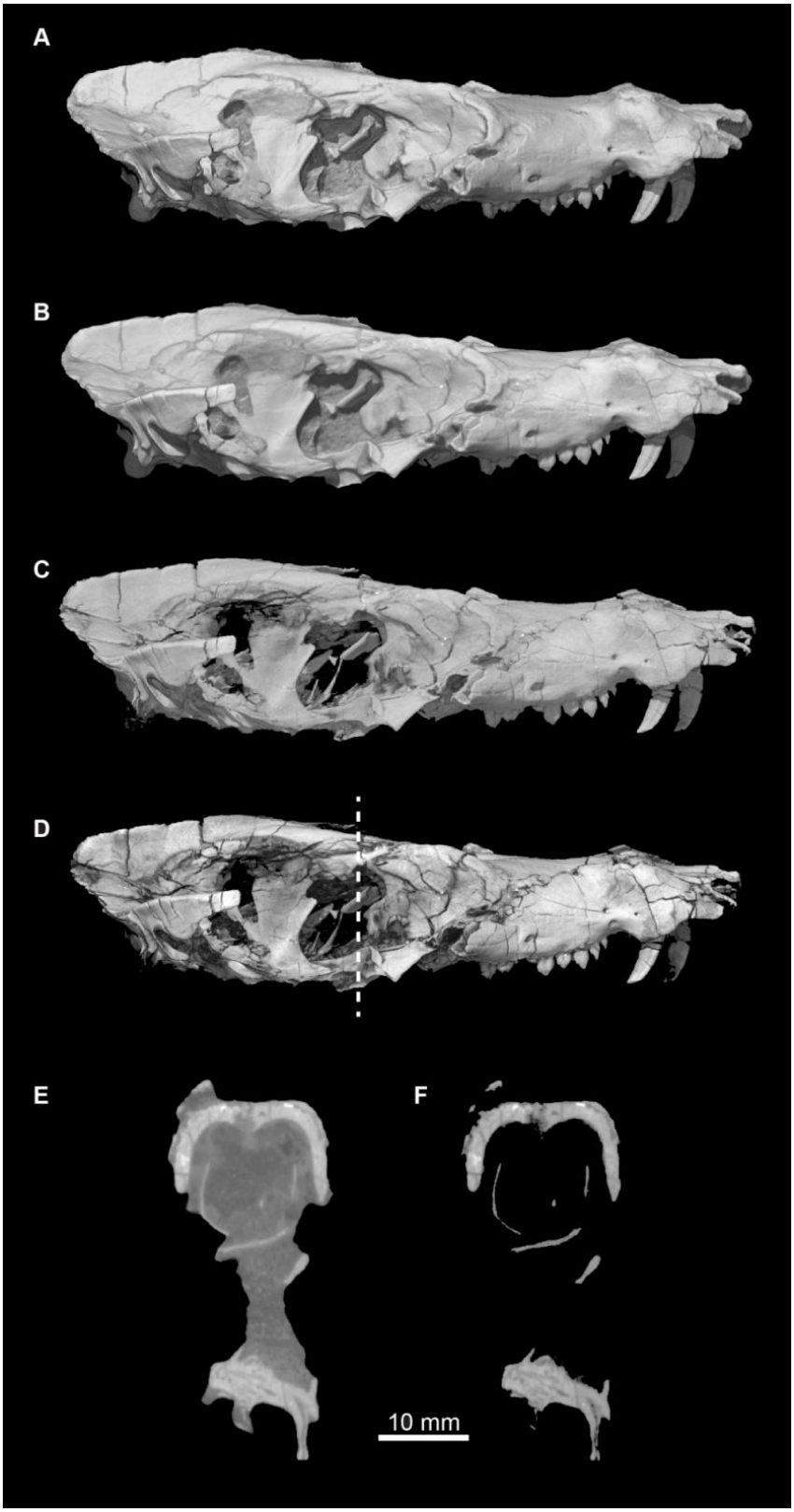

Figure 1.2.

Figure 1.2: *Pseudotherium argentinus*, a comparison of image processing methods based on μCT scans. (A) Isosurface rendering; (B) volume rendering, scattering algorithm, no digital matrix removal; (C) volume rendering, HQ scattering algorithm, digital matrix removal; (D) volume rendering, Phong algorithm, digital matrix removal; (E) cross section, no digital matrix removal; (F) cross section, digital matrix removal. Dashed line indicates position of cross sections (E) and (F).

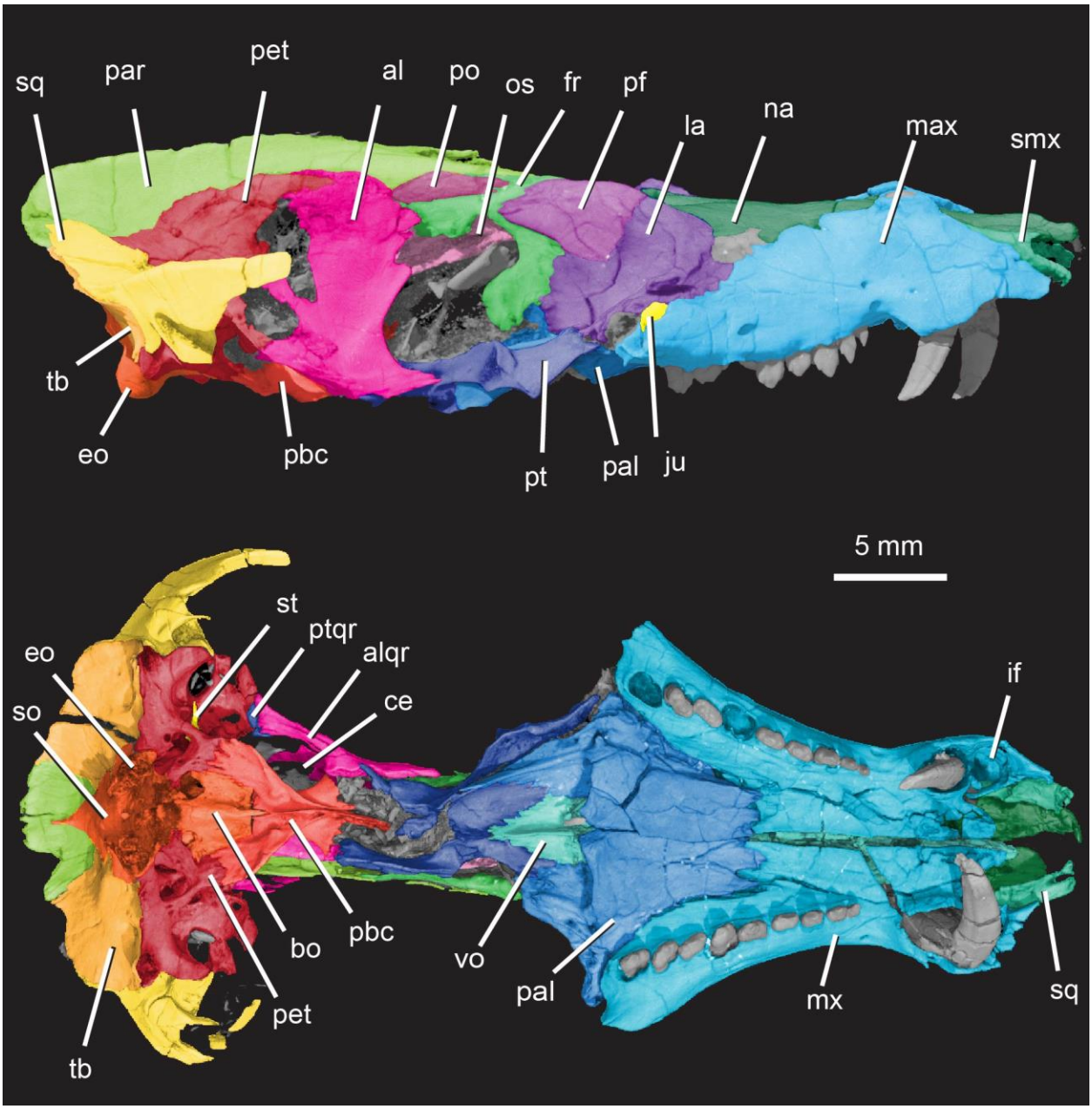

Figure 1.3: *Pseudotherium argentinus*, digitally colored 3D volume renderings of the holotype. (A) Skull in ventral and (B) right lateral views. Abbreviations: al, alisphenoid; alqr, quadrate ramus of alisphenoid; bo, basioccipital; eo, exoccipital; fr, frontal; ju, jugal; la, lacrimal; mx, maxilla; na, nasal; os, orbitosphenoid; pal, palatine; par, parietal pbc, parabasisphenoid complex; pet, petrosal (=periotic); pf, prefrontal; po, postorbital; pt, pterygoid; ptqr, quadrate ramus of pterygoid; smx, septomaxilla; so, supraoccipital; sq, squamosal; st, stapes; tb, tabular; vo, vomer.

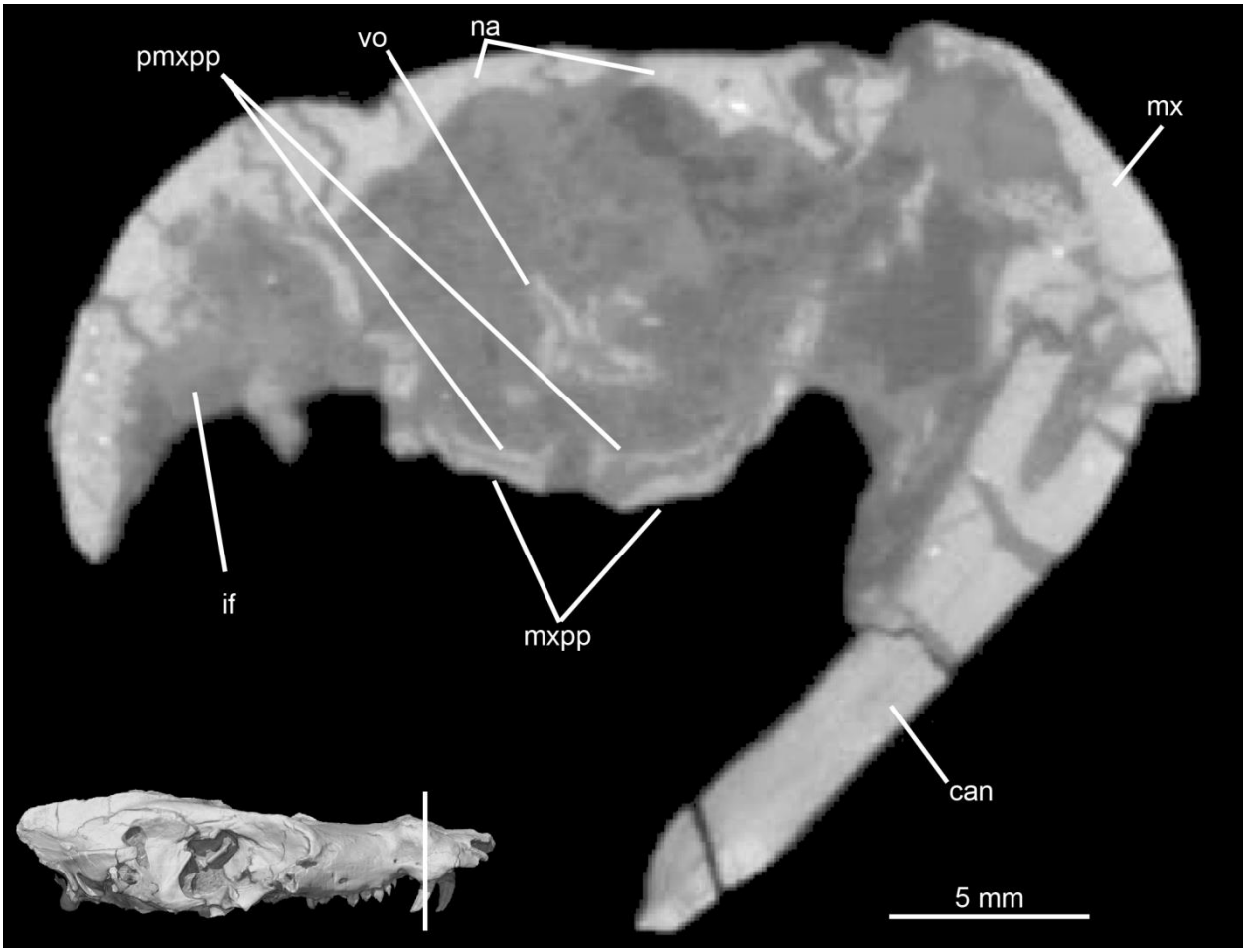

Figure 1.4: *Pseudotherium argentinus*, cross-section through the snout, showing the palatine processes of the premaxilla. Abbreviations: can, canine; if, incisive fossa for lower canine; mx, maxilla; mxpp, palatine process of maxilla; na, nasal, pmxpp, palatine process premaxilla; vo, vomer.

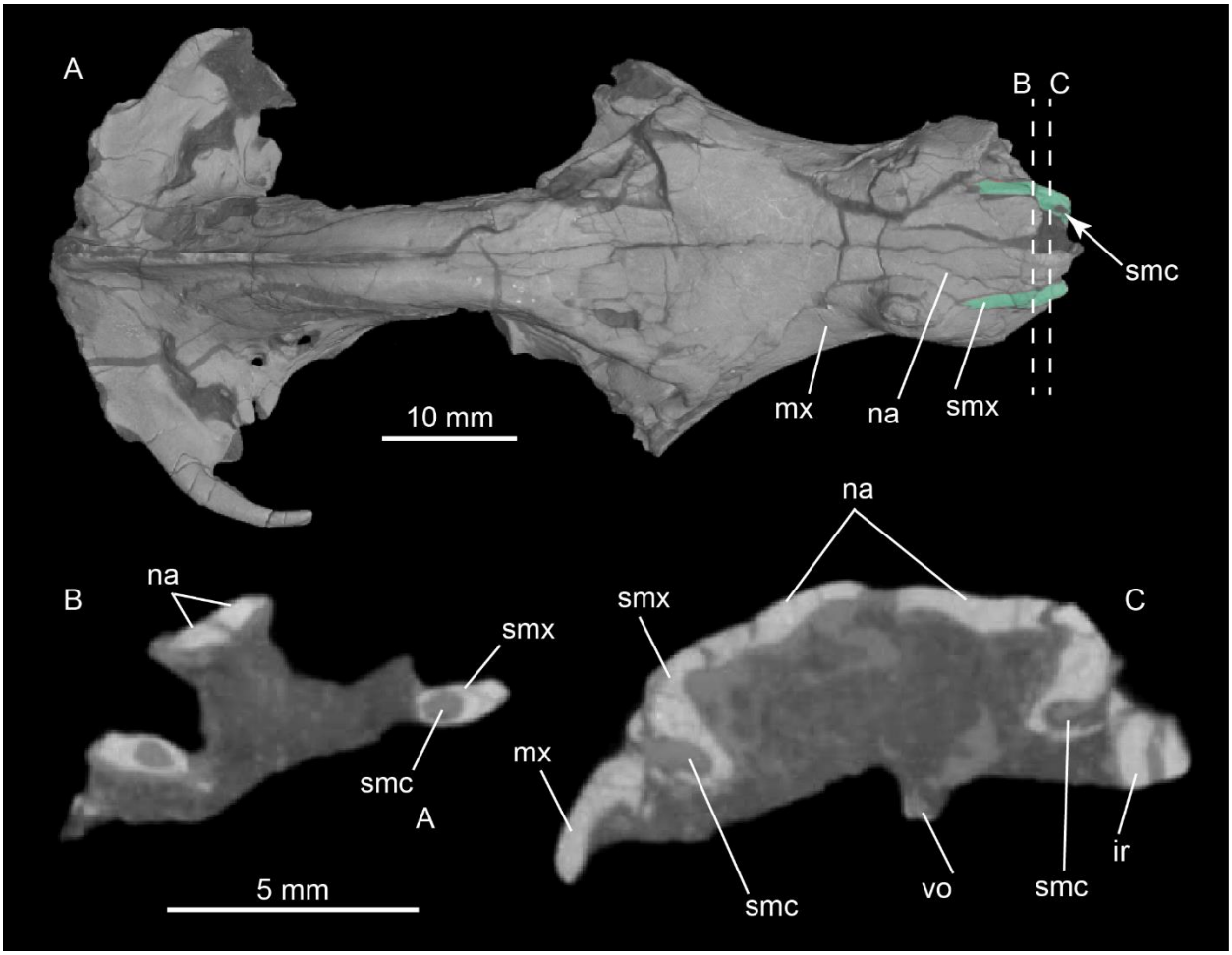

Figure 1.5: Pseudotherium argentinus, the septomaxillary canal. (A) 3D volumetric rendering of dorsal view of skull showing septomaxillae in aqua tint (A), and dashed lines that indicate positions of cross sectional CT image slices (B) and (C). Abbreviations: ir, broken incisor root; mx, maxilla; na, nasal; smc, septomaxillary canal; smx, septomaxilla, vo, vomer.

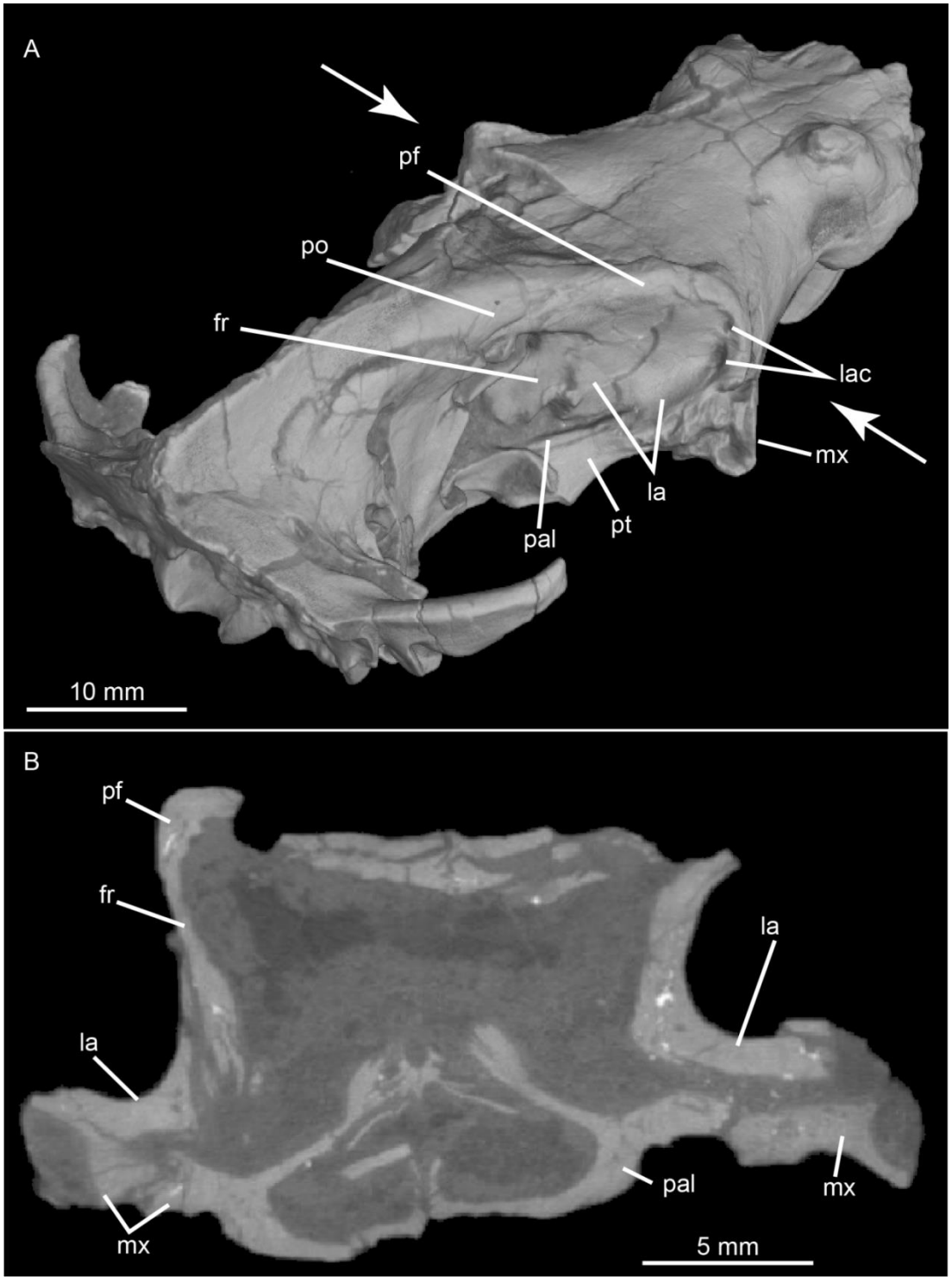

Figure 1.6.

Figure 1.6: *Pseudotherium argentinus*, wall and floor of the orbit. (A) Oblique posteriodorsal view. White arrows indicate plane of coronal slice (B). Abbreviations: fr, frontal; la, lacrimal; lac, lacrimal canal; mx, maxilla; pal, palatine; pf, prefrontal; po, postorbital; pt, pterygoid.

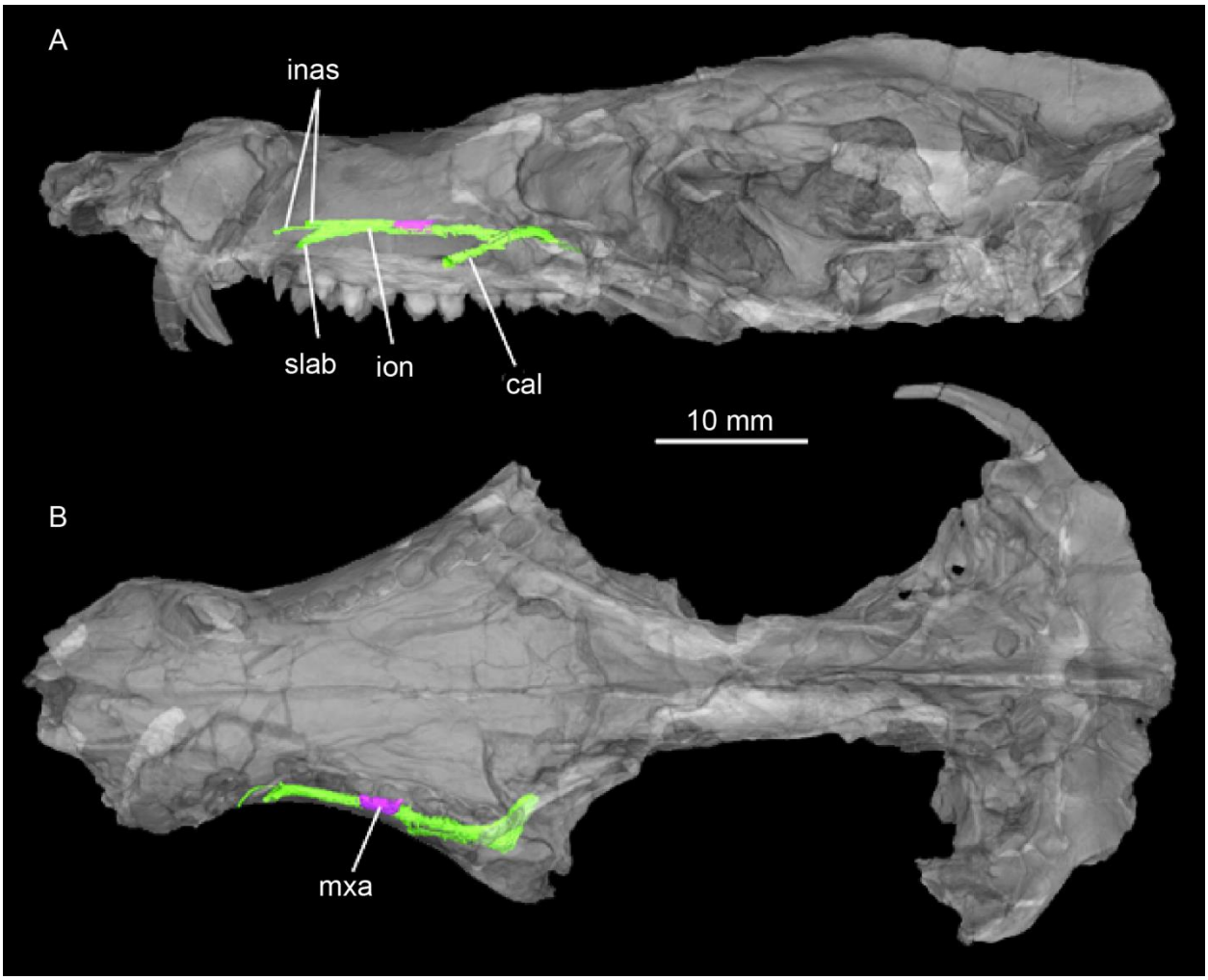

Figure 1.7: Pseudotherium argentinus, isosurface rendering of maxillary nerve. (A) skull in left lateral and (B) dorsal views. Maxillary nerve = green. Maxillary antrum = purple. Skull rendered semitransparent to view canal and antrum in situ. Abbreviations: cal, caudal alveolar ramus; inas, internal nasal rami of infraorbital nerve; ion, infraorbital nerve; mxa, maxillary antrum; slab, supralabial ramus of infraorbital nerve.

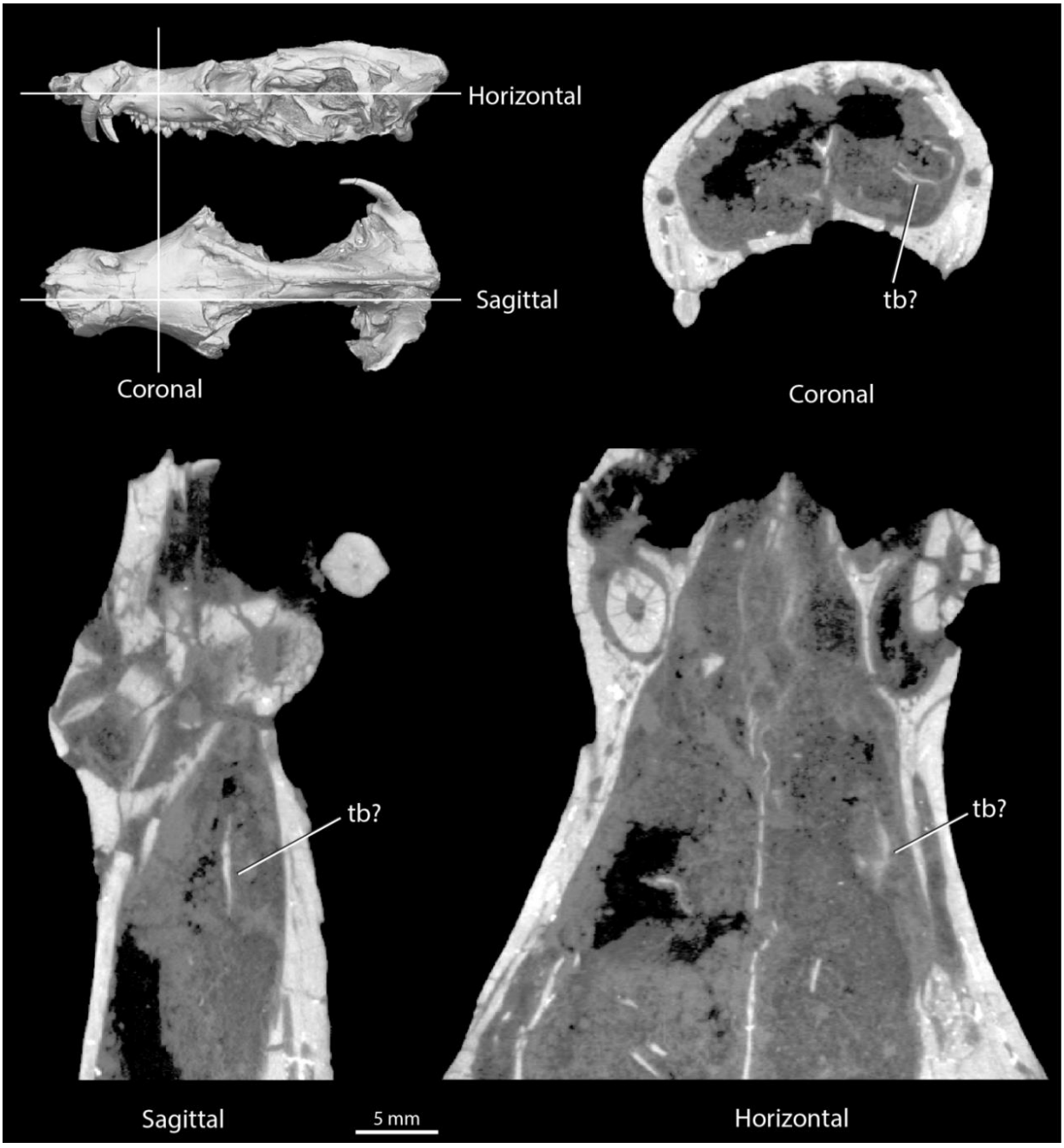

Figure 1.8: *Pseudotherium argentinus*, thin bone fragments of the nasal capsule. One may represent a turbinal (tb?), but others are probably exfoliated fragments of the nasopharyngeal wall.

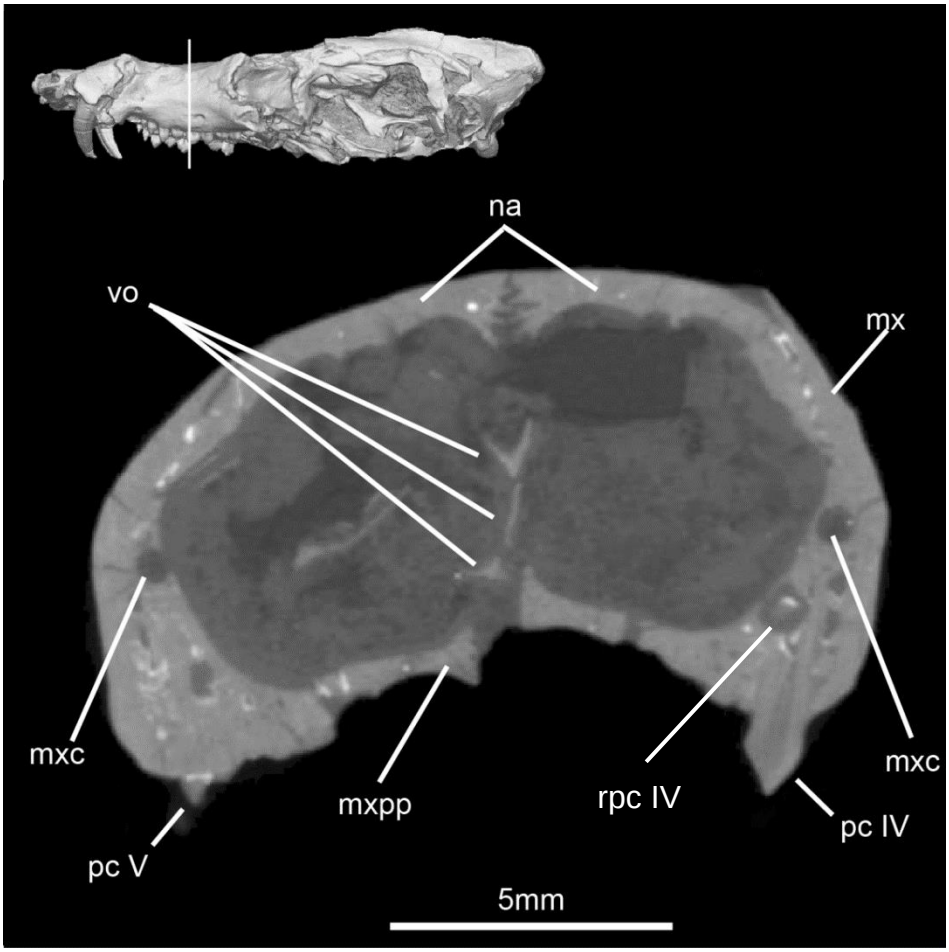

Figure 1.9. *Pseudotherium argentinus*, the tall plesiomorphic vomer. Line through *Pseudotherium* rostrum indicates position of cross sectional slice. Abbreviations: mx, maxilla; mxc, maxillary canal; mxpp, maxillary palatal process; na, nasal; pc IV, postcanine tooth IV; pc V, postcanine tooth V; rpc IV, replacement postcanine tooth IV; vo, vomer.

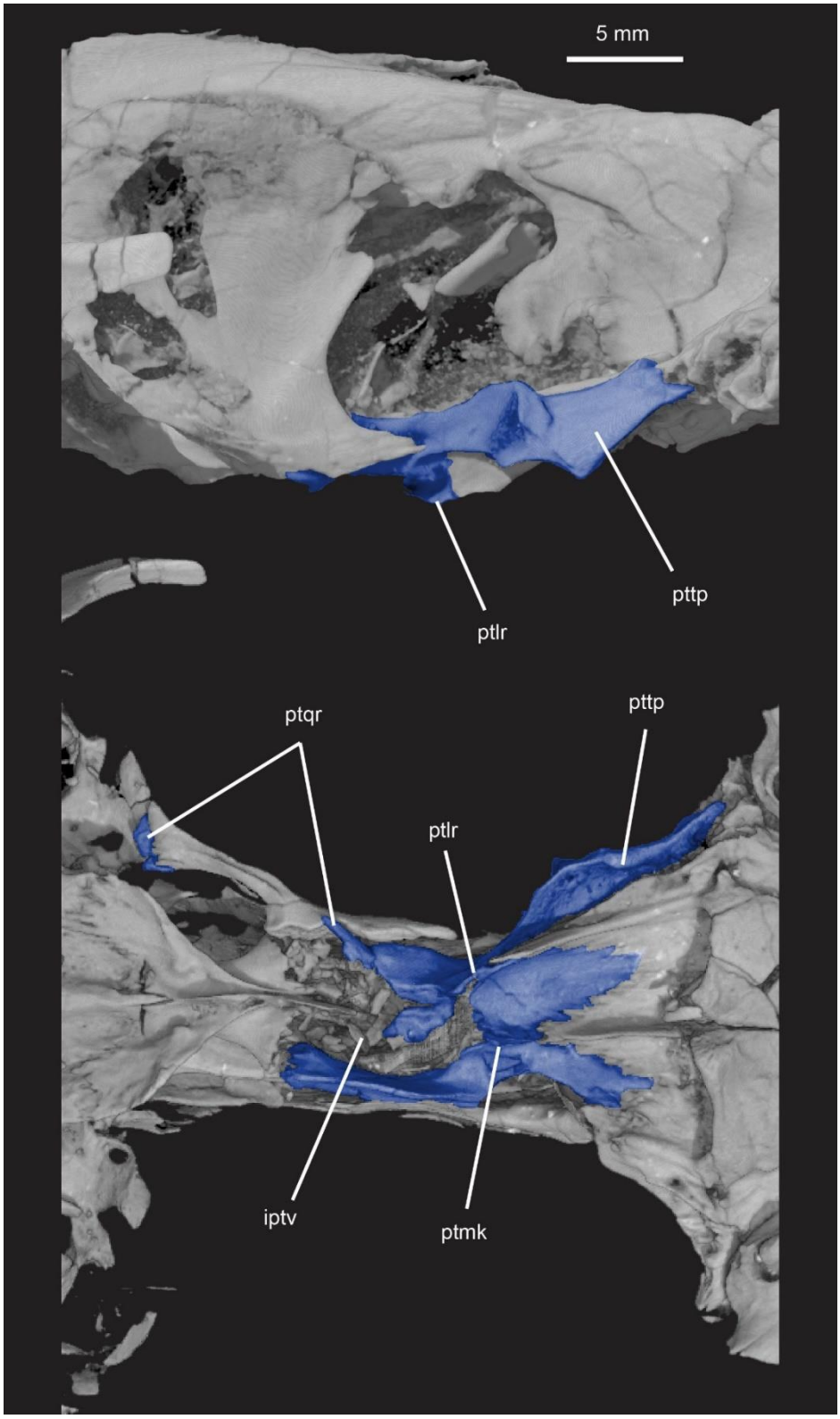

Figure 1.10.

Figure 1.10: *Pseudotherium argentinus*, pterygoid (blue) in right lateral (top) and ventral (bottom) views. Abbreviations: iptv, interpterygoid vacuity; ptlr, pterygoid lateral ridge; ptmk, pterygoid median keel; ptqr, quadrate ramus of pterygoid; pttp, pterygoid transverse process.

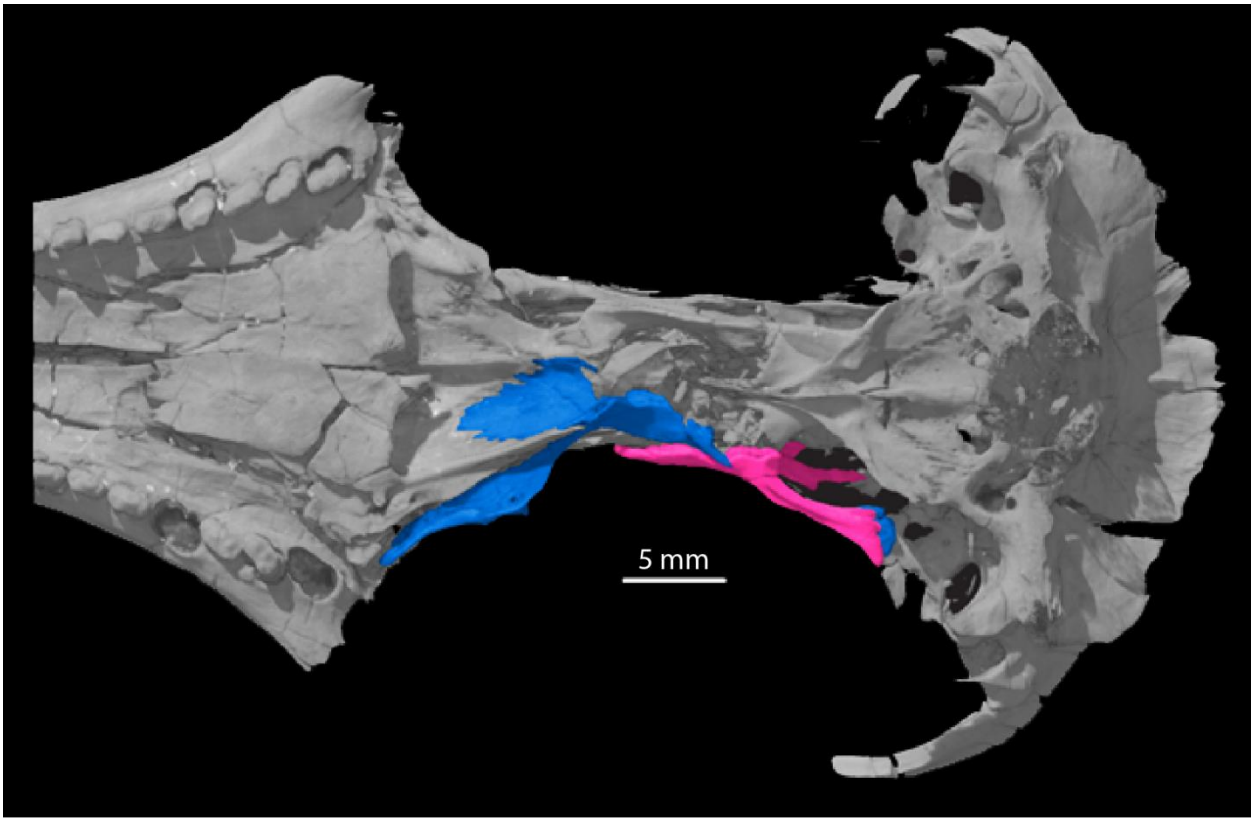

Figure 1.11: *Pseudotherium argentinus,* ventral view of skull showing quadrate processes of right alisphenoid (pink) and right pterygoid (blue). The quadrate process of the pterygoid is broken at its base but its terminal end is preserved at the distal end of the quadrate process of the alisphenoid.

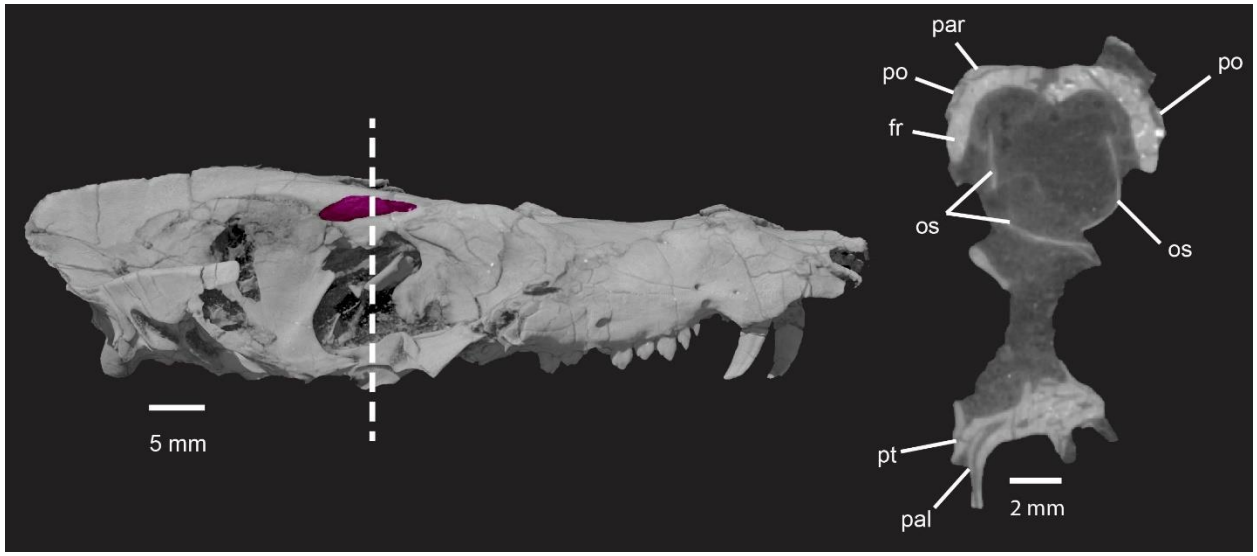

Figure 1.12: *Pseudotherium argentinus*, right lateral view of skull showing the postorbital in *Pseudotherium*. (Left) Right postorbital highlighted in magenta. (Right) Cross section through orbital region illustrating how a sliver of frontal is wedged between dorsal parietal sand ventral postorbitals. Dotted line indicates position of cross sectional slice. Abbreviations: fr, frontal; par, parietal; po, postorbital.

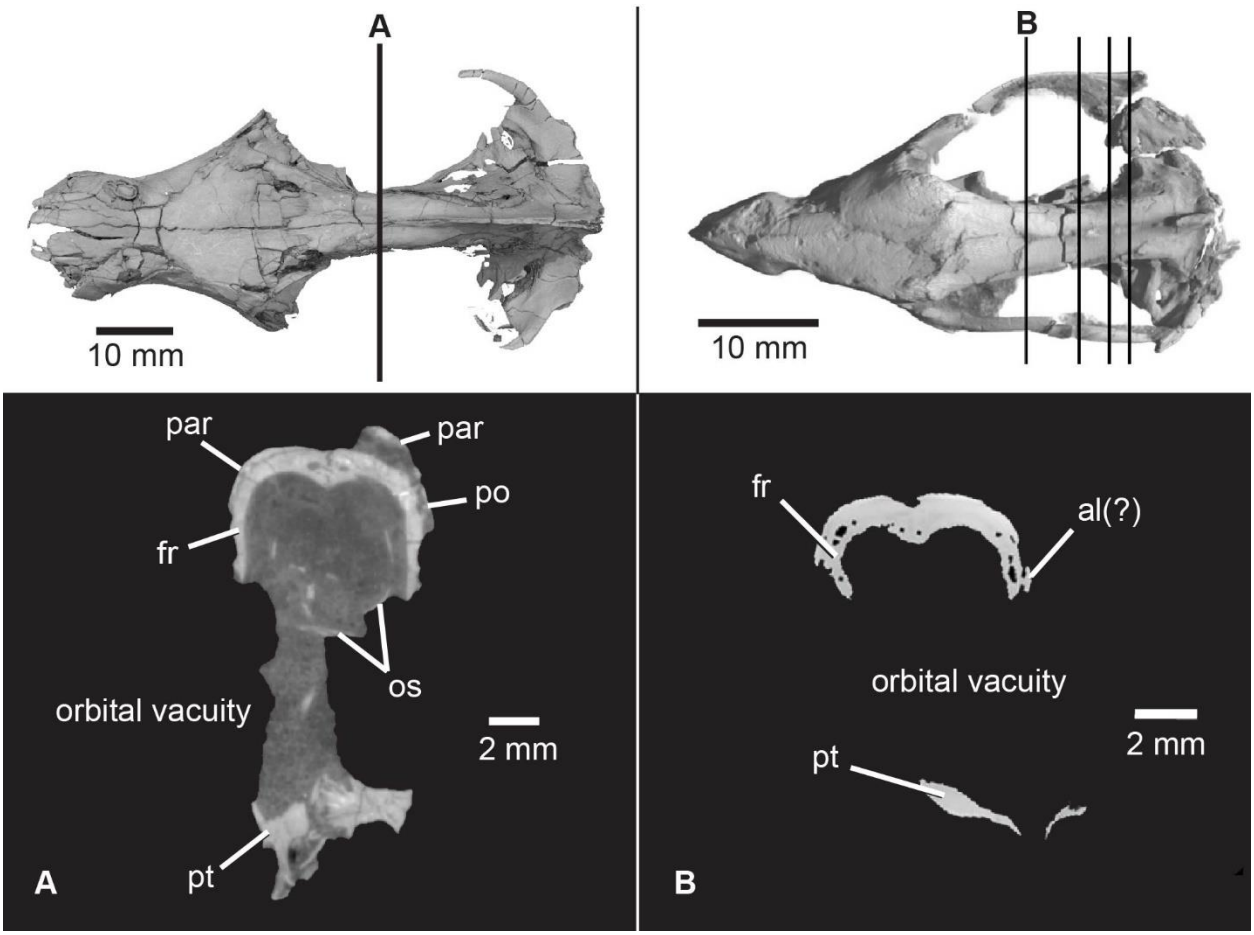

Figure 1.13: Comparison of orbital vacuities in *Pseudotherium* and *Brasilitherium riograndensis*. The ventral limit of the endocranium in *Pseudotherium* (A) is dorsal to the orbital vacuity and lined by ossified orbitosphenoids. The orbitosphenoids are missing in *Brasilitherium* (B) but were likely present, suggesting a shallower endocast than previously hypothesized. *Brasilitherium riograndensis* CT images from Rodrigues et al., (2014: fig. 3). Abbreviations: al, alisphenoid; fr, frontal; os, orbitosphenoid; par, parietal; po, postorbital; pt, pterygoid.

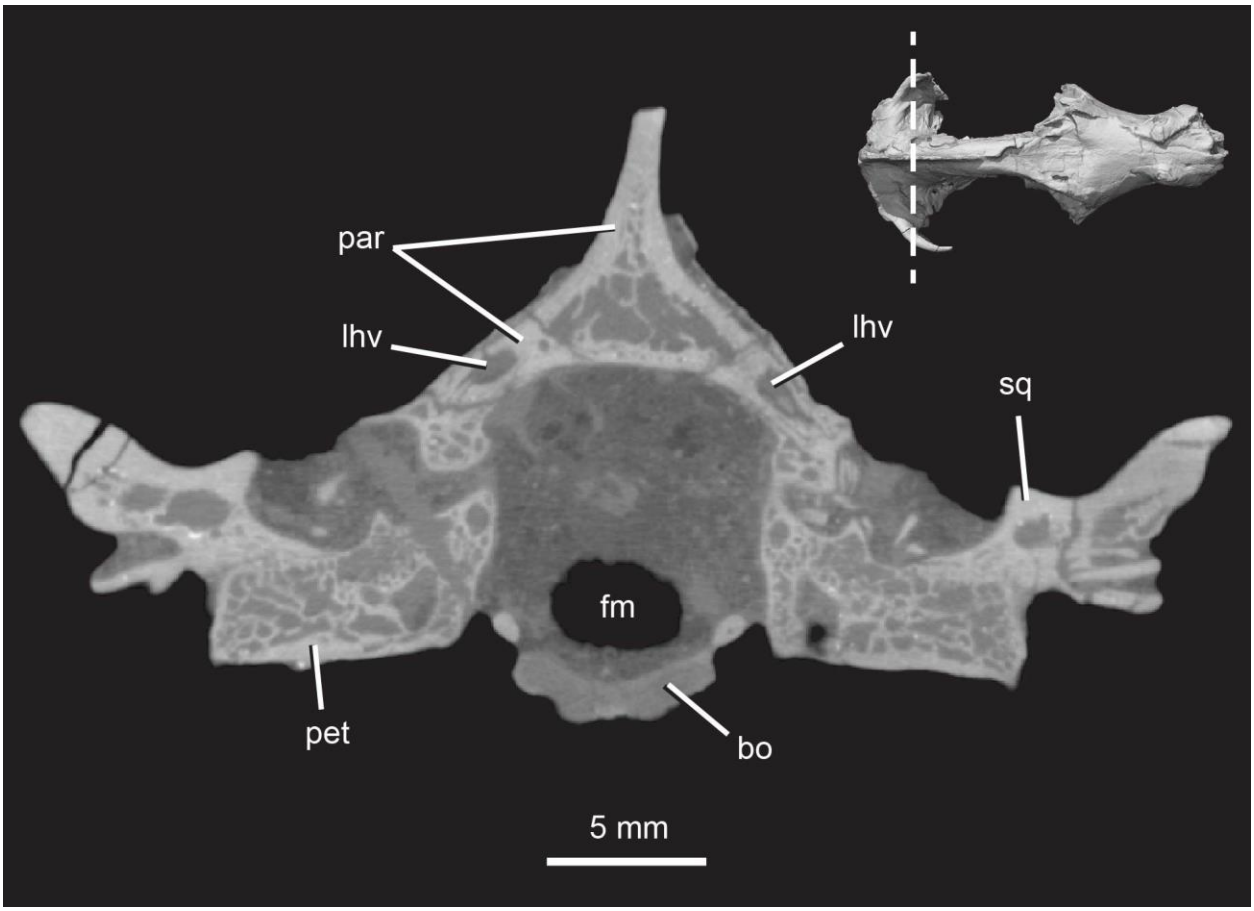

Figure 1.14: *Pseudotherium argentinus,* CT cross section through the back of the skull of the skull. Note the extensive hollow spaces in the parietal, petrosal, and squamosal. Abbreviations: bo, basioccipital; fm, foramen magnum; lhv, lateral head vein; par, parietal; pet, petrosal; sq, squamosal.

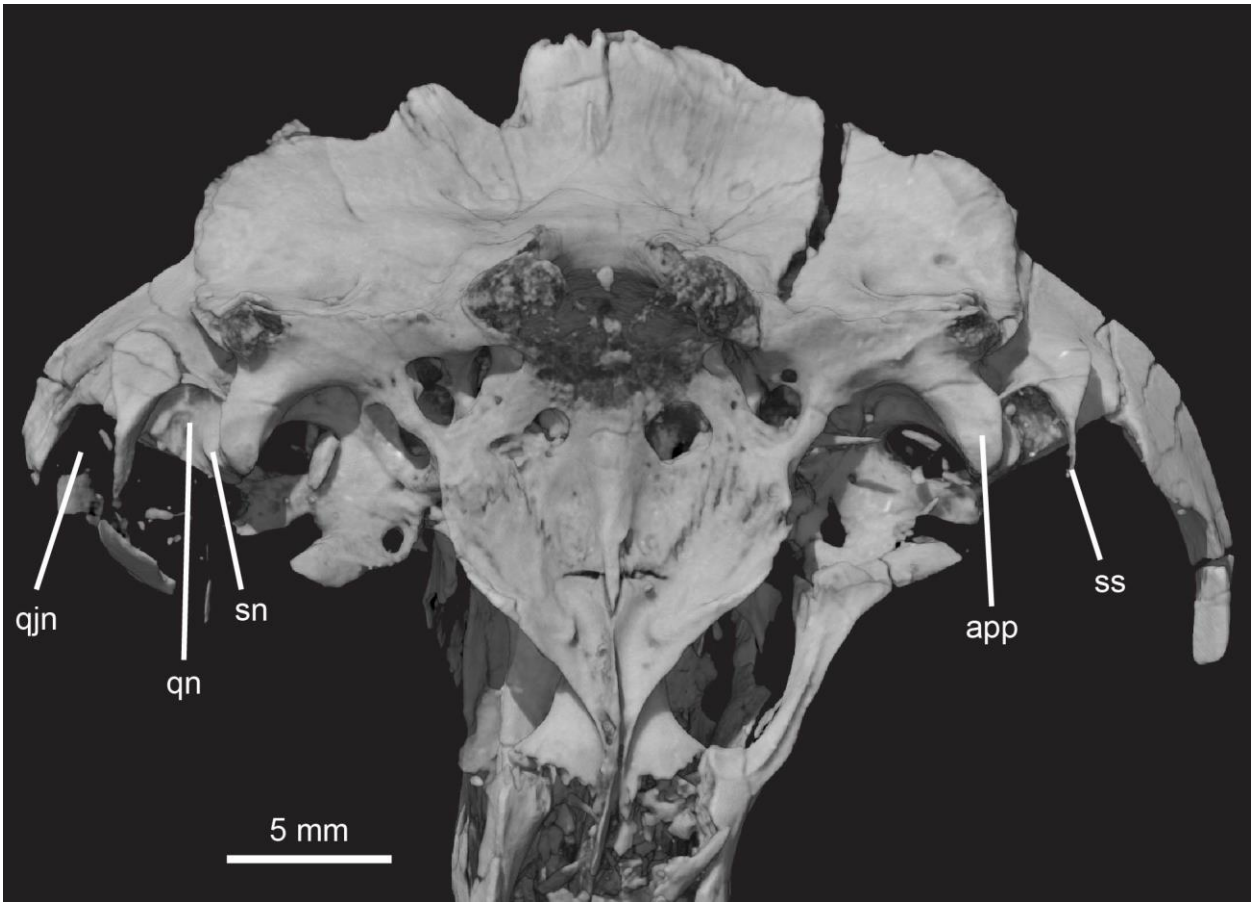

Figure 1.15: *Pseudotherium argentinus*, ventral view showing notches in temporal process of squamosal. The quadrate notch (medial) and the quadratojugal notch (lateral) are divided by a hook-shaped squamosal septum. A squamosal notch is present within the quadratojugal notch and abuts the anterior process of the bifurcated paroccipital process. The squamosal notch does not completely cover the lateral face of the anterior paroccipital process. Abbreviations: app, anterior paroccipital process; qn, quadratojugal notch; qjn, quadratojugal notch; sn, squamosal notch; ss, squamosal septum.

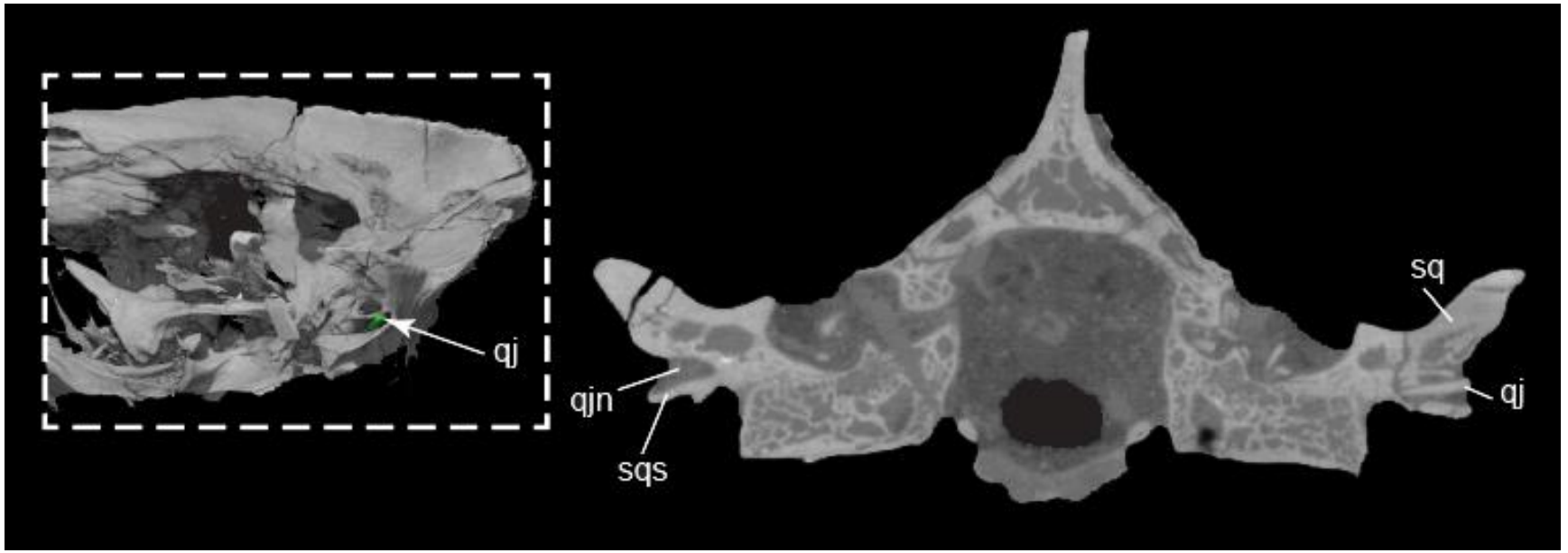

Fig. 1.16. *Pseudotherium argentinus*, the quadratojugal. (Left) Fragment of right quadratojugal (qj), green, in quadratojugal notch. (Right) Cross section through back of skull illustrating the quadratojugal inserted into quadratojugal notch in the squamosal flange. Abbreviations: qj, quadratojugal; qjn, quadratojugal notch; sq, squamosal; sqs, squamosal septum.

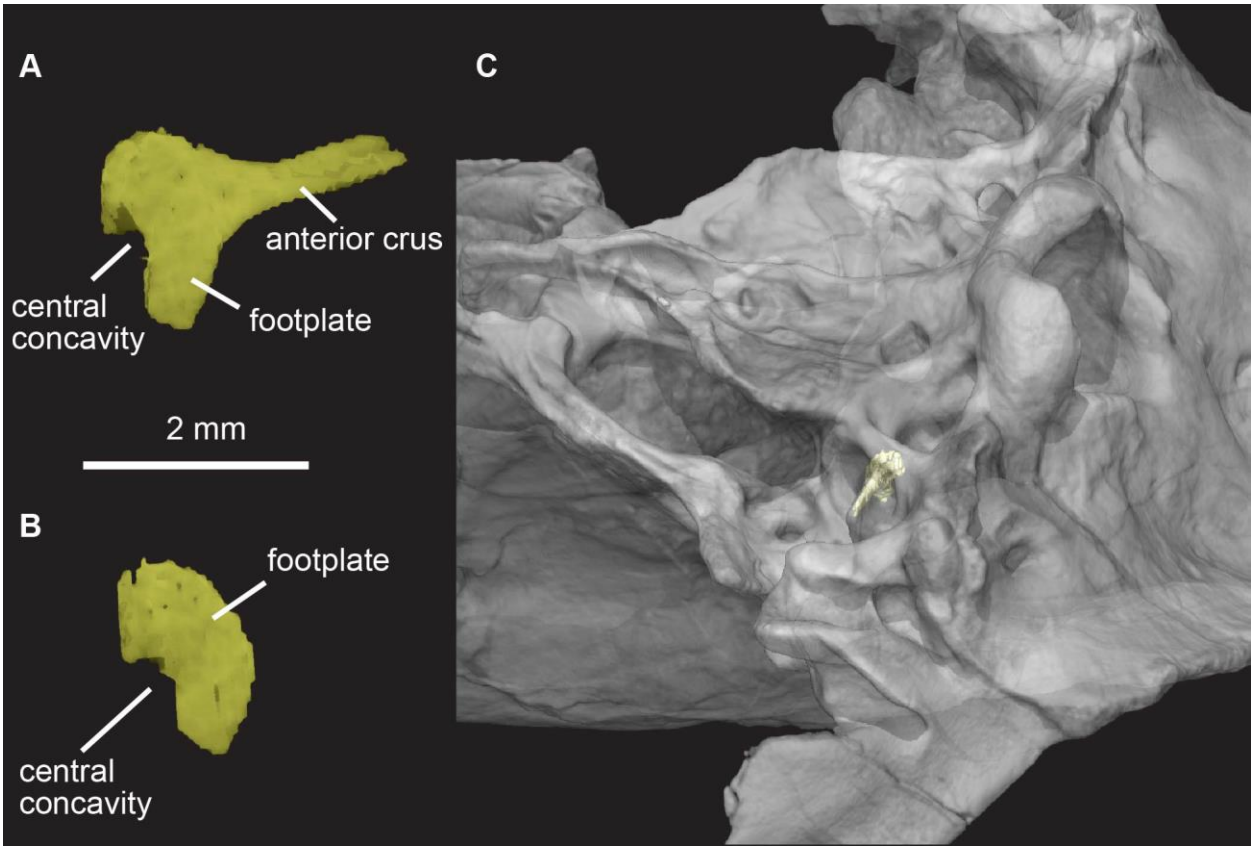

Figure 1.17: *Pseudotherium argentinus*, incomplete right stapes of *Pseudotherium*. (A) Anteromedial view of stapes, (B) medial view of footplate of stapes, and (C) semitransparent isosurface render of stapes in situ and skull in oblique-ventral view.

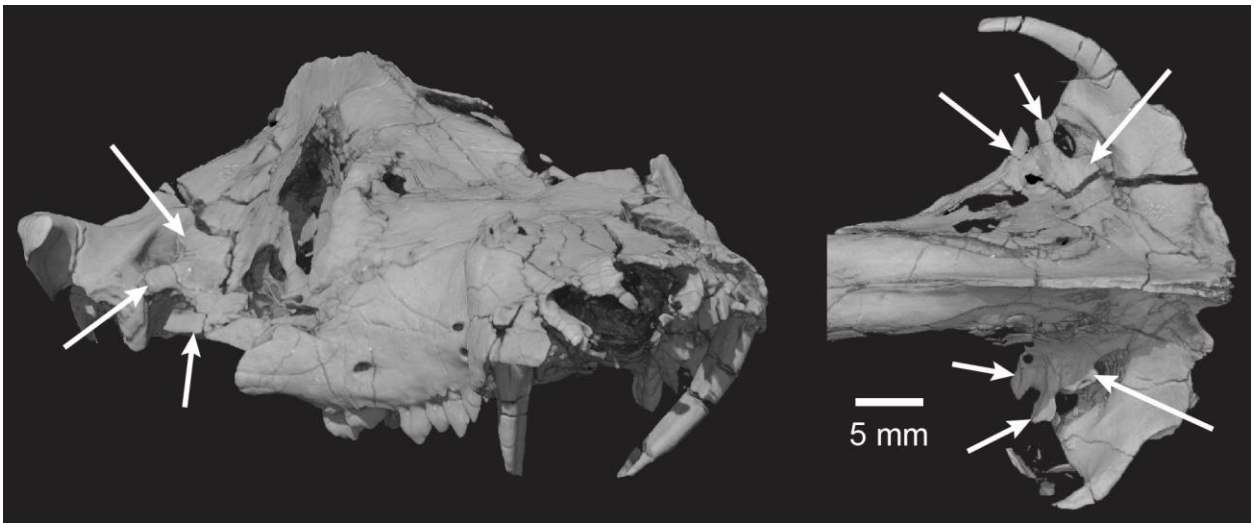

Figure 1.18: *Pseudotherium argentinus*, lateral flange of the petrosal right anterolateral (left) and dorsal (right) views. The lateral flange (indicated with arrows) is broad and has a slightly vertical slant. The lateral margin of the lateral flange bears a notch which may be apomorphic of *Pseudotherium argentinus*.

Figure 1.19: *Pseudotherium argentinus* skull in posterodorsal view illustrating open pterygoparoccipital foramina (indicated by arrows). Each pterygoparoccipital foramen is almost entirely enclosed by the lateral flange of the petrosal (periotic) anteriorly and the squamosal posteriorly. The lateral flange and the squamosal do not contact, so that pterygoparoccipital foramen is laterall open. Because each foramen is open to a similar extent, this is not likely to be an artifact of post-mortem deformation.

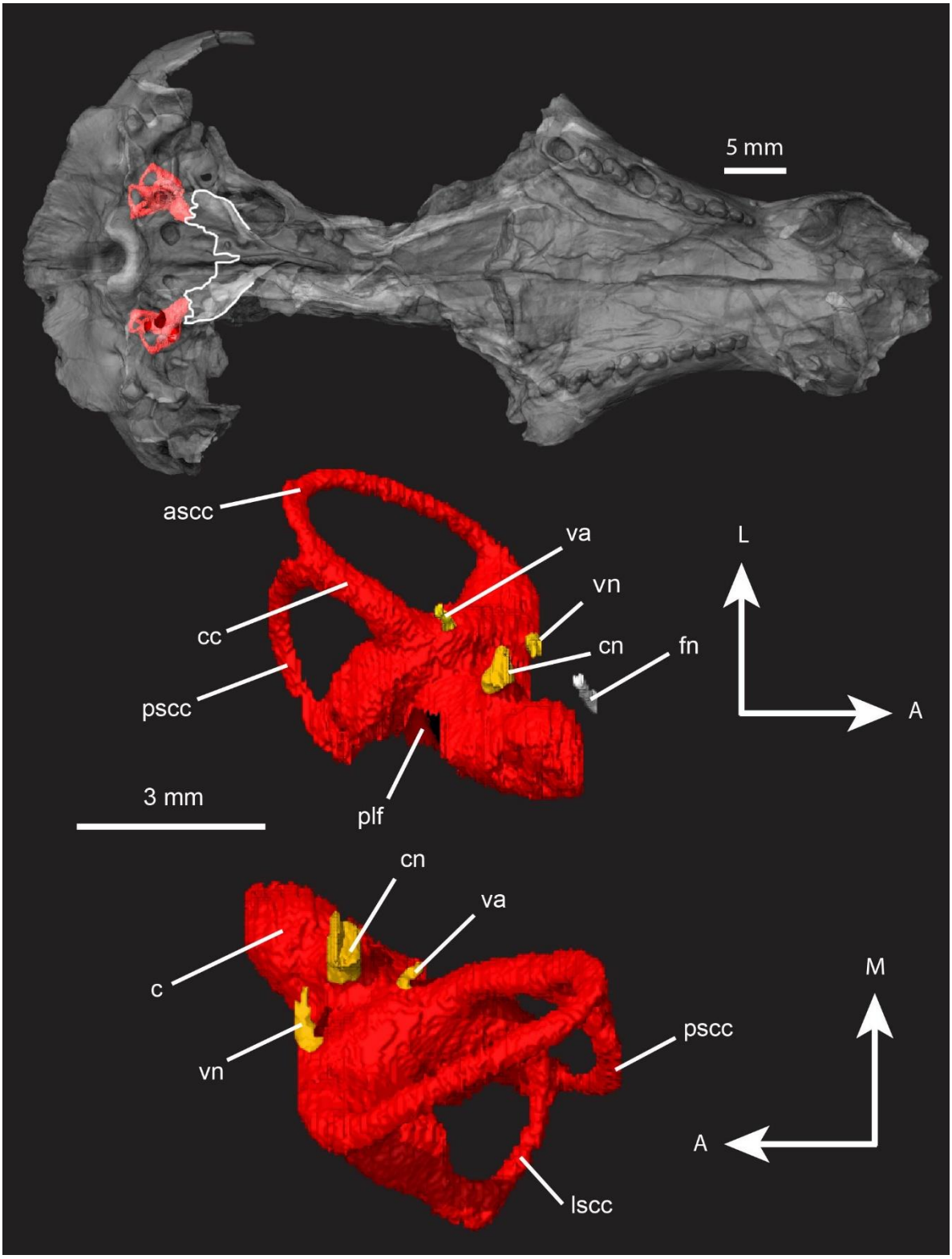

Figure 1.20.

Figure 1.20: *Pseudotherium argentinus*, inner ear volume. (Top) Ventral view of inner ear endocranial space in situ with a semitransparent isosurface model of skull. White tracings outline the parasphenoid alae and posterior border of basisphenoid. (Middle) Left inner ear volume in dorsal view. (Bottom) Left inner ear volume in ventral view. Abbreviations: ascc, anterior semicircular canal; c, cochlea; cc, common crus; cn, cochlear nerve (VIII); fn, facial nerve (VII); lscc, lateral semicircular canal; plf, perilymphatic foramen; pscc, posterior semicircular canal; va, vestibular aqueduct; vn, vestibular nerve (VIII). Arrow legend key: A = anterior, L = lateral, M = medial.

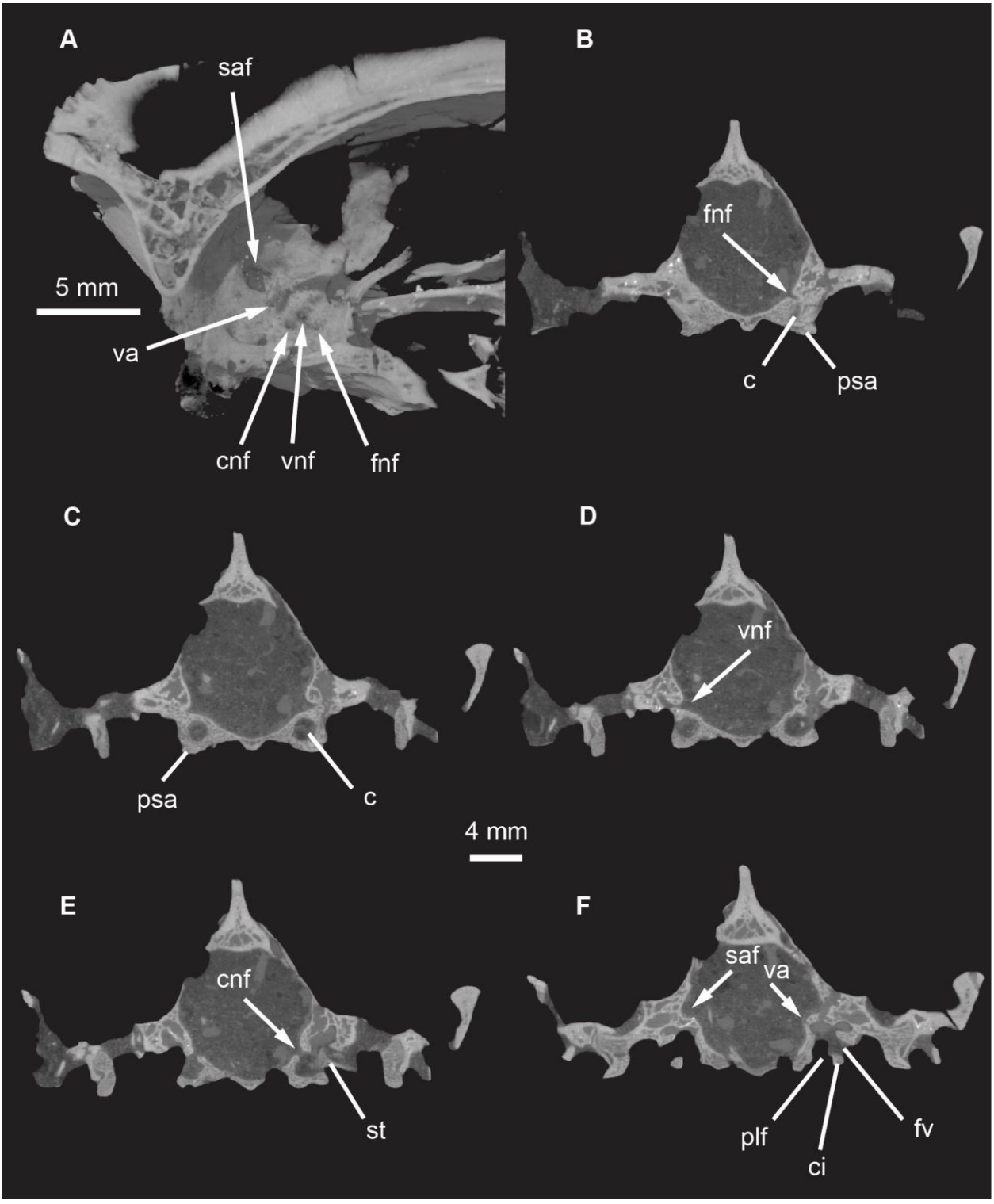
A
saf
5 mm
va
cnf
vnf
fnf
B
fnf
c
psa
C
psa
c
D
vnf
4 mm
E
cnf
st
F
saf
va
plf
ci
fv

Figure 1.21.

Figure 1.21: *Pseudotherium argentinus*, petrosal (periotic) in medial and cross sectional views. (A) Dynamic cutaway illustrating medial aspect of petrosal and its associated foramina and fossa. (B) Cross section through facial nerve foramen. (C) Cross section through vestibular nerve foramen. (D) Cross section through cochlear nerve entrance. (E) Cross section through vestibular aqueduct and subarcuate fossa. Abbreviations: c, cochlea; ci, crista interfenestralis; cnf, foramen for cochlear nerve; fnf, foramen for facial nerve; fv, foramen vestibuli; plf, parilymphatic foramen; psa, parasphenoid ala; saf, subarcuate fossa; st, stapes; va, vestibular aqueduct; vnf, foramen for vestibular nerve.

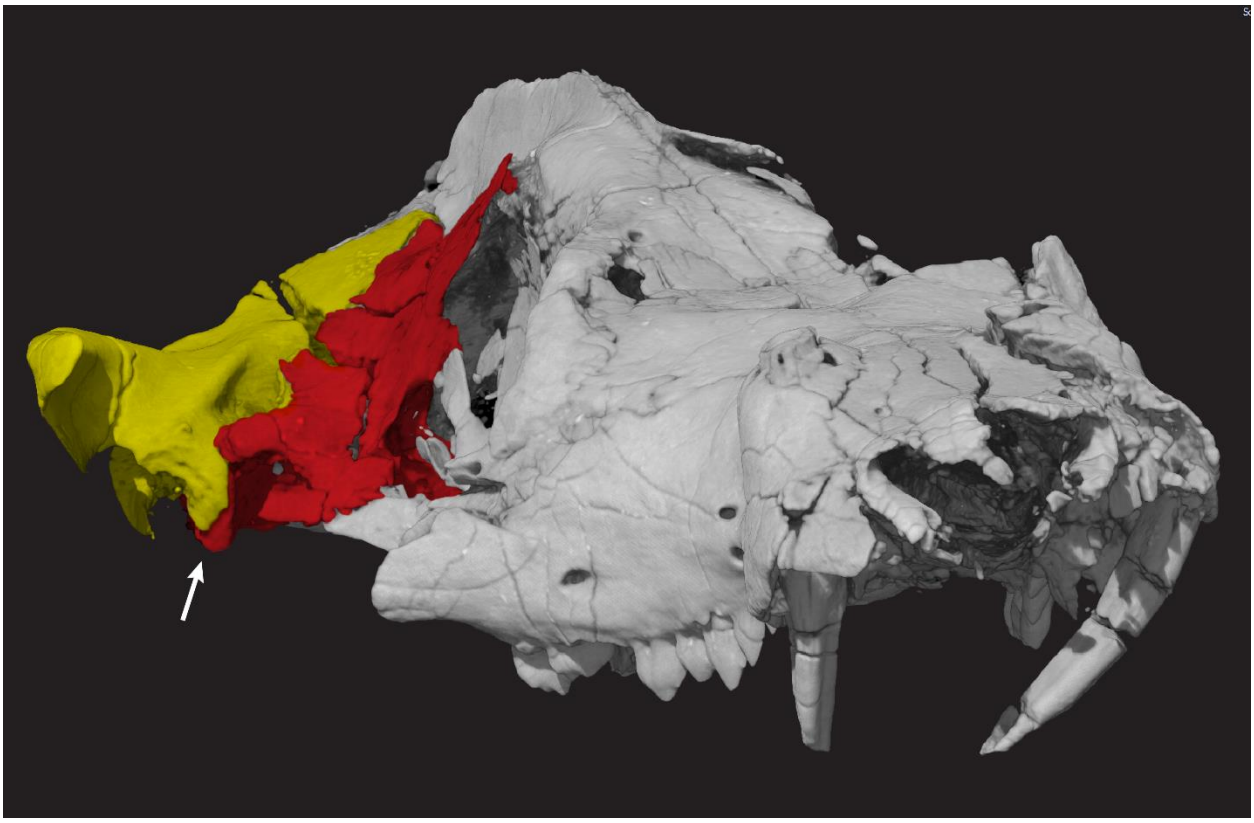

Figure 1.22: *Pseudotherium argentinus* in anterolateral view illustrating dorsal recession of squamosal to expose the lateral surface of the anterior paroccipital process (indicated by arrow). The quadrate notch is lateral to the anterior paroccipital process and would have hoursed the quadrate. Petrosal is colored red. Squamosal is colored yellow.

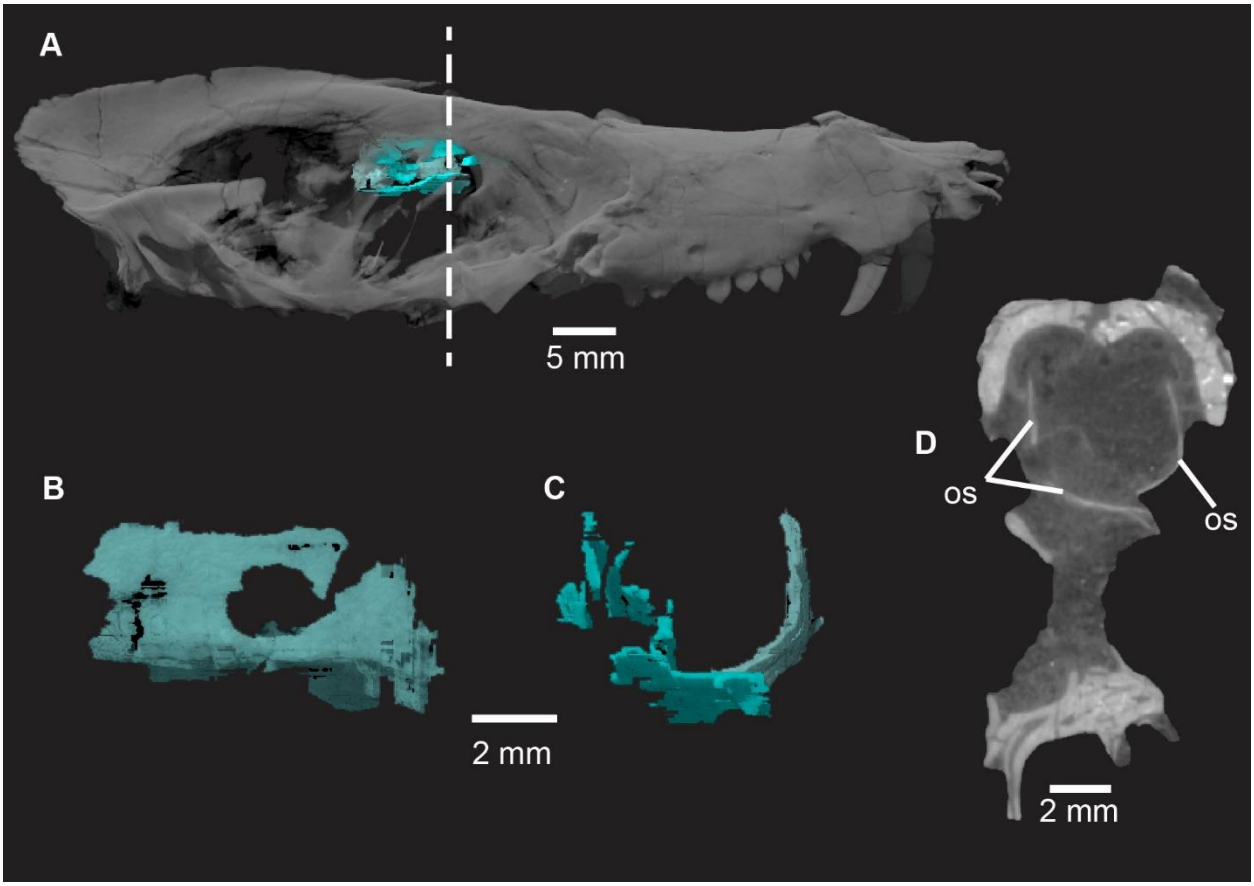

Figure 1.23: *Pseudotherium argentinus*, orbitosphenoid (os) in situ (A), left lateral view (B), anterior view (C), and cross section (D). Left and right orbitosphenoids contact ventrally at midline. Left orbitosphenoid is less fractured than right orbitosphoid and shows distinct optic foramen. Cranium rendered semitransparent to illustrate relationship of orbitosphenoid to sphenorbital fissure and surrounding bony elements. Cross section illustrates the relatively dorsal position of the brain within the cranium.

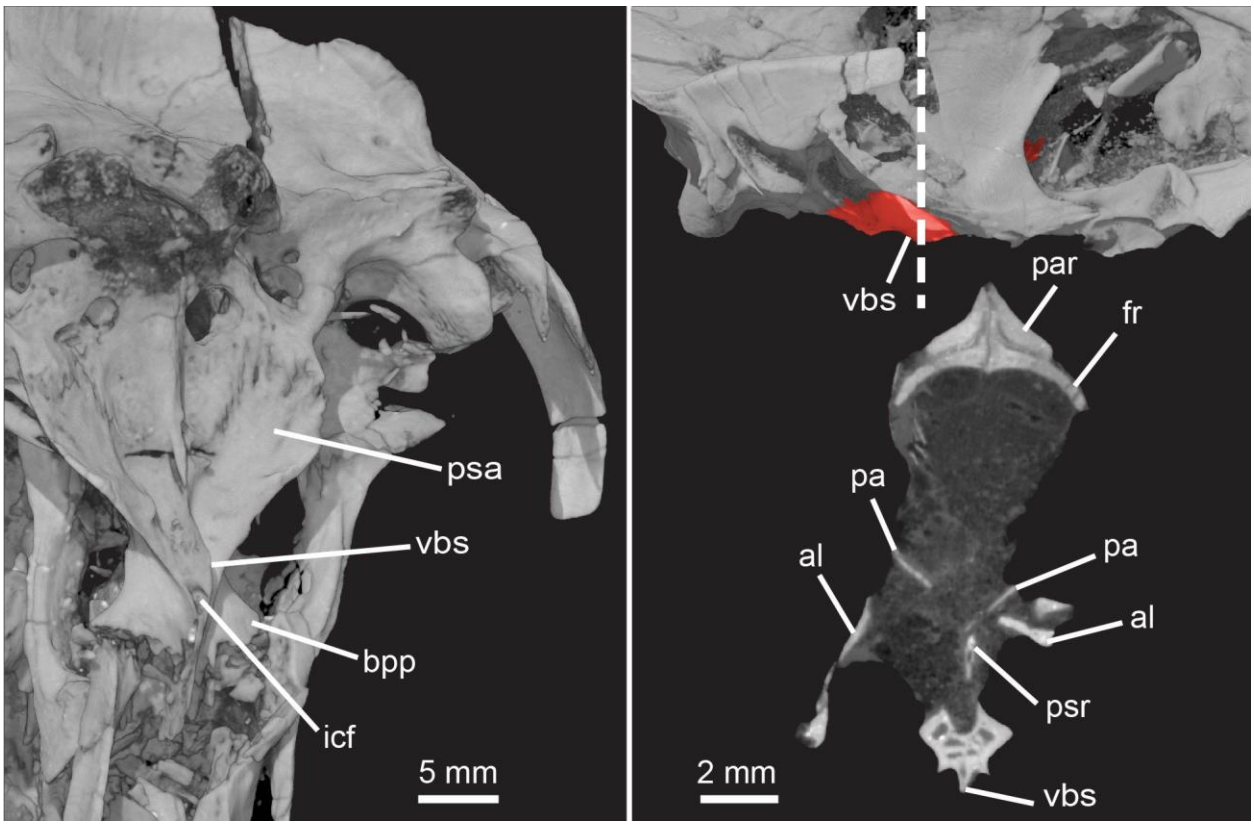

Figure 1.24: *Pseudotherium argentinus*, ventromedial crest of basisphenoid. (Left) Ventromedial crest of basisphenoid in left ventrolateral view. (Top right) Parabasisphenoid complex in left lateral view, colored red-orange, and (bottom right) ventral crest of basisphenoid (vbs) in cross section. Dashed line indicates position of cross section. Abbreviations: al, alisphenoid; bpp, basipterygoid process; fr, frontal; icf, internal carotid foramen; os, orbitosphenoid; pa, pila antotica; par, parietal; psa, parasphenoid ala; psr, parasphenoid rostrum; vbs, ventral process of basisphenoid.

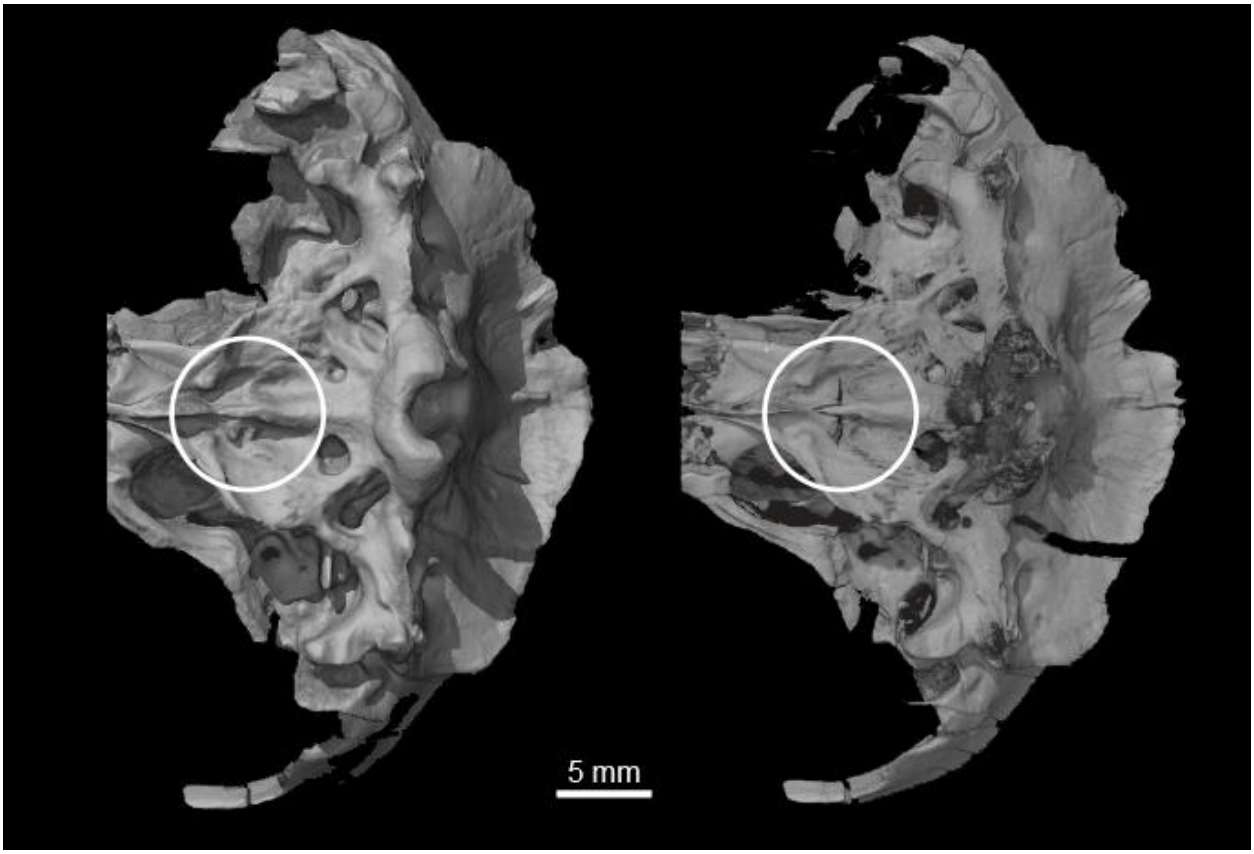

Figure 1.25: *Pseudotherium argentinus*, suture between basioccipital and basisphenoid. Suture between basioccipital and basisphenoid is indicated by the circle. The suture is distinct, marked by a wide gap and flaring articulating surfaces on both elements. An anterior process of the basioccipital overlaps the basisphenoid posteroventrally and medially. Note how different the suture looks in an isosurface model with matrix included in the rendering (left) and a digitally prepared volume render (right).

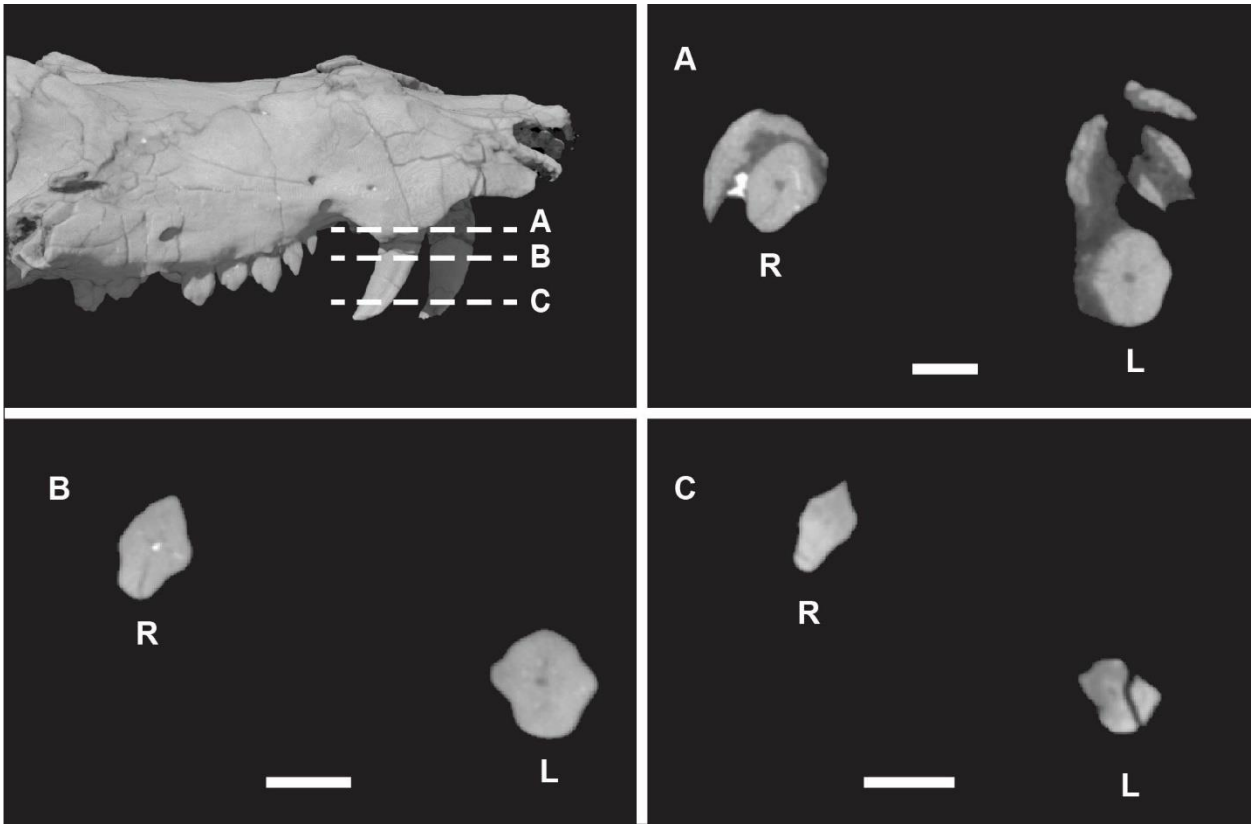

Figure 1.26: *Pseudotherium argentinus*, cross sections through canines. (A) right side of snout showing location of cross sections (B), (C), and (D). R = right, L = left. Arrows indicate labial and lingual ridges, an autapomorphy of *Pseudotherium*.

Figure 1.27.

Figure 1.27: *Pseudotherium argentinus*, left postcanine tooth row. (A) Left row in volume render. There are nine postcanines which increase in complexity from anterior to posterior, with the first postcanine being a single cusp and the penultimate postcanine having the most distinct cusps. Despite this trend, the postcanine cusps are small and blunt relative to postcanine cusps seen in other cynodonts. More posterior crowns (PC6-9) are mesiolingually in-turned. (B) Horizontal section through the snout of PVSJ 882 illustrating constricted roots with a figure-eight cross section. The pulp cavity is compressed but never completely divided between root lobes. Nutrient canals that run through each lobe of the root.

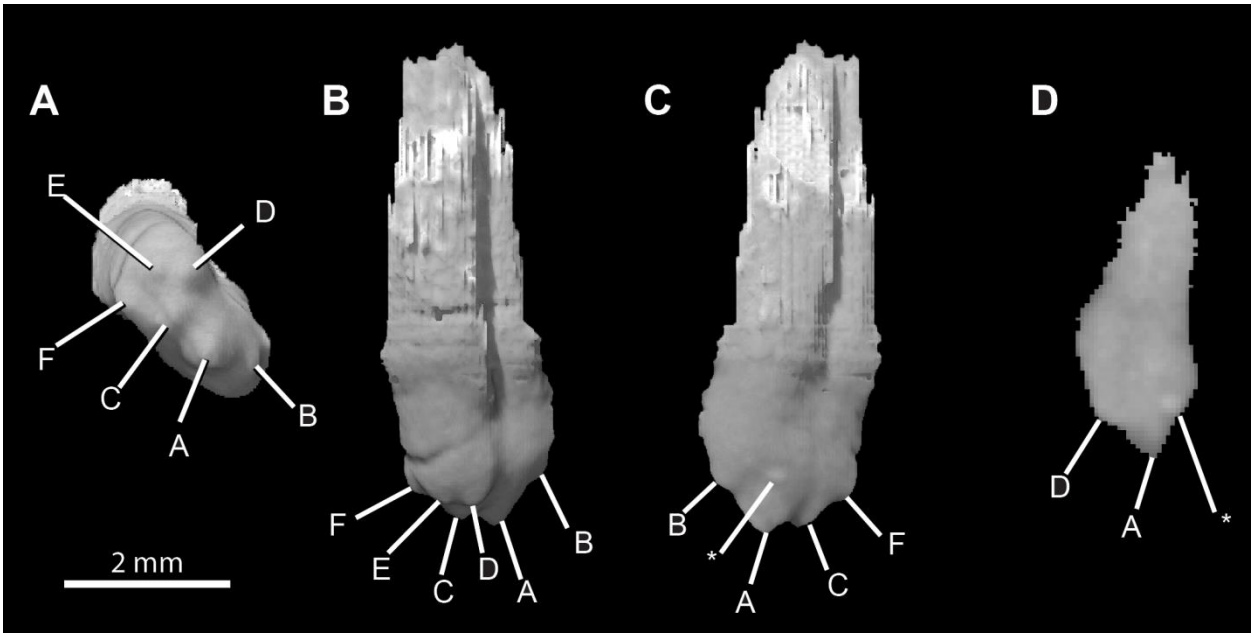

Figure 1.28: *Pseudotherium argentinus*, isolated right postcanine, PC8. (A) Occlusal, (B) buccal, (C) lingual, and (D) cross sectional views. The eighth postcanine on the right side of the skull best illustrates the cusp pattern of the distal postcanines. Three main cusps are in alignment with the longitudinal axis of the crown (A, B, C). Three accessory cusps surround the most-distal main cusp buccally (D), distally (E), and lingually (F). A small bump appears on the surface of the crown in the volume rendering (*). Cross sections confirm that it is not a cusp, but an artifact from denser material.

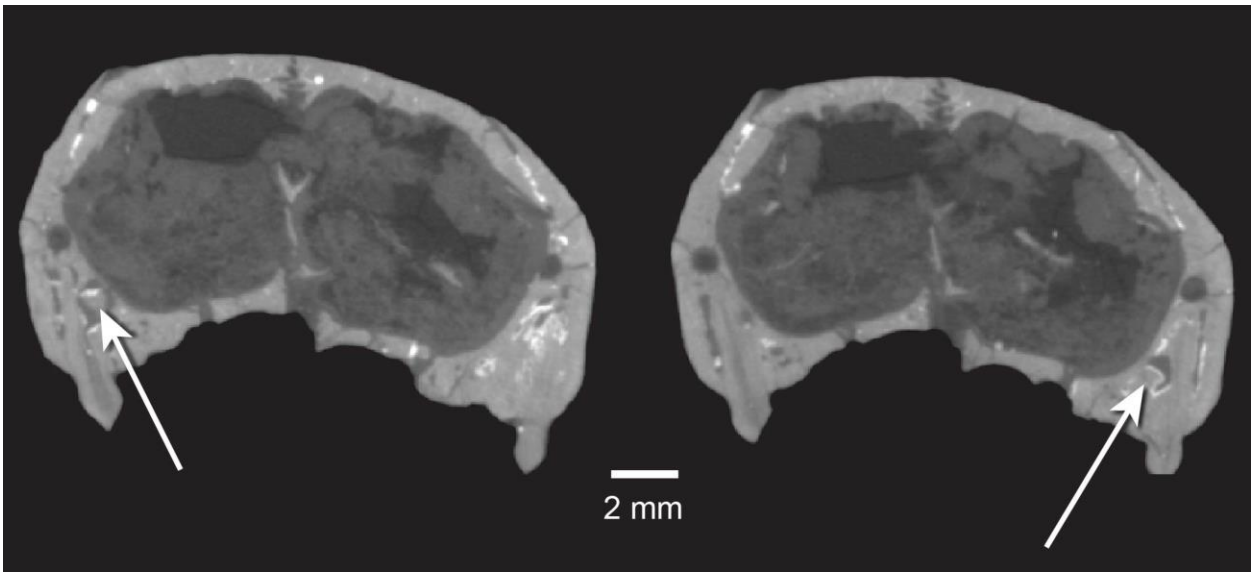

Figure 1.29: *Pseudotherium argentinus*, tooth replacement. Cross sections through left (left) and right (right) upper fourth postcanines (PC4) illustrating possible replacement teeth, indicated by arrows. Apparent replacement crowns are positioned near the distal margin and apex of the P4 roots.

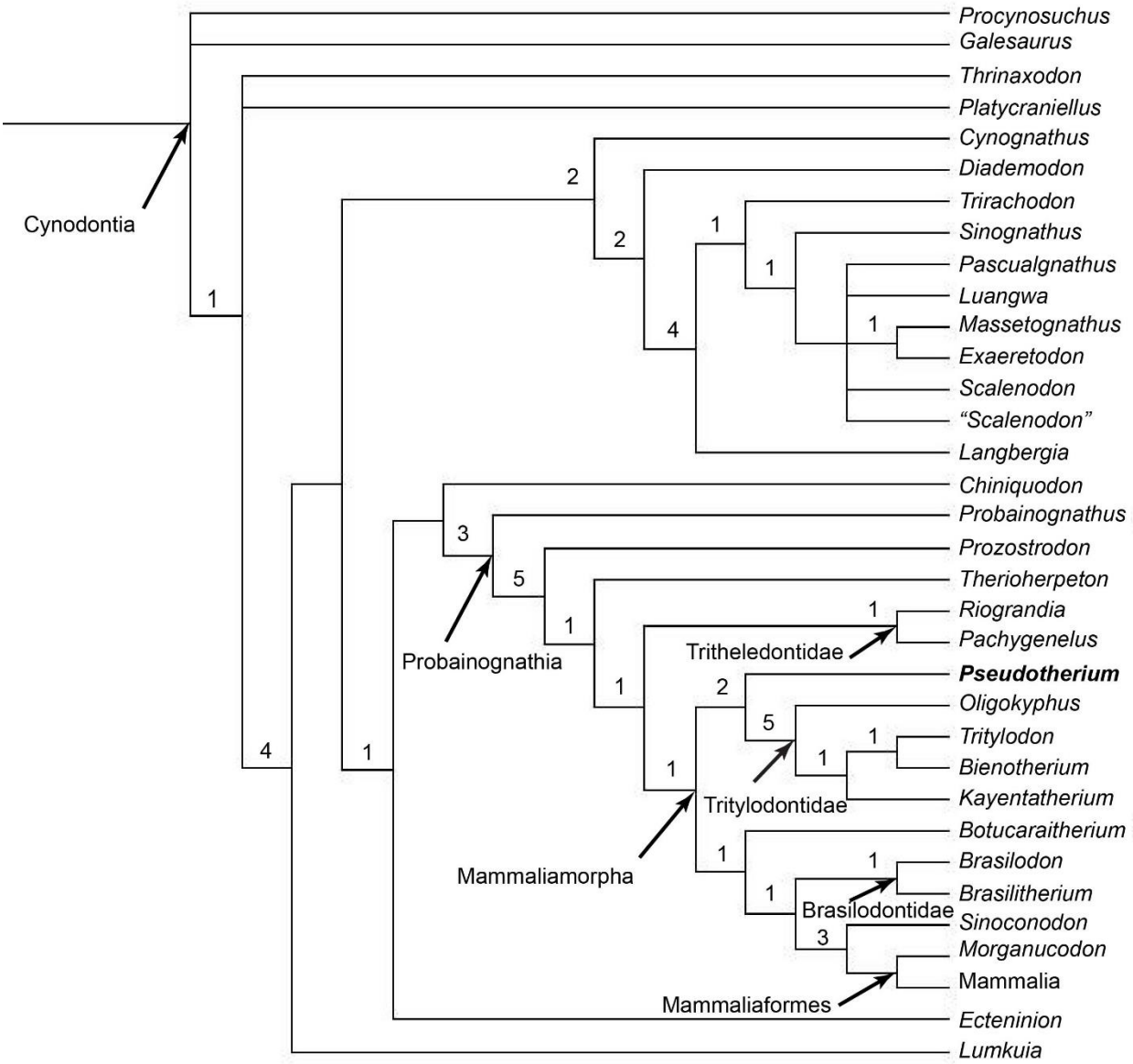

Figure 1.30: Strict consensus tree. Strict consensus tree of all eight most parsimonious trees (tree length = 443, CI = 0.4695, RI = 0.7814) obtained using PAUP*4.0b10. Characters are unordered. The number to the left of the node is the decay index of that clade.

Chapter 2: The Endocranial Cavity of *Pseudotherium argentinus* (Cynodontia, Mammaliamorpha), and Early Evolution of the Mammalian Brain[2]

INTRODUCTION

It is well known that mammals have the largest brains of any vertebrate, proportional to body size, and that increases in brain size occurred independently in several mammalian clades, most notably artiodactyls (or cetartiodactyls), proboscideans, and primates (Jerison, 1973; Nieuwenhuys et al., 1998). However, evolutionary increases in relative brain size, or 'encephalization,' are not unique to mammals, characterizing the history of many vertebrate clades (Striedter, 2005). Moreover, birds, certain non-avian reptiles, and chondrichthyans (skates and rays) have brain/body-mass ratios which overlap with the range measured in living mammals (summarized in van Dongen, 1998). Identifying which neural features besides size are unique to mammals, and understanding the timing and sequence of their evolution during early pan-mammalian history have been important research questions for several generations (summarized by Edinger, 1975; Jerison, 1973; Balanoff and Bever, 2017).

In pursuing these questions, we follow the nomenclatural recommendations based on the Phylocode that are discussed at length elsewhere (Gauthier et al., 1988; Rowe, 1988; Rowe and Gauthier, 1992; de Queiroz and Gauthier, 1992; de Queiroz, 1994; Cantino and de Queiroz, 2000). The name Mammalia refers to the crown clade (Rowe, 1988, in press A). The name Mammaliaformes (Rowe, 1988) refers to the clade stemming from the last common ancestor shared by Mammalia and *Morganucodon oehleri* (Rowe, in press B; Fig. 2.1), while the name Mammaliamorpha (Rowe, 1988) refers to a slightly more inclusive clade stemming from the last common ancestor shared by Mammalia and *Tritylodon longaevus* (Rowe, 1988, in press C; Fig. 2.1). The name Probainognathia has been construed in various ways, but is used here to refer to the clade stemming from the last common ancestor of Mammalia and *Probainognathus jenseni* (Romer, 1970; Fig. 2.1). The name Cynodontia (Rowe, in press D) refers to an even more inclusive clade stemming from the last common ancestor mammals share with the Permian *Procynosuchus delaharpeae* (Broom, 1937). The name Therapsida refers to a still more inclusive

[2] Authors: R. Wallace and T.B. Rowe. R. Wallace wrote the paper and made all figures. T.B. Rowe provided additional background.

clade stemming from the last common ancestor mammals share with the extinct Permian Biarmosuchia (Rowe, in press E), and Pan-Mammalia is used in reference to the total clade (Rowe, in press F).

Here our focus is on the endocranial space and endocast in the recently discovered Late Triassic *Pseudotherium argentinus* (Wallace et al., in prep), an extinct probainognathian cynodont that lies close to the origin of Mammaliamorpha. Phylogenetic analysis unequivocally found *Pseudotherium* to be nested within Probainognathia, but it is uncertain whether it lies just within, or just outside of Mammaliamorpha.

The endocast of *Pseudotherium* not only provides new information on brain evolution in probainoganthians, but also documents events surrounding the origin of Mammaliamorpha. This provides added context for interpreting the marked increases in encephalization documented using micro-computed tomography (μCT) in the early mammaliaform fossils *Morganucodon* and *Hadrocodium* (Rowe et al., 2011). Increases in encephalization are typically evaluated as an encephalization quotient (EQ), or the ratio of the measured endocranial volume to the endocranial volume expected for body size (Jerison, 1973). Compared to early cynodonts, a first pulse in encephalization was recognized in the Early Jurassic *Morganucodon*, in which endocranial volume increased 50% compared to more basal cynodonts such as *Probainognathus* and *Thrinaxodon*. A second encephalization pulse was described in the Early Jurassic mammaliaform *Hadrocodium*, whose EQ for the first time falls within the range measured for living mammals (Rowe et al., 2011). Once relative brain size reached that level, independent increases in encephalization occurred within numerous mammalian clades (Jerison, 1973; Macrini, 2006; Rowe et al., 2011).

These early pulses in encephalization are foreshadowed by two stem-mammaliaforms from the Late Triassic, *Adelobasileus cromptoni* (Lucas and Luo, 1993) and *Sinoconodon rigneyi* (Patterson and Olson, 1961) in which the cranial vaults are obviously expanded around enlarged brains that compare favorably with *Morganucodon* (Luo et al., 2001). Unfortunately, CT datasets are not available for their skulls, prohibiting comparison here.

Thanks to new fossil discoveries and to enhanced resolving power of μCT, it has been possible to extend Quiroga's (1984) observations on endocranial spaces in *Probainognathus* (Rowe and Wallace, in prep) and several basal mammaliamorphs that were not available to the

earlier study by Rowe et al. (2011). A study by Rodrigues et al. (2014) described a digital endocast of *Brasilitherium riograndensis*, a taxon that is closely related to *Pseudotherium* (Wallace et al., in prep). *Brasilitherium* reportedly preserves evidence of small ossifications in the nasal capsule that may represent ossified turbinals, and similar elements are visible in scans of *Pseudotherium*. A subsequent study on the endocast of the tritheledontid *Riograndia guaibensis* (Rodrigues et al., 2018) describes a digital endocast of a taxon that probably lies just outside of Mammaliamorpha. Additionally, Benoit et al., (2017) CT-scanned a number of non-mammaliaform therapsids including several basal cynodonts to provide a much broader context for understanding brain evolution in stem-mammals. This work augments a substantial body of publications on brain evolution in stem-mammals using natural endocasts and endocasts reconstructed from mechanical serial sections (e.g., Olson, 1944; Quiroga, 1979, 1980a,b, 1984; Hopson, 1979; Kielan-Jaworowska and Lancaster, 2004; Kemp 2009).

Our new data on the endocranial space of *Pseudotherium* suggest that marked changes in endocast shape are detectable in probainognathian cynodonts prior to the conspicuous encephalization events recorded in Mammaliaformes. While these changes in shape and organization are distinct in endocasts, they may not necessarily be associated with measurable changes in encephalization quotient. In light of this unexpected finding, we discuss subjective decisions that must be made to varying degrees in reconstructing the endocasts of stem-mammals, in which the endocranial cavity is not fully enclosed by bone. We also discuss whether encephalization preceding the origin of Mammalia evolved via a steady, gradual increase in size, or instead was characterized by periods of stasis punctuated by relatively rapid episodes of encephalization.

Institutional Abbreviations

PVSJ, Instituto y Museo de Ciencias Naturales, San Juan 5400, Argentina; **TMM**, Vertebrate Paleontology Laboratory of The University of Texas, Austin, Texas, USA; **USNM**, Smithsonian Institutions, United States National Museum of Natural History, Washington, D.C.

MATERIALS

Pseudotherium argentinus (PVSJ 882) is known from an isolated skull that represents a probainognathian. Its precise phylogenetic position is equivocal with other mammaliamorphs (Wallace et al., in prep). The specimen is an almost complete cranium with some post-mortem deformation. It was collected from the early Late Triassic Ischigualasto Formation in Argentina. Measuring 75.84 mm in length, it is over twice as long as its close relative *Brasilitherium* (Wallace et al., in prep). There is marked X-ray contrast between bone and matrix, and μCT scanning produced sharp, clear images of the entire skull and its endocranial space that allowed us to generate a digital endocast of the cranial cavity. The CT data of *Pseudotherium* were compared to CT data of a specimen of *Kayentatherium* (TMM 43067-10) collected from the Gold Spring locality in northern Arizona (Marsh and Rowe, in review), that also showed marked X-ray contrast between bone and matrix. The specimen measures 89.24 mm in length, and it retains replacement teeth, indicating skeletal immaturity at time of death. Breakage compromised our ability to inspect its entire endocranial space, and it was not sufficiently preserved to allow extraction of a digital endocast.

Numerous specimens of the tritylodontid *Kayentatherium wellesi* have been collected from the Early Jurassic Kayenta Formation in Arizona. The first large collection was made in the 1950s, from the type locality on Comb Ridge, near the town of Kayenta, Arizona where the many collected specimens represent a growth series (Lewis et al., 1961; Kermack, 1982). These specimens were relatively undistorted, but were buried in a fine sandstone and calcite cement that proved very difficult to prepare using conventional mechanical tools, and that also show poor X-ray contrast between bone and matrix. One specimen from this locality (USNM 317208) selected for CT scanning was a complete, slightly laterally compressed skull of a skeletally immature individual. It measures 108.76 mm in length, and CT scans show that it retains unerupted replacement teeth. Because of poor contrast between the bone and matrix, only a portion of its endocranial cavity could be clearly interpreted.

METHODS

Challenges of comparing encephalization volume reconstructions in non-mammalian cynodonts

Because soft tissues of the nervous system almost never fossilize, early efforts in using the fossil record to study brain evolution, such as the classic work of Tilly Edinger and Harry Jerison (summarized in Jerison, 1973; Edinger, 1975), were largely limited by the scarcity of natural endocasts. In most cases these studies were further limited by remnants of the preserved skull bones that obscured entire regions of the endocast. Only surfaces that were naturally exposed by erosion were generally available, because most curators were reluctant to allow destructive removal of bone to reveal the full endocast. Manual serial sectioning of fossils was occasionally used to provide details of the complete endocranial anatomy (e.g., Stensio, 1927; Fourie, 1975). However, in the last three decades, computed tomography has become a powerful, efficient, and non-destructive tool for visualizing the endocranial volumes in modern and fossil vertebrates (Rowe et al, 1995, 1997; Carlson et al., 2003), and the comparative basis for understanding brain evolution in vertebrates is growing rapidly.

The emergence of high-resolution CT and μCT has enabled digital extraction of entire endocasts, and advances in software include sophisticated tools for precise measurement of surface areas and volumes. However, comparisons between extinct pan-mammals present tenacious problems because significant regions of the sides and floor of the endocranial space were bounded in life by membranes that did not ossify and are not typically preserved. In general, the oldest and most primitive pan-mammals have the least-ossified braincases, while the braincase became successively more ossified with the origins of Cynodontia and Mammaliaformes, until it was essentially completely ossified with the origin of Mammalia (Rowe, 1988; Rowe et al., 2011). In early mammaliamorphs, broad regions of the lateral wall and floor remained unossified, presenting a source of subjectivity and uncertainty in reconstructing endocasts as well as in comparing them.

Fortunately, several bony landmarks enable an approximation of the limits of the endocranial space. The forebrain rests above the orbitosphenoid anteriorly, and the pila antotica of the prootic posteriorly. However, until the origin of Mammaliaformes the orbitosphenoid and pila antotica did not contact, leaving a gap in the ventrolateral braincase floor that must be

reconstructed. Earlier reports that the orbitosphenoid contacted the pila antotica in tritheledontids and tritylodontids (Crompton, 1958; Sues, 1986) are not supported by our new data (Fig. 2.2), nor by a more recent study by Crompton et al. (2017). Additionally, the cribriform plate beneath the olfactory bulbs did not become ossified until the origin of Mammalia (Rowe, 1988), such that the ventral surface of the olfactory bulbs must also be reconstructed. How one choses to reconstruct these regions of the endocast can be subject to *ad hoc* decisions, and reconstructions are affected by preservation and distortion, which further complicate comparisons between taxa.

An additional difficulty is that in some taxa brain size and EQ have been estimated from partially exposed natural endocasts in non-mammalian cynodonts using different geometric calculations instead of endocast dimensions. For example, using measurements from the superior view of a natural endocast of *Therioherpeton*, the entire volume of the braincase was estimated based on the formulas for the volumes of a cylinder and a truncated cone (Quiroga, 1984a). Others have used graphic double integration to estimate endocast volume (Jerison, 1973). Until these specimens are scanned, more refined estimates of brain size are unavailable. We discuss the implications of these limitations below.

For convenience, we refer to anatomical structures of the endocasts as if they were parts of the brain itself, instead of referring to them as 'casts' of neural regions. We also acknowledge that meninges and blood vessels also occupied some of these regions, and assume that their contribution to endocranial volume is similar in the taxa discussed here.

In general, to close the unossified regions of the endocranial space, we drew straight lines between bony landmarks, and our selections were guided by simultaneous observation of all three orthogonal slice planes made possible by volumetric imaging software (below).

Computed tomography

All specimens used in this analysis were scanned at The University of Texas at Austin High-Resolution X-ray Computed Tomography Facility (UTCT). *Pseudotherium* was scanned with the high-resolution Xradia scanner at 110 kV and 10 W. A 1-mm CaF_2 filter was used. A total of 1,733 slices were generated with voxel dimension of 44.21 μm.

The two *Kayentatherium* specimens were scanned with a North Star Imaging industrial CT scanner. To distinguish between rock matrix and fossil bone in the USNM specimen, it was

scanned at 150 kV and 0.24 mA with no filter. Unfortunately, in this specimen the X-ray attenuation properties of the calcite crystals growing near the bone match those of the fossil material, making it difficult to distinguish fossil-matrix boundaries throughout the specimen. A total of 3,349 slices were generated along the coronal plane with a voxel size of 39.9 μm. The TMM specimen was scanned at 180 kV and 0.15 mA. One aluminum filter was used. A total of 1,906 slices were generated along the coronal plane with voxel size of 58.2 μm.

All datasets were analyzed using Avizo Lite 9.3.1. The endocasts were hand drawn using a Wacom tablet approximately every 20 slices, and interpolated between slices. Avizo was used to measure the surface area and volume of the reconstructed endocasts. These datasets are archived at UTCT.

Encephalization volume and encephalization quotient calculations

The endocranial volume of *Pseudotherium* was manually mapped as a digital endocast and its dimensions calculated using the software Avizo Lite version 9.3.1. Some authors have systematically omitted the olfactory bulbs from brain size and EQ measurements, because its dimensions could not be consistently calculated, especially in taxa or specimens in which the cribriform plate either was not ossified or was not preserved (e.g., Jerison, 1973). Our measurements include the volume of the olfactory bulbs, and the volume of the pituitary stalk. In probainognathian cynodonts, the pineal canal is absent, and the pineal body was probably covered by an expanded telencephalon (Rowe, 1993, 2017). Thus the pineal tube does not contribute to the endocast volume in the taxa discussed here. In addition, we excluded the volumes of the inner ear and cavum epiptericum from estimates of endocast volume.

The EQ was calculated using the Eisenberg (1981) equation: $E/0.05P\text{^}.74) = EQ$, where E = endocranial volume measured in cubic centimeters, and P = body mass calculated in grams. Body mass is calculated from the skull length using a regression equation from Luo et al., 2001, based on "insectivoran" data: $Y = 3.68X - 3.83$, where X = $\log_{10}$ skull length measured in millimeters, and Y = $\log_{10}$ body mass in grams. The EQ of *Pseudotherium* was compared to the EQs of other eucynodonts from table s1 of Rowe et al., 2011, and to the EQ of *Brasilitherium* (Rodrigues et al., 2014).

DESCRIPTION OF THE BRAINCASE AND ENDOCAST OF *PSEUDOTHERIUM*

Braincase

As an aid to interpreting the endocast, we illustrate (Fig 2) and summarize the bony elements comprising the braincase in basal mammaliamorphs. Development of many of the individual bones comprising the braincase is known to track growth of specific regions of the brain in mammals (Rowe, 2017) and archosaurs (Fabbri et al., 2017), and a similar correspondence probably applies to all amniotes. The rostral braincase roof is formed by the frontal. At a level just behind the frontonasal suture, the ventral surface of the frontal bears a shallow, ovoid impression that accommodates the dorsal surface of the olfactory bulb. Descending from the midline is a shallow longitudinal ridge that marks a sulcus separating the right and left olfactory bulbs; this sulcus is absent in most non-cynodont pan-mammals (e.g., Olson, 1944; Sigurdsen et al., 2012; Benoit et al., 2017). The frontal also forms a shallow coronal (transverse) ridge that partially encircles and constricts the boundary between the olfactory bulb and the cerebral hemisphere. In mammals this ridge forms a sharp separation (the annular sulcus) between the two structures. However, in the taxa discussed here, separation of the olfactory bulb and cerebral hemisphere is marked by only a shallow, subtle constriction. Behind the olfactory bulbs, the frontal also forms a short partial roof over the dorsal surface of the rostral-most cerebral hemispheres.

The roof over the cerebral hemispheres is continued posteriorly by the parietal. A medial ridge descending from the parietal midline marks the interhemispheric sulcus (Fig. 2.3B), which separates the right and left cerebral hemispheres to varying degrees in the taxa discussed here. The parietal expands posteriorly to meet the supraoccipital, and the two meet near the junction between the cerebral hemispheres and the cerebellum.

The supraoccipital covers the dorsal and posterior surfaces of the cerebellum and forms the roof of the foramen magnum, through which the spinal cord passes. In immature individuals, the vermis of the cerebellum protrudes through a narrow aperture that rises vertically from the foramen magnum; it eventually closes to fully enclose the vermis, leaving a more-or-less circular foramen magnum (Simon, 2013).

The exoccipitals form the lateral sides of the foramen magnum and cover the posterolateral surfaces of the cerebellar hemispheres. The ventral rim of the foramen magnum is formed by the basioccipital, which also forms a floor beneath the ventral surface of the medulla. The basisphenoid forms the braincase floor beneath the pituitary, and encloses the circle of Willis of the internal carotid artery.

Lateral surfaces of the cerebellum are enclosed by the petrosal (=periotic), which represents the fused prootic and opisthotic ossifications of the otic capsule. The petrosal encloses the membranous labyrinth and vestibule of the inner ear. In the taxa discussed here the vestibule is slightly elongated compared to more basal cynodonts such as *Thrinaxodon* (Fourie, 1974; Rowe et al., 1995), and in mammaliamorphs it might properly be called the cochlea. The petrosal also houses the parafloccular lobe of the cerebellum in its subarcuate fossa, which extends beneath the arch of the anterior semicircular canal. In mammaliamorphs, the internal auditory meatus is partially closed by a thin wall of bone that is penetrated by foramina for the vestibulocochlear nerve and a branch of the facial nerve (Kemp, 1983; Rowe, 1988).

The orbitotemporal portion of the braincase is not completely ossified in early mammaliamorphs. The lateral and ventral surfaces of the telencephalon were partially enclosed by the orbitosphenoid anteriorly, and by the pila antotica (pleurosphenoid, Presley and Steel, 1976) of the prootic posterolaterally. These elements do not contact one another in *Pseudotherium* or in *Kayentatherium*, or in any other non-mammaliaform cynodonts (Crompton et al., 2017) These elements are not common in fossil specimens as they tend to be thin and fragile, and seldom survive the fossilization and preparation processes. In *Pseudotherium*, the pila antotica arises from the petrosal near its suture with the basioccipital. The pila antotica is mediolaterally broad and projects anterodorsally. It terminates above the anterior end of the sella turcica. Left and right pila antoticae do not contact one another medially, and the pituitary stalk passed between them (Figs. 3 and 4). Given these relationships, the pila antotica supported the diencephalon (thalamus), and may have supported part of the telencephalon as well.

The orbitosphenoid lies medially within the sphenorbital fissure, which is enclosed between the frontal and alisphenoid. The orbitosphenoid is a paired element that contacts its partner ventromedially to form a floor beneath part of the telencephalon, and it is supported by a median, ventral ‘stem’ that may correspond to the presphenoid in mammals (Crompton et al.,

2017). In *Pseudotherium*, the dorsal flange of each orbitosphenoid lies medial to a descending, orbital process of the frontal. In life they were probably attached to the frontal (Crompton et al., 2017), but in the specimen studied here they are separated from it, probably as a result of post-mortem deformation (Wallace et al., in prep: fig. 18). The orbitosphenoid contains a large foramen for the optic nerve. The orbitosphenoid does not contact the pila antotica, nor the parasphenoid rostrum.

The secondary braincase wall is formed by the anterior lamina of the petrosal and the ascending process of the alisphenoid. The alisphenoid ossifies adjacent to the caudolateral pole of the piriform (olfactory) cortex in mammals and their extinct cynodontian relatives (Rowe and Shepherd, 2016; Rowe 2017). Together these elements surround a large cavum epiptericum that housed the semilunar ganglion of the trigeminal nerve (C.N. V) (Kuhn and Zeller, 1987).

Three regions in the braincase of *Pseudotherium* are not ossified. One region is beneath the anteroventral surface of the olfactory bulb, leaving a gap that would eventually be filled by the ossified cribriform plate of the ethmoid in Mammalia. The second gap is along the ventrolateral floor of the braincase between the orbitosphenoid and pila antotica. The third gap lies between the left and right pila antoticae and the zone between them and the sella turcica of the basisphenoid. When reconstructing the brain volume in these unossified regions, the meninges were assumed to pass straight from one bony element to the next (Fig. 2.3D). These are the regions most prone to interpretation when reconstructing an endocast.

Endocast

The endocast of *Pseudotherium* (Fig. 2.5) is narrow and positioned high in the skull, as was the case in cynodonts ancestrally (Kemp, 1979, 2009). The endocast has a convex dorsal curvature between the olfactory bulbs and the dorsal lip of the foramen magnum. The length of this curve in sagittal plane is equal to 62% of the distance from the tip of the rostrum to the back of the occipital condyle. The ventral surface of the endocast is also concave and flexes sharply at the pons. In dorsal view, it maintains a consistent width for much of its length, but posteriorly the caudolateral poles of the cerebral hemispheres widen over the midbrain and cerebellum just anterior to the subarcuate fossae, and they diverge laterally where they are enclosed by the

alisphenoid. In lateral view, the endocast gradually deepens from anterior to posterior. The endocast has a total volume of 1338.46 mm^3.

Forebrain (Telencephalon + Diencephalon)

The olfactory bulbs occupied a relatively large space of about 200.96 mm^3, comprising approximately 15.02% of the total endocranial volume (Table 2.1). The olfactory bulb is convex dorsally. Ventrally, the cartilaginous cribriform plate was not ossified. The olfactory fossa was interpreted as being closed by a flat anteroventral surface (see methods) representing the cartilaginous cribriform plate. In contrast to non-cynodont pan-mammalian condition in which the endocasts fail to record separation between right and left olfactory bulbs, there is a distinct sulcus between the two bulbs in *Pseudotherium*.

Each olfactory bulb terminates in a small, midline projection from its anterodorsal surface (Fig. 2.6). Similar projections are illustrated in other digital endocasts of early mammaliaforms and mammals (e.g., Macrini et al., 2006, 2007a, b; Rowe et al., 2011). They represent the vomeronasal and terminal (C.N. 0) nerves which make their first synapse in the accessory olfactory bulb, an anatomically distinct region located dorsally on the olfactory bulb. These two nerves and the accessory olfactory bulb are part of the vomeronasal system and are not involved in the main olfactory system (Rowe et al., 2005); the accessory olfactory bulb has not been identified in the endocast in any non-mammalian cynodont. The accessory olfactory bulb does not leave an impression on the skull roof in *Pseudotherium*.

The cerebral hemispheres form tall domes that are deeply divided by a median interhemispheric sulcus. In endocasts of the more basal cynodonts *Thrinaxodon* (Rowe et al. 1995; Hopson, 1979), *Diademodon* (Macrini, 2006) *Massetognathus* (Quiroga, 1979), and *Trirachodon* (Hopson, 1979), no interhemispheric sulcus is evident and the forebrain endocast appears tubular and cylindrical. Like the forebrain in vertebrates generally, the telencephalon must have been differentiated into right and left hemispheres, but the forebrain was not sufficiently large that its cerebral hemispheres produced separated impressions in the roof of the braincase. In contrast, in *Probainognathus* the interhemispheric sulcus is deep and separates high-domed cerebral hemispheres. The cerebral hemispheres are elongated, and their caudolateral poles protrude laterally against the alisphenoid. In these features, the forebrain in

Probainognathus closely resembles *Pseudotherium*, *Brasilitherium, Riograndia*, and *Kayentatherium*. The caudal pole of each cerebral hemisphere expands laterally to such an extent that they now exceed the width of the cerebellum. This reflects further expansion of the piriform (olfactory) cortex, a trend that can be traced to enhancement of the olfactory system in the most basal cynodonts (Rowe and Shepherd, 2016; Rowe, 2017). The cerebral hemispheres terminate where they meet the cerebellum above the level of the posterior limit of the paraflocculus root.

The pineal gland is not visible in the endocast of *Pseudotherium*, and it was probably covered by the cerebral hemispheres. The hypophyseal fossa is relatively small. With a total volume of about 4.20 mm^3, the hypophyseal fossa comprises approximately 0.314% of the total endocranial volume. The pituitary stalk left no bony trace, but the boundaries of the endocranial space in which it resided may be estimated between the left and right pila antoticae, and the hypophyseal fossa ventrally. The region which contained the pituitary stalk is estimated to be about 6.61 mm^3, giving the entire hypophyseal region a volume of 10.81 mm^3 or about 0.808% of the total endocranial volume (Table 2.1).

Midbrain (Mesencephalon)

The midbrain is not visible in the endocast of *Pseudotherium*. The cerebral hemispheres terminate where they meet the cerebellum. In more basal cynodonts, the midbrain is exposed dorsally between the cerebrum and the cerebellum (Rowe et al., 1995; Kielan-Jaworowska et al., 2004; Macrini, 2006). In the taxa of interest here, expansion and contact of the cerebrum and cerebellum covers the midbrain from surficial exposure.

At their junction, above the position of the subarcuate fossae of the petrosal, the endocast is smooth. The dorsal surface of the midbrain was covered by the cerebral hemispheres and by dural venous sinuses. The cerebral peduncles are not visible in ventral view as they are obscured by the flexure between the region of the pons and the hypothalamus.

Hindbrain (Metencephalon + Myelencephalon)

The cerebellum was overlapped anteriorly by the cerebral hemispheres. The cerebellum has a dorsomedial vermis that slightly interrupts the dorsal margin of the foramen magnum,

causing it to have a triangular shape (Fig. 2.7). The left and right cerebellar hemispheres bulge on either side of the vermis.

The paraflocculars and flocculars lobes of the cerebellum are histologically differentiated structures in living mammals (Voogd and Glickstein, 1998), but they are impossible to differentiate in endocasts of fossils. Both names have been used interchangeably in the literature in reference to the anatomically singular cerebellar lobe which occupies the subarcuate fossa of the petrosal. We neutrally use the term 'paraflocculus'. The function of this distinct structure has been debated. Some authors consider it to be a mere extension of a cerebellar lobule, a 'packaging solution' in which part of the cerebellum squeezed into the subarcuate fossa as it grew, and that it had no intrinsic functional identity (e.g., Larsell, 1952). However, Olson (1944) regarded the size of the paraflocculus as corresponding with agility in basal pan-mammals. In living mammals, neurons in the paraflocculus and adjacent parts of the cerebellum project to vestibular nuclei (Voogd and Glickstein, 1998; Voogd et al., 2012). Ablation experiments that bilaterally bisected the paraflocculus demonstrated that it plays a role in the vestibulo-occular reflex system involved in smooth eye-tracking of moving objects and smooth eye-tracking during pursuit (Zee et al., 1981). Still, it is unclear to what degree the lobe distinguishable in endocasts preserves a functional identity that coincides with its anatomical identity; whether its relative size corresponds with some measure of agility; or if it is simply a part of the larger vestibulo-occular reflex system of the cerebellum.

The left subarcuate fossa in *Pseudotherium* measures approximately 2.42 mm long and 1.6 mm wide, and the combined volume of the subarcuate fossae contributes to approximately 0.681% of total endocast volume. In *Brasilitherium*, whose skull is half the length of *Pseudotherium*, the subarcuate fossa contributes to about 2% of the total endocast (Rodrigues et al., 2014). In *Pseudotherium*, the subarcuate fossa is continuous with the post-temporal recess, which probably transmitted vessels from the post-temporal fenestra in certain Mesozoic mammals (Kielan-Jaworowska et al., 2004).

The pons and medulla oblongata cannot be differentiated from one another on the endocast. However, foramina for cranial nerves VII-XII suggest their relative positions, as nerves VII and VIII arise from the pontomedullary junction and nerves IX-XII arise from the medulla oblongata (Fig. 2.4). Cranial nerve VII and the cochlear and vestibular branches of VIII cluster anteroventral

to the paraflocculus. They penetrate the cranium just posterior to the ascent of the pila antotica, which marks the boundary between metencephalon and myelencephalon.

Vessels

The endocranial vault contains paired longitudinal grooves on either side of the cerebral hemispheres for the lateral head veins. Posterior to the cerebral hemispheres, the endocast is smooth over the region of the midbrain and anterior portion of the cerebellum. This is interpreted to be the confluence of the sagittal and transverse. This endocast feature was similarly identified as one of the dural sinuses in the tritheledont *Riograndia guabensis* (Rodrigues et al., 2018).

Encephalization quotient of *Pseudotherium*

The endocranial volume of *Pseudotherium* measures 1.34 mL. The body mass of *Pseudotherium* was estimated using skull length as is common for non-mammalian cynodonts. Skull length of *Pseudotherium* measures 75.84 mm, and the body mass equation from Luo et al. (2001) yields a body mass estimate of 1224.63 grams. With this body mass estimate and the estimated endocranial volume, the equation developed by Eisenberg (1981) yields an EQ of 0.13, which is within the range of non-mammaliaform cynodonts (Rowe et al., 2011), and probably below that of the stem-mammaliforms *Sinoconodon* (Luo et al., 2001) and *Adelobasileus* (Lucas and Luo, 1993).

DISCUSSION

Caveats and limitations in endocasts

In measuring brain weight in extant mammals, Jerison (1973:30-31) explained some of the many pitfalls: “Should it [the brain] be weighed with our without cerebrospinal fluid? Should the dura be left intact or should it be removed? Should the brain be weighed fresh or after fixation, and, if after fixation how long should it be pickled?....One should probably consider any measurements of brain weight as involving an inherent error of the order of at least 5 or 10%, and possibly more, because of the vagueness of the definition of weight.”

A comparable degree of uncertainty involves estimating brain volume from reconstructed endocasts. For example, assumptions must be made in bounding certain unossified regions of the

endocranial space that inevitably affect volume measuremens. Like Rodrigues et al. (2014), we explicitly describe how we delimited those spaces that are not enclosed by bone, although we differ on how it should be done. A few others have also been explicit in their assumptions about bounding unossified spaces (e.g., Jerison, 1973; Rowe et al., 2011; Balanoff and Bever, 2017; Benoit et al., 2017) but in many cases, the assumptions have gone unreported. Moreover, measurements of digital and natural endocasts are made in fundamentally different ways, and even natural endocasts are measured in different ways (above).

Body weight presents another set of problems. In extant mammals, body weight measurements are fairly straightforward. However, estimating body weight in extinct stem mammals generally extrapolates from linear measurement, causing additional uncertainty in EQ calculations (Jerison, 1973; Quiroga, 1984). For example, different regression coefficients (e.g., Jerison, 1973; Eisenberg, 1981; Hurlburt 1999) have been proposed for different sets of living mammals. Additionally, both body weight and EQ can be affected by maturity at time of death for any particular specimen. EQ is probably systematically overestimated in immature mammals; so far as we are aware, maturity at time of death has never been addressed when measuring or comparing EQs.

Jerison (1973) consistently excluded measurements of olfactory bulbs from his estimates of mammal and extinct cynodont endocasts. He also operated under the notion that the brain generally did not fill the endocranial cavity, so he arbitrarily corrected for this. In his various studies of early cynodonts, Quiroga (1980, 1984a, 1984b) used different equations to estimate body mass, and different methods to estimate brain size. Rowe et al. (2011) were consistent in the methods used to measure and report EQs, but their overall sample size for non-mammaliaform cynodonts was small. A much larger sample of therapsid (including mammals) EQs was recently reported by Benoit et al. (2017) based on new CT data, but many of their reported measurements were harvested from older publications. Suffice it to say that some error margin should be kept in mind while comparing EQ estimates.

Encephalization in early pan-mammalian evolution

The earliest amniotes and earliest (‘pelycosaur-grade’) pan-mammals had very small brains compared to living mammals (Case, 1906; Romer, 1956; Jerison, 1973; Rowe, 2017).

Only the floor and rear parts of the braincase, behind the pituitary fossa, were ossified. Whereas the right and left cerebral hemispheres must have been differentiated, as they are in all other vertebrates (Nieuwenhuys et al., 1998), the endocasts in early pan-mammals preserve little more than the dorsal surface of the forebrain, which appears featureless and cylindrical with no apparent interhemispheric sulcus. The cerebellum was wider than the narrow forebrain (Case, 1906; Olson, 1944). The olfactory bulbs were small and presumably mounted on long stalks but there was no bony separation between the bulbs, nor any preserved impression of the stalks. A fairly large pineal eye was present, and the midbrain was exposed dorsally between the telencephalon and cerebellum (Case, 1906; Romer, 1956; Jerison, 1973). The uncertainties surrounding measurements of EQ are probably greatest in these earliest and most basal pan-mammals in which large areas of the braincase are unossified, requiring extensive reconstruction of the endocranial cavity. About the most that can be said from endocasts is that there was little measureable change in encephalization of stem-mammals for ~100 million years following the divergence of Pan-Mammalia from the ancestral amniote in the Carboniferous, approximately 310 million years ago (Rowe, 2017).

Encephalization in early therapsid evolution

The plesiomorphic pan-mammalian condition carried into early therapsids, which arose in the mid-Permian, roughly 50 million years after pan-mammals diverged from other amniotes. Although therapsids preserve skeletal evidence of longer limbs and increased agility, which implies an increase in encephalization (Gauthier et al., 1988; Kemp, 2006; Rowe, 2017), no unequivocal increase has yet been measured. According to a study by Benoit et al. (2017) based on new CT scans of a number of Permian therapsid fossils, early therapsid EQ was effectively unchanged from basal amniotes. Benoit et al. (2017) reported EQs for non-mammaliaform therapsids based on three different regressions, viz., Jerison (1973), Hurlburt et al. (1999), and Manger (2006). The estimates using Jerison's regression (1973) returned the lowest EQs, while Hurlburt et al. (1999) returned the highest values, but in all analyses, non-probainognathian values fluctuated between ~0.06 and ~ 0.2 (on the Jerison scale), with no apparent phylogenetic signal in the variance.

The only exceptions were consistently low EQs for the large, herbivorous head-butting dinocephalians. Another exception was reported for the fossorial dicynodonts *Kawingasaurus* and *Cistecephalus* (Laaß and Kaestner. 2017). Their anomalously high EQ values approach the range observed in extant mammals, and are reported to include 'neocortex-like structures.' However, the CT imagery published in that paper and personal inspection of those specimens indicates that large volumes of the temporal fossae were erroneously added to the reconstructed endocast, and suggests that their endocranial cavities were small and resembled other dicynodonts (e.g., Cluver, 1975) and non-cynodonts therapsids.

Encephalization in early cynodont evolution

Using the Eisenberg equation, Rowe et al. (2011) measured a slight increase in EQ (~0.21) in basal cynodont *Thrinaxodon*, compared to more basal therapsids. Early cynodonts are notable in having an interbulbar sulcus that separates the olfactory bulbs on the endocast for the first time. Slightly lower EQ values were measured in other early non-mammaliaform cynodonts, and there was no clear phylogenetic signal in this variance. In light of the uncertainties in measuring EQ, it remains to be seen whether early cynodonts reflect a genuine increase in encephalization. As with early Therapsida, however, a large number of skeletal transformations in early cynodonts imply neurosensory enhancements that might correlate to an increased EQ.

Early evolutionary transformation of the cynodont skull included ossification of the alisphenoid to enclose the lateral braincase wall around an expanded olfactory (piriform) cortex in the lateral wall of the telencephalon. The secondary palate appeared and effected separation of the nasopharyngeal passage from the mouth. An occlusal dentition and the development of teeth with long roots and a periodontal ligament also appeared early in cynodont history. The double occipital condyle afforded broad arcs of stable, rapid head movement. Differentiation of thoracic and lumbar vertebrae probably signaled the origin of diaphragmatic breathing and possibly also the rapid sniffing of scent tracking (Rowe and Shepherd, 2016).

The origin of Cynodontia corresponded with a profound re-organization in feeding behavior in a crown-ward direction that was probably driven by a fundamental transformation in olfactory performance and early emergence of the integrated sense of ortho-retronasal olfaction (Rowe and Shepherd, 2016). Extant mammals generally retain the primitive tetrapod olfaction

mode of sniffing known as ‘orthonasal’ smell, in which airborne environmental odorant molecules are drawn through the nares (nostrils) into the nose to activate the olfactory epithelium. However, orthonasal smell in mammals takes on its own special characteristics owing to their huge olfactory receptor (OR) genome. Approximately ~1200 OR genes are inferred to have been present in mammals ancestrally, compared to ~100 that were present ancestrally in Tetrapoda and Amniota (Niimura, 2009, 2012). Mammals also employ a system of diaphragmatic ventilation that, together with a distinctive craniovertebral joint, confers unique attributes to mammalian orthonasal smell, such as their abilities in scent-tracking.

‘Retronasal’ smell is the counterpart to orthonasal smell. In retronasal smell, air exhaled from the lungs carries with it an entirely new domain of odor molecules liberated in the mouth through the breakdown of food by chewing, saliva, and actions of the tongue. These molecules pass forward from the back of the mouth via the choana (internal naris) and across the main olfactory epithelium before being expelled through the nares. In retronasal smell, olfaction combines with taste and other senses (e.g., somatosensation, vision, hearing) to generate our sensation of flavor (Shepherd, 2004, 2006, 2012).

In mammals, orthonasal smell, retronasal smell, taste, and somatosensory signals from the lips, tongue and teeth all converge in the neocortical area known as the orbitofrontal cortex (De Araujo et al., 2003; Small et al., 2007; Rolls and Grabenhorst, 2008). Ortho-retronasal olfaction, or flavor, is thus a high-level multisensory map in which distinct classes of information are integrated. This has been demonstrated in clinical data from patients who lost olfactory sensation following nasal infection or cranial trauma (Cullen and Leopold, 1999; Franselli et al., 2004; Bonfils et al., 2005) and from laboratory experiments (e.g., Heilmann and Humel, 2004; Sun and Halpern, 2005; Gautam and Verhagen, 2012). Ortho-retronasal olfaction is unique to mammals among living species. However, many facets of ortho-retronasal olfaction are dependent on the spatial organization and mechanical performance of the skull, dentition, and postcranial skeleton and thus its origins can be traced through the fossil record to the origin of Cynodontia (Rowe and Shepherd, 2016; Rowe, 2017).

Whereas we might expect an increase in encephalization in association with some of these changes, one of the major conclusions of the larger study by Benoit et al. (2017) was that nearly all non-mammaliaform taxa sampled, including early cynodonts, had EQs that fit close to

a single regression line that lies on the upper range of variation in amphibians and non-avian reptiles, and that lies below the regression line for Mammaliaformes (Benoit et al., 2017). Included in their sample were a number of non-mammaliaform cynodonts. What seems remarkable in these findings is that little evolution in relative brain size was detected despite the remarkable skeletal transformation documented in non-mammaliaform therapsids and cynodonts (Gauthier et al., 1988; Rowe, 2017). Nevertheless, if the Benoit et al. (2017) study is taken at face value, skeletal reorganization in early cynodonts may not have coincided with an increase in the relative size of the brain, or it was sufficiently small as to be masked by the margin of error implicit in measuring EQ in these small-brained pan-mammals.

Encephalization in early probainognathian evolution

In the mid-Triassic *Probainognathus* the surface of the endocast for the first time takes on a more detailed resemblance to the mammalian brain (Fig. 2.8, Node 4). The probainognathian brain was evidently packed more tightly into the braincase to impress more vivid details of its shape into the braincase roof. There is now a median sulcus that separates the right and left cerebral hemispheres, and the hemispheres extend forward to closely approach the olfactory bulbs. However, a short length of the olfactory peduncles is still visible between the olfactory bulb and cerebral hemisphere. The caudolateral poles of the cerebral hemispheres, corresponding to the olfactory (piriform) cortex, project laterally and are approximately as wide as the cerebellum between the roots of its paraflocculars lobes (Quiroga, 1979, 1980, 1984). This suggests that enhancement in olfaction was an important influence in the origin of Probainognathia. Despite the marked increase in its ‘brain-like’ appearance, the EQ measured from a natural endocast of *Probainognathus* was estimated at 0.19 (Quiroga, 1980, 1984), and EQ for the slightly more derived *Therioherpeton* was estimated at a value of 0.18 (Quiroga, 1984). This may be another indication that EQ is insufficiently imprecise to detect relatively small changes in relative brain size, even if the changes seem significant in terms of relative brain region size. The endocasts in *Riograndia, Pseudotherium, Brasilitherium*, *Therioherpeton*, and tritylodontids all show a general resemblance to *Probainognathus*.

Comparison of the endocast of *Pseudotherium* to *Brasilitherium* and other probainognathians

The endocranial volume of *Pseudotherium* reconstructed for this analysis differs from the reconstruction of the closely related *Brasilitherium* endocranial volume in several ways. One difference concerns the shape of the olfactory bulbs. The floor of the olfactory bulbs is not ossified in *Brasilitherium* (Rodrigues et al., 2014) or in *Pseudotherium*. Reconstructions of the olfactory bulbs of *Brasilitherium* infer their shape from the shape of the roof of the olfactory fossa, assuming that the olfactory bulbs are dorsoventrally symmetrical. As a result, *Brasilitherium* was estimated to have the largest olfactory bulb volume of any known non-mammaliaform cynodont by one order of magnitude. While the proportion of olfactory bulb length to entire endocast length is notably long when viewed dorsally, the entire reconstructed volume of the olfactory bulbs, which comprise 35% of the total endocast, may have been overestimated for *Brasilitherium.*

In contrast, we reconstruct the floor of the olfactory fossa as a flat plane extending beneath the olfactory fossa from the frontal to the orbitosphenoid. Our estimates of olfactory bulb volume may underestimate their volume in life. However, developmental interdependencies observed in the ontogeny of extant mammals suggest that this may be more realistic.

As odorant receptor genes are expressed and odorant receptors mature on the olfactory epithelium of the nose, their axons pass backwards to the rostral end of the telencephalon where they make their first synapse (Rowe et al., 2005). This induces the formation of olfactory glomeruli and differentiation of the olfactory bulb (Farbman 1988, 1990; Mombaerts, 2001; Chen and Shepherd, 2005; Bargmann, 2006). The number of expressed OR genes is correlated with the size of the cribriform plate and olfactory bulb (Bird et al., 2018). Olfactory ‘images’ produced in the olfactory bulbs are passed to the olfactory (piriform) cortex for higher level processing before being sent on to the dorsal cortex (Shepherd and Rowe, 2017). There is a general correspondence between size of the expressed olfactory genome, the cribriform plate, olfactory bulbs, and size of the piriform cortex (Macrini et al., 2007; Rowe and Shepherd, 2016). To have a greatly enlarged olfactory bulb without a corresponding enlargement in the piriform cortex is difficult to understand in light of these interdependencies that affect the olfactory system as a whole.

Quiroga (1980) speculated that a neocortical plate on the dorsal cortex was present in *Probainognathus.* While it may be true that the observed inflation of the cerebral hemispheres reflects an early stage in the transition from the plesiomorphic 3-layer dorsal cortex to 6-layer neocortex, it is a difficult proposition to test in known specimens of early probainognathians. The case for emergence of a neocortex is stronger in mammaliaforms, in which a pelt of modern aspect is preserved in at least one remarkable fossil, and the brain is much larger and subspherical in shape (Rowe et al., 2011). Regardless, the relatively larger olfactory bulbs in *Probainognathus* are correlated with an enlarged olfactory cortex, and it appears that the early ontogenetic interdependencies within the olfactory system of mammals played out in early probainognathians. The same interdependencies have been observed in extant chelonians and lepidosaurs (Bruce and Bradford, 2009) and are probably a general organizational feature in amniotes that have only a three-layered dorsal cortex (Rowe and Shepherd, 2016).

If we assume that the olfactory bulb casts reconstructed for *Brasilitherium* are overestimated by 25%-50%, then reducing their volume by those percentages drops the EQ of *Brasilitherium* from 0.22 to 0.21 or 0.19, respectively (using the equation of Eisenberg, 1981), placing it in the range of other basal (non-mammaliaform) cynodonts. This also diminishes the proportion of the olfactory bulbs in *Brasilitherium* to between 28% and 17% of the overall endocast, which is closer to the 15% measured in *Pseudotherium*.

Other differences between the *Pseudotherium* and *Brasilitherium* endocasts are that the former was reconstructed with a relatively small region for the pituitary stalk while the *Brasilitherium* endocast depicts a large pituitary stalk region. Without bony landmarks it is difficult to judge which is more accurate. Another difference is that our reconstruction of *Pseudotherium* excludes the cavum epiptericum, whereas at least part of the cavum epitptericum was included in the *Brasilitherium* endocast. The cavum epiptericum is an extracranial space housing the semilunar ganglion of the trigeminal nerve. While enclosed by the osseous cranium in mammals, it remains an extradural space (Meckel's cave) that is contained within the secondary braincase wall. The rationale for inclusion of the cavum epiptericum in the *Brasilitherium* endocast study was that the space was historically included in basal cynodont endocast studies because it was preserved in natural endocasts. Additionally, the space for the semilunar ganglion is often included in endocranial volume reconstructions for Mammalia, as it

is housed within the mammalian endocranium. Our rationale for deleting the cavum epiptericum is that the published digital endocasts of non-mammalian cynodonts generally exclude it (Rowe et al., 2011), and these seemed the most relevant taxa for comparison. Both arguments have a measure of validity, but only uniformity in approach will increase the comparative sensitivity of EQ.

In most other respects, the endocasts of *Pseudotherium* and *Brasilitherium* are quite similar to the endocast of *Probainognathus*, which is the most basal cynodont in which the cerebral hemispheres form tall domes separated by a deep interhemispheric sulcus. In *Pseudotherium* and *Brasilitherium* they are further elongated and contact the cerebellum to cover the midbrain and exclude its dorsal exposure. As in *Probainognathus*, the caudolateral poles of cerebral hemispheres, representing the olfactory (piriform) cortex, protrude laterally to approximate the width of the cerebellum between its paraflocculus roots. While no discernable increase in EQ has been measured in basal probainognathans, that these features are sharply delineated on the endocasts suggest that the brain is more inflated and more tightly packed into the braincase to leave such detailed impressions of its outer surface on the inner surfaces of the endocranial cavity.

So far as we can judge, the shape of tritylodont endocasts is effectively identical to *Pseudotherium*, although published EQ values suggest that it may have been slightly smaller (Benoit et al., 2017). The cerebral hemispheres are expanded enough to bulge into the skull roof, leaving an interhemispheric sulcus on the cranial vault (Fig. 2.9). In the tritheledontid *Riograndia* (Rodrigues et al., 2018), the olfactory bulbs and cerebral hemispheres apparently are in contact, covering the olfactory tracts and eliminating dorsal exposure of the olfactory peduncles. Further, its cerebral hemispheres are proportionally wider than any other more distantly related cynodont. However, the cerebral hemispheres are primitive in that they do not extend far enough posterior to cover part of the cerebellum as they do in *Therioherpeton*. Thus there is some minor variation in shape or ‘packaging’ among these early probainognathians, despite little measurable variation in relative brain size.

We note that compared to *Probainognathus*, the cochlea is more elongate and medially in-turned in *Brasilitherium* (Rodrigues et al., 2013), *Pseudotherium* (Wallace et al., in press), and in tritylodontids (Luo, 2001), suggesting sensitivity to a wider range of high-frequency sound.

Further, the cochlea is walled medially and housed within a promontorium of the periotic in *Pseudotherium* and *Brasilitherium*. These apparent enhancements in audition also came about without a discernable increase in encephalization, if published EQ values are taken at face value.

Encephalization in early mammaliaforms

Estimations of EQ become more accurate in Mammaliaformes, where much more of the endocranial cavity is ossified, and corresponding changes in cranial architecture can be seen. In *Morganucodon*, a 50% increase in EQ, to ~0.35 corresponds with obvious expansion of the braincase around a voluminous, sub-spherical forebrain, in which greatly enlarged olfactory bulbs and piriform cortex can be observed in the endocasts (Rowe et al., 2011). Enhancement of the olfactory system was the primary driver of encephalization in early mammaliaforms, but other factors were involved as well.

By this time a small neocortex was almost surely present, and contributed in a small degree to encephalization. Dominating the neocortex is a single primary somatosensory field that maps sensation from mechanoreceptors in the skin, hair follicles, muscle spindles, and joint receptors (Kaas, 2009). This peripheral somatosensory input is mapped to the neocortex as an 'animunculus.' The presence of a pelt of modern aspect is known from the remarkably preserved Early Jurassic mammaliaform *Castorocauda lutrisimilis* (Ji et al., 2006), in which both guard hairs and velus underfur are preserved. In mammals, guard hairs are equipped with several different kinds of mechanoreceptors that are responsible for inducing the differentiation of the neocortical somatosensory map (Zelená, 1994). A parallel neocortical motor map, made of pyramidal neurons, gives origin to the pyramidal tract. This tract projects directly from the neocortex to all other downstream parts of the brain and into the spinal column, where it programs and executes skilled movements requiring precise control of distal musculature (Rowe et al., 2011; Shepherd and Rowe, 2017). Its appearance is associated with considerable expansion of the foramen magnum (Wallace et al., in prep).

A second encephalization pulse to an EQ of ~0.5 is recorded in a digital endocast of the Early Jurassic mammaliaform *Hadrocodium* (Rowe, et al., 2011). It was also driven largely by olfaction and it more than doubled the relative size of the brain in stem-mammals, compared to early cynodonts. *Hadrocodium* carried relative brain size into the range measured among living

mammals. The origin of Mammalia was tied to a third pulse in olfactory elaboration in which the nasal capsule became extensively filled by an elaborate, ossified scaffold of turbinals that support extensive olfactory and respiratory epithelia (Rowe et al., 2011).

CONCLUSIONS

From the origin of Pan-Mammalia in the Carboniferous, some ~310 million years ago, to the origin of Probainognathia in the mid-Triassic, ~ 230 million years ago, there was little measurable change in encephalization quotient. The forebrains in the basal-most taxa were cylindrical and featureless except for the pineal stalk. The forebrain lacked a deep interhemispheric sulcus and was narrower than the cerebellum. Because less of their braincase was ossified, greater subjectivity surrounds reconstructing endocasts and estimating EQ in the early small-brained pan-mammals. Given the many sources of error, current EQ measurements measuring in the range between ~0.1 to ~0.2 should probably be considered as effectively equivalent.

The skeletal evidence of increased agility in early therapsids implies enhanced neural performance that seems consistent with an increase in EQ. However, no unequivocal increase in the relative size of a basal therapsid endocast has yet been measured. The origin of Cynodontia probably also corresponds to an increased EQ, one that was driven by elaboration of the olfactory system. The first qualitative evidence can be found in early cynodonts with the division between olfactory bulbs by a shallow interbulbar sulcus, formed by a short midline septum from the frontal, and by the ossification of the alisphenoid around the caudolateral poles of the olfactory (piriform) cortex. However, uncertainties in reconstructing endocasts tend to limit interpretation of whatever small increase in EQ may have occurred at that time.

At the origin of Probainognathia, the brain is more tightly packed within the braincase so that the endocast represents recognizable brain morphology. In *Pseudotherium* and *Brasilitherium*, the cerebral hemispheres are tall-domed, and elongated such that they closely approach the olfactory bulbs anteriorly, while posteriorly they contact the cerebellum. All of these changes seem consistent with an enlarged brain, but inconsistencies in how endocasts of early probainognathians are extracted from fossil crania, and how they are measured

compromises quantitative comparisons. Nevertheless, from the outer shape of the endocast in *Pseudotherium*, *Brasilitherium*, and the other basal probainognathians, it is easy to see that they possess a combination of ancestral pan-mammal and derived early mammaliaform neauroanatomical traits.

In light of the many assumptions and different methods that have been used to generate endocasts and to measure EQ, it seems possible that some small degree of gradual increase in early pan-mammalian brain evolution may have gone un-measured. Taken at face value, however, reported EQ values suggest that relative brain size was effectively static in early pan-mammals for some 90 million years. The evidence available at present is not sufficiently precise to completely reject either hypothesis. However, what is presently known of EQ seems more consistent with the interpretation of long periods of effective stasis that were punctuated by more rapid episodes of brain expansion. As others have speculated, a punctuation in EQ eventually may be measured near the origin of Therapsida. Less equivocal are episodes of rapid, if relatively minor encephalization with the origin of Cynodontia followed by another with the origin of Probainognathia. The acceleration seen and measured in Mammaliaformes seems unequivocal. Once EQ entered the range of variation measured in extant mammals, a tremendous diversification of brain size and organization followed. CT scanning all of the relevant fossils, consideration of their maturity at time of death, consistency in how endocasts are reconstructed and how body mass is estimated may lend greater precision to EQ as a comparative measure and reveal a more nuanced sequence of events than current estimates portray.

Table 2.1 Linear and volumetric measurements from the endocast of *Pseudotherium*.

Olfactory bulb length	11.66 mm
Olfactory bulb width	6.62 mm
Olfactory bulb volume	200.96 mm^3
Cerebral hemisphere length	18.38 mm
Cerebral hemisphere width, anterior	6.08 mm
Cerebral hemisphere width, posterior	10.4 mm
Hypophysis and stalk cast depth (from adjacent ventral surface)	4.44 mm
Hypophyseal seat width	1.52 mm
Hypophyseal seat length	1.92 mm
Hypophysis and stalk cast volume	10.81 mm^3
Cerebellum width, posterior to paraflocculus	7.58 mm
Paraflocculus length	2.42 mm
Paraflocculus width	1.6 mm
Maximum width, between paraflocculi	13.2 mm
Volume total	1338.46 mm^3

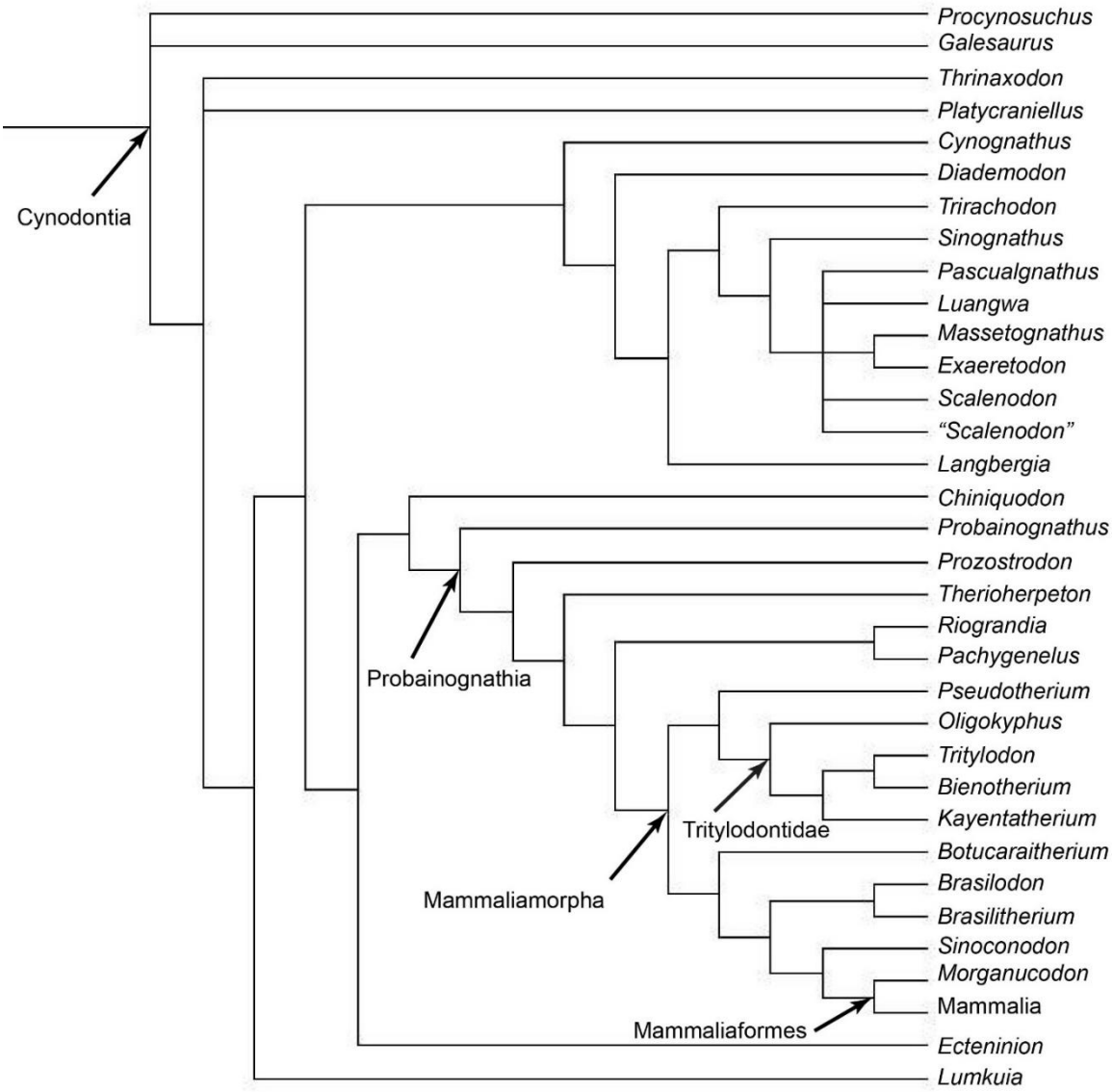

Figure 2.1: Phylogeny of cynodonts based on analysis from Wallace et al., in prep, using modified matrix from Liu and Olsen, 2010.

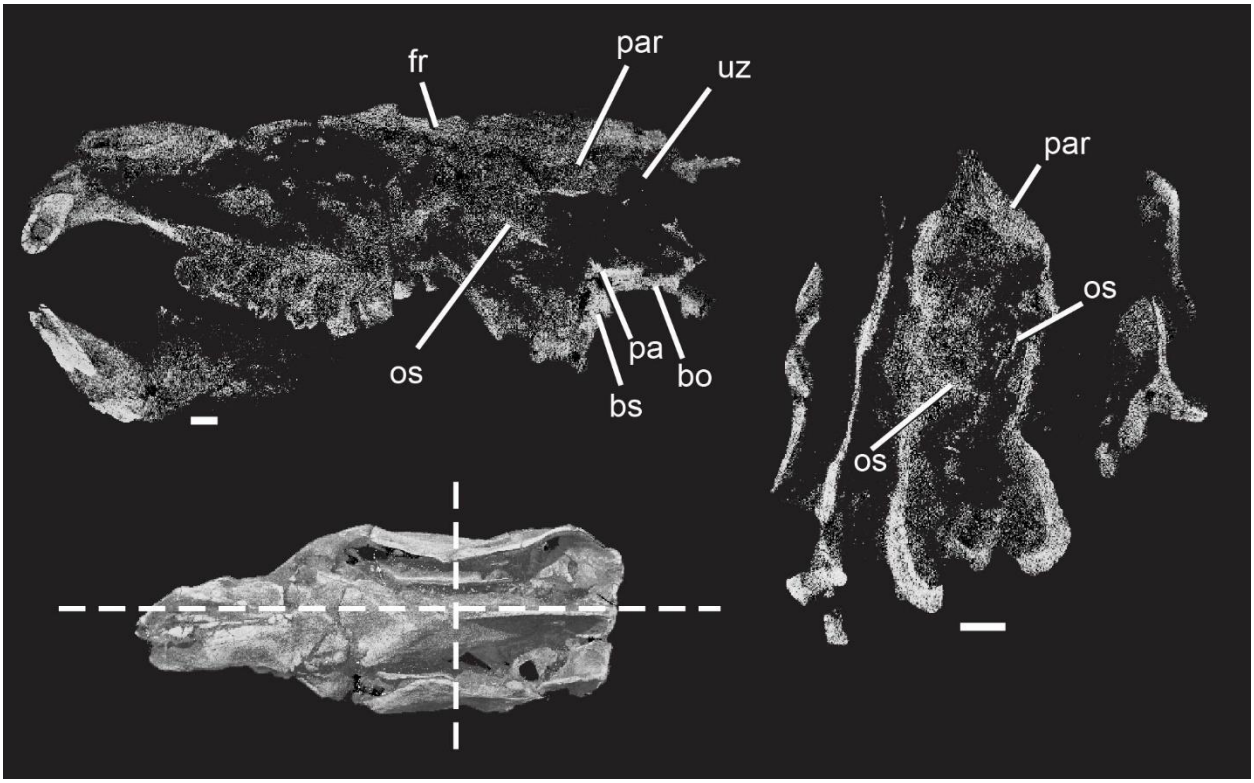

Figure 2.2: Cross sections through *Kayentatherium* USNM 317208. Parasagittal section (upper left) shows the orbitosphenoid (or) and pila antotica (pa) forming the ventral limit of the braincase in a typical non-mammalian cynodont arrangement. The bones do not contact one another. The coronal section (right) shows the paired orbitosphenoids high within the skull and oriented so that they contact one another medially. Scale bars = 5 mm. Abbreviations: **bo**, basioccipital; **bs**, basisphenoid; **fr**, frontal; **os**, orbitosphenoid; **pa**, pila antotica; **par**, parietal; **uz**, unossified zone.

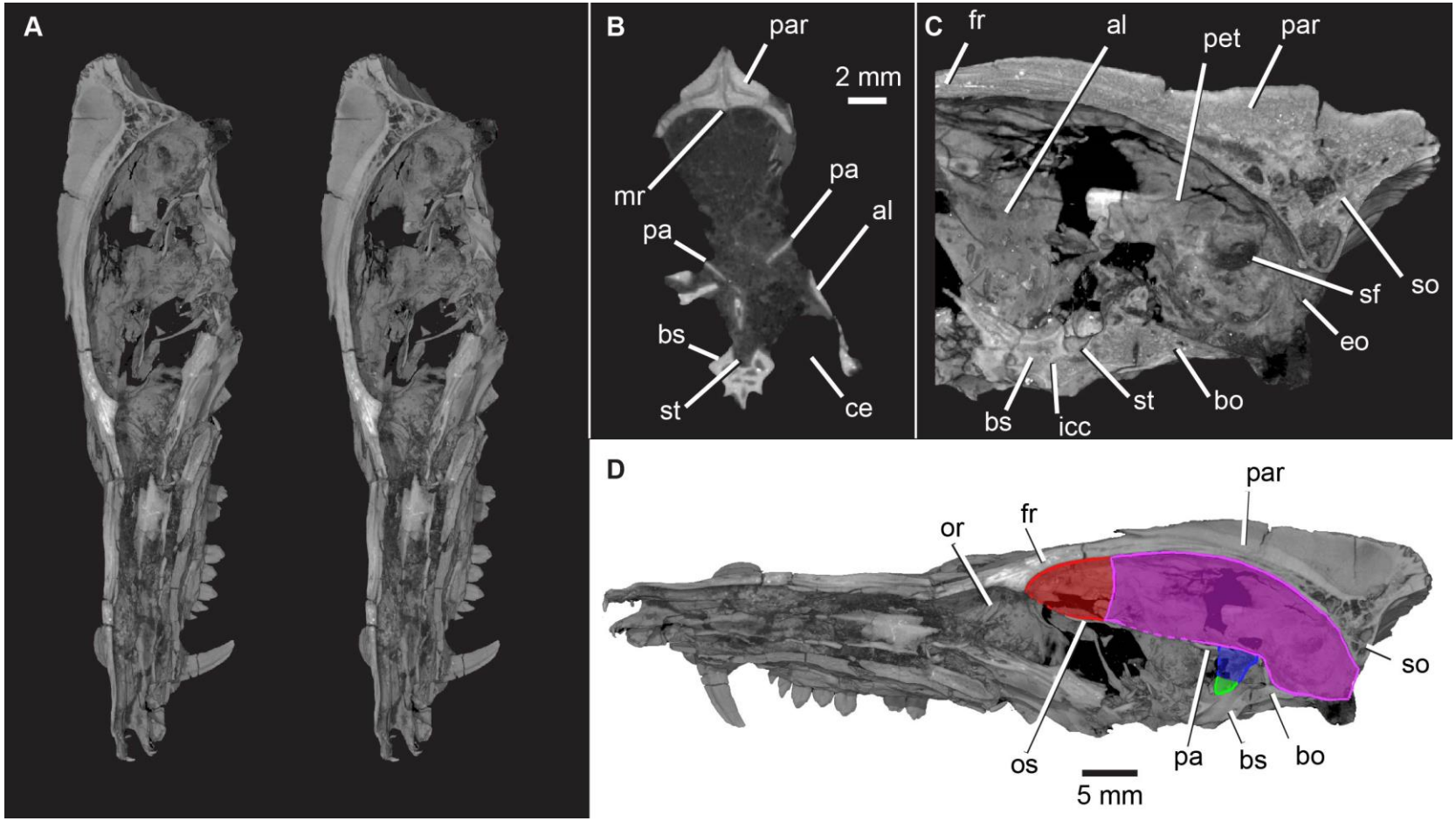

Figure 2.3: Braincase of *Pseudotherium* PVSJ 882. **A.** Stereoscopic sagittal cutaway. **B.** Cross section through sella turcica (st) showing medial ridge (mr) of parietal roof dividing cerebral hemispheres. **C.** Labeled posterior end of braincase. **D.** Schematic depicting endocast's relationship to braincase elements. Dashed outline indicates where endocast had to be inferred due to absence of ossification. Abbreviations: **al**, alisphenoid; **bo**, basioccipital; **bs**, basisphenoid; **ce**, cavum

epiptericum; **eo**, exoccipital; **fr**, frontal; **icc**, internal carotid canal; **mr**, medial ridge; **os**, orbitosphenoid; **or**, olfactory region; **pa**, pila antotica; **par**, parietal; **pet**, petrosal; **so**, supraoccipital; **st**, sella turcica.

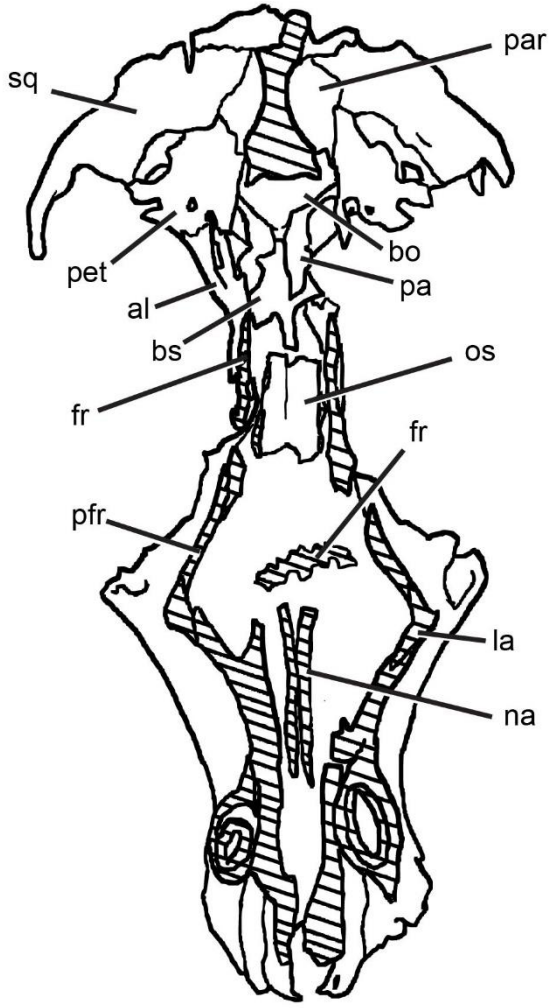

Figure 2.4.

Figure 2.4: Horizontal cutaway through braincase of *Pseudotherium*. **Left:** stereoscopic volume renderings with horizontal cutaway. **Right:** labeled illustration of horizontal cutaway. Hashed lines represent cutaway bone. Scale bar = 5 mm. Abbreviations: **al**, alisphenoid; **bo**, basioccipital; **bs**, basisphenoid; **fr**, frontal; **la**¸lacrimal; **na**, nasal; **os**, orbitosphenoid; **pa**, pila antotica; **par**, parietal; **pet**, petrosal; **pfr**, prefrontal; **sq**, squamosal.

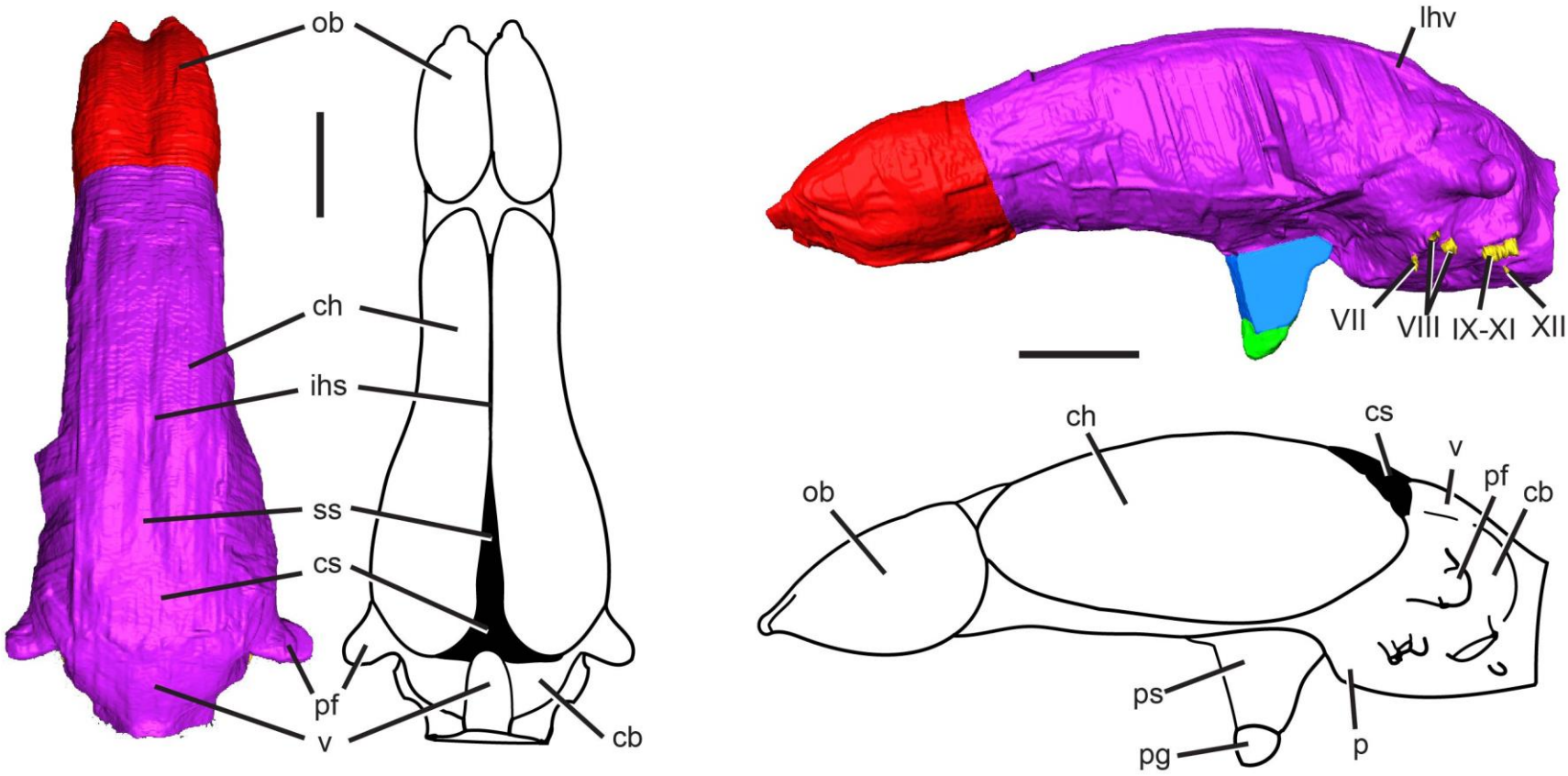

Figure 2.5: Endocast of *Pseudotherium* in dorsal (left) and left lateral (right) views. Scale bars = 5 mm. Roman numerals: **VII**, facial nerve; **VIII**, vestibulocochlear nerve; **IX**, glossopharyngeal nerve; **X**, vagus; **XI**, accessory nerve; **XII**, hypoglossal nerve. Abbreviations: **cb**, cerebellum; **ch**, cerebral hemisphere; **cs**, confluence of sinuses; **ihs**, interhemispheric sulcus; **lhv**, lateral head vein; **ob**, olfactory bulb; **p**, pons; **pf**, paraflocculus; **pg**, pituitary gland; **ps**, pituitary stalk region; **v**, vermis.

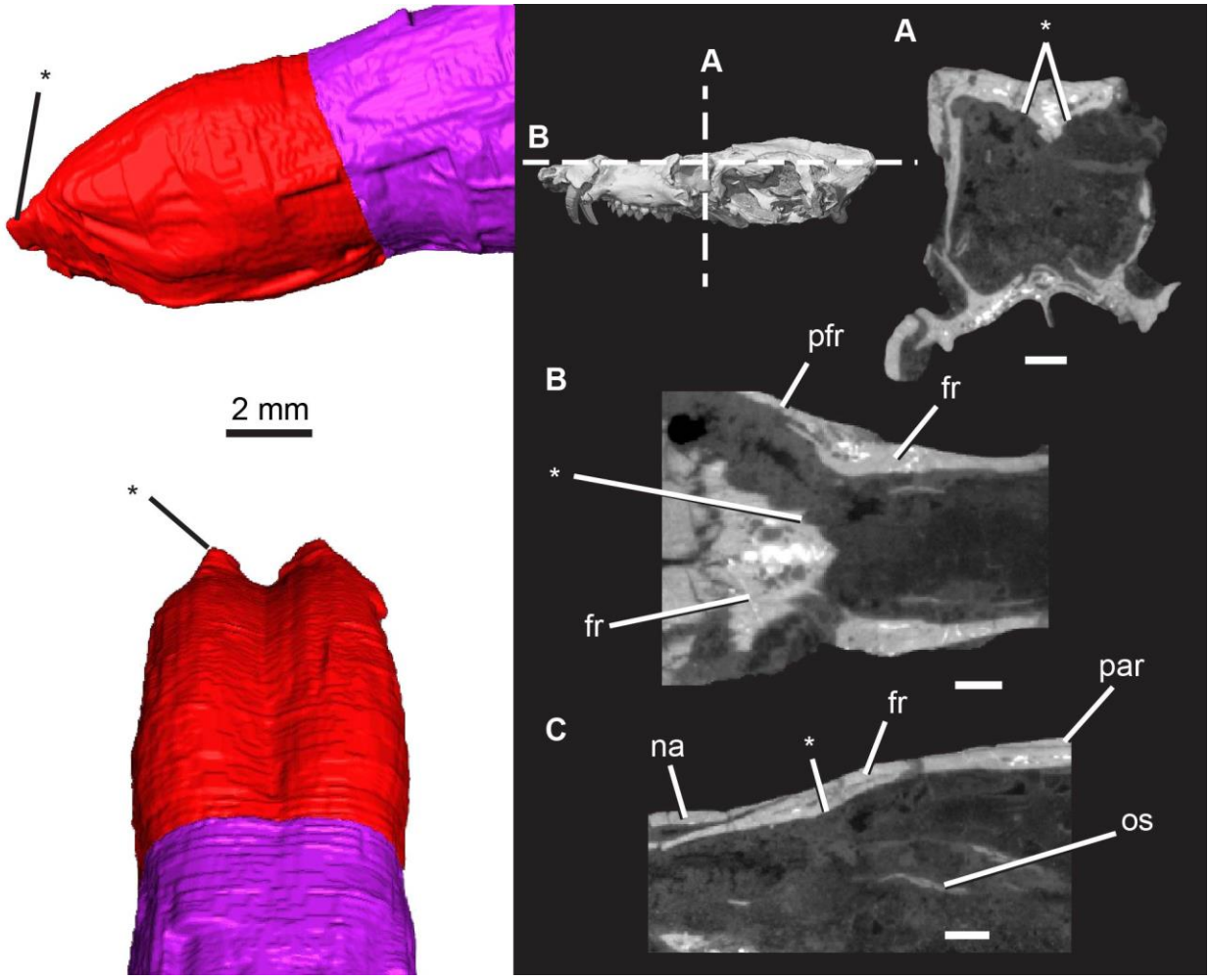

Figure 2.6: Vomeronasal and terminal nerves in *Pseudotherium*. **Left:** Anterior end of olfactory bulb casts with space for vomeronasal and terminal nerves (*). **Right:** Cross section (A), horizontal (B) and parasagittal sections through regions of vomeronasal and terminal nerves. Scale bars = 2 mm. Abbreviations: **fr**, frontal; **na**, nasal; **os**, orbitosphenoid; **par**, parietal; **pfr**, prefrontal.

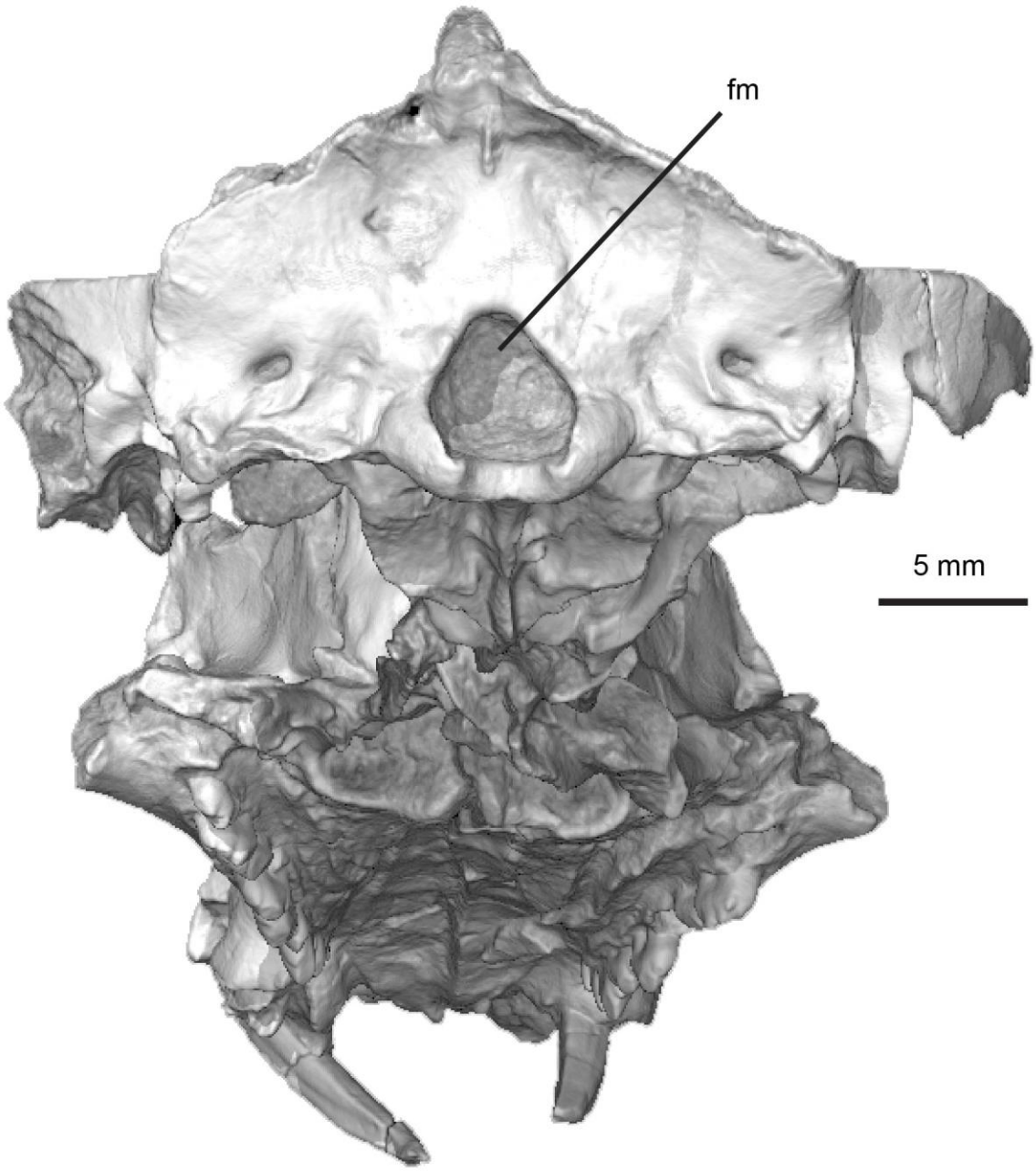

Figure 2.7: Foramen magnum (fm) of *Pseudotherium* in occipital view with skull oriented in a natural position inferred from imaginary vertical plane between opisthion and basion of foramen magnum.

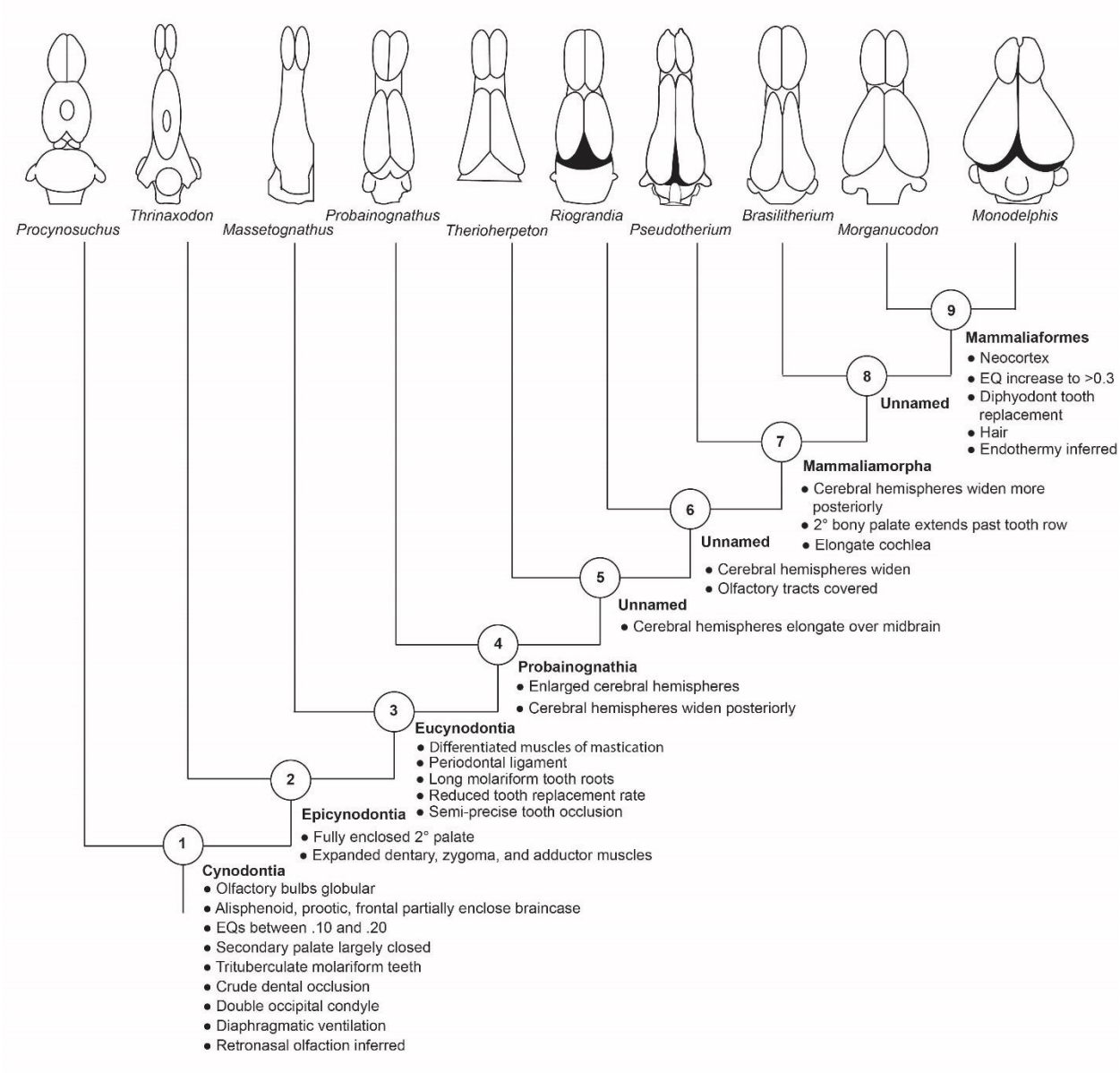

Figure 2.8: Evolution of the mammalian brain and schematic representations of select cynodont brains. *Procynosuchus* was modified from Kemp, 1979. Note that the large size of the olfactory bulbs is likely inaccurate. *Thrinaxodon* and *Monodelphis* were modified from Rowe et al., 2011. *Massetognathus*, *Probainognathus*, *Riograndia*, *Brasilitherium*, and *Morganucodon* were modified from Rodrigues et al., 2018: fig. 7. *Therioherpeton* was modified from Quiroga, 1984.

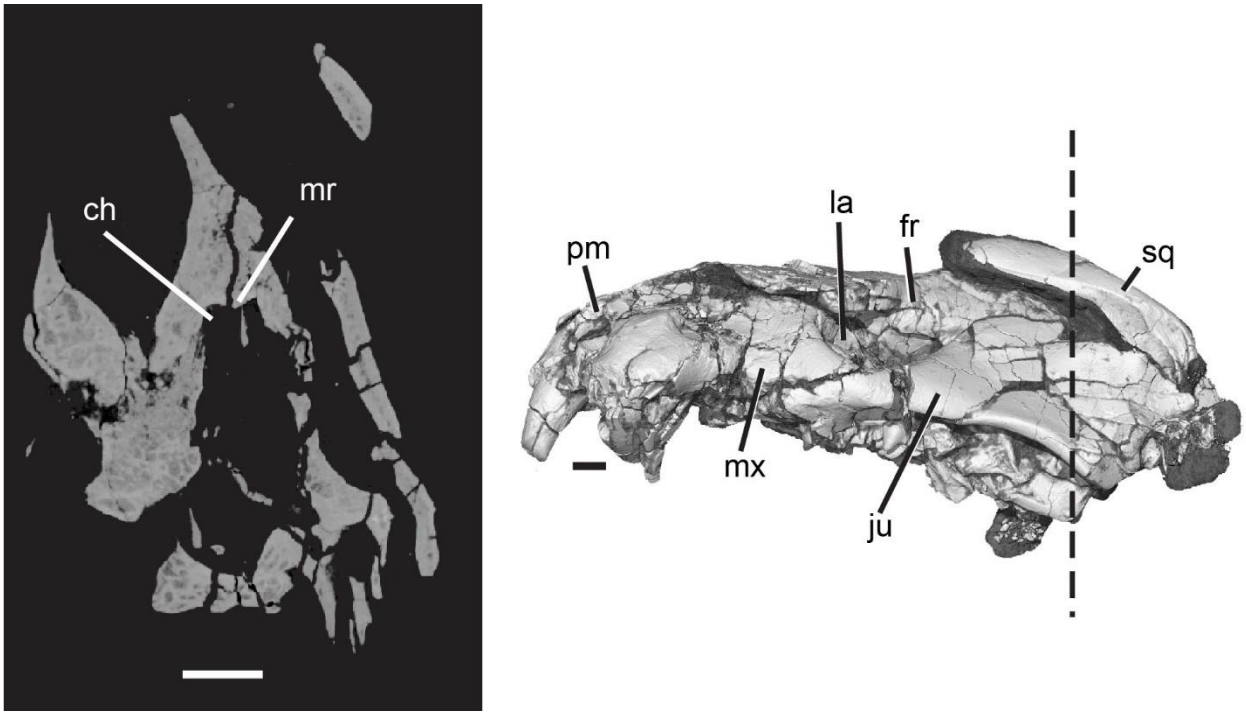

Figure 2.9: Braincase and volume rendering of *Kayentatherium* TMM 43647-10. The endocranial cavity preserves the impression of the cerebral hemispheres (ch) on the parietal. A medial ridge (mr) indicates an interhemispheric sulcus between the cerebral hemispheres. Scale bars = 5 mm. Abbreviations: **ch**, cerebral hemispheres; **fr**, frontal; **ju**, jugal; **la**, lacrimal; **mr**, medial ridge; **mx**¸maxilla; **pm**, premaxilla; **sq**, squamosal.

Chapter 3: The foramen magnum as a proxy for cynodont endocranial volume and the origin of the mammalian pyramidal tract[3]

INTRODUCTION

Large brains are a distinguishing feature of all mammals and are generally regarded as instrumental to the diversification and long evolutionary success of Mammalia. Understanding the evolutionary history of changing brain size relative to body size, or encephalization, among pan-mammals is of great interest to paleontologists and neontologists alike. In the oldest and most primitive members of the mammalian stem-group, the brain was small and the braincase only partially ossified. The lateral and ventral surfaces of the forebrain are not completely enclosed by bone. Additionally, the orbitosphenoid and pila antotica of the prootic, two bony elements associated with the ventral surface of the forebrain, are not sutured together and leave gaps in the ventral braincase. They are thin, delicate bones positioned within the skull, medial to the cranial roofing bones and secondary braincase wall (epipterygoid). Often, they are not preserved or easily observed, and they are inconsistently described in fossils. Consequently, reconstructing endocasts and measuring brain size relative to body mass (Encephalization Quotient or EQ) involves subjective decisions on bounding the endocranial cavity, and is a source of error in comparative studies. These effects are most pronounced in the most primitive and oldest pan –mammals, while error margins diminish somewhat as the braincase becomes more fully ossified in those taxa more closely related to crown mammals (Wallace et al., in prep).

High-resolution X-ray computed tomography (CT) scans of some fossils permits non-destructive visualization of these hidden braincase bones. Further, the boundaries of the brain and its associated meninges, nerves, and blood vessels can be digitally reconstructed from CT datasets using voxel-rendering software. Digital endocasts have now been reconstructed and described for a variety of non-mammalian therapsids including biarmosuchians and dinocephalians (Benoit et al., 2017a,b); dicynodonts (Laaß, 2015; Laaß and Kaestner, 2017); therocephalians (Sigurdsen et al., 2012); stem probainognathians including the tritheledontid

[3] Authors: R. Wallace and G. Wallace. R. Wallace wrote the paper and made figures. G. Wallace assisted with statistical analysis.

Riograndia (Rodrigues et al., 2018), *Brasilitherium* (Rodrigues et al., 2014), and *Pseudotherium* (Wallace et al., in prep); and the mammaliaforms *Morganucodon* and *Hadrocodium* (Rowe et al., 2011). Still others have been reconstructed and measured but not formally described (e.g., *Thrinaxodon* and *Diademodon* Rowe et al., 2011; *Massetognathus*, *Tritylodon*, therocephalians, and gorgonopsians Benoit et al., 2017b). X-ray computed tomography is the most common source of digital data, neutron tomography is another imaging techniques now applied to fossils (Laaß, 2015a,b; Laaß and Kaestner, 2017).

While CT technology has significantly facilitated endocast reconstruction, it is not a panacea. For instance, not all fossils are amenable to scanning. When the X-ray attenuation properties of the rock matrix match those of the fossil bone, distinguishing matrix from fossil can be a nearly impossible task. Further, digital endocasts are subject to the same limitation as natural endocasts. Even when specimens scan well, the endocasts have some fundamental limitations. Both natural and digital endocasts only depict the impression of the meninges and blood vessels surrounding the brain that leave an impression on the inner surface of the skull, and thus only approximates the shape of the brain (Bauchot and Stephan, 1967; Jerison, 1975; Kielan-Jaworowska and Lancaster, 2004). Methodologically, the boundaries of the endocranial space in most stem-mammals have to be delimited in digital endocast reconstruction for any place that is not defined by bone. This can lend a certain arbitrariness to the reconstructed endocast shape and size.

For example, the roof of the olfactory bulbs leaves a clear impression on the ventral surface of the frontals, but the floor of the olfactory bulbs leaves no bony trace or only leaves a partial trace if the orbitosphenoids happen to be preserved. The shape of the olfactory bulbs in the probainognathian *Brasilitherium* was approximated by mirroring the dorsal half of the olfactory bulb mold in the underside of the frontal (Rodrigues et al., 2014).

While objective, this method has the potential to inflate estimated brain volume. A comparable study of its close relative *Pseudotherium* enclosed missing segments of the braincase walls using straight lines and planar surfaces. This may systematically underestimate brain volumes, but may be more defensible (Wallace et al., in prep).

Similarly, reconstruction of the space that houses the infundibulum, or pituitary stalk, have also been subject to conflicting measurements. The mammalian pituitary gland fits snugly

into the sella turcica of the basisphenoid, and is connected to the hypothalamus by a thin stalk that contributes very little to brain volume. However, endocasts reconstructed for stem-mammals sometimes include a thick cylindrical volume between the sella turcica and the hypothesized diencephalon. Given the rarity of natural endocasts, the subjective uncertainties of producing virtual endocasts, and differing methods for measuring them, an alternative approach to estimating encephalization for stem-mammals and mammal fossils would be beneficial.

The foramen magnum, a large opening at the back of the skull for the passage of the spinal cord and other structures, has previously attracted attention from those seeking to estimate brain volume. In an early attempt to associate foramen magnum size with brain volume, the foramen magnum area was crudely approximated from width and height measurements using the equation $A = 1/4wh$ for 117 diverse placental mammal species (Radinsky, 1967). The log of the foramen magnum area was plotted against the log of the endocranial volume measured from the same specimens and a significant correlation was found between the two measurements for each mammalian clade sampled. The strong correlation between foramen magnum size and brain size was subsequently confirmed in a separate analysis of nine 'insectivoran' and primate taxa, again using crude measurements of foramen magnum area (Jerison, 1973: appendix III).

It is important to note that more than central nervous system tissue passes through the foramen. In addition to the transition between medulla oblongata and spinal cord, meninges (dura, arachnoid, and pia mater including the first denticulate ligament), tectorial membrane, alar ligaments, blood vessels to the brain (vertebral and spinal arteries), and a branch of cranial nerve XI (spinal portion of accessory nerve) all pass through the foramen magnum. Despite all this, foramen magnum size is strongly correlated with medulla oblongata size (Radinsky, 1967; Jerison, 1973: appendix III).

The size of the medulla oblongata and other brain regions, excepting the olfactory bulbs, are highly correlated with one another and with absolute brain volume. This concerted scaling has been described in mammals, and even in sharks, suggesting that brains follow a concerted model of evolution across vertebrates (Finlay and Darlington, 1995; Striedter, 2005; Finlay et al., 2001; Yopak et al., 2010). The cerebrum and cerebellum tend to vary in relative size across different taxa, supporting a mosaic model of brain evolution where brain regions evolve independently from other regions. Often, cerebrum and cerebellum enlargement coincides with

an increase in overall brain size following a hyperallometric model (Yopak et al., 2010). Concerted scaling of the vertebrate brain means that the foramen magnum area, which is correlated with medulla oblongata size, should allow us to predict absolute brain size in non-mammalian cynodonts.

Here, I collect endocast volumes from the literature and compare those values with the foramen magnum area of those specimens. The goal of this study is to quantify the relationship between endocranial volume and foramen magnum area in non-mammalian cynodonts. Another goal of this analysis will be to identify a relationship between foramen magnum area and cranial length in various amniote taxa. Results from this analysis may help predict encodranial volume from foramen magnum area for taxa that are not amenable to digital endocast reconstruction. Results may also assist with a diagnosis of taxa near the origin of mammals by revealing differences in relative foramen magnum size, and therefore a difference in relative brain size.

MATERIALS AND METHODS

Skull measurements collected for this study were taken from CT datasets archived at DigiMorph.org, at the University of Texas at Austin High-Resolution X-ray Computed Tomography Facility (UTCT). The lengths of skulls and area of foramen magna were measured from a total of 97 amniote taxa. Forty-eight were extinct and extant mammalian taxa, and seven were from stem-mammals. Skull length and foramen magnum area were also collected from 17 extant avians, and 25 extant lepidosaurs. X-ray computed tomography datasets for the taxa compared in this study were rendered as 3-D visualizations using the program VGStudio Max v. 2.1.

Reconstructed skulls were image-captured in the optimal view for measuring the foramen magnum's surface area. The angle and position of the foramen magnum relative to the plane of the face and braincase varies from taxon to taxon. Ancestrally, the foramen magnum opens posteriorly on the back of the skull. In some derived taxa, the foramen magnum may be angled ventrally relative to the plane of the braincase (e.g., the armadillo, *Dasypus* sp.) or anywhere in between. By marking the opisthion and basion (dorsal- and ventral-most points on the foramen magnum) in VGStudio, a plane of the foramen magnum could be established and oriented vertically. Then the skull could be rotated along the X-axis until the foramen magnum is

completely in view, with its dorsoventral plane parallel to the viewer. An image of the skull in this view was captured and opened in ImageJ. Using the polygon tool in ImageJ, the perimeter of the foramen magnum was outlined by applying polygon anchor points by hand on the bone-air interface, and the area was measured (Fig. 3.1).

Endocranial volumes were collected from the literature (Rowe et al., 2011: table S1; Colbert et al., 2005; Wallace and Rowe, in press). Endocranial volumes were collected for a total of eleven stem-mammals, and twenty-three mammals. The foramen magnum area was gathered from the same specimens to minimize any effects on size from sex and/or ontogeny. Some taxa have a notch in the dorsal margin of the foramen magnum (e.g., monotremes), that is filled in early development by the vermis of the cerebellum (Edinger, 1947; Simon, 2013). Because the notch is only a transient structure during ontogeny in tritylodonts, monotremes and some other mammals (Simon, 2013), the notch was not included in foramen magnum measurements. Appendix 3.A is the data table of the endocranial volume, foramen magnum area, and skull length data analyzed for this study.

Skull lengths of CT renderings were measured in ImageJ. Skull length for lepidosaurs were measured from the tip of the premaxilla to the distal-most point of the occipital condyles (Fig. 3.1A). Because birds are bipedal and have large brains, the foramen magnum is positioned horizontally under the endocranial cavity and the occiput balloons posteriorly beyond the foramen magnum. Therefore, avian skull length was measured from the tip of the bony part of the beak to the posterior end of the occiput (Fig. 3.1B). Finally, in mammals, landmarks for measuring skull length were more variable. Many different measurements are employed by mammalogists, depending on the species and the purpose for measuring (e.g., species identification, sex identification; Elbroch, 2006). These include condylobasal, basilar, basal, occipitonasal, and greatest skull length measurements. Basal length (tip of premaxilla to lower edge of foramen magnum) and condylobasal length (tip of premaxilla to posterior end of occipital condyles) were used most frequently in this study (Fig. 3.1C). All skull length measurements were recorded in millimeters.

Linear regressions were conducted using R (2017). Nonlinear regression were conducted using the R package “minpack.lm” (Elzhov et al., 2016). Type-1 error rate was set at $\alpha = 0.05$. For

post-hoc comparisons, family-wise error rates were controlled using the Tukey-Kramer method implemented in the R package "lsmeans" (Lenth, 2017). See Appendix 3.B for code.

RESULTS

Model selection

Endocranial volume and foramen magnum area are expected to scale allometrically with body size. Allometric scaling often follows a power law relationship, which may be fit to data with either nonlinear regression or linear regression log-log transformed data. The choice of model depends on the variance structure of the data (Xiao, 2011). If variance is additive on the original measurement model, residuals should be normally distributed and nonlinear models should provide a better fit. If variance is multiplicative on the original measurement scale, model residuals should be lognormally distributed (normally distributed on the log-log scale) and linear models of log-log transformed data should provide a better fit. To determine which models were appropriate, a nonlinear and a log-log linear model were fit for both the relationship between endocranial volume and foramen magnum area and the relationship between foramen magnum area and skull length. The four following models were fit, with $\varepsilon \sim N(0, \sigma)$.

$$E_i = A * (F_i)b + \varepsilon \quad \text{Equation 1}$$

$$Log(E_i) = a + b * \log(F_i) + \varepsilon \quad \text{Equation 2}$$

$$F_i = A * (S_i)^b + \varepsilon \quad \text{Equation 3}$$

$$Log(F_i) = a + b * log(S_i) + \varepsilon \quad \text{Equation 4}$$

Where E = endocranial volume in mL, F = foramen magnum area in mm^2, and S = skull length in mm.

Model fits were evaluated via AIC. The linear log-log models (Equations 2 and 4) provided a substantially better fit to the data compared to the nonlinear models (Equations 1 and 3) ($\Delta AIC_{eq2\text{-}eq1}$=903.773, $\Delta AIC_{eq4\text{-}eq3}$=228.8007). The Shapiro-Wilkes tests indicated residual errors were not normally distributed for the nonlinear models (W_{eq1} = 0.56382, p-value $_{eq1}$ = 5.547e-08; W_{eq3} = 0.56381, p-value $_{eq3}$ = 5.545e-08), but were normally distributed for the log-log transformed linear models (W_{eq2} = 0.96509, p-value $_{eq2}$ = 0.4568; W_{eq4} = 0.98276, p-value $_{eq4}$ = 0.2342). Thus, linear

models of log-log transformed data were selected to compare the relations between foramen magnum area vs. endocranial volume and skull length vs. foramen magnum area.

Endocranial volume and foramen magnum area

The relationship between endocranial volume and foramen magnum area was modeled including an effect for clade, with levels (Mammal, non-mammalian mammaliaforms, non-mammaliaform cynodonts). Mammals were set as the reference comparison.

$$Log(EV_i) = a + b * log(FM_i) + Clade + \varepsilon$$ Equation 5

Analysis of variance demonstrated that adding a clade term and an interaction term did not significantly improve the model fit (ANOVA Table 3.1).

Endocranial volume allometrically scales with foramen magnum area in all clades (Fig. 3.2; Model 3.3 in Appendix 3.B). Table 3.2 summarizes the results from modeling the linear correlation between log endocranial volume and log foramen magnum area in extinct and extant cynodonts.

The relationship of the endocranial volume to foramen magnum area in non-mammaliaform cynodonts is:

$$E_{NMC} = 1.59334F_{NMC} - 4.82421$$ Equation 6

Where E_{NMC} = log endocranial volume in milliliters, and F_{NMC} = log foramen magnum area in squared millimeters.

The relationship of the endocranial volume to foramen magnum area in non-mammalian mammaliaforms is:

$$E_{NMM} = 1.59334F_{NMM} - 5.5332$$ Equation 7

Where E_{NMM} = log endocranial volume in milliliters, and F_{NMM}= log foramen magnum area in squared millimeters.

The model in Equation 5 reveals a significant mean difference between mammals and non-mammalian mammaliaforms, upon Tukey-Kramer post-hoc testing (q = 2.545, df= 24, p = 0.0472, Table 3.3). However non-mammalian mammaliaforms only have two members in this sample, thus this difference finding may be spurious due to low power.

Foramen magnum area and skull length

The relationship between foramen magnum area and skull length was modeled including an effect for clade (Mammal, stem-mammals, Aves, and Lepidosaur). Mammals were set as the reference comparison.

$$Log(FM_i) = a + b * log(SL_i) + \varepsilon \quad \text{Equation 8}$$

Analysis of variance demonstrates that adding a clade term significantly improves model fit, while adding an interaction term does not significantly improve model fit (ANOVA Table 3.4).

Foramen magnum area allometrically scales with skull length in all clades ($p < 2e\text{-}16$). Table 3.5 summarizes the regression statistics between log skull length and log foramen magnum area in a linear regression model (Model 5.1 in Appendix 3.B). Extinct and extant mammaliaforms have a significantly larger foramen magnum proportional to skull length than do other amniotes, including non-mammaliaform cynodonts (Fig. 3.3). Tukey-Kramer post-hoc testing supports significant mean difference in foramen magnum size between mammals and non-mammaliaform amniotes (i.e., birds, lepidosaurs, and non-mammaliaform cynodonts), but not between mammals and mammaliaforms (Table 3.6). Thus the fossils *Morganucodon* and *Hadrocodium* scale with mammals, rather than non-mammaliaform cynodonts.

DISCUSSION

Endocranial volume is correlated with foramen magnum area

Endocranial volume and foramen magnum area are strongly correlated in cynodonts. This has been repeatedly shown in extant placental mammals (Radinsky, 1967; Jerison, 1973: appendix III), and now in extinct cynodont taxa as well. The sample size for non-mammalian cynodonts is small, with only two non-mammalian mammaliaforms and five non-mammaliaform cyndonts represented. More sampling will strengthen the predictive power of the equation. Although the endocranial volumes for numerous taxa are currently published, they could not be incorporated here because the occipital views of the specimens from which the volumes were measured were not published, and because the CT datasets are not archived on a publicly accessible online database. Therefore, foramen magnum measurements of those taxa are not presently available. This study demonstrates how the occipital view contains practical data, and

should be included in figures of descriptive analyses, along with measured foramen magnum area. This study also underscores the importance of publicly archiving digital data (Rowe and Frank, 2011). Multiple digital 3-D data repositories are available and should be utilized (Davies et al., 2017).

Results of this study show that equations 6 and 7 can be used for a rough approximation of endocranial volume E in stem-mammals when only the surface of the skull is available. All that is necessary is the presence of the complete foramen magnum for variable F. In other words, brain size can still be approximated for specimens that are not amenable to CT scanning, or that cannot be scanned for whatever reason. Similarly, these equations may be useful for incomplete specimens, or specimens with distorted braincases.

Relative size of the foramen magnum

Foramen magnum size is larger in mammaliaforms than in other amniotes including non-mammaliaform cynodonts. This increase in foramen magnum size correlates with an increase in olfactory bulb and cortex size, cerebellum size, and the origin of the six-layered neocortex, which collectively brought encephalization quotients up from about 0.1-0.22 in non-mammaliaform cynodonts to about 0.32 to 0.5 and greater in Mammaliaformes (Rowe et al., 2011). The foramen magnum area is strongly correlated with medulla oblongata size (Radinsky, 1967), and brain size in general (Finlay and Darlington, 1995; Striedter, 2005). This simultaneous increase of these brain regions supports a concerted model of brain evolution in Mammaliaformes, rather than a mosaic model. Mosaic brain evolution has been hypothesized within Mammalia (Barton and Harvey, 2000; Hager et al., 2012) in the context of concerted scaling (Striedter, 2005; Herculano-Houzel et al., 2014). One explanation may be that brain growth in mammals is restricted by the near cessation of adult neurogenesis (Finlay and Darlington, 1995; Finlay et al., 2001), though some claim this hypothesis to be weakly supported (Hager et al., 2012). However, it might explain why birds independently enlarged their brains without simultaneously enlarging their foramen magnum. Birds and other non-mammalian vertebrates are not limited by the same neurogenerative constraints as mammals because neurogenesis continues over their lifespan (Finlay and Darlington, 1995; Finlay et al., 2001), and indeed, mosaic brain evolution is documented across avian clades (Striedter and Charvet, 2008). Therefore, it seems likely that the pattern of

mammalian neurogenesis developed at least as early as Mammaliaformes. More thorough comparisons of brain region proportions in other synapsids can narrow in on when this developmental pattern arose in the synapsid lineage.

The evolution of the pyramidal tract

What contributed to the enlargement of the foramen magnum in Mammaliaformes? Unlike other vertebrates, the mammalian brain features paired motor tracts which are visible on the ventral service of the medulla oblongata called the medullary pyramids. The medullary pyramids are composed of axons that descend to the spinal cord from upper motor neurons residing in the neocortex. A majority of these axons decussate, or cross over, near the level of the foramen magnum and continue caudally in the lateral funiculus of the spinal cord. These motor axons terminate at various spinal segments, mostly in the cervical and lumbar enlargements, where they synapse with lower motoneurons and interneurons. This tract is therefore referred to as the corticospinal tract. Other upper motor neurons in the neocortex synapse with lower motor neurons in the brainstem, forming a tract called the corticobulbar tract. Together, the corticospinal tract and the corticobulbar tract comprise the pyramidal tract. The corticospinal tract acts in conjunction with other motor tracts, the rubrospinal tract and the reticulospinal tract. In these descending motor pathways, motoneurons and interneurons in the spinal cord are innervated by efferent neurons that reside in the brainstem, as opposed to the cortex. The cortex initiates movement in these pathways, but it does not synapse with alpha motoneurons as it does in the corticospinal tract. The rubrospinal and reticulospinal tracts are ancestral pathways used by other amniotes and possibly other vertebrates (Cruce and Newman, 1984). Therefore, the pyramidal tract is a novel addition to the mammalian central nervous system, and is significant in that the neocortex exhibits direct control over voluntary movement. This is believed to influence fine motor skill and coordination. Interestingly, the termination parameters of corticospinal axons (i.e., the spinal cord segment and the depth of the ventral horn where upper motor neurons synapse) are better predictors of dexterity than parameters of the corticospinal tract itself (i.e., area of the tract, fiber size, and fiber number; Heffner and Masterton, 1975).

The simultaneous evolution of near modern encephalization and large foramen magnum area suggests that the pyramidal tract emerged in concert with the origin of the neocortex.

Following Deacon's (1990) rule of 'large equals well connected' (Striedter, 2005, 2006), the origin of the neocortex in Mammaliaformes signifies major organizational changes in brain connectivity, and the origin of the pyramidal tract. In mammaliaforms such as *Morganucodon*, the pyramidal tract would have been small, terminated in the upper cervical segments of the spinal cord, and its axons would have mostly synapsed with spinal interneurons in the dorsal horn, as this is the condition in basal therians (Turner, 1924; Schieber, 2007). The pyramidal tract of the echidna *Tachyglossus aculeatus* differs from basal therians for having a more cranial decussation at the pons and a derived caudal termination at about the 24th spinal segment (Goldby, 1939). This is likely because the monotremes are derived with large neocortices, rather than a reflection of the ancestral condition. Convergent corticospinal pathways have arisen in birds including finches (Wild and Williams, 2000), owls (Karten, 1971), and parrots (Kalischer, 1905) in which the Wulst connects directly to the spinal cord. Therefore, it is not unreasonable to hypothesize that the pyramidal tract originated in Mammaliaformes when the enlarged dorsal cortex evolved and expanded control over descending motor pathways.

CONCLUSIONS

Foramen magnum area is a parameter that can be effectively used to estimate brain size in mammals and non-mammalian cynodonts. It is a particularly useful for non-mammalian cynodonts because the fossils are often crushed, incomplete, have an incompletely ossified braincase, and/or do not scan well with CT. A limit to relying on foramen magnum area is that the foramen magnum is not always preserved or is distorted from post-mortem deformation. Beyond encephalization estimation, the foramen magnum may have significance for studying the origin and evolution of the pyramidal tract. A preliminary comparison of foramen magnum size and skull length in lepidosaurs, avians, mammals, and a few non-mammalian cynodonts suggests that the foramen magnum enlarged when encephalization approached modern proportions in Mammaliaformes. Because the pyramidal tract is an additional descending motor pathway running along the ventral surface of the medulla oblongata and passes through the foramen magnum, this size change likely marks the origin of the pyramidal tract. More foramen magnum data on synapsids is needed, and it is therefore recommended that posterior views of skulls be published, and CT data be publicly archived. Because the pyramidal tract is involved in dexterity and coordination, it is clear that a

comparative anatomical approach to the appendicular skeleton across Synapsida would further shed light on the origin of the pyramidal tract.

Table 3.1: ANOVA comparing effect of clade on relationship between log endocranial volume and log foramen magnum area.

Analysis of Variance Table

```
Model 1: log(Endocranial_volume) ~ log(FM_area)
Model 2: log(Endocranial_volume) ~ log(FM_area) + Clade
Model 3: log(Endocranial_volume) ~ log(FM_area) * Clade
  Res.Df    RSS Df Sum of Sq      F  Pr(>F)
1     26 6.9079
2     24 5.4098  2    1.4981 3.3514 0.05364 .
3     22 4.9173  2    0.4925 1.1017 0.34994
---
Signif. codes:  0 ‘***’ 0.001 ‘**’ 0.01 ‘*’ 0.05 ‘.’ 0.1 ‘ ’ 1
```

Table 3.2: Statistics for linear correlation modeling relationship between log endocranial volume (mL) and log foramen magnum area (mm^2).

```
Call:
lm(formula = log(Endocranial_volume) ~ log(FM_area) + Clade,
    data = Skull_FM_EV)

Residuals:
     Min       1Q   Median       3Q      Max
-0.70665 -0.30244 -0.08282  0.33232  1.13542

Coefficients:
                  Estimate Std. Error t value Pr(>|t|)
(Intercept)       -4.56596    0.32333 -14.122 4.01e-13 ***
log(FM_area)       1.59334    0.07072  22.531  < 2e-16 ***
CladeMammaliaform -0.96739    0.38316  -2.525   0.0186 *
CladeNMC          -0.25825    0.29427  -0.878   0.3889
---
Signif. codes:  0 ‘***’ 0.001 ‘**’ 0.01 ‘*’ 0.05 ‘.’ 0.1 ‘ ’ 1

Residual standard error: 0.4748 on 24 degrees of freedom
  (76 observations deleted due to missingness)
Multiple R-squared:  0.9659,   Adjusted R-squared:  0.9616
F-statistic: 226.5 on 3 and 24 DF,  p-value: < 2.2e-16
```

Table 3.3: Tukey-Kramer post-hoc results testing differences of endocranial volume in clade means, controlling for foramen magnum size.

contrast	estimate	SE	df	t.ratio	p.value
Mammal - Mammaliaform	0.9673933	0.3831590	24	2.525	0.0472
Mammal - NMC	0.2582472	0.2942680	24	0.878	0.6593
Mammaliaform - NMC	-0.7091461	0.4484518	24	-1.581	0.2728

Results are given on the log (not the response) scale.
P value adjustment: tukey method for comparing a family of 3 estimates

Table 3.4: ANOVA comparing effect of clade on relationship between log foramen magnum area and log skull length.

```
Analysis of Variance Table

Model 1: I(log(FM_area)) ~ I(log(Skull_length))
Model 2: I(log(FM_area)) ~ I(log(Skull_length)) + Clade
Model 3: I(log(FM_area)) ~ I(log(Skull_length)) * Clade
  Res.Df    RSS Df Sum of Sq       F    Pr(>F)
1     95 28.015
2     91 11.880  4   16.1342 30.2657 8.867e-16 ***
3     87 11.595  4    0.2858  0.5361    0.7095
---
Signif. codes:  0 ‘***’ 0.001 ‘**’ 0.01 ‘*’ 0.05 ‘.’ 0.1 ‘ ’ 1
```

Table 3.5: Statistics for linear model comparing log foramen magnum area (mm^2) and log skull length (mm).

```
Call:
lm(formula = I(log(FM_area)) ~ I(log(Skull_length)) + Clade,
    data = Skull_FM_EV)

Residuals:
     Min       1Q   Median       3Q      Max
-0.92467 -0.23931 -0.02501  0.19077  1.10021

Coefficients:
                    Estimate Std. Error t value Pr(>|t|)
(Intercept)         -2.38030    0.23350 -10.194  < 2e-16 ***
I(log(Skull_length))  1.52231    0.05412  28.126  < 2e-16 ***
CladeAves           -0.75238    0.10212  -7.368 7.64e-11 ***
CladeLepidosaur     -0.82219    0.10076  -8.160 1.78e-12 ***
CladeMammaliaform   -0.01285    0.26902  -0.048    0.962
CladeNMC            -1.04874    0.17273  -6.072 2.88e-08 ***
---
Signif. codes:  0 ‘***’ 0.001 ‘**’ 0.01 ‘*’ 0.05 ‘.’ 0.1 ‘ ’ 1

Residual standard error: 0.3613 on 91 degrees of freedom
  (7 observations deleted due to missingness)
Multiple R-squared:  0.9391,   Adjusted R-squared:  0.9358
F-statistic: 280.9 on 5 and 91 DF,  p-value: < 2.2e-16
```

Table 3.6. Tukey-Kramer post-hoc results testing differences in foramen magnum size between clade means, controlling for skull length.

contrast	estimate	SE	df	t.ratio	p.value
Mammal - Aves	0.75238261	0.1021184	91	7.368	<.0001
Mammal - Lepidosaur	0.82218852	0.1007582	91	8.160	<.0001
Mammal - Mammaliaform	0.01285069	0.2690189	91	0.048	1.0000
Mammal - NMC	1.04874479	0.1727318	91	6.072	<.0001
Aves - Lepidosaur	0.06980591	0.1250760	91	0.558	0.9807
Aves - Mammaliaform	-0.73953192	0.2794061	91	-2.647	0.0704
Aves - NMC	0.29636217	0.1857018	91	1.596	0.5039
Lepidosaur - Mammaliaform	-0.80933783	0.2662047	91	-3.040	0.0251
Lepidosaur - NMC	0.22655626	0.1937277	91	1.169	0.7687
Mammaliaform - NMC	1.03589410	0.3177458	91	3.260	0.0133

P value adjustment: tukey method for comparing a family of 5 estimates

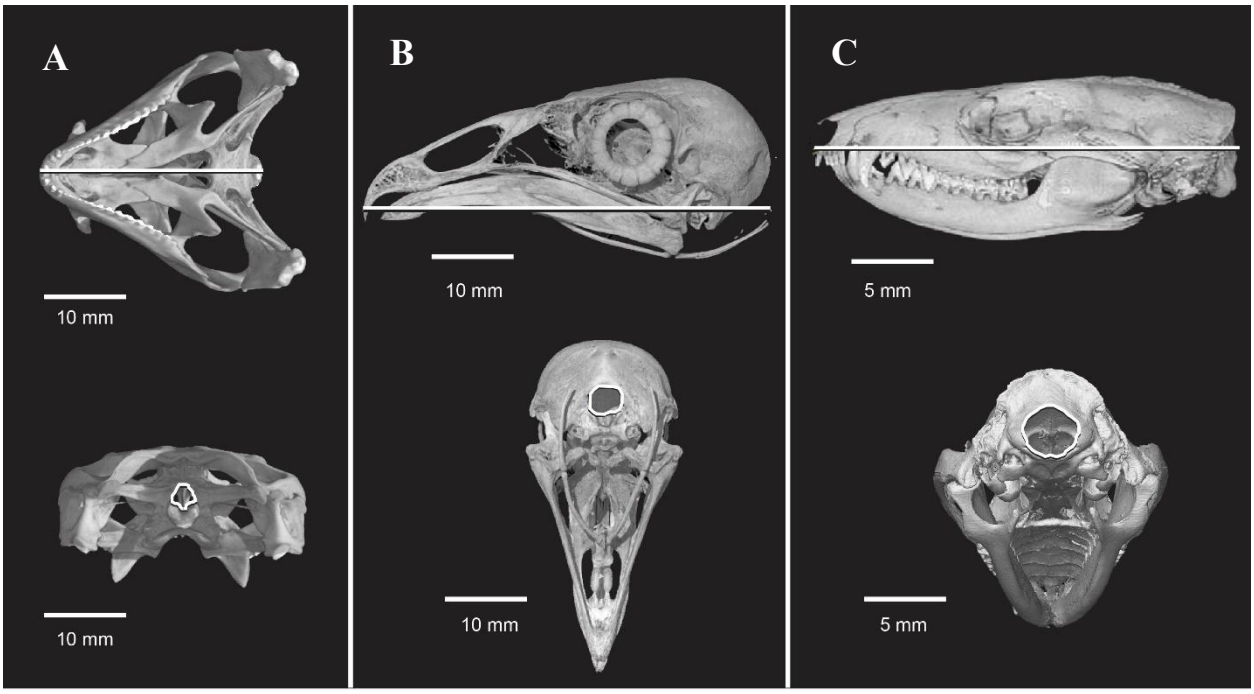

Figure 3.1: Examples of skull length (top) and foramen magnum (bottom) measurements for lepidosaurs (e.g., *Pogona vitticeps*, A), birds (e.g., *Coragyps atratus*, B), and mammals (*Monodelphis domestica*, C).

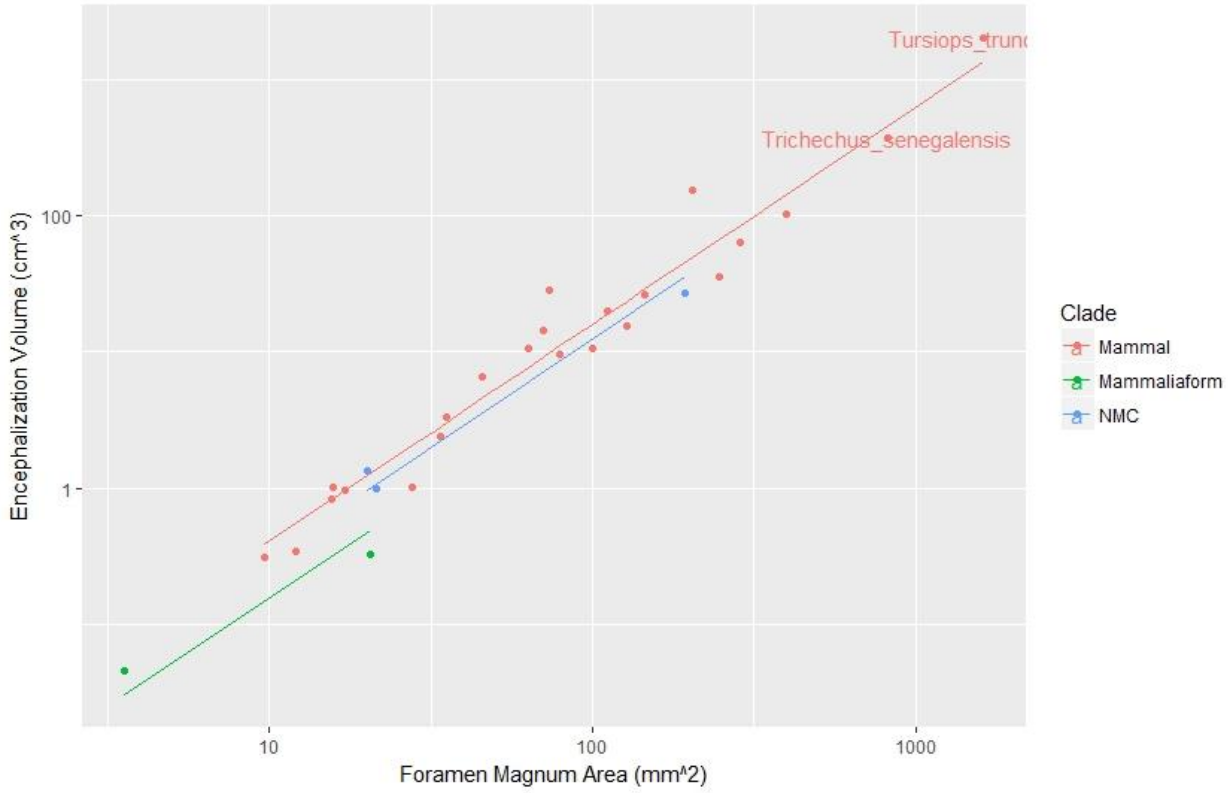

Figure 3.2: Scatterplot of endocranial volume (mm^3) and foramen magnum area (mm^2) for mammals, non-mammalian mammaliaforms ("Mammaliaform"), and non-mammaliaform cynodonts ("NMC").

Figure 3.3: Scatterplot of skull length (mm) and foramen magnum area (mm2) data for mammals, non-mammalian mammaliaforms ("Mammaliaforms"), non-mammaliaform cynodonts ("NMC"), avians, and lepidosaurs, transformed on a logarithmic scale.

Appendices

APPENDIX 1.A: CHARACTER LIST

Phylogenetic Analysis

The present phylogenetic analysis uses the Liu and Olsen (2010) morphological character matrix for Eucynodontia, with some modifications from Soares et al. (2014), and Martinelli et al. (2016, 2017). Such modifications include the recognition of *Brasilodon* and *Brasilitherium* as distinct taxa; the scorings for these taxa follow the scorings of Soares et al. (2014), with the exception of Character 13 pertaining to the prefrontal. Character state changes suggested by Soares et al., 2014 were used because the authors' justification for the character state changes were supported by the literature. The only exception was to the scoring of *Prozostrodon* for characters 13 and 14, which changed the character state from presence of prefrontal and postorbital by Liu and Olsen, 2010, to absence. Character 37, describing the relative length of the palatine in the secondary palate, was the only character change made by Soares et al. (2014), that was not accepted since the change did not impact the scoring of any taxa. Most changes to the scorings of taxa by Martinelli et al. (2016, 2017) were adopted in this analysis, except for those that came into conflict with the character changes made in the present study. For example, *Brasilodon* was rescored by Martinelli et al., 2016, for character 11 to a state that has been removed in this study; therefore, that change was not accepted.

1) Changes in character definition

Character 11. Lateral expansion of braincase in parietal region: absent (0); well-developed (1).

The braincase was described as lacking any lateral expansion (0), having a moderately developed lateral expansion (1), or being well-developed (2) and had the option of being analyzed as an ordered character. State 0 would reflect the plesiomorphic, tubular brain of most eucynodonts, while State 2 would reflect the unambiguously encephalized cranium of *Moranucodon* and mammals. *Therioherpeton*, *Riograndia*, *Pachygenelus*, and *Brasilodon* were scored State 1 (Liu and Olsen, 2010), with the implication that they exhibit an intermediate morphology in a trend toward increased encephalization. Later, brasilodontids were scored as having a well-developed, laterally expanded braincase (Soares et al., 2014), likely based on a

Brasilitherium endocast study (Rodrigues et al., 2013), the results of which are discussed in the anatomical description of *Pseudotherium*. *Morganucodon* has an unambiguously wide braincase relative to other eucynodonts, along with other cranial morphologies expected to accompany an enlarged brain including a low and lateral orbitosphenoid and floored cavum epiptericum (possibly the result of the lateral flange being pushed ventrally by the expanding brain in development). The comparably well-encephalized braincase of brasilodontids is dubious, and they lack those accompanying cranial morphologies. No definition has been provided for a plesiomorphic braincase width versus a moderate, or well-developed, laterally expanded braincase; discrepancies in identifying the brasilodontid braincase as moderately laterally expanded or well-developed suggests one is needed. After comparing figures of tritylodontids, tritheledonts, and brasilodontids, whose braincases appear comparable in width relative to snout width, there is no reason to have character states beyond a narrow braincase (0), and a well-developed, laterally expanded braincase (1), where non-mammaliaforms exhibit the primitive condition, and mammaliaforms exhibit the derived condition.

Character 62. Paroccipital process: undifferentiated (0); differentiated (1).

The paroccipital process character has been simplified from a three-state character to a two-state character. Morphological character matrices have described the paroccipital process as either undifferentiated, or differentiated into an anterior process and a bulbous posterior process (as is commonly described for tritylodontids), or a quadrate and mastoid process (scored for *Morganucodon*). For this analysis, this character was reduced to two states, describing a differentiated process and an undifferentiated process. In its original publication, the character was written as a two-state character, with states undifferentiated (0), or differentiated into a quadrate and mastoid process (1) (Rowe, 1988). The character has persisted in all subsequent phylogenetic analyses of eucynodonts. Eventually the character was modified to a more general absence (0) or presence (1) of bifurcation (Luo, 1994; Luo et al., 2001; Bonaparte et al., 2005), but still remained as two states. In both the original publication, and in subsequent publications, other characters were written to describe the shape of the anterior and posterior processes of the bifurcated paroccipital process. A third character state was recently added to include the shape of the bifurcated processes within the one character (Abdala, 2007). The character states for the paroccipital process included undifferentiated (0), differentiated in quadrate and mastoid

processes (1), or differentiated into anterior and posterior processes (2). The polarity of the character states has changed in subsequent publications (e.g., Liu and Olsen, 2010; Ruta et al., 2013), and the character state describing the anterior-posterior bifurcation has even been embellished to specify a "bulbous" anterior process (Liu and Olsen, 2010), no doubt elucidating the intent to distinguish between the bifurcated paroccipital process of the tritylodontids from the bifurcated paroccipital process of mammaliaforms. For this analysis, the character was reduced to the original two-state condition for two reasons. First, the distinction between the anterior and posterior processes of a bifurcated paroccipital process in tritylodontids vs. the quadrate and mastoid processes in mammaliaforms is not adequately defined. Further, brasilodontids do have a bifurcated paroccipital process, but a bulbous anterior process does not describe the condition in brasilodontids, nor does the quadrate and mastoid processes seem to be applicable. Second, the quadrate and mastoid process state seems to only apply to taxa within Mammaliaformes. Because this analysis is investigating the relationship of non-mammaliaform eucynodonts, such a distinction is not relevant. Therefore, reducing the paroccipital process character to its original two-state condition is more conservative and reasonable for the scope of this project.

Character 81. Shape of squamosal articulated surface for mandible: small and medially or anteromedially facing facet (0); wide, ventrally directed glenoid cavity (1).

Originally, Character 81 was a three-state character statement and State 0 read "absent." However, this state is not independent of Character 79, which describes the variation of craniomandibular joint composition. A quadrate/articular jaw joint (State 0 of Character 79) necessitates the absence of a mandibular articular surface on the squamosal. Further, Character 81 is a transformational character. "Absent" is not a shape and including it in a transformational character is a logical shortcoming (Sereno, 2007). Contingency coding, scoring inapplicable for taxa lacking the character, is recommended in this situation.

2) Changes in scoring of taxa

Character state changes from latest iteration of character matrix (Martinelli et al., 2017) for *Prozostrodon*, *Brasilodon*, and *Brasilitherium*

Character 13: *Prozostrodon* changes from 1 to 0 based on Bonaparte and Barbarena, 2001.

Brasilitherium changes from 1 to 0 based on Ruf et al., 2014.

Character 14: *Prozostrodon* changes from 2 to 1 based on Bonaparte and Barbarena, 2001.

Character 62: *Brasilodon* changes from 0 to 1 based on Bonaparte et al., 2003: figs. 3, 5b, and 6
Brasilitherium changes from ? to 2 based on CT images published in Rodrigues et al., 2013.

Character List

The following morphological character list was used in the present phylogenetic analysis of *Pseudotherium argentinus*. It uses the character list provided by Liu and Olsen, 2010, with changes to characters 96, 106, and 107 as suggested by Soares et al., 2014. Changes to characters 11 and 62 were made for the present analysis. Italicized acronyms indicate differences in how the character is written between present study and previous author(s). Acronyms and numbers refer to authors and their published character numbers: R, (Rowe, 1988); W, (Wible, 1991); WH, (Wible & Hopson, 1993); LL,(Lucas & Luo, 1993); L, (Luo, 1994); LC, (Luo & Crompton, 1994); M, (Martinez et al.,1996); H, (Hopson & Kitching, 2001); LCS, (Luo et al., 2001); B, (Bonaparte et al., 2003); S, (Sidor & Smith, 2004); MA, (Martinelli et al., 2005), BO, (Bonaparte, Martinelli & Schultz, 2005b); SH, (Sidor & Hancox, 2006); A, (Abdala, 2007); LO, (Liu and Olsen, 2010); SMO, (Soares et al., 2014). "#" before the character indicates that character is ordered in some analyses.

Rostrum

1. #Premaxillary extranasal process: absent or with very little exposure (0); large but not contacting nasal (1); contacting nasal (2). [*R2, W36*, L82, M14, A0]

2. Septomaxilla facial process: long, far beyond the posterior border of the external nares (0); short, almost limited in the external nares (1). [*S1, A1*, LO2]

3. #Snout in relation to the temporal region (to the posterior border, not the parietal crest): longer (0); subequal (1); shorter (2). [*A10*, LO3]

4. Paracanine fossa in relation to the upper canine: anteromedial (0), medial or posteromedial (1), anterior (2), paracanine fossa absent (3). [A13]

5. Premaxilla forms posterior border of the incisive foramen: absent (0), present (1). [M19, H1, B21, BO27, MA24, *A12*, LO5]

6. Maxillary platform lateral to the teeth series: absent (0); present (1). [M15, H77, BO15, *A22*, LO6]

7. Maxilla: excluded from (0), or participates in (1) border of subtemporal fenestra. [R15, W14, *L62*, M16, A20]

Skull roof

8. Profile of skull roof: nearly flat (0); remarkably concave (the parietal crest is higher than the extension of anterior surface) (1); convex (the parietal crest is lower than the extension of anterior surface) (2). [*S7*, *A64*, LO8]

9. Parietal foramen: present (0); absent (1). [R8, W12, LL34, L64, M31, H7, B24, BO34, MA28, A6]

10. Interparietal (postparietal) in adult: separate bone in adult (0); fused with other bones (1). [R21, W15, *LL36*, M34]

11. #Lateral expansion of braincase in parietal region: absent (0); well-developed (1). [*L67, M33, LO11*]

12. Parietal crest posteriorly extending close to or reach the posteriomost position of the occipital crest: absent (0); present (1). [LO12]

Orbital region

13. Prefrontal: present (0); absent (1). [R4, W1, M28, H3, B22, BO30, MA25, A3]

14. #Postorbital bar and postorbital: present (0); postorbital present but not forming postorbital bar (1); both absent (2). [*R7, W2, LL33, L55, M29, H5, B23, B40, BO31, BO32, MA 50, A5*, LO14]

15. #Palatine: do not meet the frontal (0); meets frontal but two elements without significant contribution to medial orbit wall (1); meets frontal and two elements with significant contribution to medial orbit wall (2). [*R6, R31, W17, W37, L56, L60, M24, M30, H23, B29, BO46, MA38, A62*, LO15]

16. Sphenopalatine foramen: absent (0); present (1). [*L57, M26*, LO16]

Zygomatic arch

17. Zygomatic arch dorsoventral height relative to skull length: moderately deep (10~18%) (0); very deep (>18%) (1); slender (2) (<10%). [*R16, W40, L54, M39, H18, S5, BO40, MA33, A68*, LO17]

18. The anteroventral corner of the zygomatic arch: lie at the same level as (0); or remarkably higher than (1) the postcanine line. [LO18]

19. Infraorbital process: absent (0); suborbital angulation between maxilla and jugal (1); descending process of the jugal (2). [*M18*, *H21*, *H41*, *A25*, *B38*, *BO29*, *BO44*, *MA36*, *MA46*, A69, LO19]

20. #Zygomatic arch dorsal extent: below middle of orbit (0); above middle of orbit but still level within orbit (1); beyond the upper border of the orbit (2). [*H19*, LO20]

21. Posterior extension of jugal along zygomatic arch: extending back near quadratojugal notch of squamosal (0), extending back near squamosal glenoid (1), reduced and receding from glenoid (2). [*L28*, LO21]

22. The posteroventral process of jugal: low (0); high, forming more than half height of zygomatic arch (1). [*H20*, *BO43*, *A70*, LO22]

23. The width of temporal fossa: reach greatest near middle (0); same throughout or little change (1); strongly increase backward, the posterior width much bigger than the anterior width (2). [*H39*, *BO42*, *MA44*, A73, LO23]

24. Squamosal groove for external auditory meatus: without or with an incipient depression (0); deep (1). [*M55*, *H22*, *B28*, *S18*, *BO45*, *MA37*, *A72*, LO24]

25. Posterior extension of the squamosal dorsal to the squamosal sulcus in zygomatic arch: incipient (0); well developed (1) [*A71*, LO25]

26. The notch separating lambdoidal crest from zygomatic arch: shallow (0); deep, "V"-shape (1). [*H43*, *S17*, *BO55*, *A74*, LO26]

Palatal complex

27. Palatine: excluded from subtemporal border of orbit (0); participates in subtemporal border by displacing pterygoid posteriorly (1). [L58]

28. Vomer exposure in incisive foramen (at anterior ends of maxillae on palate): present (0); absent (1). [*M21*, LO28]

29. Vomer: with (0) or without (1) vertical septum extending posterior to level of secondary palate. [SH63]

30. Ectopterygoid: does not contact maxilla (0); contacts maxilla (1); absent (2). [*R32, H9, S15, A19*, LO30]

31. Interpterygoid vacuity in adults between pterygoid flanges: present (0); absent (1). [M27, H10, B25, BO35, MA29, A24]

32. Secondary palatal plate on maxilla reaches midline: absent (0); present (1). [H12, S11, *A15*, LO32]

33. Secondary palatal plate on palatine reaches midline: absent (0); present (1). [H13, S12, *A15*, LO33]

34. Posterior extent of osseous secondary palate: far from (0), close to or beyond (1) rear upper postcanine row. [R30, W16, *L68*, M23, LCS40, *H14, B26, BO36, MA30, A17*, LO34]

35. #The posterior end of secondary osseous palate relative to anterior border of orbit: anterior (0); about equal level (1); posterior (2). [H15, B27, BO38]

36. Osseous palate extension: 45% of skull length or less (0); more than 45% of skull length (1). [A16]

37. Contribution of palatine to osseous secondary palate: short (less than 1/3) (0); long (greater than 1/3) (1) [M22, *H40, B37, BO53, MA45, A18*, LO37]

38. Middle of pterygoid: smooth (0); a boss (1); a distinct median crest (2). [*LL12, L71, A25*, LO38]

39. The nasopharyngeal roof posterior to the transverse process of pterygoid: narrow,

deep, ventrally forms a keel (0); wide, flat, the narrowest place greater than half the width of the transverse process (1). [LO39]

40. Quadrate ramus of pterygoid: present (0); absent (1). [R38, W47, *LC10*, M40, H30, B34, BO52, S20, MA43, A29]

41. Quadrate articulation with quadrate ramus of epipterygoid: absent (0); present (1). [*LC11*, M53, *A30*, LO41]

Basicranium, and lateral wall of the braincase

42. Frontal-epipterygoid contact: present (0), absent (1). [*R39, W48, L61*, H35, S24, A63]

43. Epipterygoid ascending process at level of trigeminal foramen: greatly expanded (0); moderately expanded (1). [H32, B35, A66]

44. The anterior part of the basisphenoid: narrow (0); wide, and the width greater than half the width of the transverse process (1). [*L69, LCS44*, LO44]

45. Parasphenoid ala: at the same level as the basicranium (0); ventrally expanded below the basicranium (1). [*H17, BO39*, *MA32,* A28, LO45]

46. #Basisphenoid wing (parasphenoid ala): long, border the fenestra vestibuli (0); slightly reduced and excluded from oval window, overlap the entire prootic cochlear housing (1); greater reduced and overlapping a part of the pars cochlearis (cochlear housing) (2); basisphenoid does not overlap the petrosal pars cochlearis (3). [*R40, W49*, L74, *M41, M49, LCS37, A27*, LO46]

47. #Overlap of the basioccipital to the pars cochlearis: entire cochlear housing (0);

the medial side of the promontorium (1); no overlapping (2). [LCS 38]

48. Internal carotid foramina in basisphenoid: present (0); absent (1). [*R42, W50, WH23,* LL14, L72, M45, H26, B31, BO48, MA40, A26]

49. Prootic and opisthotic: separated (0); fused at early ontogenetic stage to form petrosal (=periotic) (1). [R51, W5, WH29, L34, BO56, A36]

50. Promontorium (Pars cochlearis of petrosal): absent (0); present (1). [R52, W6, *LL1*, *L35,* LCS9, *BO57,* A34]

51. Internal auditory meatus: open (0); walled (1). [*R53, W7, WH12, L39, M47, H36, B36,* A37]

52. #The trigeminal ganglion (semilular ganglion): open ventrally (0); partial prootic floor (1); complete prootic floor (2). [W54, A33]

53. Lateral trough floor anterior to the tympanic aperture of the prootic canal and/or the primary facial foramen: absent (0); present (1). [*R49, LL6, L43, M44,* LCS 15]

54. Vascular foramen in the posterior part of the lateral flange (Foramen "X" of (Rougier et al., 1992) (p205)): absent (0); present (1). [*LL30*, *L53, M43*, LCS29]

55. Foramen and passage of prootic sinus on lateral trough: absent (0); present (1). [*R50, W28, LL3, L45, MA49, BO58, A35*, LO55]

56. Route of the venous drainage exiting from the back of the cavum epiptericum: only lateral flange vascular groove (0); absent (1); lateral flange vascular canal present (foramina on lateral surface) (2). [W53, WH22, *H27*, LO56]

57. #Maxillary and mandibular branch (V2+3) of the trigeminal nerve exit: via single foramen between prootic and epipterygoid (0); via two foramina between prootic and epipterygoid (1); via separate foramina, some enclosed by anterior lamina of prootic (petrosal) (2). [*L50, M48, H28, B33 BO51, S27, MA42, A65*, LO57]

58. Pterygoparoccipital foramen: squamosal does not contribute to enclosure of foramen (0); squamosal contributes to enclosure of foramen (1); open (2). [*LL23, L51*]

59. Vertical component of lateral flange of prootic ("L-shaped" and forming a vertical wall to pterygoparoccipital foramen): absent (0); present (1). [*L52*, LCS25]

60. Anterior part of paroccipital process: the lateral aspect covered by the squamosal (0); exposed due to dorsally withdrawn of the squamosal (1). [*L47*, LCS22]

61. Hyoid (stapedial) muscle fossa on the paroccipital process: absent (0); present (1). [R55, W56, WH35, LL7, L40, M59, LCS32, MA48, BO61, *A38*, LO61]

62. Paroccipital process: undifferentiated (0); differentiated (1). [*R56, W18, L46, L47, M50, LCS21, LCS30, BO66, A43, LO62*]

63. Separation of fenestra rotunda and jugular foramen: confluent (0); completely and widely separated (1). [R60, W29, *LL10, L42*, M46, *HK42*, LCS33, *B39*, *BO60*, A40]

64. Articulation of the paroccipital process with the quadrate: absent (0); present (1). [*R19, W41, M52, H29, A32*, LO64]

Occipital region

65. Paroccipital process in the base of the posttemporal fossa: absent (0); present (1). [*H24, A44*, LO65]

66. Tabular: present (0), absent (1). [R22, LL19, L80, *LCS 47*, LO66]

67. The relationship of hypoglossal foramen (condylar foramen) with the jugular foramen: confluent or sharing a depression (0); at least one foramen completely separated from the jugular foramen (1). [*LL11, L75, M51, LCS39, BO65*]

68. Shape of the occipital condyles (in lateral view): bulbous (0); ovoid to cylindrical (1). [*LL15, L77*, LCS51]

Craniomandibular joint

69. #Rotation of dorsal plate relative to trochlear axis on quadrate: less than 10 degree (0); about 45 degrees (1); around 90 degrees (2); parallel to trochlear axis (3). [L30, LC1]

70. Curvature of the contact facet on the posterior side of the dorsal plate of quadrate: flat or convex (0); concave (1). [*L29, LC2, M56*, LO70]

71. Size of the lateral trochlear condyle relative to the medial trochlear condyle on quadrate: the lateral condyle larger than the medial condyle (0); the medial condyle equal or larger than the lateral condyle (1). [*LC3*, LO71]

72. Shape of the trochlear of quadrate: cylindrical (0); trough-shaped (1). [LC4]

73. #Lateral margin of the dorsal plate of quadrate: straight (0); flaring posteriorly (1); flaring and rotated posteromedially (2). [LC5]

74. #Medial margin of the dorsal plate of quadrte: straight (0); flaring anteriorly (1); flaring and rotated anterolaterally (2). [LC6]

75. Dorsal margin of dorsal plate of quadrate: retains pointed angle (0); has rounded margin (1) [L31, LC7]

76. #Lateral notch and neck of quadrate (separation of the lateral margin of the contact facet from the trochlear): the lateral notch is absent or poorly developed (0); lateral notch developed, separating the lateral margin of the contact facet from the lateral end of the trochlear (1); lateral notch is broader and separation of the lateral margin of contact facet for the trochlear is wider, the lateral margin is shifted medially (2); development of the neck with raise the contact facet away from the trochlear (3). [*L32*, LC8]

77. Articulation of the quadrate with the squamosal: via concave recess in the squamosal (0); covered dorsally by the squamosal (1); little or no contact with the squamosal (2). [*WH7, LC12*, M54, *H31, A60*, LO77]

78. Articulation of the quadrate with the stapes: via a broad recess on the medial margin and the median end of the trochlear (0); the stapedial contact restricted to the medial end of the trochlear (1); via a projection from the medial margin of the dorsal plate (2); via a medial vertical ridge in the neck (3); via a projection from the neck of the quadrate (4). [*R20, W42*, *L33*, LC14]

79. Craniomandibular articulation; quadrate/articular (0); main quadrate/articular, secondary surangular/squamosal (1); incipient dentary/squamosal (2); main dentary/squamosal (3). [*R66*, *R67*, *W9*, *W60*, *L23*, *L24*, *M60*, *H25*, *LCS 70*, *B30*, *S19*, *BO26*, *MA39, A58*, LO79]

80. Craniomandibular articulation: lies around the same height (0), much lower (1) or

remarkably higher (2) than the postcanine line. [*L25*, *A59*, LO80]

81. Shape of squamosal articulation surface for mandible: small and medially or anteromedially facing facet (0); wide, ventrally directed glenoid cavity (1). [*L26*, *B19*, *BO37*, *MA22*, *A57*, LO81]

Mandible

82. Dentary symphysis: unfused (0); fused (1). [R68, W10, L19, LCS56, H44, B17, S34, BO21, MA21, A61]

83. #Lateral ridge of the dentary: absent (0); incipient (1); moderatly developed (2); strongly projected (3). [A47]

84. Angle of the dentary: close to the position of postorbital bar (0); close to the jaw joint (1). [*A54*, LO84]

85. Position of dentary-surangular dorsal contact relative to postorbital bar and jaw joint: around midway (0); closer to jaw joint (1). [*H48*, *A55*, LO85]

86. Mediolateral thickening of the anterior margin of the coronoid process: absent (0); present (1). [M66, H50, A51]

87. Splenial: large and deep, reaches ventral border of the dentary (0); reduced to thin splint covering dentary groove (1). [M64]

88. #Postdentary bones: large, with tall surangular (0); angular, surangular, and prearticular reduced in height and lying in dentary groove (1); further reduced to single gracile rod in postdentary trough (2). [R74, W59, M65, H49]

89. Reflected lamina of angular posterior extent relative to distance from angle of dentary to jaw joint: greater than 1/2 the distance (0); less than l/2 the distance (1). [H51]

90. #Reflected lamina of angular shape: spoon-shaped plate with slight depressions (0); hook-like lamina (1); reduced to thin process (2) [*M62, H52, S44,* A56]

91. Mandibular movement during occlusion: orthal movement during power stroke (0); posteriorly directed power stroke (1); moderate rotation along the longitudinal axis in power stroke (2). [*R79, W62, L2,* LCS74, *B2, BO2,* LO91]

Dentition

92. Postcanine occlusion: lack consistent contact relationship (0); bilateral, interdigitating occlusion between multiple cusps (1); precise unilateral occlusion (2) [*R84, R86, W33, L1, L14, M8, LCS 73, LCS 81, B1, BO1, MA1, A87,* LO92]

93. Relationships of wear facet to main cusp: wear facet absent (0); simple longitudinal facet on crown (1); main cusp bears two distinct facets (2); multiple cusps with each cusp bearing one or two transverse and crescentic facets (3). [*L17, B16, MA19, BO20,* LO93]

94. Upper incisors number: five or more (0); four (1); three or less (2). [*R81, W63, L5, M1, H53, B3,* S45, BO3, MA3, A76]

95. Lower incisor number: four or more (0); three (1); two or less (2). [L5, M2, H54, B4, S46, BO4, MA4, A77]

96. Incisor size: all of similar size (0); some incisors large (1). [H56, *B5, B6, BO5, MA5,*

MA6, *MA7*, A78, LO96, SMO96]

97. Incisor cutting margins: smoothly ridged (0); serrated (1); denticulated (2). [*H55*, *A79*, LO97]

98. Distinct upper incisor/canine diastema: present (0); absent (1). [*A81*, LO98]

99. Upper canine: large (0); reduced in size (<10% of skull length) (1); absent (2). [*L6*, H57, A83]

100. Lower canine: large (0); reduced in size (1); absent (2). [L6, H58, A84]

101. Canine serrations: absent (0); present (1). [H59, A8]

102. Upper postcanine morphology: sectorial without or with incipient cingulum broadening the crown (0); sectorial with a well-developed lingual cingulum (1); bucco-lingually expanded (2). [*L13*, *M5*, *M9*, *H60*, *H62*, *A7*, *S51*, *S55*, *B10*, *BO8*, *A89*, LO102]

103. #Anteriormost one-cusped tooth: present till adult (0); present only in juvenile (1); absent (2). [LO103]

104. #Posteriormost gomphodont postcanine(s) in adults: absent (0); absent in juvenile but present in adult (1); present from juvenile (2). [H80]

105. Posterior postcanines with strongly curved main cusp: absent (0); present (1). [*S52*, A90]

106. Upper postcanine roots: single (0); constricted root, with longitudinal groove (1); divided into two longitudinal aligned roots (2); multiple roots (more than two) (3). [*R88, W65, W66, L9, M6, LCS77, B8, BO6, MA9, A95, LO106, SMO106*]

107. Lower postcanine roots: single (0); constricted root, with longitudinal groove (1); divided (2). [*R88*, W65, *L9*, M7, *B8, BO6, MA9, A94*, *LO107, SMO107*]

108. Buccal (external) cingulum on sectorial upper postcanines: absent (0); present (1). [*R85, H61, B9, BO7, MA10, A91*, LO108]

109. Number of upper cusps in transverse row: one (0); two (1); three or more (2). [H63, A9*2*]

110. Position of upper transverse cusp row on crown: midcrown (almost to posterior margin) (0); on anterior half of crown (1); at posterior margin (no posterior cingulum) (2). [H64]

111. Central cusp of upper transverse row: absent (0), midway between buccal and lingual cusps (1); closer to lingual cusp (2). [H65]

112. Arrangement of main cups of upper postcanines: in single longitudinal row (0); multiple cusps in multiple rows (1). [L13, LCS78]

113. Interlocking of lower postcanines: absent (0); distal cuspule ‘d’ of anterior molar fits into embayment between cusp ‘b’ and cusp ‘e’ of the succeeding molar (1). [L11, B14, BO18]

114. Number of lower cusps in transverse row: two (0), three or more (1). [*H73*, LO114]

115. Lingual cingulum on lower postcanine: present (0); vestigial or absent (1) [*L12*,

LCS80, *B11*, *B12*, *BO9*, *BO10*, *S56*, *A93*, LO115]

116. Lower posterior basin: absent (0); present (1). [H75]

117. Axis of posterior part of maxillary tooth row: directed lateral to subtemporal fossa (0); directed toward center of fossa (1); directed toward medial rim of the fossa and diverged (2); directed toward medial rim of the fossa and parallel (3). [*R80*, *M12*, *H78*, *B13*, *MA17*, *MA20*, *BO14*, *BO16*, *BO17*, *A86*, LO117]

118. Upper tooth series posterior extension: below the orbit and anterior to the subtemporal fenestra (0); anterior to the orbit (1); behind the anterior border of the subtemporal fenestra (2). [*H79*, *A75*, LO118]

119. Postcanine replacement pattern: alternating (0); delayed (1); at most single replacement for one position (2); sequential addition of postcanines, no replacement (3). [*L7*, *H81*, *LCS89*, *B7*, LO119]

Postcranial skeleton

120. Vertebral centra: amphicoelous (0); platycoelous (1). [R108, H101, B51, BO78, MO61]

121. Axis centrum: cylindrical (0) or depressed (1). [R98]

122. Dens: absent or vestigial (0) or strongly developed (1) [R99]

123. Posterior thoracic vertebrate (or middle of the dorsal vertebrate): neural spines slightly inclined or nearly vertical (0) or strongly inclined (1). [*R102*, LO123]

124. Anapophysis: absent (0); present (1). [LO124]

125. Expanded costal plates on dorsal ribs: absent (0); present (1). [H82]

126. Lumbar costal plates with ridge overlapping preceding rib: absent (0); present (1). [H83]

127. #Acromion process: absent (0); weak to moderate (1); strongly developed and close to level of glenoid (2). [R115, H85]

128. Scapular constriction below the acromion process: absent (0); present (1). [H86]

129. Scapular elongation between the acromion and glenoid: absent (0); present (1). [H87, *B41, BO68, MO51,* LO129]

130. Procoracoid in glenoid: present (0); barely present or absent (1). [R116, H88, B42, BO 71, MO52]

131. Procoracoid contact with scapula: greater than coracoid contact (0); equal to or less than coracoid contact (1). [H89, B43, BO72, MO53]

132. Humeral ectepicondylar foramen: present (0); absent (1). [R124, H90, B44, BO73, MO54]

133. Ulnar olecranon process: unossified or poorly ossified (0); well ossified (1). [*R128, H91, B45, MO55,* LO133]

134. Manual digit III phalanx number: four (0); three (1). [H92]

135. Manual digit IV phalanx number: four (0); three (1). [H93]

136. Dorsal profile of ilium: strongly convex (0); flat to concave (1). [R130, H96, B48, BO75]

137. Length of anterior process of ilium anterior to acetabulum (relative to diameter of acetabulum): less than 1.5 (0); greater than 1.5 (1). [H94, B46, BO74, MO56]

138. Lateral surface of iliac blade: concave or nearly flat (0); convex (1); a longitudinal ridge divides it into dorsal and ventral moieties (1). [*R131*, LO138]

139. Posterior iliac spine: robust and extends beyond acetabulum (0); reduced to small nub that lies entirely anterior to acetabulum (1). [R132, *R133*, LO139]

140. Cotyloid (acetabular) notch: lies between the ischial and iliac part of the acetabulum, mainly on ilium (0); between acetabular facet and pubic process of the ischium, on ischium (1). [*R134*, LO140]

141. The diameter of the obturator foramen greater than that of the acetabulum: absent (0); present (1). [*R139*, LO141]

142. Femoral head: rounded and predominately in plane of shaft (0); subspherical and inflected dorsally (1). [R141]

143. Greater trochanter separated from femoral head by distinct notch: absent (0); present (1). [R143, H98, B49, BO76, MO59]

144. Lesser trochanter position: on ventromedial surface of femoral shaft (0); on medial surface of femoral shaft (1). [R144, H100, B50, BO77, MO60]

145. Lesser trochanter location near the level of the femoral head: absent (0); present

(1). [BO80, MO63]

APPENDIX 1.B: PAUP OUTPUT

```
P A U P *
Version 4.0b10 for 32-bit Microsoft Windows
Thu Jul 06 13:05:28 2017

      -----------------------------NOTICE---------------------------
        This is a beta-test version.  Please report any crashes,
        apparent calculation errors, or other anomalous results.
        There are no restrictions on publication of results obtained
        with this version, but you should check the WWW site
        frequently for bug announcements and/or updated versions.
        See the README file on the distribution media for details.
      --------------------------------------------------------------

Heuristic search settings:
  Optimality criterion = parsimony
    Character-status summary:
      Of 145 total characters:
        All characters are of type 'unord'
        All characters have equal weight
        All characters are parsimony-informative
    Gaps are treated as "missing"
    Multistate taxa interpreted as uncertainty
  Starting tree(s) obtained via stepwise addition
  Addition sequence: random
    Number of replicates = 1000
    Starting seed = 1080186551
  Number of trees held at each step during stepwise addition = 1
  Branch-swapping algorithm: tree-bisection-reconnection (TBR)
  Steepest descent option not in effect
  Initial 'MaxTrees' setting = 100
  Branches collapsed (creating polytomies) if maximum branch length is zero
  'MulTrees' option in effect
  Topological constraints not enforced
  Trees are unrooted

Heuristic search completed
    Total number of rearrangements tried = 37498754
    Score of best tree(s) found = 444
    Number of trees retained = 8
    Time used = 9.36 sec

Tree-island profile:
                 First      Last                 First   Times
```

Island	Size	tree	tree	Score	replicate	hit
1	8	1	8	444	1	964
2	14	-	-	447	673	1
3	6	-	-	447	267	1
4	5	-	-	447	58	7*
5	3	-	-	447	143	1
6	2	-	-	447	136	5*
7	1	-	-	447	22	19*
8	0	-	-	447	345	2*

Note(s):
* Multiple hits on islands of unsaved trees may in fact represent different islands

8 trees saved to file "C:\Users\Dell Laptop\Documents\PhD\Phylogenetic analyses\Brasilodontid analysis\Jan 11 2017\Character81edit.tre"

Strict consensus of 8 trees:

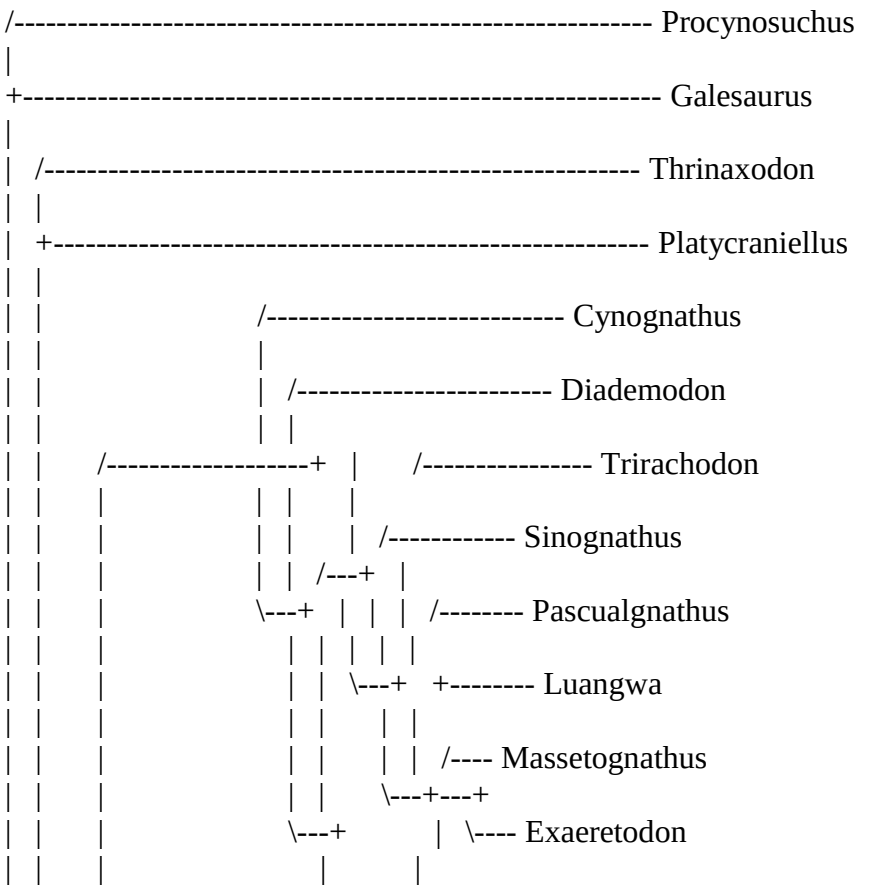

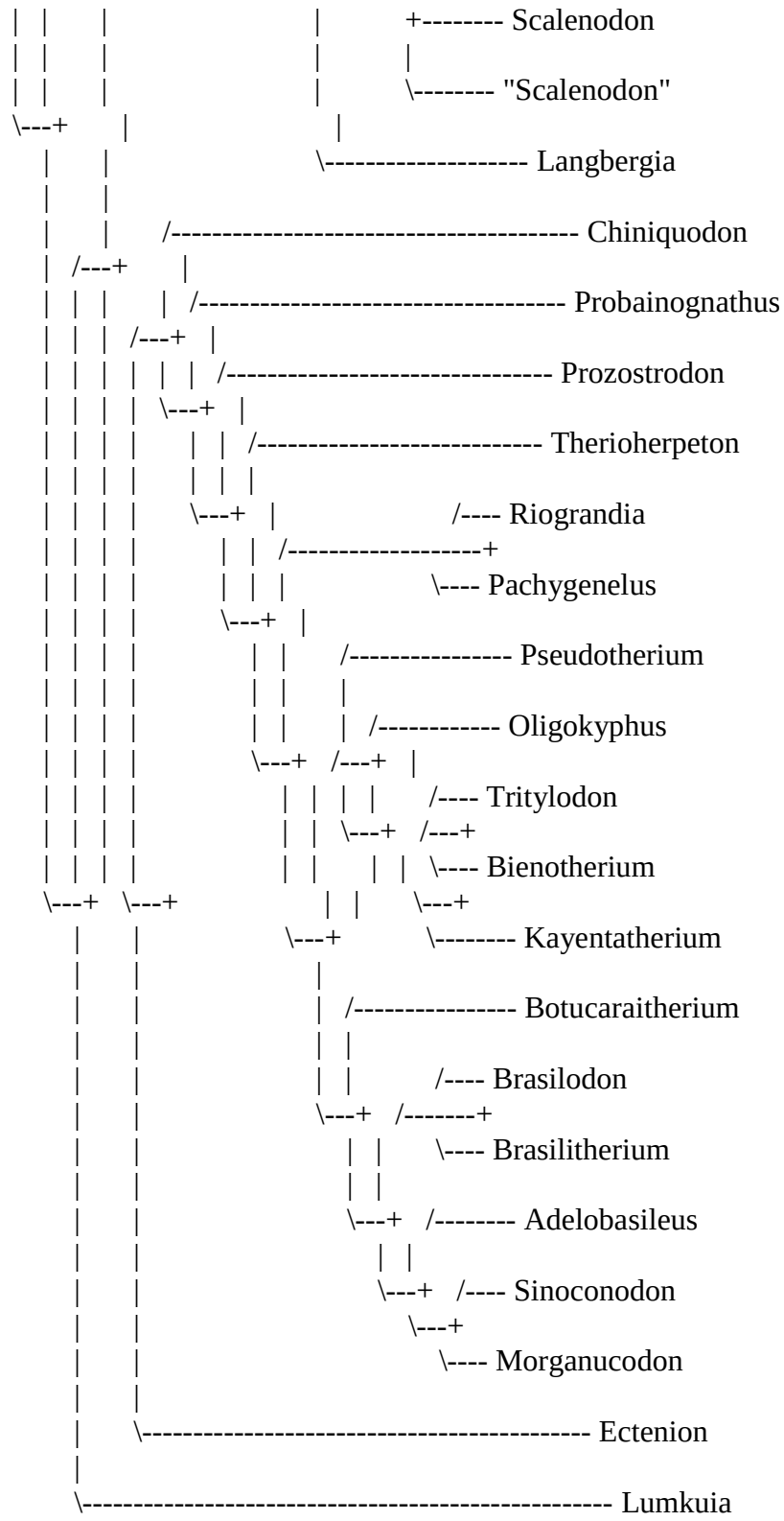
Scalenodon
"Scalenodon"
Langbergia
Chiniquodon
Probainognathus
Prozostrodon
Therioherpeton
Riograndia
Pachygenelus
Pseudotherium
Oligokyphus
Tritylodon
Bienotherium
Kayentatherium
Botucaraitherium
Brasilodon
Brasilitherium
Adelobasileus
Sinoconodon
Morganucodon
Ectenion
Lumkuia

Consensus tree(s) written to treefile: C:\Users\Dell Laptop\Documents\PhD\Phylogenetic analyses\Brasilodontid analysis\Jan 11 2017\character81edit_sc.tre

Tree description:

Unrooted tree(s) rooted using outgroup method
Optimality criterion = parsimony
Character-status summary:
Of 145 total characters:
All characters are of type 'unord'
All characters have equal weight
All characters are parsimony-informative
Gaps are treated as "missing"
Multistate taxa interpreted as uncertainty
Character-state optimization: Accelerated transformation (ACCTRAN)

Tree number 1 (rooted using default outgroup)

Tree length = 444
Consistency index (CI) = 0.4707
Homoplasy index (HI) = 0.5293
Retention index (RI) = 0.7812
Rescaled consistency index (RC) = 0.3677

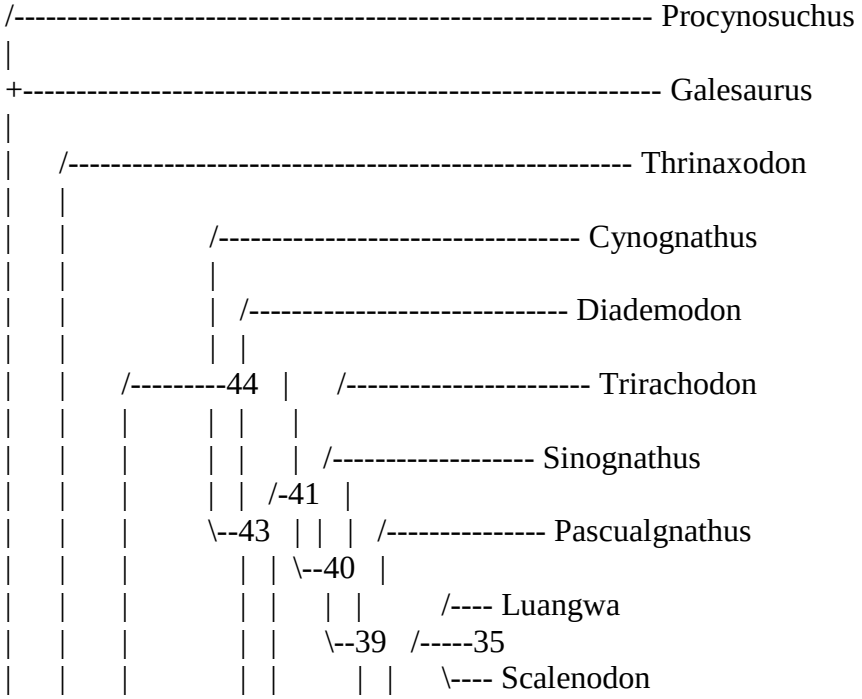

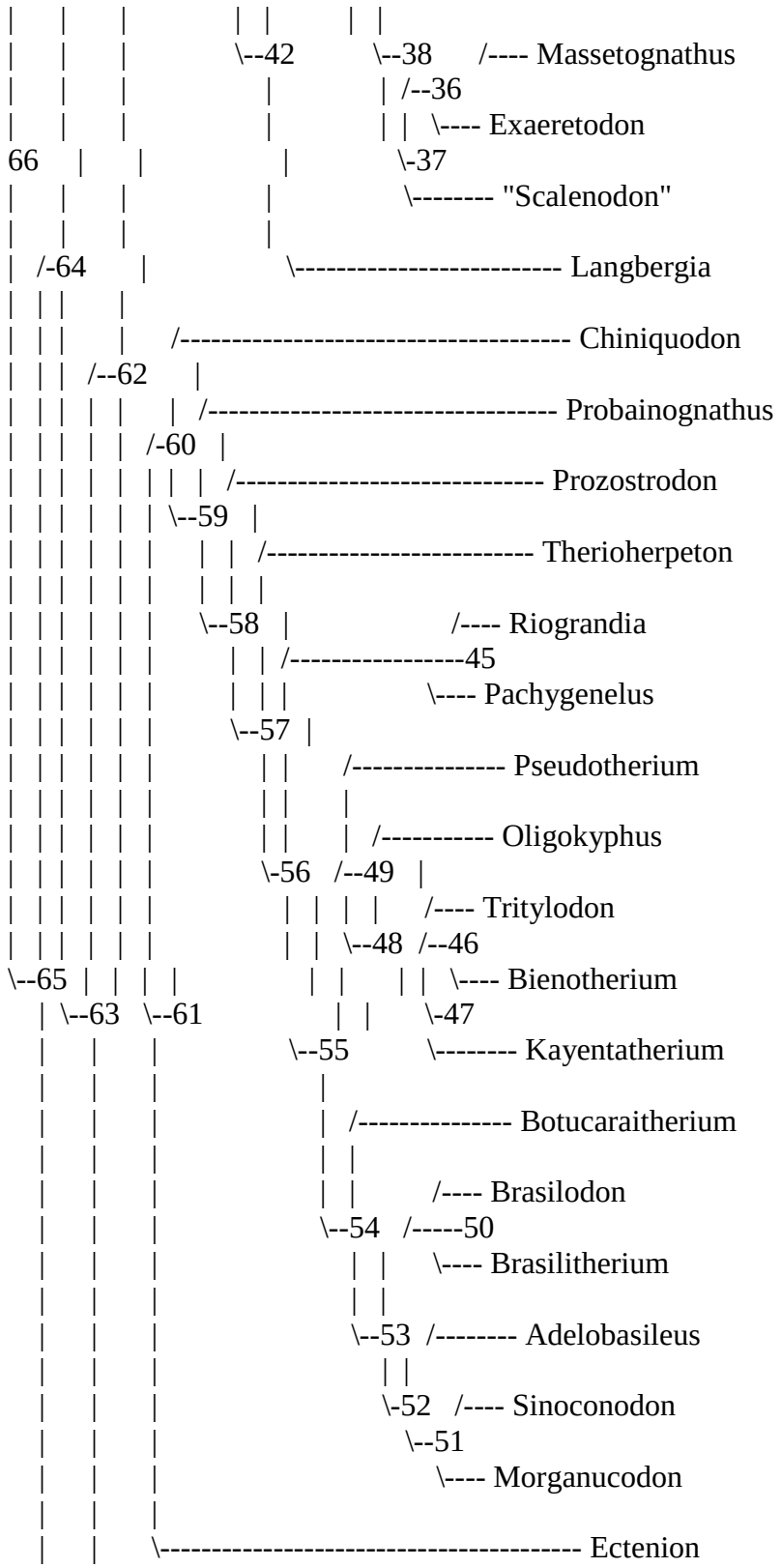
Massetognathus
Exaeretodon
"Scalenodon"
Langbergia
Chiniquodon
Probainognathus
Prozostrodon
Therioherpeton
Riograndia
Pachygenelus
Pseudotherium
Oligokyphus
Tritylodon
Bienotherium
Kayentatherium
Botucaraitherium
Brasilodon
Brasilitherium
Adelobasileus
Sinoconodon
Morganucodon
Ectenion

```
|     |
|     \------------------------------------------------ Lumkuia
|
\---------------------------------------------------------- Platycraniellus
```

Apomorphy lists:

Branch	Character	Steps	CI	Change
node_66 --> Procynosuchus	2 (Septomaxilla)	1	0.143	1 ==> 0
	8 (Profile of sk)	1	0.400	0 ==> 1
	64 (Articulation)	1	0.250	0 ==> 1
	78 (Articulation)	1	1.000	1 ==> 0
	83 (#Lateral rid)	1	0.429	1 ==> 0
	94 (Upper inciso)	1	0.250	1 ==> 0
	95 (Lower inciso)	1	0.286	1 ==> 0
	102 (Upper postc)	1	0.286	0 ==> 1
	124 (Anapophysis)	1	0.200	1 ==> 0
node_66 --> Galesaurus	19 (Infraorbital)	1	0.286	0 --> 1
	25 (Posterior ex)	1	0.250	1 ==> 0
	30 (Ectopterygoi)	1	0.286	0 --> 1
	31 (Interpterygo)	1	0.167	0 --> 1
	105 (Posterior p)	1	0.250	0 ==> 1
	115 (Lingual cin)	1	0.167	0 --> 1
	125 (Expanded co)	1	0.250	0 --> 1
node_66 --> node_65	3 (#Snout in rel)	1	0.250	0 ==> 1
	32 (Secondary pa)	1	1.000	0 ==> 1
	33 (Secondary pa)	1	1.000	0 ==> 1
	73 (#Lateral mar)	1	1.000	0 ==> 1
	76 (#Lateral not)	1	0.600	0 ==> 1
	85 (Position of)	1	0.500	0 --> 1
	89 (Reflected la)	1	1.000	0 --> 1
	90 (#Reflected l)	1	1.000	0 --> 1
node_65 --> node_64	31 (Interpterygo)	1	0.167	0 --> 1
	98 (Distinct upp)	1	0.500	1 ==> 0
	115 (Lingual cin)	1	0.167	0 --> 1
node_64 --> Thrinaxodon	85 (Position of)	1	0.500	1 --> 0
	102 (Upper postc)	1	0.286	0 ==> 1
	125 (Expanded co)	1	0.250	0 --> 1
node_64 --> node_63	2 (Septomaxilla)	1	0.143	1 --> 0
	9 (Parietal fora)	1	0.250	0 --> 1
	26 (The notch se)	1	0.200	0 --> 1
	29 (Vomer)	1	0.333	0 --> 1
	40 (Quadrate ram)	1	0.500	0 ==> 1

42 (Frontal-epip) 1 0.200 0 ==> 1
46 (#Basisphenoi) 1 0.600 0 ==> 1
79 (Craniomandib) 1 0.750 0 ==> 1
82 (Dentary symp) 1 0.500 0 ==> 1
83 (#Lateral rid) 1 0.429 1 ==> 2
90 (#Reflected l) 1 1.000 1 --> 2
105 (Posterior p) 1 0.250 0 ==> 1
127 (#Acromion p) 1 1.000 0 ==> 1
134 (Manual digi) 1 1.000 0 --> 1
135 (Manual digi) 1 1.000 0 --> 1
node_63 --> node_62 20 (#Zygomatic a) 1 0.286 0 --> 1
41 (Quadrate art) 1 0.333 0 ==> 1
48 (Internal car) 1 0.333 0 ==> 1
87 (Splenial) 1 1.000 0 ==> 1
88 (#Postdentary) 1 1.000 0 ==> 1
101 (Canine serr) 1 0.200 0 --> 1
node_62 --> node_44 3 (#Snout in rel) 1 0.250 1 --> 0
9 (Parietal fora) 1 0.250 1 --> 0
17 (Zygomatic ar) 1 0.250 2 ==> 0
19 (Infraorbital) 1 0.286 0 ==> 2
23 (The width of) 1 0.333 0 ==> 2
24 (Squamosal gr) 1 0.500 0 ==> 1
25 (Posterior ex) 1 0.250 1 ==> 0
29 (Vomer) 1 0.333 1 --> 0
72 (Shape of the) 1 0.500 0 --> 1
97 (Incisor cutt) 1 0.500 0 ==> 1
125 (Expanded co) 1 0.250 0 --> 1
126 (Lumbar cost) 1 0.500 0 ==> 1
node_44 --> Cynognathus 26 (The notch se) 1 0.200 1 --> 0
38 (Middle of pt) 1 0.400 0 ==> 1
65 (Paroccipital) 1 0.333 0 ==> 1
71 (Size of the) 1 0.250 0 ==> 1
118 (Upper tooth) 1 0.500 0 ==> 1
124 (Anapophysis) 1 0.200 1 ==> 0
node_44 --> node_43 22 (The posterov) 1 0.200 0 ==> 1
57 (#Maxillary a) 1 0.667 0 --> 1
91 (Mandibular m) 1 0.667 0 ==> 1
92 (Postcanine o) 1 0.667 0 ==> 1
93 (Relationship) 1 0.600 0 ==> 3
102 (Upper postc) 1 0.286 0 ==> 2
109 (Number of u) 1 0.400 0 --> 1
112 (Arrangement) 1 0.500 0 ==> 1
115 (Lingual cin) 1 0.167 1 --> 0
119 (Postcanine) 1 0.667 0 ==> 1

node_43 --> Diademodon 20 (#Zygomatic a) 1 0.286 1 ==> 2
30 (Ectopterygoi) 1 0.286 0 ==> 1
72 (Shape of the) 1 0.500 1 --> 0
80 (Craniomandib) 1 1.000 0 ==> 1
111 (Central cus) 1 0.500 1 ==> 0
node_43 --> node_42 3 (#Snout in rel) 1 0.250 0 --> 1
18 (The anterove) 1 0.250 0 ==> 1
23 (The width of) 1 0.333 2 ==> 1
28 (Vomer exposu) 1 0.500 0 ==> 1
35 (#The posteri) 1 0.250 0 ==> 1
42 (Frontal-epip) 1 0.200 1 --> 0
56 (Route of the) 1 0.667 0 ==> 2
69 (#Rotation of) 1 0.750 0 ==> 1
70 (Curvature of) 1 0.500 0 --> 1
74 (#Medial marg) 1 0.667 0 ==> 1
76 (#Lateral not) 1 0.600 1 --> 2
83 (#Lateral rid) 1 0.429 2 ==> 1
109 (Number of u) 1 0.400 1 --> 2
114 (Number of l) 1 0.500 0 --> 1
117 (Axis of pos) 1 0.500 0 ==> 1
136 (Dorsal prof) 1 0.500 0 --> 1
node_42 --> node_41 1 (#Premaxillary) 1 0.333 0 ==> 1
6 (Maxillary pla) 1 0.500 0 ==> 1
9 (Parietal fora) 1 0.250 0 --> 1
103 (#Anteriormo) 1 0.500 0 ==> 1
104 (#Posteriorm) 1 0.667 0 --> 1
node_41 --> Trirachodon 2 (Septomaxilla) 1 0.143 0 ==> 1
38 (Middle of pt) 1 0.400 0 ==> 2
42 (Frontal-epip) 1 0.200 0 --> 1
node_41 --> node_40 3 (#Snout in rel) 1 0.250 1 --> 2
29 (Vomer) 1 0.333 0 ==> 1
30 (Ectopterygoi) 1 0.286 0 --> 2
97 (Incisor cutt) 1 0.500 1 ==> 0
101 (Canine serr) 1 0.200 1 ==> 0
105 (Posterior p) 1 0.250 1 --> 0
114 (Number of l) 1 0.500 1 --> 0
117 (Axis of pos) 1 0.500 1 ==> 2
126 (Lumbar cost) 1 0.500 1 --> 0
128 (Scapular co) 1 0.500 0 --> 1
node_40 --> Sinognathus 19 (Infraorbital) 1 0.286 2 ==> 0
22 (The posterov) 1 0.200 1 ==> 0
95 (Lower inciso) 1 0.286 1 ==> 2
104 (#Posteriorm) 1 0.667 1 --> 0
node_40 --> node_39 23 (The width of) 1 0.333 1 --> 2

41 (Quadrate art) 1 0.333 1 --> 0
83 (#Lateral rid) 1 0.429 1 ==> 2
94 (Upper inciso) 1 0.250 1 --> 2
111 (Central cus) 1 0.500 1 --> 0
116 (Lower poste) 1 1.000 0 ==> 1
node_39 --> Pascualgnathus 20 (#Zygomatic a) 1 0.286 1 ==> 2
109 (Number of u) 1 0.400 2 ==> 1
110 (Position of) 1 1.000 0 ==> 1
node_39 --> node_38 1 (#Premaxillary) 1 0.333 1 --> 0
3 (#Snout in rel) 1 0.250 2 --> 1
16 (Sphenopalati) 1 0.333 0 --> 1
58 (Pterygoparoc) 1 0.333 0 ==> 1
111 (Central cus) 1 0.500 0 --> 2
137 (Length of a) 1 0.500 0 ==> 1
node_38 --> node_35 9 (Parietal fora) 1 0.250 1 ==> 0
94 (Upper inciso) 1 0.250 2 --> 1
97 (Incisor cutt) 1 0.500 0 ==> 1
101 (Canine serr) 1 0.200 0 ==> 1
node_35 --> Luangwa 3 (#Snout in rel) 1 0.250 1 ==> 0
17 (Zygomatic ar) 1 0.250 0 ==> 2
22 (The posterov) 1 0.200 1 ==> 0
23 (The width of) 1 0.333 2 --> 1
node_35 --> Scalenodon 19 (Infraorbital) 1 0.286 2 ==> 0
node_38 --> node_37 15 (#Palatine) 1 0.333 0 --> 1
99 (Upper canine) 1 0.500 0 --> 1
110 (Position of) 1 1.000 0 ==> 2
124 (Anapophysis) 1 0.200 1 --> 0
130 (Procoracoid) 1 0.500 0 --> 1
node_37 --> node_36 4 (Paracanine fo) 1 1.000 0 ==> 1
5 (Premaxilla fo) 1 0.500 0 ==> 1
98 (Distinct upp) 1 0.500 0 ==> 1
100 (Lower canin) 1 0.500 0 ==> 1
node_36 --> Massetognathus 2 (Septomaxilla) 1 0.143 0 ==> 1
15 (#Palatine) 1 0.333 1 --> 0
16 (Sphenopalati) 1 0.333 1 --> 0
19 (Infraorbital) 1 0.286 2 ==> 0
23 (The width of) 1 0.333 2 --> 1
35 (#The posteri) 1 0.250 1 ==> 2
55 (Foramen and) 1 0.333 0 ==> 1
94 (Upper inciso) 1 0.250 2 --> 1
97 (Incisor cutt) 1 0.500 0 ==> 2
node_36 --> Exaeretodon 7 (Maxilla) 1 0.200 0 ==> 1
52 (#The trigemi) 1 0.500 0 ==> 1
84 (Angle of the) 1 0.500 0 ==> 1

99 (Upper canine) 1 0.500 1 --> 0
109 (Number of u) 1 0.400 2 ==> 1
111 (Central cus) 1 0.500 2 ==> 0
118 (Upper tooth) 1 0.500 0 ==> 2
125 (Expanded co) 1 0.250 1 ==> 0
133 (Ulna olecra) 1 0.500 0 ==> 1
node_37 --> "Scalenodon" 95 (Lower inciso) 1 0.286 1 ==> 2
node_42 --> Langbergia 17 (Zygomatic ar) 1 0.250 0 ==> 2
node_62 --> node_61 5 (Premaxilla fo) 1 0.500 0 --> 1
8 (Profile of sk) 1 0.400 0 --> 2
15 (#Palatine) 1 0.333 0 --> 1
28 (Vomer exposu) 1 0.500 0 --> 1
56 (Route of the) 1 0.667 0 ==> 1
69 (#Rotation of) 1 0.750 0 ==> 1
70 (Curvature of) 1 0.500 0 ==> 1
74 (#Medial marg) 1 0.667 0 ==> 1
76 (#Lateral not) 1 0.600 1 ==> 2
77 (Articulation) 1 0.667 0 ==> 1
83 (#Lateral rid) 1 0.429 2 --> 0
128 (Scapular co) 1 0.500 0 --> 1
130 (Procoracoid) 1 0.500 0 --> 1
136 (Dorsal prof) 1 0.500 0 --> 1
141 (The diamete) 1 1.000 0 --> 1
node_61 --> node_60 2 (Septomaxilla) 1 0.143 0 --> 1
7 (Maxilla) 1 0.200 0 --> 1
30 (Ectopterygoi) 1 0.286 0 ==> 2
34 (Posterior ex) 1 0.500 0 ==> 1
35 (#The posteri) 1 0.250 0 --> 1
36 (Osseous pala) 1 0.500 0 --> 1
37 (Contribution) 1 0.500 0 ==> 1
42 (Frontal-epip) 1 0.200 1 --> 0
101 (Canine serr) 1 0.200 1 --> 0
124 (Anapophysis) 1 0.200 1 ==> 0
node_60 --> Chiniquodon 1 (#Premaxillary) 1 0.333 0 ==> 1
8 (Profile of sk) 1 0.400 2 --> 0
17 (Zygomatic ar) 1 0.250 2 ==> 0
19 (Infraorbital) 1 0.286 0 ==> 1
35 (#The posteri) 1 0.250 1 --> 2
83 (#Lateral rid) 1 0.429 0 --> 2
node_60 --> node_59 18 (The anterove) 1 0.250 0 ==> 1
21 (Posterior ex) 1 0.667 0 ==> 1
48 (Internal car) 1 0.333 1 ==> 0
81 (Squamosal ar) 1 0.667 0 --> 1
105 (Posterior p) 1 0.250 1 ==> 0

117 (Axis of pos) 1 0.500 0 ==> 1
123 (Posterior t) 1 1.000 0 --> 1
131 (Procoracoid) 1 1.000 0 --> 1
137 (Length of a) 1 0.500 0 ==> 1
node_59 --> Probainognathus 7 (Maxilla) 1 0.200 1 --> 0
36 (Osseous pala) 1 0.500 1 --> 0
42 (Frontal-epip) 1 0.200 0 --> 1
55 (Foramen and) 1 0.333 0 ==> 1
81 (Squamosal ar) 1 0.667 1 --> 2
118 (Upper tooth) 1 0.500 0 ==> 1
node_59 --> node_58 1 (#Premaxillary) 1 0.333 0 --> 2
10 (Interparieta) 1 1.000 0 --> 1
12 (Parietal cre) 1 1.000 0 --> 1
15 (#Palatine) 1 0.333 1 --> 2
16 (Sphenopalati) 1 0.333 0 ==> 1
17 (Zygomatic ar) 1 0.250 2 --> 1
20 (#Zygomatic a) 1 0.286 1 --> 0
26 (The notch se) 1 0.200 1 --> 0
31 (Interpterygo) 1 0.167 1 --> 0
39 (The nasophar) 1 1.000 0 --> 1
41 (Quadrate art) 1 0.333 1 --> 0
44 (The anterior) 1 0.500 0 --> 1
46 (#Basisphenoi) 1 0.600 1 --> 2
51 (Internal aud) 1 1.000 0 --> 1
58 (Pterygoparoc) 1 0.333 0 --> 2
63 (Separation o) 1 0.500 0 --> 1
65 (Paroccipital) 1 0.333 0 --> 1
67 (The relation) 1 0.500 0 --> 1
69 (#Rotation of) 1 0.750 1 --> 2
71 (Size of the) 1 0.250 0 --> 1
73 (#Lateral mar) 1 1.000 1 --> 2
74 (#Medial marg) 1 0.667 1 --> 2
75 (Dorsal margi) 1 0.333 0 --> 1
76 (#Lateral not) 1 0.600 2 --> 3
78 (Articulation) 1 1.000 1 --> 3
79 (Craniomandib) 1 0.750 1 --> 2
82 (Dentary symp) 1 0.500 1 ==> 0
83 (#Lateral rid) 1 0.429 0 --> 3
86 (Mediolateral) 1 1.000 0 ==> 1
93 (Relationship) 1 0.600 0 ==> 1
94 (Upper inciso) 1 0.250 1 --> 0
103 (#Anteriormo) 1 0.500 0 ==> 1
106 (Upper postc) 1 0.750 0 ==> 1
107 (Lower postc) 1 0.500 0 ==> 1

108 (Buccal (ext) 1 1.000 0 ==> 1
115 (Lingual cin) 1 0.167 1 ==> 0
121 (Axis centru) 1 1.000 0 --> 1
122 (Dens) 1 1.000 0 --> 1
129 (Scapular el) 1 0.500 0 --> 1
133 (Ulna olecra) 1 0.500 0 --> 1
138 (Lateral sur) 1 1.000 0 ==> 1
139 (Posterior i) 1 1.000 0 ==> 1
140 (Cotyloid (a) 1 1.000 0 ==> 1
node_58 --> Prozostrodon 95 (Lower inciso) 1 0.286 1 ==> 0
101 (Canine serr) 1 0.200 0 ==> 1
102 (Upper postc) 1 0.286 0 ==> 1
node_58 --> node_57 2 (Septomaxilla) 1 0.143 1 --> 0
13 (Prefrontal) 1 0.333 0 ==> 1
14 (#Postorbital) 1 1.000 0 ==> 2
94 (Upper inciso) 1 0.250 0 --> 2
96 (Incisor size) 1 0.500 0 --> 1
144 (Lesser troc) 1 1.000 0 ==> 1
145 (Lesser troc) 1 1.000 0 ==> 1
node_57 --> Therioherpeton 117 (Axis of pos) 1 0.500 1 ==> 0
node_57 --> node_56 120 (Vertebral c) 1 1.000 0 ==> 1
142 (Femur head) 1 1.000 0 ==> 1
143 (Greater tro) 1 1.000 0 ==> 1
node_56 --> node_45 4 (Paracanine fo) 1 1.000 0 ==> 3
68 (Shape of the) 1 0.333 0 ==> 1
99 (Upper canine) 1 0.500 0 ==> 1
node_45 --> Riograndia 17 (Zygomatic ar) 1 0.250 1 ==> 2
27 (Palatine) 1 0.333 0 ==> 1
65 (Paroccipital) 1 0.333 1 --> 0
100 (Lower canin) 1 0.500 0 ==> 1
115 (Lingual cin) 1 0.167 0 ==> 1
node_45 --> Pachygenelus 35 (#The posteri) 1 0.250 1 ==> 2
95 (Lower inciso) 1 0.286 1 ==> 2
106 (Upper postc) 1 0.750 1 ==> 0
107 (Lower postc) 1 0.500 1 ==> 0
117 (Axis of pos) 1 0.500 1 ==> 2
node_56 --> node_55 1 (#Premaxillary) 1 0.333 2 --> 0
18 (The anterove) 1 0.250 1 --> 0
25 (Posterior ex) 1 0.250 1 --> 0
38 (Middle of pt) 1 0.400 0 ==> 2
49 (Prootic and) 1 0.333 0 ==> 1
50 (Promontorium) 1 0.500 0 --> 1
54 (Vascular for) 1 0.500 0 --> 1
56 (Route of the) 1 0.667 1 ==> 2

57 (#Maxillary a) 1 0.667 0 --> 1
62 (Paroccipital) 1 0.500 0 ==> 1
64 (Articulation) 1 0.250 0 --> 1
119 (Postcanine) 1 0.667 0 --> 1
132 (Humerus ect) 1 1.000 0 ==> 1
138 (Lateral sur) 1 1.000 1 ==> 2
node_55 --> node_49 1 (#Premaxillary) 1 0.333 0 --> 1
8 (Profile of sk) 1 0.400 2 ==> 1
17 (Zygomatic ar) 1 0.250 1 --> 0
20 (#Zygomatic a) 1 0.286 0 --> 2
21 (Posterior ex) 1 0.667 1 --> 0
22 (The posterov) 1 0.200 0 --> 1
46 (#Basisphenoi) 1 0.600 2 --> 1
59 (Vertical com) 1 0.500 0 ==> 1
60 (Anterior par) 1 0.500 0 ==> 1
61 (Hyoid (stape) 1 0.500 0 --> 1
69 (#Rotation of) 1 0.750 2 --> 3
78 (Articulation) 1 1.000 3 --> 2
79 (Craniomandib) 1 0.750 2 ==> 0
84 (Angle of the) 1 0.500 0 --> 1
91 (Mandibular m) 1 0.667 0 --> 1
100 (Lower canin) 1 0.500 0 --> 2
103 (#Anteriormo) 1 0.500 1 --> 0
107 (Lower postc) 1 0.500 1 --> 2
119 (Postcanine) 1 0.667 1 --> 2
127 (#Acromion p) 1 1.000 1 --> 2
129 (Scapular el) 1 0.500 1 --> 0
node_49 --> Pseudotherium 2 (Septomaxilla) 1 0.143 0 ==> 1
7 (Maxilla) 1 0.200 1 ==> 0
13 (Prefrontal) 1 0.333 1 ==> 0
14 (#Postorbital) 1 1.000 2 ==> 1
15 (#Palatine) 1 0.333 2 ==> 1
40 (Quadrate ram) 1 0.500 1 ==> 0
46 (#Basisphenoi) 1 0.600 1 --> 3
54 (Vascular for) 1 0.500 1 --> 0
66 (Tabular) 1 0.333 0 ==> 1
node_49 --> node_48 3 (#Snout in rel) 1 0.250 1 --> 2
6 (Maxillary pla) 1 0.500 0 ==> 1
18 (The anterove) 1 0.250 0 --> 1
24 (Squamosal gr) 1 0.500 0 ==> 1
34 (Posterior ex) 1 0.500 1 --> 0
35 (#The posteri) 1 0.250 1 ==> 2
44 (The anterior) 1 0.500 1 --> 0
45 (Parasphenoid) 1 1.000 0 ==> 1

48 (Internal car) 1 0.333 0 --> 1
50 (Promontorium) 1 0.500 1 --> 0
52 (#The trigemi) 1 0.500 0 ==> 1
63 (Separation o) 1 0.500 1 ==> 0
80 (Craniomandib) 1 1.000 0 ==> 2
92 (Postcanine o) 1 0.667 0 ==> 1
93 (Relationship) 1 0.600 1 ==> 3
99 (Upper canine) 1 0.500 0 ==> 2
102 (Upper postc) 1 0.286 0 ==> 2
103 (#Anteriormo) 1 0.500 0 --> 2
104 (#Posteriorm) 1 0.667 0 ==> 2
106 (Upper postc) 1 0.750 1 ==> 3
109 (Number of u) 1 0.400 0 ==> 2
112 (Arrangement) 1 0.500 0 ==> 1
117 (Axis of pos) 1 0.500 1 ==> 3
118 (Upper tooth) 1 0.500 0 ==> 2
node_48 --> Oligokyphus 67 (The relation) 1 0.500 1 ==> 0
71 (Size of the) 1 0.250 1 ==> 0
75 (Dorsal margi) 1 0.333 1 ==> 0
node_48 --> node_47 23 (The width of) 1 0.333 0 ==> 1
26 (The notch se) 1 0.200 0 ==> 1
node_47 --> node_46 31 (Interpterygo) 1 0.167 0 ==> 1
node_46 --> Tritylodon 22 (The posterov) 1 0.200 1 ==> 0
75 (Dorsal margi) 1 0.333 1 ==> 0
95 (Lower inciso) 1 0.286 1 ==> 2
node_46 --> Bienotherium 58 (Pterygoparoc) 1 0.333 2 ==> 0
node_47 --> Kayentatherium 27 (Palatine) 1 0.333 0 ==> 1
node_55 --> node_54 3 (#Snout in rel) 1 0.250 1 --> 0
47 (#Overlap of) 1 1.000 0 --> 1
53 (Lateral trou) 1 1.000 0 --> 1
55 (Foramen and) 1 0.333 0 --> 1
57 (#Maxillary a) 1 0.667 1 --> 2
94 (Upper inciso) 1 0.250 2 --> 1
96 (Incisor size) 1 0.500 1 --> 0
102 (Upper postc) 1 0.286 0 ==> 1
113 (Interlockin) 1 0.500 0 ==> 1
124 (Anapophysis) 1 0.200 0 --> 1
node_54 --> node_53 100 (Lower canin) 1 0.500 0 ==> 1
node_53 --> node_50 68 (Shape of the) 1 0.333 0 ==> 1
81 (Squamosal ar) 1 0.667 1 --> 0
node_50 --> Brasilodon 49 (Prootic and) 1 0.333 1 ==> 0
node_50 --> Brasilitherium 13 (Prefrontal) 1 0.333 1 ==> 0
17 (Zygomatic ar) 1 0.250 1 ==> 2
37 (Contribution) 1 0.500 1 ==> 0

94 (Upper inciso) 1 0.250 1 ==> 0
node_53 --> node_52 4 (Paracanine fo) 1 1.000 0 --> 2
8 (Profile of sk) 1 0.400 2 ==> 0
11 (#Lateral exp) 1 1.000 0 ==> 1
25 (Posterior ex) 1 0.250 0 --> 1
27 (Palatine) 1 0.333 0 --> 1
35 (#The posteri) 1 0.250 1 --> 2
52 (#The trigemi) 1 0.500 0 ==> 2
64 (Articulation) 1 0.250 1 --> 0
66 (Tabular) 1 0.333 0 --> 1
77 (Articulation) 1 0.667 1 --> 0
78 (Articulation) 1 1.000 3 --> 4
79 (Craniomandib) 1 0.750 2 --> 3
88 (#Postdentary) 1 1.000 1 --> 2
91 (Mandibular m) 1 0.667 0 --> 2
93 (Relationship) 1 0.600 1 --> 0
95 (Lower inciso) 1 0.286 1 --> 0
106 (Upper postc) 1 0.750 1 --> 2
107 (Lower postc) 1 0.500 1 --> 2
node_52 --> Adelobasileus 58 (Pterygoparoc) 1 0.333 2 ==> 1
62 (Paroccipital) 1 0.500 1 ==> 0
node_52 --> node_51 31 (Interpterygo) 1 0.167 0 ==> 1
43 (Epipterygoid) 1 1.000 0 ==> 1
46 (#Basisphenoi) 1 0.600 2 ==> 3
61 (Hyoid (stape) 1 0.500 0 ==> 1
node_51 --> Sinoconodon 59 (Vertical com) 1 0.500 0 ==> 1
66 (Tabular) 1 0.333 1 --> 0
102 (Upper postc) 1 0.286 1 ==> 0
113 (Interlockin) 1 0.500 1 ==> 0
115 (Lingual cin) 1 0.167 0 ==> 1
node_51 --> Morganucodon 21 (Posterior ex) 1 0.667 1 ==> 2
30 (Ectopterygoi) 1 0.286 2 ==> 1
47 (#Overlap of) 1 1.000 1 ==> 2
60 (Anterior par) 1 0.500 0 ==> 1
64 (Articulation) 1 0.250 0 --> 1
68 (Shape of the) 1 0.333 0 ==> 1
77 (Articulation) 1 0.667 0 --> 2
92 (Postcanine o) 1 0.667 0 ==> 2
93 (Relationship) 1 0.600 0 --> 2
node_61 --> Ectenion 15 (#Palatine) 1 0.333 1 --> 2
20 (#Zygomatic a) 1 0.286 1 --> 0
26 (The notch se) 1 0.200 1 --> 0
38 (Middle of pt) 1 0.400 0 ==> 2
52 (#The trigemi) 1 0.500 0 ==> 1

```
                        58 (Pterygoparoc)      1  0.333  0 ==> 1
      node_63 --> Lumkuia         7 (Maxilla)           1  0.200  0 ==> 1
                        30 (Ectopterygoi)      1  0.286  0 ==> 2
                        31 (Interpterygo)      1  0.167  1 --> 0
                        35 (#The posteri)      1  0.250  0 ==> 1
                        38 (Middle of pt)      1  0.400  0 ==> 1
                        49 (Prootic and )      1  0.333  0 ==> 1
                        58 (Pterygoparoc)      1  0.333  0 ==> 1
                        76 (#Lateral not)      1  0.600  1 ==> 0
      node_65 --> Platycraniellus  19 (Infraorbital)      1  0.286  0 --> 1
                        20 (#Zygomatic a)      1  0.286  0 ==> 1
                        30 (Ectopterygoi)      1  0.286  0 --> 1
                        71 (Size of the )      1  0.250  0 ==> 1
```

Tree description:

```
  Unrooted tree(s) rooted using outgroup method
  Optimality criterion = parsimony
    Character-status summary:
      Of 145 total characters:
        All characters are of type 'unord'
        All characters have equal weight
        All characters are parsimony-informative
    Gaps are treated as "missing"
    Multistate taxa interpreted as uncertainty
    Character-state optimization: Delayed transformation (DELTRAN)
```

Tree number 1 (rooted using default outgroup)

Tree length = 444
Consistency index (CI) = 0.4707
Homoplasy index (HI) = 0.5293
Retention index (RI) = 0.7812
Rescaled consistency index (RC) = 0.3677

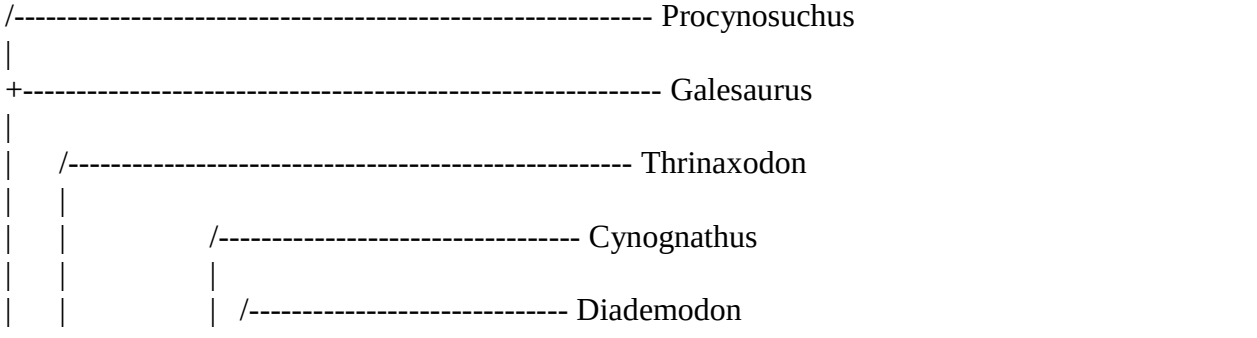

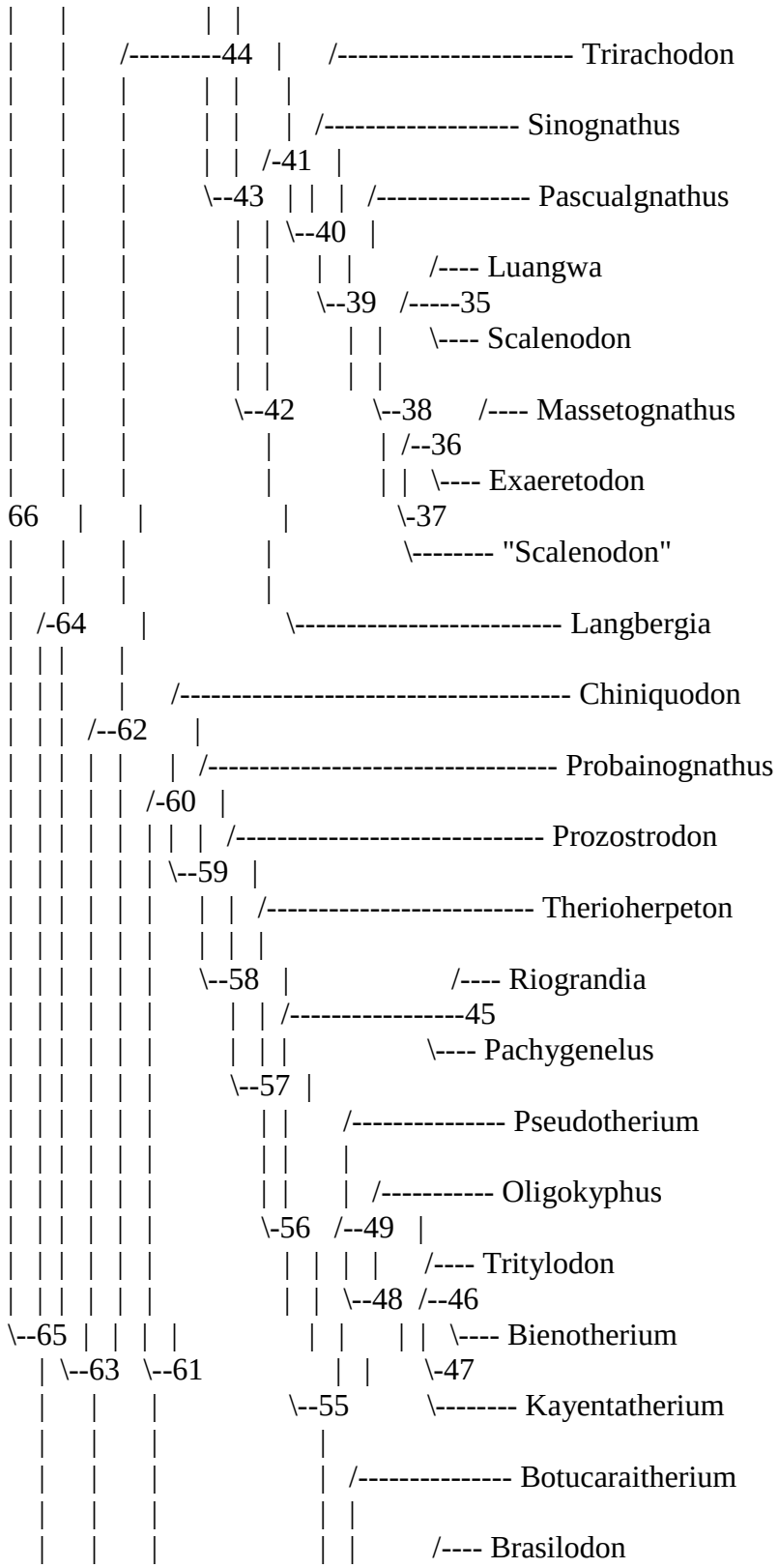
Trirachodon
Sinognathus
Pascualgnathus
Luangwa
Scalenodon
Massetognathus
Exaeretodon
"Scalenodon"
Langbergia
Chiniquodon
Probainognathus
Prozostrodon
Therioherpeton
Riograndia
Pachygenelus
Pseudotherium
Oligokyphus
Tritylodon
Bienotherium
Kayentatherium
Botucaraitherium
Brasilodon

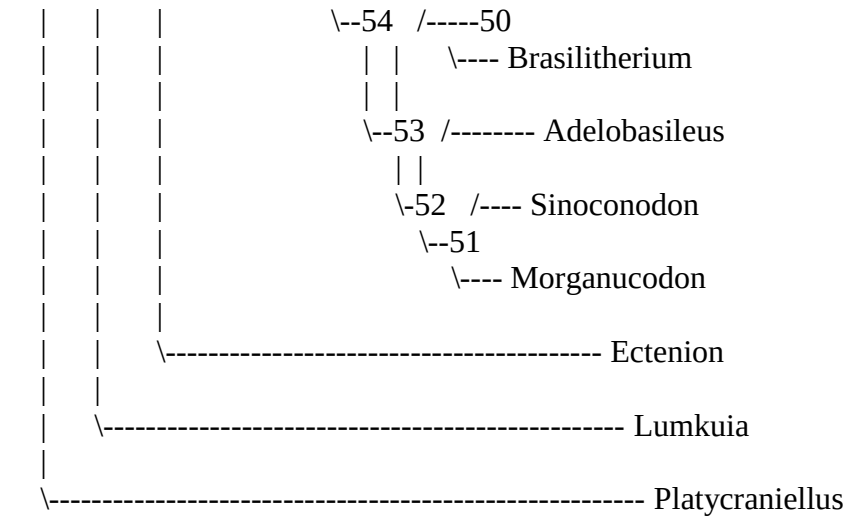

Apomorphy lists:

Branch	Character	Steps	CI	Change
node_66 --> Procynosuchus	2 (Septomaxilla)	1	0.143	1 ==> 0
	8 (Profile of sk)	1	0.400	0 ==> 1
	64 (Articulation)	1	0.250	0 ==> 1
	78 (Articulation)	1	1.000	1 ==> 0
	83 (#Lateral rid)	1	0.429	1 ==> 0
	94 (Upper inciso)	1	0.250	1 ==> 0
	95 (Lower inciso)	1	0.286	1 ==> 0
	102 (Upper postc)	1	0.286	0 ==> 1
	124 (Anapophysis)	1	0.200	1 ==> 0
node_66 --> Galesaurus	19 (Infraorbital)	1	0.286	0 --> 1
	25 (Posterior ex)	1	0.250	1 ==> 0
	30 (Ectopterygoi)	1	0.286	0 --> 1
	31 (Interpterygo)	1	0.167	0 --> 1
	105 (Posterior p)	1	0.250	0 ==> 1
	115 (Lingual cin)	1	0.167	0 --> 1
	125 (Expanded co)	1	0.250	0 --> 1
node_66 --> node_65	3 (#Snout in rel)	1	0.250	0 ==> 1
	32 (Secondary pa)	1	1.000	0 ==> 1
	33 (Secondary pa)	1	1.000	0 ==> 1
	73 (#Lateral mar)	1	1.000	0 ==> 1
	76 (#Lateral not)	1	0.600	0 ==> 1
node_65 --> node_64	89 (Reflected la)	1	1.000	0 --> 1
	98 (Distinct upp)	1	0.500	1 ==> 0
	115 (Lingual cin)	1	0.167	0 --> 1
node_64 --> Thrinaxodon	31 (Interpterygo)	1	0.167	0 --> 1

90 (#Reflected l) 1 1.000 0 --> 1
102 (Upper postc) 1 0.286 0 ==> 1
125 (Expanded co) 1 0.250 0 --> 1
node_64 --> node_63 40 (Quadrate ram) 1 0.500 0 ==> 1
42 (Frontal-epip) 1 0.200 0 ==> 1
46 (#Basisphenoi) 1 0.600 0 ==> 1
79 (Craniomandib) 1 0.750 0 ==> 1
82 (Dentary symp) 1 0.500 0 ==> 1
83 (#Lateral rid) 1 0.429 1 ==> 2
85 (Position of) 1 0.500 0 --> 1
90 (#Reflected l) 1 1.000 0 --> 2
105 (Posterior p) 1 0.250 0 ==> 1
127 (#Acromion p) 1 1.000 0 ==> 1
node_63 --> node_62 31 (Interpterygo) 1 0.167 0 --> 1
41 (Quadrate art) 1 0.333 0 ==> 1
48 (Internal car) 1 0.333 0 ==> 1
87 (Splenial) 1 1.000 0 ==> 1
88 (#Postdentary) 1 1.000 0 ==> 1
134 (Manual digi) 1 1.000 0 --> 1
135 (Manual digi) 1 1.000 0 --> 1
node_62 --> node_44 2 (Septomaxilla) 1 0.143 1 --> 0
17 (Zygomatic ar) 1 0.250 2 ==> 0
19 (Infraorbital) 1 0.286 0 ==> 2
20 (#Zygomatic a) 1 0.286 0 --> 1
23 (The width of) 1 0.333 0 ==> 2
24 (Squamosal gr) 1 0.500 0 ==> 1
25 (Posterior ex) 1 0.250 1 ==> 0
97 (Incisor cutt) 1 0.500 0 ==> 1
101 (Canine serr) 1 0.200 0 --> 1
125 (Expanded co) 1 0.250 0 --> 1
126 (Lumbar cost) 1 0.500 0 ==> 1
node_44 --> Cynognathus 3 (#Snout in rel) 1 0.250 1 --> 0
38 (Middle of pt) 1 0.400 0 ==> 1
65 (Paroccipital) 1 0.333 0 ==> 1
71 (Size of the) 1 0.250 0 ==> 1
72 (Shape of the) 1 0.500 0 --> 1
118 (Upper tooth) 1 0.500 0 ==> 1
124 (Anapophysis) 1 0.200 1 ==> 0
node_44 --> node_43 22 (The posterov) 1 0.200 0 ==> 1
26 (The notch se) 1 0.200 0 --> 1
91 (Mandibular m) 1 0.667 0 ==> 1
92 (Postcanine o) 1 0.667 0 ==> 1
93 (Relationship) 1 0.600 0 ==> 3
102 (Upper postc) 1 0.286 0 ==> 2

112 (Arrangement) 1 0.500 0 ==> 1
119 (Postcanine) 1 0.667 0 ==> 1
node_43 --> Diademodon 3 (#Snout in rel) 1 0.250 1 --> 0
20 (#Zygomatic a) 1 0.286 1 ==> 2
30 (Ectopterygoi) 1 0.286 0 ==> 1
80 (Craniomandib) 1 1.000 0 ==> 1
109 (Number of u) 1 0.400 0 --> 1
111 (Central cus) 1 0.500 1 ==> 0
node_43 --> node_42 18 (The anterove) 1 0.250 0 ==> 1
23 (The width of) 1 0.333 2 ==> 1
28 (Vomer exposu) 1 0.500 0 ==> 1
35 (#The posteri) 1 0.250 0 ==> 1
56 (Route of the) 1 0.667 0 ==> 2
57 (#Maxillary a) 1 0.667 0 --> 1
69 (#Rotation of) 1 0.750 0 ==> 1
74 (#Medial marg) 1 0.667 0 ==> 1
83 (#Lateral rid) 1 0.429 2 ==> 1
109 (Number of u) 1 0.400 0 --> 2
115 (Lingual cin) 1 0.167 1 --> 0
117 (Axis of pos) 1 0.500 0 ==> 1
node_42 --> node_41 1 (#Premaxillary) 1 0.333 0 ==> 1
6 (Maxillary pla) 1 0.500 0 ==> 1
70 (Curvature of) 1 0.500 0 --> 1
72 (Shape of the) 1 0.500 0 --> 1
76 (#Lateral not) 1 0.600 1 --> 2
103 (#Anteriormo) 1 0.500 0 ==> 1
node_41 --> Trirachodon 2 (Septomaxilla) 1 0.143 0 ==> 1
38 (Middle of pt) 1 0.400 0 ==> 2
104 (#Posteriorm) 1 0.667 0 --> 1
114 (Number of l) 1 0.500 0 --> 1
node_41 --> node_40 9 (Parietal fora) 1 0.250 0 --> 1
29 (Vomer) 1 0.333 0 ==> 1
42 (Frontal-epip) 1 0.200 1 --> 0
97 (Incisor cutt) 1 0.500 1 ==> 0
101 (Canine serr) 1 0.200 1 ==> 0
117 (Axis of pos) 1 0.500 1 ==> 2
node_40 --> Sinognathus 3 (#Snout in rel) 1 0.250 1 --> 2
19 (Infraorbital) 1 0.286 2 ==> 0
22 (The posterov) 1 0.200 1 ==> 0
95 (Lower inciso) 1 0.286 1 ==> 2
node_40 --> node_39 83 (#Lateral rid) 1 0.429 1 ==> 2
104 (#Posteriorm) 1 0.667 0 --> 1
105 (Posterior p) 1 0.250 1 --> 0
116 (Lower poste) 1 1.000 0 ==> 1

126 (Lumbar cost) 1 0.500 1 --> 0
136 (Dorsal prof) 1 0.500 0 --> 1
node_39 --> Pascualgnathus 3 (#Snout in rel) 1 0.250 1 --> 2
20 (#Zygomatic a) 1 0.286 1 ==> 2
23 (The width of) 1 0.333 1 --> 2
94 (Upper inciso) 1 0.250 1 --> 2
109 (Number of u) 1 0.400 2 ==> 1
110 (Position of) 1 1.000 0 ==> 1
111 (Central cus) 1 0.500 1 --> 0
node_39 --> node_38 58 (Pterygoparoc) 1 0.333 0 ==> 1
111 (Central cus) 1 0.500 1 --> 2
128 (Scapular co) 1 0.500 0 --> 1
137 (Length of a) 1 0.500 0 ==> 1
node_38 --> node_35 9 (Parietal fora) 1 0.250 1 ==> 0
97 (Incisor cutt) 1 0.500 0 ==> 1
101 (Canine serr) 1 0.200 0 ==> 1
node_35 --> Luangwa 3 (#Snout in rel) 1 0.250 1 ==> 0
16 (Sphenopalati) 1 0.333 0 --> 1
17 (Zygomatic ar) 1 0.250 0 ==> 2
22 (The posterov) 1 0.200 1 ==> 0
node_35 --> Scalenodon 19 (Infraorbital) 1 0.286 2 ==> 0
23 (The width of) 1 0.333 1 --> 2
node_38 --> node_37 30 (Ectopterygoi) 1 0.286 0 --> 2
41 (Quadrate art) 1 0.333 1 --> 0
110 (Position of) 1 1.000 0 ==> 2
node_37 --> node_36 1 (#Premaxillary) 1 0.333 1 --> 0
4 (Paracanine fo) 1 1.000 0 ==> 1
5 (Premaxilla fo) 1 0.500 0 ==> 1
98 (Distinct upp) 1 0.500 0 ==> 1
100 (Lower canin) 1 0.500 0 ==> 1
124 (Anapophysis) 1 0.200 1 --> 0
130 (Procoracoid) 1 0.500 0 --> 1
node_36 --> Massetognathus 2 (Septomaxilla) 1 0.143 0 ==> 1
19 (Infraorbital) 1 0.286 2 ==> 0
35 (#The posteri) 1 0.250 1 ==> 2
55 (Foramen and) 1 0.333 0 ==> 1
97 (Incisor cutt) 1 0.500 0 ==> 2
99 (Upper canine) 1 0.500 0 --> 1
node_36 --> Exaeretodon 7 (Maxilla) 1 0.200 0 ==> 1
15 (#Palatine) 1 0.333 0 --> 1
16 (Sphenopalati) 1 0.333 0 --> 1
23 (The width of) 1 0.333 1 --> 2
52 (#The trigemi) 1 0.500 0 ==> 1
84 (Angle of the) 1 0.500 0 ==> 1

94 (Upper inciso) 1 0.250 1 --> 2
109 (Number of u) 1 0.400 2 ==> 1
111 (Central cus) 1 0.500 2 ==> 0
118 (Upper tooth) 1 0.500 0 ==> 2
125 (Expanded co) 1 0.250 1 ==> 0
133 (Ulna olecra) 1 0.500 0 ==> 1
node_37 --> "Scalenodon" 15 (#Palatine) 1 0.333 0 --> 1
94 (Upper inciso) 1 0.250 1 --> 2
95 (Lower inciso) 1 0.286 1 ==> 2
99 (Upper canine) 1 0.500 0 --> 1
node_42 --> Langbergia 17 (Zygomatic ar) 1 0.250 0 ==> 2
42 (Frontal-epip) 1 0.200 1 --> 0
114 (Number of l) 1 0.500 0 --> 1
node_62 --> node_61 9 (Parietal fora) 1 0.250 0 --> 1
29 (Vomer) 1 0.333 0 --> 1
56 (Route of the) 1 0.667 0 ==> 1
69 (#Rotation of) 1 0.750 0 ==> 1
70 (Curvature of) 1 0.500 0 ==> 1
74 (#Medial marg) 1 0.667 0 ==> 1
76 (#Lateral not) 1 0.600 1 ==> 2
77 (Articulation) 1 0.667 0 ==> 1
128 (Scapular co) 1 0.500 0 --> 1
node_61 --> node_60 5 (Premaxilla fo) 1 0.500 0 --> 1
15 (#Palatine) 1 0.333 0 --> 1
28 (Vomer exposu) 1 0.500 0 --> 1
30 (Ectopterygoi) 1 0.286 0 ==> 2
34 (Posterior ex) 1 0.500 0 ==> 1
37 (Contribution) 1 0.500 0 ==> 1
124 (Anapophysis) 1 0.200 1 ==> 0
130 (Procoracoid) 1 0.500 0 --> 1
136 (Dorsal prof) 1 0.500 0 --> 1
node_60 --> Chiniquodon 1 (#Premaxillary) 1 0.333 0 ==> 1
7 (Maxilla) 1 0.200 0 --> 1
17 (Zygomatic ar) 1 0.250 2 ==> 0
19 (Infraorbital) 1 0.286 0 ==> 1
20 (#Zygomatic a) 1 0.286 0 --> 1
26 (The notch se) 1 0.200 0 --> 1
35 (#The posteri) 1 0.250 0 --> 2
36 (Osseous pala) 1 0.500 0 --> 1
42 (Frontal-epip) 1 0.200 1 --> 0
node_60 --> node_59 8 (Profile of sk) 1 0.400 0 --> 2
18 (The anterove) 1 0.250 0 ==> 1
21 (Posterior ex) 1 0.667 0 ==> 1
35 (#The posteri) 1 0.250 0 --> 1

48 (Internal car) 1 0.333 1 ==> 0
105 (Posterior p) 1 0.250 1 ==> 0
117 (Axis of pos) 1 0.500 0 ==> 1
137 (Length of a) 1 0.500 0 ==> 1
node_59 --> Probainognathus 20 (#Zygomatic a) 1 0.286 0 --> 1
26 (The notch se) 1 0.200 0 --> 1
55 (Foramen and) 1 0.333 0 ==> 1
81 (Squamosal ar) 1 0.667 0 --> 2
83 (#Lateral rid) 1 0.429 2 --> 0
118 (Upper tooth) 1 0.500 0 ==> 1
node_59 --> node_58 15 (#Palatine) 1 0.333 1 --> 2
16 (Sphenopalati) 1 0.333 0 ==> 1
82 (Dentary symp) 1 0.500 1 ==> 0
83 (#Lateral rid) 1 0.429 2 --> 3
86 (Mediolateral) 1 1.000 0 ==> 1
93 (Relationship) 1 0.600 0 ==> 1
103 (#Anteriormo) 1 0.500 0 ==> 1
106 (Upper postc) 1 0.750 0 ==> 1
107 (Lower postc) 1 0.500 0 ==> 1
108 (Buccal (ext) 1 1.000 0 ==> 1
115 (Lingual cin) 1 0.167 1 ==> 0
138 (Lateral sur) 1 1.000 0 ==> 1
139 (Posterior i) 1 1.000 0 ==> 1
140 (Cotyloid (a) 1 1.000 0 ==> 1
141 (The diamete) 1 1.000 0 --> 1
node_58 --> Prozostrodon 1 (#Premaxillary) 1 0.333 0 --> 2
94 (Upper inciso) 1 0.250 1 --> 0
95 (Lower inciso) 1 0.286 1 ==> 0
101 (Canine serr) 1 0.200 0 ==> 1
102 (Upper postc) 1 0.286 0 ==> 1
node_58 --> node_57 7 (Maxilla) 1 0.200 0 --> 1
12 (Parietal cre) 1 1.000 0 --> 1
13 (Prefrontal) 1 0.333 0 ==> 1
14 (#Postorbital) 1 1.000 0 ==> 2
17 (Zygomatic ar) 1 0.250 2 --> 1
36 (Osseous pala) 1 0.500 0 --> 1
123 (Posterior t) 1 1.000 0 --> 1
144 (Lesser troc) 1 1.000 0 ==> 1
145 (Lesser troc) 1 1.000 0 ==> 1
node_57 --> Therioherpeton 117 (Axis of pos) 1 0.500 1 ==> 0
node_57 --> node_56 2 (Septomaxilla) 1 0.143 1 --> 0
10 (Interparieta) 1 1.000 0 --> 1
31 (Interpterygo) 1 0.167 1 --> 0
39 (The nasophar) 1 1.000 0 --> 1

41 (Quadrate art) 1 0.333 1 --> 0
42 (Frontal-epip) 1 0.200 1 --> 0
44 (The anterior) 1 0.500 0 --> 1
51 (Internal aud) 1 1.000 0 --> 1
58 (Pterygoparoc) 1 0.333 0 --> 2
63 (Separation o) 1 0.500 0 --> 1
67 (The relation) 1 0.500 0 --> 1
69 (#Rotation of) 1 0.750 1 --> 2
71 (Size of the) 1 0.250 0 --> 1
73 (#Lateral mar) 1 1.000 1 --> 2
74 (#Medial marg) 1 0.667 1 --> 2
75 (Dorsal margi) 1 0.333 0 --> 1
76 (#Lateral not) 1 0.600 2 --> 3
78 (Articulation) 1 1.000 1 --> 3
79 (Craniomandib) 1 0.750 1 --> 2
120 (Vertebral c) 1 1.000 0 ==> 1
131 (Procoracoid) 1 1.000 0 --> 1
133 (Ulna olecra) 1 0.500 0 --> 1
142 (Femur head) 1 1.000 0 ==> 1
143 (Greater tro) 1 1.000 0 ==> 1
node_56 --> node_45 1 (#Premaxillary) 1 0.333 0 --> 2
4 (Paracanine fo) 1 1.000 0 ==> 3
46 (#Basisphenoi) 1 0.600 1 --> 2
68 (Shape of the) 1 0.333 0 ==> 1
94 (Upper inciso) 1 0.250 1 --> 2
96 (Incisor size) 1 0.500 0 --> 1
99 (Upper canine) 1 0.500 0 ==> 1
node_45 --> Riograndia 17 (Zygomatic ar) 1 0.250 1 ==> 2
27 (Palatine) 1 0.333 0 ==> 1
100 (Lower canin) 1 0.500 0 ==> 1
115 (Lingual cin) 1 0.167 0 ==> 1
node_45 --> Pachygenelus 35 (#The posteri) 1 0.250 1 ==> 2
65 (Paroccipital) 1 0.333 0 --> 1
81 (Squamosal ar) 1 0.667 0 --> 1
95 (Lower inciso) 1 0.286 1 ==> 2
106 (Upper postc) 1 0.750 1 ==> 0
107 (Lower postc) 1 0.500 1 ==> 0
117 (Axis of pos) 1 0.500 1 ==> 2
129 (Scapular el) 1 0.500 0 --> 1
node_56 --> node_55 38 (Middle of pt) 1 0.400 0 ==> 2
49 (Prootic and) 1 0.333 0 ==> 1
56 (Route of the) 1 0.667 1 ==> 2
62 (Paroccipital) 1 0.500 0 ==> 1
65 (Paroccipital) 1 0.333 0 --> 1

121 (Axis centru) 1 1.000 0 --> 1
122 (Dens) 1 1.000 0 --> 1
132 (Humerus ect) 1 1.000 0 ==> 1
138 (Lateral sur) 1 1.000 1 ==> 2
node_55 --> node_49 8 (Profile of sk) 1 0.400 2 ==> 1
57 (#Maxillary a) 1 0.667 0 --> 1
59 (Vertical com) 1 0.500 0 ==> 1
60 (Anterior par) 1 0.500 0 ==> 1
79 (Craniomandib) 1 0.750 2 ==> 0
node_49 --> Pseudotherium 2 (Septomaxilla) 1 0.143 0 ==> 1
7 (Maxilla) 1 0.200 1 ==> 0
13 (Prefrontal) 1 0.333 1 ==> 0
14 (#Postorbital) 1 1.000 2 ==> 1
15 (#Palatine) 1 0.333 2 ==> 1
18 (The anterove) 1 0.250 1 --> 0
40 (Quadrate ram) 1 0.500 1 ==> 0
46 (#Basisphenoi) 1 0.600 1 --> 3
50 (Promontorium) 1 0.500 0 --> 1
66 (Tabular) 1 0.333 0 ==> 1
103 (#Anteriormo) 1 0.500 1 --> 0
node_49 --> node_48 1 (#Premaxillary) 1 0.333 0 --> 1
6 (Maxillary pla) 1 0.500 0 ==> 1
20 (#Zygomatic a) 1 0.286 0 --> 2
21 (Posterior ex) 1 0.667 1 --> 0
22 (The posterov) 1 0.200 0 --> 1
24 (Squamosal gr) 1 0.500 0 ==> 1
25 (Posterior ex) 1 0.250 1 --> 0
35 (#The posteri) 1 0.250 1 ==> 2
45 (Parasphenoid) 1 1.000 0 ==> 1
52 (#The trigemi) 1 0.500 0 ==> 1
54 (Vascular for) 1 0.500 0 --> 1
61 (Hyoid (stape) 1 0.500 0 --> 1
63 (Separation o) 1 0.500 1 ==> 0
64 (Articulation) 1 0.250 0 --> 1
69 (#Rotation of) 1 0.750 2 --> 3
78 (Articulation) 1 1.000 3 --> 2
80 (Craniomandib) 1 1.000 0 ==> 2
84 (Angle of the) 1 0.500 0 --> 1
91 (Mandibular m) 1 0.667 0 --> 1
92 (Postcanine o) 1 0.667 0 ==> 1
93 (Relationship) 1 0.600 1 ==> 3
94 (Upper inciso) 1 0.250 1 --> 2
96 (Incisor size) 1 0.500 0 --> 1
99 (Upper canine) 1 0.500 0 ==> 2

100 (Lower canin) 1 0.500 0 --> 2
102 (Upper postc) 1 0.286 0 ==> 2
103 (#Anteriormo) 1 0.500 1 --> 2
104 (#Posteriorm) 1 0.667 0 ==> 2
106 (Upper postc) 1 0.750 1 ==> 3
107 (Lower postc) 1 0.500 1 --> 2
109 (Number of u) 1 0.400 0 ==> 2
112 (Arrangement) 1 0.500 0 ==> 1
117 (Axis of pos) 1 0.500 1 ==> 3
118 (Upper tooth) 1 0.500 0 ==> 2
119 (Postcanine) 1 0.667 0 --> 2
127 (#Acromion p) 1 1.000 1 --> 2
node_48 --> Oligokyphus 67 (The relation) 1 0.500 1 ==> 0
71 (Size of the) 1 0.250 1 ==> 0
75 (Dorsal margi) 1 0.333 1 ==> 0
node_48 --> node_47 3 (#Snout in rel) 1 0.250 1 --> 2
17 (Zygomatic ar) 1 0.250 1 --> 0
23 (The width of) 1 0.333 0 ==> 1
26 (The notch se) 1 0.200 0 ==> 1
34 (Posterior ex) 1 0.500 1 --> 0
44 (The anterior) 1 0.500 1 --> 0
48 (Internal car) 1 0.333 0 --> 1
node_47 --> node_46 31 (Interpterygo) 1 0.167 0 ==> 1
node_46 --> Tritylodon 22 (The posterov) 1 0.200 1 ==> 0
75 (Dorsal margi) 1 0.333 1 ==> 0
95 (Lower inciso) 1 0.286 1 ==> 2
node_46 --> Bienotherium 58 (Pterygoparoc) 1 0.333 2 ==> 0
node_47 --> Kayentatherium 27 (Palatine) 1 0.333 0 ==> 1
node_55 --> node_54 102 (Upper postc) 1 0.286 0 ==> 1
113 (Interlockin) 1 0.500 0 ==> 1
node_54 --> node_53 3 (#Snout in rel) 1 0.250 1 --> 0
18 (The anterove) 1 0.250 1 --> 0
46 (#Basisphenoi) 1 0.600 1 --> 2
47 (#Overlap of) 1 1.000 0 --> 1
50 (Promontorium) 1 0.500 0 --> 1
53 (Lateral trou) 1 1.000 0 --> 1
54 (Vascular for) 1 0.500 0 --> 1
55 (Foramen and) 1 0.333 0 --> 1
57 (#Maxillary a) 1 0.667 0 --> 2
100 (Lower canin) 1 0.500 0 ==> 1
119 (Postcanine) 1 0.667 0 --> 1
129 (Scapular el) 1 0.500 0 --> 1
node_53 --> node_50 64 (Articulation) 1 0.250 0 --> 1
68 (Shape of the) 1 0.333 0 ==> 1

node_50 --> Brasilodon 49 (Prootic and) 1 0.333 1 ==> 0
node_50 --> Brasilitherium 13 (Prefrontal) 1 0.333 1 ==> 0
17 (Zygomatic ar) 1 0.250 1 ==> 2
25 (Posterior ex) 1 0.250 1 --> 0
37 (Contribution) 1 0.500 1 ==> 0
94 (Upper inciso) 1 0.250 1 ==> 0
node_53 --> node_52 8 (Profile of sk) 1 0.400 2 ==> 0
11 (#Lateral exp) 1 1.000 0 ==> 1
52 (#The trigemi) 1 0.500 0 ==> 2
node_52 --> Adelobasileus 58 (Pterygoparoc) 1 0.333 2 ==> 1
62 (Paroccipital) 1 0.500 1 ==> 0
66 (Tabular) 1 0.333 0 --> 1
node_52 --> node_51 4 (Paracanine fo) 1 1.000 0 --> 2
27 (Palatine) 1 0.333 0 --> 1
31 (Interpterygo) 1 0.167 0 ==> 1
35 (#The posteri) 1 0.250 1 --> 2
43 (Epipterygoid) 1 1.000 0 ==> 1
46 (#Basisphenoi) 1 0.600 2 ==> 3
61 (Hyoid (stape) 1 0.500 0 ==> 1
79 (Craniomandib) 1 0.750 2 --> 3
81 (Squamosal ar) 1 0.667 0 --> 1
88 (#Postdentary) 1 1.000 1 --> 2
91 (Mandibular m) 1 0.667 0 --> 2
95 (Lower inciso) 1 0.286 1 --> 0
106 (Upper postc) 1 0.750 1 --> 2
107 (Lower postc) 1 0.500 1 --> 2
node_51 --> Sinoconodon 59 (Vertical com) 1 0.500 0 ==> 1
77 (Articulation) 1 0.667 1 --> 0
93 (Relationship) 1 0.600 1 --> 0
102 (Upper postc) 1 0.286 1 ==> 0
113 (Interlockin) 1 0.500 1 ==> 0
115 (Lingual cin) 1 0.167 0 ==> 1
node_51 --> Morganucodon 21 (Posterior ex) 1 0.667 1 ==> 2
30 (Ectopterygoi) 1 0.286 2 ==> 1
47 (#Overlap of) 1 1.000 1 ==> 2
60 (Anterior par) 1 0.500 0 ==> 1
64 (Articulation) 1 0.250 0 --> 1
66 (Tabular) 1 0.333 0 --> 1
68 (Shape of the) 1 0.333 0 ==> 1
77 (Articulation) 1 0.667 1 --> 2
78 (Articulation) 1 1.000 3 --> 4
92 (Postcanine o) 1 0.667 0 ==> 2
93 (Relationship) 1 0.600 1 --> 2
124 (Anapophysis) 1 0.200 0 --> 1

node_61 --> Ectenion 2 (Septomaxilla) 1 0.143 1 --> 0
8 (Profile of sk) 1 0.400 0 --> 2
15 (#Palatine) 1 0.333 0 --> 2
38 (Middle of pt) 1 0.400 0 ==> 2
52 (#The trigemi) 1 0.500 0 ==> 1
58 (Pterygoparoc) 1 0.333 0 ==> 1
83 (#Lateral rid) 1 0.429 2 --> 0
101 (Canine serr) 1 0.200 0 --> 1
node_63 --> Lumkuia 7 (Maxilla) 1 0.200 0 ==> 1
9 (Parietal fora) 1 0.250 0 --> 1
26 (The notch se) 1 0.200 0 --> 1
29 (Vomer) 1 0.333 0 --> 1
30 (Ectopterygoi) 1 0.286 0 ==> 2
35 (#The posteri) 1 0.250 0 ==> 1
38 (Middle of pt) 1 0.400 0 ==> 1
49 (Prootic and) 1 0.333 0 ==> 1
58 (Pterygoparoc) 1 0.333 0 ==> 1
76 (#Lateral not) 1 0.600 1 ==> 0
node_65 --> Platycraniellus 19 (Infraorbital) 1 0.286 0 --> 1
20 (#Zygomatic a) 1 0.286 0 ==> 1
30 (Ectopterygoi) 1 0.286 0 --> 1
71 (Size of the) 1 0.250 0 ==> 1
85 (Position of) 1 0.500 0 --> 1

APPENDIX 3.A: DATA TABLE

Taxon	Clade	Skull_length	Body_mass	FM_area	log_FM_area	Encephalization_volume	EV_source	Mass_source	Specimen number
Brasilitherium	NMC	38.03	98.57			0.378436	Rodrigues et al., 2014	Rodrigues et al., 2014	
Diademodon	NMC	330	50000	194.245	2.288349849	26.971	Macrini, 2006	Jerison, 1973	
Exaeretodon sp.	NMC	278	46877			19.91	Skull length + EV: Quiroga, 1980	BM eq.: Liu et al., 2001	
Hadrocodium	Mammaliaform	12	2	3.576	0.55339751	0.04515	Macrini, 2006	Luo et al., 2001	
Kayentatherium	NMC	108.756	4614.238	63.307	1.801451734		N/A	This study	USNM 317208
Kayentatherium	NMC	89.236	2228.371	21.378	1.329967073	0.9939	This study	This study	TMM
Kryptobataar	Mammal	26.3	28.1	12.053	1.081095157	0.343	Macrini, 2006	Macrini and Rowe, unpublished data	
Massetognathus sp.	NMC	95	2805.58136			3.33	Skull length + EV: Quiroga, 1980; BM eq.: Liu et al., 2001		
Morganucodon	Mammaliaform	32.5	51	20.5275	1.312336061	0.325	Rowe et al., 2011	Rowe et al., 2011	
Obdurodon	Mammal	141.795	2038	127.0683333	2.104037334	15.443	Macrini et al., 2006	Macrini et al., 2006	
Probainognathus jenseni	NMC	65	590			1.2	Skull length + EV: Quiroga, 1980	BM eq.: Liu et al., 2001	
Probelesodon sp.	NMC	120	3807			4.33	Skull length + EV: Quiroga, 1980	BM eq.: Liu et al., 2001	
Pseudotherium argentinus	NMC	75.839	1224.63	20.073	1.302612285	1.34	This study	This study	

Pucadelphys andinus	Mammal	30.944	49	9.693666667	0.986488082	0.312	Macrini et al., 2007a	Macrini et al., 2007a	
Therioherpeton	NMC	33	57.3			0.36	Quiroga, 1984	BM eq.: Liu et al., 2001	
Trirachodon	NMC	104.231	3946.649952	46.63533333	1.668715085		N/A		
Vincelestes	Mammal	57.033	900	33.687	1.527462337	2.371	Macrini et al., 2007b	Macrini et al., 2007b	
Zalambdalestes 108	Mammal	46.256	82.69	27.704	1.442542479	1.02	Kielan-Jaworowska, 1984	Kielan-Jaworowska, 1984	PSS-MAE130
Zalambdalestes 130	Mammal	27.704	82.69	15.73633333	1.172515363	1.02	Kielan-Jaworowska, 1984	Kielan-Jaworowska, 1984	PSS-MAE108
Allactaga_major	Mammal	44.135		46.852					
Artibeus_jamaicensis	Mammal	26.862		17.3					
Bradypus_variegatus	Mammal	72.907		62.411					
Callicebus_moloch	Mammal	68.793		40.333					
Callimico_goeldi	Mammal								
Canis_lupus	Mammal	221.774	36500	203.169	2.307857443	153.937	Macrini, 2006	Macrini, 2006	
Carollia_perspicillata	Mammal	20.374		7.555					
Cavia_porcellus	Mammal	66.783		42.513					
Cebus_apella	Mammal	86.423		113.995					
Chrysochloris_sp	Mammal	24		12.338					
Cynomys_ludovicianus	Mammal	50.874		25.483					
Cynopterus_brachyotis	Mammal	27.304		10.531					
Dasypus_novemcinctus	Mammal	51.389	4000	100.12	2.000520841	10.546	Macrini, 2006	Macrini, 2006	
Dasyurus_hallucatus	Mammal	36.053	401	35.288	1.547627045	3.339	Macrini et al., 2007a	Macrini et al., 2007a	

Didelphis_virginiana	Mammal	107.835	2800	45.62	1.659155281	6.608	Macrini et al., 2007a	Macrini et al., 2007a
Dolichotis patagonum	Mammal	118.614		104.632				
Dromiciops_australis	Mammal	28.454	21.5	15.53	1.191171456	0.821	Macrini et al., 2007a	Macrini et al., 2007a
Eptesicus_fuscus	Mammal	19.121		9.556				
Felis_silvestris	Mammal	88.361	4500	73.332	1.86529353	28.276	Macrini, 2006	Macrini, 2006
Glaucomys_volans	Mammal	35.34		19.876				
Gorilla_gorilla	Mammal	263.86		590.22				
Hemicentetes semispinosus	Mammal	39.204		19.272				
Heterocephalus glaber	Mammal	20.58		12.492				
Hipposideros giga	Mammal	35.948		19.788				
Homo_sapiens	Mammal	186.351		544.146				
Hyaena_hyaena	Mammal	215.51		172.635				
Hypsignathus_monstrosus	Mammal	59.27		30.06				
Lemur_fulvus	Mammal	90.349		103.589				
Lepus_californicus	Mammal	97.806		101.114				
Loris_tardigradus	Mammal	51.144		26.44				
Macropus_eugenii	Mammal	120.536		126.212				
Macroscelides_proboscideus	Mammal	34.455		16.257				
Manis_tricuspis	Mammal	45.041	4500	63.211	1.800792661	10.711	Macrini, 2006	Macrini, 2006
Monodelphis_domestica	Mammal	38.873	80.4	17.157	1.234441351	0.954	Macrini et al., 2007a	Macrini et al., 2007a
Ornithorhynchus_anatinus	Mammal	92.167	1389	79.5325	1.900544634	9.732	Macrini, 2006	Macrini, 2006

Orycteropus_afer	Mammal	250.455	60000	398.351	2.600265912	103.943	Macrini, 2006	Macrini, 2006
Phascolarctos_cinereus	Mammal	120	9500	145.846	2.163894523	26.275	Macrini et al., 2007a	Macrini et al., 2007a
Procavia_capensis	Mammal	109.6	3800	70.458	1.847930311	14.337	Macrini, 2006	Macrini, 2006
Tachyglossus_aculeatus	Mammal	101.972	4250	111.534	2.047407278	20.013	Macrini, 2006	Macrini, 2006
Trichechus_senegalensis	Mammal	190.345	140000	820.785	2.914229411	374.556	Macrini, 2006	Macrini, 2006
Tursiops_truncatus	Mammal	430	385500	1622.959	3.210307549	2048.23	Colbert et al., 2005	http://www.nmfs.noaa.gov/pr/species/mammals/dolphins/bottlenose-dolphin.html
Vombatus_ursinus	Mammal	106.875	25000	285.8445	2.45612984	63.553	Macrini et al., 2007a	Macrini et al., 2007a
Zaglossus_bruijni	Mammal	160.217	7500	246.4785	2.391779042	36.049	Macrini, 2006	Macrini, 2006
Agama_agama	Lepidosaur	24.953		7.605				
Anolis_carolinensis	Lepidosaur	19.816		2.359				
Basiliscus_basiliscus	Lepidosaur	41.915		10.481				
Callopistes_maculatus	Lepidosaur	33.027		7.909				
Chamaeleo_laevigatus	Lepidosaur	20.538		3.982				
Cnemidophorus_tigris	Lepidosaur	25.437		5.666				
Crotaphytus_collaris	Lepidosaur	27.87		6.81				
Ctenosaura_pectinata	Lepidosaur	64.688		21.827				
Dipsosaurus_dorsalis	Lepidosaur	22.92		6.024				

Draco_quinquefasciatus	Lepidosaur	18.248	2.47
Eublepharis_macularius	Lepidosaur	22.477	4.092
Gonatodes_albogularis	Lepidosaur	11.574	1.525
Lacerta_viridis	Lepidosaur	11.567	1.59
Latastia_longicaudata	Lepidosaur	15.453	2.763
Lepidophyma_flavimaculatum	Lepidosaur	23.71	4.241
Phrynosoma_platyrhinos	Lepidosaur	13.531	4.539
Pogona_vitticeps	Lepidosaur	40.297	11.2
Sphenodon_punctatus	Lepidosaur	55.244	24.067
Teius_teyou	Lepidosaur	26.624	7.546
Tupinambus_teguixin	Lepidosaur	59.444	23.111
Uta_stansburiana	Lepidosaur	12.676	2.16
Varanus_acanthurus	Lepidosaur	30.875	7.602
Varanus_exanthematicus	Lepidosaur	56	18.18
Varanus_komodoensis	Lepidosaur	198	92.144
Xenosaurus_grandis	Lepidosaur	27.296	4.683
Alca_tordus	Aves	98.427	47.62
Anas_platyrhynchos	Aves	125.918	67.171
Brotogeris_chrysopterus	Aves	34.333	11.486
Chauna_chavaria	Aves	87.443	48.841

Coragyps_atratus	Aves	90.482	35.031
Crypturellus_cinnamomeus	Aves	56.5	13.847
Gallus_gallus	Aves	66.047	35.017
Gavia_immer	Aves	148.636	68.181
Grus_canadensis	Aves	180	60.308
Haliaeetus_leucocephalus	Aves	126.477	86.93
Melanerpes_aurifrons	Aves	48.471	19.812
Podilymbus_podiceps	Aves	53.583	21.805
Ptilinopus_melanospila	Aves	42.214	15.352
Rhea_americana	Aves	77.922	30.241
Seiurus_aurocapillus	Aves	30.708	6.304
Struthio_camelus	Aves	76.867	48.923
Tyto_alba	Aves	69.663	26.052

APPENDIX 3.B: R CODE

```
#Load packages
library(tidyverse)
library(nlme)
library(car)

#Load Data
Skull_FM_EV <- read_csv("Skull_FM_EV.csv") %>%
  mutate(Skull_length_centered =Skull_length - mean(Skull_length, na.rm = T),
         Clade = relevel(as.factor(Clade), ref = "Mammal"))

nonmam <- filter(Skull_FM_EV, Clade != "Mammal")
cor.test(nonmam$Skull_length, nonmam$Encephalization_volume)
cor.test(nonmam$Body_mass, nonmam$Encephalization_volume)
cor.test(Skull_FM_EV$FM_area, Skull_FM_EV$Encephalization_volume)

plot(Skull_FM_EV$Encephalization_volume, Skull_FM_EV$FM_area)
model1 <- lm(Encephalization_volume ~ FM_area, data = Skull_FM_EV)
summary(model1)

model1.2 <- lm(log(Encephalization_volume) ~ log(FM_area), data = Skull_FM_EV)
summary(model1.2)
```

```
AIC(model1, model1.2)

model2 <- lm(Encephalization_volume ~ FM_area * Clade, data = Skull_FM_EV)
summary(model2)

aq_mam <- c("Trichechus_senegalensis", "Tursiops_truncatus")

model3 <- lm(Encephalization_volume ~ FM_area,
             data = Skull_FM_EV)
summary(model3)
plot(model3)
View(Skull_FM_EV[!(Skull_FM_EV$Taxon %in% aq_mam),])

model3.2 <- lm(log(Encephalization_volume) ~ log(FM_area),
               data = Skull_FM_EV)
summary(model3.2)

model3.3 <- lm(log(Encephalization_volume) ~ log(FM_area) * Clade,
               data = Skull_FM_EV)
summary(model3.3)

AIC(model3, model3.2, model3.3)

Skull_FM_EV %>%
```

```
  #filter(!(Skull_FM_EV$Taxon %in% aq_mam)) %>%
  ggplot(aes(x = FM_area, y = Encephalization_volume)) +
    geom_point() +
    geom_smooth(method = lm,
                se = FALSE) +
    geom_text(aes(label = ifelse(Taxon %in% aq_mam, Taxon, ""))) +
    scale_x_log10() +
    scale_y_log10() +
    labs(x = "Foramen Magnum Area (mm^2)",
         y = "Encephalization Volume (cm^3)")



#modling FM_area as a function of skull length
model4 <- lm(FM_area~Skull_length_centered*Clade,
             data = Skull_FM_EV)
summary(model4)
plot(model4)

#Accounting for allometry
model5 <- lm(I(log(FM_area))~ I(log(Skull_length))*Clade,
             data = Skull_FM_EV)
summary(model5)
#Accounting for allometry
model6 <- lm(I(log(FM_area)) ~ I(log(Skull_length))*I(Clade %in% c("Mammal", "Mammaliaform")),
```

```
            data = Skull_FM_EV)
summary(model6)


anova(model5, model6)
AIC(model5, model6)


Skull_FM_EV %>%
  filter(!(Taxon %in% aq_mam)) %>%
  ggplot(aes(y = FM_area, x = Skull_length_centered, color = Clade, shape = Clade)) +
  geom_point() +
  geom_smooth(method = lm,
              se = FALSE) +
  geom_text(aes(label = ifelse(FM_area > 150, Taxon, "")), vjust = 0, hjust = 1) +
  labs(title = "Foramen magnum area vs. skull length",
       x = "Skull Length - mean(Skull Length) (mm)",
       y = "Foramen Magnum Area (mm^2)")


Skull_FM_EV %>%
  group_by(Clade) %>%
  summarize(Taxon = Taxon[which.min(Skull_length)], min_Skull_Length =  min(Skull_length))


NMC_predictions <- data.frame(Clade= "NMC",
                              FM_area = seq(0, 200))
```

```
NMC_predictions <- data.frame(NMC_predictions, predict(model3, NMC_predictions,
interval="predict"))

NMC_predictions %>%

  ggplot(aes(x = FM_area, y = fit)) +

  geom_line(color = "blue") +

  geom_ribbon(aes(x = FM_area, ymin = lwr, ymax = upr),

              color = "grey",

              alpha = 0.5) +

  geom_point(aes(x = FM_area, y = Encephalization_volume, color = Taxon),

             data = filter(Skull_FM_EV, Clade == "NMC")) +

  labs(y = "Encephalization Volume [cm^3]",

       x = "Average Foramen Magnum Area [mm^2]")



#Allometric Plot

Skull_FM_EV %>%

  ggplot(aes(y = FM_area, x = Skull_length, color = Clade, shape = Clade)) +

  geom_point() +

  geom_smooth(method = lm,

              se = FALSE) +

  geom_text(aes(label = ifelse(Taxon %in% aq_mam, Taxon, ""))) +

  scale_x_log10() +

  scale_y_log10() +

  labs(title = "Foramen magnum area vs. skull length",
```

```
      x = "Skull Length (mm)",
      y = "Foramen Magnum Area (mm^2)")

#NLS no effect of
#Accounting for allometry
model7 <- lm(I(log(FM_area)) ~ I(log(Skull_length)),
             data = Skull_FM_EV)

model8 <- nlsLM(FM_area ~ A * Skull_length^c,
       data = Skull_FM_EV,
       start = list(A = coef(model7)[1], c = coef(model7)[2]))
summary(model8)

model9 <- nlme(FM_area ~ (A * Skull_length^c),
               fixed = A + c ~1 ,
               groups = ~ Clade,
                 data = Skull_FM_EV %>%
                   select(Taxon, Clade, FM_area, Skull_length) %>%
                   na.omit,
                 start = c(A = coef(model7)[1], c = coef(model7)[2]))
summary(model9)
coef(model9)

model10 <- nlme(FM_area ~ (A * Skull_length^c),
```

```
            fixed = A + c ~ 1,
            groups = ~I(Clade %in% c("Mammal")),
              data = Skull_FM_EV %>%
              select(Taxon, Clade, FM_area, Skull_length) %>%
              na.omit,
            start = c(A = coef(model7)[1], c = coef(model7)[2]))
summary(model10)
coef(model10)

anova.lme(model9, model10)

#Nonlinear Plot
Skull_FM_EV %>%
  select(Taxon, Clade, FM_area, Skull_length) %>%
  na.omit %>%
  mutate(pred9 = predict(model9)) %>%
  ggplot(aes(y = FM_area, x = Skull_length, color = Clade, shape = Clade)) +
  geom_point() +

  geom_line(aes(x = Skull_length, y = pred9))+
  labs(title = "Foramen magnum area vs. skull length",
       x = "Skull Length (mm)",
       y = "Foramen Magnum Area (mm^2)")
```

```
AIC(model4, model5, model6, model7, model8, model9, model10)


Skull_FM_EV %>%
  select(Skull_length, FM_area, Clade) %>%
  na.omit %>%
  mutate(pred6 = predict(model6),
         resid6 = residuals(model6)) %>%
  ggplot(aes(x = log(FM_area), y = resid6)) +
    geom_point() +
    facet_wrap(~Clade)


Skull_FM_EV %>%
  select(Skull_length, FM_area, Clade) %>%
  na.omit %>%
  mutate(pred6 = predict(model6),
         resid6 = residuals(model6)) %>%
         {leveneTest(.$resid6 ~ .$Clade)}


gls1 <- gls(I(log(FM_area)) ~ I(log(Skull_length)),
         data = Skull_FM_EV %>%
           select(FM_area, Skull_length, Taxon, Clade) %>%
           na.omit)


summary(gls1)
```

```
coef(gls1)

gls2 <- gls(I(log(FM_area)) ~ I(log(Skull_length)) * Clade,
            data = Skull_FM_EV %>%
              select(FM_area, Skull_length, Taxon, Clade) %>%
              na.omit)

summary(gls2)

gls3 <- gls(I(log(FM_area)) ~ I(log(Skull_length)) * Clade,
            data = Skull_FM_EV %>%
              select(FM_area, Skull_length, Taxon, Clade) %>%
              na.omit,
            weights = varIdent(form = ~ Clade))
summary(gls3)

gls4 <- gls(I(log(FM_area)) ~ I(log(Skull_length)) * I(Clade %in% c("Mammal", "Mammaliaform")),
            data = Skull_FM_EV %>%
              select(FM_area, Skull_length, Taxon, Clade) %>%
              na.omit,
            weights = varIdent(form = ~ I(Clade %in% c("Mammal", "Mammaliaform"))))
summary(gls4)
anova(gls3, gls4)
```

```
AIC(gls1, gls2, gls3, gls4, model5, model6)

AIC(model7, model5, model6)

anova(model7, model5, model6)
```

References

Abdala, F. 2007. Redescription of *Platycraniellus elegans* (Therapsida, Cynodontia) from the lower Triassic of South Africa, and the cladistic relationships of eutheriodonts. Palaeontology 50: 591-618.

Balanoff, A.M., and Bever, G.S. 2017. The role of endocasts in the study of brain evolution. In J. Kaas (Ed.), Evolution of Neurosensory Systems, Volume 1 (pp. 223-241). Amsterdam, Netherlands: Elsevier.

Barghusen, H.R. 1986. On the evolutionary origin of the therian tensor veli palatini and tensor tympani muscles. In N.H. Hotton III, P.D. MacLean, J.J. Roth, and E.C. Roth (Eds.), The ecology and biology of mammal-like reptiles (pp. 256-262). Washington, D.C.: Smithsonian Institution Press.

Bargmann, C.I. 2006. Comparative chemosensation from receptors to ecology. Nature 444: 295-301.

Barton, R.A., and Harvey, P.H. 2000. Mosaic evolution of brain structure in mammals. Nature 405: 1055-1058.

Bauchot, R. and Stephan, H. 1967. Encéphales et moulages endocraniens de quelques insectivores et primates actuels. In: Problemes actuels in paleontologie (Évolution des Vertébrés): Colloques Interanationaux de Centre National de la Recherche Scientifique. Paris, France, 6-11 June 1966. Editions du Centre National de la Recherché Scientifique, 163: 575-586.

Benoit, J., Manger, P.R., Rubidge, B.S. 2016. Palaeoneurological clues to the evolution of defining mammalian soft tissue traits. Scientific Reports 6: 25604. Available from: https://www.nature.com/articles/srep25604 DOI: 10.1038/srep25604

Benoit, J., Manger, P.R., Norton, L., Fernandez, F., and Rubidge, B.S. 2017a. Synchrotron scanning reveals the palaeoneurology of the head-butting *Moschops capensis* (Therapsida, Dinocephalia). PeerJ 5: e3496. DOI 10.7717/peerj.3496

Benoit, J., Fernandez, V., Manger, P.R., and Rubidge, B.S. 2017b. Endocranial casts of pre-mammalian therapsids reveal an unexpected neurological diversity at the deep evolutionary root of mammals. Brain, Behavior, and Evolution 90: 311-333.

Bird, D.J., Murphy, W.J., Fox-Rosales, L., Hamid, I., Eagle, R.A., and Van Valkenburgh, B. 2018. Olfaction written in bone: cribriform plate size parallels olfactory receptor gene repertoires in Mammalia. Proceedings of the Royal Society of London B 285: 20180100. DOI: 10.1098/rspb.2018.0100

Bonaparte, J.F. 1962. Descripción del cráneo y mandíbula de *Exaeretodon frenguellii*, Cabrera y su comparación con Diademodontidae, Tritylodontidae y los cinodontes sudamericanos. Publicaciones del Museo Municipal de Ciencias Naturales y Tradicionales de Mar del Plata 1:135-202.

Bonaparte, J.F. 2013. Evolution of the Brasilodontidae (Cynodontia-Eucynodontia). Historical Biology 25: 643-653.

Bonaparte, J.F., and Barberena, M.C. 1975. A possible mammalian ancestor from the Middle Triassic of Brazil (Therapsida-Cynodontia). Journal of Paleontology 49: 931-936.

Bonaparte, J.F., and Barberena, M.C. 2001. On two advanced carnivorous cynodonts from the Late Triassic of southern Brazil. Bulletin of the Museum of Comparative Zoology 156: 37-48.

Bonaparte, J.F., Martinelli, A.G., Schultz, C.L., and Rubert, R. 2003. The sister group of mammals: small cynodonts from the Late Triassic of southern Brazil. Revista Brasileira de Paleontologia 5: 5-27.

Bonaparte, J.F., Martinelli, A.G., Schultz, C.L., and Rubert, R. 2005. New information on *Brasilodon* and *Brasilitherium* (Cynodontia, Probainognathia) from the late Triassic of southern Brazil. Revista Brasileira Paleontologia 8: 25-46.

Bonaparte, J.F., Soares, M.B., and Martinelli, A.G. 2013. Discoveries in the Late Triassic of Brazil improve knowledge on the origin of mammals. Historia Natural, Fundación Felix de Azara, Tercera Series 2: 5-30.

Bonaparte, J.F., Martinelli, A.G., Schultz, C.L., and Rubert, R. 2005. New information on *Brasilodon* and *Brasilitherium* (Cynodontia, Probainognathia) from the late Triassic of southern Brazil. Revista Brasileira de Paleontologia 8: 25-46.

Broom, R. 1905. On the use of the term Anomodontia. Records of the Albany Museum, (Grahmstown, South Africa) 4: 266-269.

Broom, R. 1912. On a new type of cynodont from the Stormberg. Annals of the South African Museum 7: 334-336.

Broom, R. 1929. On some recent new light on the origin of mammals. Proceedings of the Linnean Society of New South Wales 54: 688–694.

Broom, R. 1932. The mammal-like reptiles of South Africa and the origin of mammals. London: HF & G Witherby. p. 376.

Broom, R. 1936. On some new genera and species of Karroo fossil reptiles, with notes on some others. Annals of the Transvaal Museum 18: 349-386.

Broom, R. 1937. A further contribution to our knowledge of the fossil reptiles of the Karroo. Proceedings of the Zoological Society of London, Series B 107: 299–318.

Cantino, P.D., and de Queiroz, K. 2002. PhyloCode: a phylogenetic code of biological nomenclature. Available from: https://www.ohio.edu/PhyloCode/PhyloCode2a.pdf

Cantino, P.D., and de Queiroz, K. 2002. PhyloCode: a phylogenetic code of biological nomenclature. Available from: https://www.ohio.edu/PhyloCode/PhyloCode2a.pdf

Carlson, W.D., Rowe T., Ketcham, R.A., and Colbert, M.W. 2003. Applications of high-resolution X-ray computed tomography in petrology, meteoritics and palaeontology. Geological Society, London, Special Publications 215: 7-22.

Case, E.C. 1907. Revision of the Pelycosauria of North America. Washington, Carnegie Institution of Washington Publications.

Chen, W.R., and Shepherd, G.M. 2005. The olfactory glomerulus: a cortical module with specific functions. Journal of Neurocytology 34: 353-360.

Cluver, M.A. 1971. The cranial morphology of the dicynodont genus *Lystrosaurus*. Annals of the South African Museum 56: 155-274.

Colbert, M.W., Racicot, R., and Rowe, T. 2005. Anatomy of the cranial endocast of the bottlenose dolphin, *Tursiops truncatus*, based on HRXCT. Journal of Mammalian Evolution 12: 195-207. DOI: 10.1007/s10914-005-4861-0

Crompton, A.W. 1955. A revision of the Scalaposauridae with special reference to kinetism in this family. Researches Nasionale Museum. Bloemfontein. 1: 150-183.

Crompton, A.W. 1958. The cranial morphology of a new genus and species of ictidosaurian. Journal of Zoology 130: 183-216.

Crompton, A.W., and Luo, Z.-X. 1993. Relationships of the Liassic mammals *Sinoconodon*, *Morganucodon oehleri*, and *Dinnetherium*. In Mammal Phylogeny (pp. 30-44). New York: Springer.

Crompton, A.W., and Sun, A.L. 1985. Cranial structure and relationships of the Liassic mammal *Sinoconodon*. Zoological Journal of the Linnean Society 85: 99-119.

Crompton, A.W., Owerkowicz, T., Bhullar, B.-A., and Musinsky, C. 2017. Structure of the nasal region of non-mammalian cynodonts and mammaliaforms: speculations on the evolution of mammalian endothermy. Journal of Vertebrate Paleontology 37: e1269116. DOI: 10.1080/02724634.2017.1269116

Cruce, W.L.R. and Newman, D.B. 1984. Evolution of motor systems: the reticulospinal pathways. American Society of Zoologists 24: 733-753.

Currie, B.S., Colombi, C.E., Tabor, N.J., Shipman, T.C., and Montañez, I.P. 2009. Stratigraphy and architecture of the Upper Triassic Ischigualasto Formation, Ischigualasto Provincial Park, San Juan, Argentina. Journal of South American Earth Sciences 27:74–87.

Davies, T.G., Rahman, I.A., Lautenschlager, S., Cunningham, J.A., Asher, R.J., Barrett, P.M., et al. 2017. Open data and digital morphology. Proceedings of the Royal Society B 284: 20170194. Available from: http://rspb.royalsocietypublishing.org/content/284/1852/20170194 DOI: DOI: 10.1098/rspb.2017.0194

Deacon, T.W. 1990. Rethinking mammalian brain evolution. American Zoologist 30: 629-705.

De Beer, G.R. 1937. The Development of the Vertebrate Skull. Chicago: University Chicago Press. p. 554.

de Queiroz, K., and Gauthier, J.A. 1992. Phylogenetic taxonomy. Annual Review of Ecology and Systematics 23: 449-80.

de Queiroz, K., and Gauthier, J.A. 1994. Toward a phylogenetic system of biological nomenclature. Trends in Ecology & Evolution 9: 27-31.

Donoghue, M., Doyle, J., Gauthier, J.A., Kluge, A.G., and Rowe, T.B. 1989. Importance of fossils in phylogeny reconstruction. Annual Review of Ecology and Systematics 20: 431-460.

Edinger, T. 1941. The brain of *Pterodactylus*. American Journal of Science 239: 665-682.

Edinger, T. 1975. Paleoneurology 1804–1966: an annotated bibliography. Advances in Anatomy Embryology and Cell Biology 49 (1-6): 1-258.

Eisenberg, J.F. 1981. The Mammalian Radiations. Chicago, IL: University of Chicago.

Elbroch, M. 2006. Animal skulls: a guide to North American species. Mecanicsburg, PA: Stackpole Books. p. 727

Elzhov, T.V., Mullen, K.M., Spiess, A.-N., and Bolker, B. 2016. Minpack.lm: R interface to the Levenberg-Marquardt nonlinear least-squares algorithm found in MINPACK, Plus support for bounds. R package version 1.2-1. http://CRAN.R-project.org/package=minpack.lm

Estes, R. 1961. Cranial anatomy of the cynodont reptile *Thrinaxodon liorhinus*. Bulletin of the Museum of Comparative Zoology 125: 165-180.

Fabbri, M., Koch, N.M., Pritchard, A.C., Hanson, M., Hoffman, E., Bever, G.S., Balanoff, A.M., Morris, Z.S., Field, D.J., Camacho, J., Rowe, T.B., Norell, M.A., Smith, R.M., Abzhanov, A., and B.-A.S. Bhullar. 2017. The skull roof tracks the brain during the evolution and development of reptiles including birds. Nature Ecology & Evolution 1: 1543. DOI: 10.1038/s41559-017-0288-2

Farbman, A.I. 1988. Cellular interactions in the development of the vertebrate olfactory system. In Margolis, F.L., Getchell, T.V. (Eds), Molecular neurobiology of the olfactory system (pp. 319-332). New York, NY: Plenum Press.

Farbman, A.I. 1990. Olfactory neurogenesis: genetic or environmental controls? Trends in Neurosciences 13: 362-365.

Finlay, B.L., and Darlington, R.B. 1995. Linked regularities in the development and evolution of mammalian brains. Science 268: 1578-1584. DOI: 10.1126/science.7777856

Finlay, B.L., Darlington, R.B., and Nicastro, N. 2001. Developmental structure in brain evolution. Behavioral and Brain Sciences 24: 263-308.

Fourie, S. 1974. The cranial morphology of *Thrinaxodon liorhinus* Seeley. Annals of the South African Museum 65: 337-400.

Gauthier, J.A., Kluge, A.G., and Rowe, T.B. 1988. Amniote phylogeny and the importance of fossils. Cladistics 4: 105-209.

Goldby, F. 1939. An experimental investigation of the motor cortex and pyramidal tract of *Echidna aculeata*. Journal of Anatomy 73: 509-524.

Hager, R., Lu, L., Rosen, G.D., and Williams, R.W. 2012. Genetic architecture supports mosaic brain evolution and independent brain-body size regulation. Nature Communications 3: 1079. Available from: https://www.nature.com/articles/ncomms2086 DOI: 10.1038/ncomms2086

Haughton, S.H., and Brink, A.S. 1954. A bibliographic list of Reptilia from the Karroo beds of Africa. Palaeontologica Africana 2: 1-187.

Heffner, R., and Masterton, B. 1975. Variation in form of the pyramidal tract and its relationship to digital dexterity. Brain, Behavior, and Evolution 12: 161-200.

Herculano-Houzel, S., Manger, P.R., and Kaas, J.H. 2014. Brain scaling in mammalian evolution as a consequence of concerted and mosaic changes in numbers of neurons and average neuronal cell size. Frontiers in Neuroanatomy 8: 1-28. DOI: 10.3389/fnana.2014.00077

Hopson, J. 1971. Postcanine replacement in the gomphodont cynodont *Diademodon*. Zoological Journal of the Linnean Society 50: 1-21.

Hopson, J.A. 1979. Paleoneurology. In Gans, C., Northcutt, R.G., and Ulinski, P.S. (Eds.), Biology of the Reptilia, vol. 9: Neurology A (pp. 39-146). New York, NY: Academic Press.

Hopson, J.A. 1990. Cladistic analysis of therapsid relationships. Journal Vertebrate Paleontology 10(S3): 28A.

Hopson, J.A., and Barghusen, H.R. 1986. An analysis of therapsid relationships. In: Roth JJ, Roth EC, McLean PO, and Hotton III N (Eds), Ecology and Biology of Mammal-Like Reptiles (pp. 83-106). Washington, D.C.: Smithsonian Institution and Institute of Mental Health.

Hopson, J.A., and Kitching, J.W. 2001. Probainognathian cynodont from South Africa. Bulletin of the Museum of Comparative Zoology 156: 5-35.

Hurlburt, G.R. 1999. Comparison of body mass estimation techniques, using recent reptiles and the pelycosaur *Edaphosaurus boanerges*. Journal of Vertebrate Paleontology 19:338–350.

Jerison, H.J. 1973. Evolution of the brain and intelligence. New York, NY: Academic Press.

Jerison, H.J. 1975. Fossil evidence of the evolution of the human brain. Annual Review of Anthropology 4:27-58. Available from: https://www.annualreviews.org/doi/pdf/10.1146/annurev.an.04.100175.000331

Ji, Q., Luo, Z.-X., Yuan, C.-X., and Tabrum, A.R. 2006. A swimming mammaliaform from the Middle Jurassic and ecomorphological diversification of early mammals. Science 311: 1123-1127.

Kaas, J.H. 2009. Reconstructing the organization of the forebrain of the first mammals. In Kaas, J.H. (Ed.), Evolutionary Neuroscience (pp. 523-544). New York, NY: Academic Press.

Kalischer, O. 1905. Das Grosshirn der Papageien in anatomischer und physiologischer Beziehung. Abhandlungen der Preussischen AkademiederWissenschaften, p 1–105.

Karten, H.J. 1971. Efferent projections of the Wulst of the owl. Anatomical Record (abstract) 169: 353.

Kemp, T.S. 1979. The primitive cynodont *Procynosuchus*: structure, function, and evolution of the postcranial skeleton. Philosophical Transactions of the Royal Society of London, Series B 288: 217-258.

Kemp, T.S. 1982. Mammal-like Reptiles and the Origin of Mammals. London and New York: Academic Press Inc.

Kemp, T.S. 1983. The relationships of mammals. Zoological Journal Linnean Society 77: 353-384.

Kemp, T.S. 2005. The origin and evolution of mammals. Oxford: Oxford University Press.Kemp, T.S. 2006. The origin and early radiation of the therapsid mammal-like reptiles: a palaeobiological hypothesis. Journal of Evolutionary Biology 19: 1231-1247.

Kemp, T.S. 2009. The endocranial cavity of the nonmammalian cynodonts *Chiniquodon theotenicus* and its implications for the origin of the mammalian brain. Journal of Vertebrate Paleontology 29: 1188-1198.

Kermack, K.A., Mussett, F., and Rigney, H.W. 1981. The skull of *Morganucodon*. Zoological Journal of the Linnean Society 71: 1-158.

Kermack, D.M. 1982. A new tritylodontid from the Kayenta Formation of Arizona. Zoological Journal of the Linnean Society 76:1-17.

Ketcham, R.A., and Carlson, W.D. 2001. Acquisition, optimization and interpretation of X-ray computed tomographic imagery: applications to the geosciences. Computers & Geosciences 27: 381-400.

Kielan-Jaworowska, Z., and Lancaster, T.E. 2004. A new reconstruction of mutituberculate endocranial casts and encephalization quotient of *Kryptobaatar*. Acta Palaeontologica Polonica 49: 177-188.

Kielan-Jaworowska Z., Cifelli R.L., and Luo Z.-X. 2004. Mammals from the age of dinosaurs. New York: Columbia University Press.

Krause, D.W., and Kielan-Jaworowska, Z. 1993. The endocranial cast and encephalization quotient of *Ptilodus* (Multituberculata, Mammalia). Palaeovertebrata 22: 99-112.

Kuhn, H.-J., and Zeller, U. 1987. The cavum epiptericum in monotremes and therian mammals: Morphogenesis of the mammalian skull. Mammalia Depicta 13: 51-70.

Laaß, M. 2015a. The origins of the cochlea and impedance matching hearing in synapsids. Acta Palaeontologica Polonica 61:267-280. Available from: http://www.bioone.org/doi/full/10.4202/app.00140.2014

Laaß, M. 2015b. Virtual reconstruction and description of the cranial endocast of *Pristerodon mackayi* (Therapsida, Anomodontia). Journal of Morphology 276:1089–1099. DOI: 10.1002/jmor.20397

Laaß, M., and Kaestner, A. 2017. Evidence for convergent evolution of a neocortex-like structure in a late Permian therapsid. Journal of Morphology 278: 1033-1057. DOI: 10.1002/jmor.20712

Lenth, R.V. 2016. Least-squares means: the R package lsmeans. Journal of Statistical Software 69: 1-33. DOI: 10.18637/jss.v069.i01

Larsell, O. 1952. The morphogenesis and adult pattern of the lobules and tissues of the cerebellum of the white rat. Journal of Comparative Neurology 97: 281–356.

Lewis, G.E., Irwin, J.H., and Wilson, R.F. 1961. Age of the Glen Canyon Group (Triassic and Jurassic) on the Colorado Plateau. Geological Society of America Bulletin 72: 1437-1440.

Lillegraven, J.A., and Kielan-Jaworowska, Z., Clemens, W.A. (Eds.). 1979. Mesozoic mammals: the first two-thirds of mammalian history. Berkeley, CA: University of California Press.

Liu, J., and Abdala, F. 2014. Phylogeny and taxonomy of the Traversodontidae. In C.F. Kammerer, K.D. Angielczyk, and J. Fröbisch (Eds.), Early evolutionary history of the Synapsida (pp. 255-279). Netherlands: Springer.

Liu, J., and Olsen, P. 2010. The phylogenetic relationships of Eucynodontia (Amniotoa, Synapsida). Journal of Mammalian Evolution 17: 151-176.

Lucas, S.G., and Luo, Z.1993. *Adelobasileus* from the Upper Triassic of West Texas: the oldest mammal. Journal of Vertebrate Paleontology 13: 309-334.

Luo, Z.-X. 1994. Sister-group relationships of mammals and transformations of diagnostic mammalian characters. In N.C. Fraser, H.-D. Sues (Eds.), In the shadow of the dinosaurs: Early Mesozoic tetrapods (98-128). Cambridge, NY: Cambridge University Press.

Luo, Z.-X. 2001. The inner ear and its bony housing in tritylodontids and implications for evaluation of the mammalian ear. Bulletin of the Museum of Comparative Zoology 156: 81-97.

Luo, Z.-X. 2007. Transformation and diversification in early mammal evolution. Nature 450: 1011-1019. DOI: 0.1038/nature06277

Luo, Z.-X. 2011. Developmental patterns in Mesozoic evolution of mammal ears. Annual Review of Ecology, Evolution, and Systematics 42: 355-380. DOI: 10.1146/annurev-ecolsys-032511-142302

Luo, Z.-X., and Crompton, A.W. 1994. Transformation of the quadrate (incus) through the transition from non-mammalian cynodonts to mammals. Journal of Vertebrate Paleontology 14: 341-374.

Luo, Z.-X., Crompton, A.W., and Lucas, S.G. 1995. Evolutionary origins of the mammalian promontorium and cochlea. Journal of Vertebrate Paleontology 15: 113-121.

Luo, Z.X., Crompton, A.W., and Sun, A.L. 2001. A new mammaliaform from the early Jurassic and evolution of mammalian characteristics. Science 292: 1535-1540. DOI: 10.1126/science.1058476

Luo, Z.-X., Gatesy, S.M., Jenkins, F.A., Amaral, W.W., and Shubin, N.H. 2015. Mandibular and dental characteristics of Late Triassic mammaliaform *Haramiyavia* and their ramifications for basal mammal evolution. Proceedings of the National Academy of Sciences 112: e7101-9. DOI: 10.1073/pnas.1519387112

Luo, Z.-X., Schultz, J.A., and Ekdale, E.G. 2016. Evolution of the middle and inner ears of mammaliaforms: the approach to mammals. In J.A. Clack, R.R. Fay, and A.N. Popper (Eds.), Evolution of the vertebrate ear—evidence from the fossil record (pp. 139-174). Netherlands: Springer Handbook of Auditory Research. Available from: https://link.springer.com/chapter/10.1007/978-3-319-46661-3_6 DOI: 10.1007/978-3-319-46661-3_6

Macrini, T.E. 2006. The evolution of endocranial space in mammals and non-mammalian cynodonts [Dissertation]. Austin: University of Texas.

Macrini, T.E., Rowe, T.B., and Archer, M. 2006. Description of a cranial endocast from a fossil platypus, *Obdurodon dicksoni* (Monotremata, Ornithorhynchidae), and the relevance of endocranial characters to monotreme phylogeny. Journal of Morphology 267: 1000-1015.

Macrini, T.E., Muizon, C. de, Cifelli, R.L., and Rowe, T. 2007a. Digital cranial endocast of *Pucadelphys andinus*, a Paleocene metatherian. Journal of Vertebrate Paleontology 27: 99-107.

Macrini, T.E., Rougier, G.W., and Rowe, T. 2007b. Description of a cranial endocast from the fossil mammal *Vincelestes neuquenianus* (Theriiformes) and its relevance to the evolution of endocranial characters in therians. The Anatomical Record 290: 875-892.

Macrini, T.E., Rowe, T.B., and VandeBerg, J. 2007c. Cranial endocasts from a growth series of *Monodelphis domestica* (Didelphidae, Marsupialia): a study of individual and ontogenetic variation. Journal of Morphology 268:844-865.

Marsh, A.D., and Rowe, T.B. In review. Anatomy and systematics of *Sarahsaurus aurifontanalis* from the Early Jurassic Kayenta Formation. PLoSOne, 155 pp, 50 figures, 3 supplements,

Martinelli, A.F., Bonaparte, J.F., Schultz, C.L., and Rubert, R. 2005. A new tritheledontid (Therapsida, Eucynodontia) from the Late Triassic of Rio Grande do Sul (Brazil) and its phylogenetic relationships among carnivorous non-mammalian eucynodonts. Ameghiniana 42: 191-208.

Martinelli, A.F., and Rougier, G.W. 2007. On *Chaliminia musteloides* (Eucynodontia: Tritheledontidae) from the Late Triassic of Argentina, and a phylogeny of ictidosauria. Journal of Vertebrate Paleontology 27: 442-460.

Martinelli, A.F., and Bonaparte, J.F. 2011. Postcanine replacement in *Brasilodon* and *Brasilitherium* (Cynodontia, Probainognathia) and its bearing in cynodont evolution. In J. Calvo, J. Porfiri, B.G. Riga, and D.D. Santos DD (Eds.), Paleontología y dinosaurios desde América Latina (pp. 179-186). Mendoza, Argentina: Editorial de la Universidad Nacional de Cuyo.

Martinelli, A.F., Soares, M.B., and Schwanke, C. 2016. Two new cynodonts (Therapsida) from the Middle-Early Late Triassic of Brazil and comments on South American probainognathians. PLoS ONE 11: e0162945. Available from: http://journals.plos.org/plosone/article?id=10.1371/journal.pone.0162945 DOI:10.1371/journal.pone.0162945

Martinelli, A.F., Eltink, E., Da-Rosa, A.S., and Langer, M.C. 2017. A new cynodont from the Santa Maria Formation, South Brazil, improves Late Triassic probainognathian diversity. Papers in Palaeontology 3: 1-23. DOI: 10.1002/spp2.1081

Martinez, R.N., May, C.L., and Forster, C.A. 1996. A new carnivorous cynodont from the Ischigualasto Formation (Late Triassic, Argentina), with comments on eucynodont phylogeny. Journal of Vertebrate Paleontology 16: 271-284.

Martínez, R.N, and Alcober, O.A. 2009. A basal sauropodomorph (Dinosauria: Saurischia) from the Ischigualasto Formation (Triassic, Carnian) and the early evolution of Sauropodomorpha. PLoS ONE 4: e4397. Available from: http://journals.plos.org/plosone/article?id=10.1371/journal.pone.0004397 DOI: 4310.1371/journal.pone.0004397

Martínez, R.N., Apaldetti, C., Colombi, C., Alcober, O., Sereno, P.C., Fernandez, E., et al. 2012. Vertebrate succession in the Ischigualasto Formation. Journal of Vertebrate Paleontology 32(S1): 10-30. DOI: 10.1080/02724634.2013.818546

Martínez, R.N., Sereno, P.C., Alcober, O.A., Colombi, C.E., Renne, P.R., Montañez, I.P., et al. 2011. A basal dinosaur from the dawn of the dinosaur era in southwestern Pangaea. Science 331: 201-210.

Mombaerts, P. 2001. How smell develops. Nature Neuroscience 4: 1192-1198.

Nieuwenhuys, R., Hans, J., and Nicholson, C. 1998. The central nervous system of vertebrates. New York, NY: Springer.

Olson, E.C. 1944. Origin of mammals based upon cranial morphology of the therapsid suborders. Geological Society of America Special Papers 55: 1–136.

Owen, R. 1861. Paleontology or a systematic summary of extinct animals and their geological relations (2nd ed). Edinburgh: Adams and Charles Black.

Patterson, B., and Olson, E.C. 1961. A triconodontid mammal from the Triassic of Yunnan. In G. Vanderbroek (ed.), International Colloquium on the Evolution of Lower and Non-Specialized Mammals (pp. 129-191). Brussels, Belgium: Koninklijke Vlaamse Academiie voor Wetenschappen, Letteren en Schone Kunsten van Belgie.

Presley, R. and Steel, F.L.D. 1976. On the homology of the alisphenoid. Journal of Anatomy 121: 441-459.Rogers, R.R., Swisher III, C.C., Sereno, P.C., Monetta, A.M., Forster, C.A., and Martínez, R.N. 1993. The Ischigualasto tetrapod assemblage, Late Triassic, Argentina, and 40Ar/39Ar dating of dinosaur origins. Science 260: 794–797.

Quiroga, J.C. 1979. The brain of two mammal-like reptiles (Cynodontia — Therapsida). The Journal für Hirnforschung 20: 341-350.

Quiroga, J.C. 1980a. Further studies on cynodont endocasts (Reptilia — Therapsida). Zeitschrift fur Mikroskopisch-Anatomische Forschung 94: 580-592.

Quiroga, J.C. 1980b. The brain of the mammal-like reptile *Probainognathus jenseni* (Therapsida — Cynodontia). A correlative neurological approach to the neocortex at the reptile-mammal transition. The Journal für Hirnforschung 21: 299-336.

Quiroga, J.C. 1984. The endocranial cast of the advanced mammal-like reptile *Therioherpeton cargnini* (Therapsida — Cynodontia) from the Middle Triassic of Brazil. The Journal für Hirnforschung 25: 285-290.

R Core Team. 2017. R: A language and environment for statistical computing. R Foundation for Statistical Computing, Vienna, Austria. URL https://www.R-project.org/

Rodrigues, P.G., Ruf, I., and Schultz, C.L. 2013. Digital reconstruction of the otic region and inner ear of the non-mammalian cynodont *Brasilitherium riograndensis* (Late Triassic, Brazil) and its relevance to the evolution of the mammalian ear. Journal of Mammalian Evolution 20: 291-307. DOI: 10.1007/s10914-012-9221-2

Rodrigues, P.G., Ruf, I., and Schultz, C.L. 2014. Study of a digital cranial endocast of the non-mammaliaform cynodont *Brasilitherium riograndinsis* (Late Triassic, Brazil) and its relevance to the evolution of the mammalian brain. Paläontologische Zeitschrift 88: 329-352. DOI: 10.1007/s12542-013-0200-6

Rodrigues, P.G., Martinelli, A.G., Schultz, C.L., Corfe, I.J., Gill, P.G., Soares, M.B., and Rayfield, E.J. 2018. Digital cranial endocast of *Riograndia guaibensis* (Late Triassic, Brazil) sheds light on the evolution of the brain in non-mammalian cynodonts. Historical Biology, 1-18. Available from: https://doi.org/10.1080/08912963.2018.1427742 DOI: 10.1080/08912963.2018.1427742

Romer, A.S. 1956. Osteology of the reptilia. Chicago: University of Chicago Press.

Romer, A.S. 1970. The Chanares (Argentina) Triassic reptile fauna. VI. A chiniquodontid cynodont with an incipient squamosal-dentary jaw articulation. Breviora 344: 1-8.

Rougier, G.W., Wible, J.R., and Hopson, J.A. 1992. Reconstruction of the cranial vessels in the Early Cretaceous mammal *Vincelestes neuquenianus*: implications for the mammalian cranial vascular system. Journal of Vertebrate Paleontology 12: 188-216.

Rougier, G.W., Apesteguía, S., Gaetano, L.C. 2011. Highly specialized mammalian skulls from the Late Cretaceous of South America. Nature 479: 98-102.

Rodrigues, P.G., Ruf, I., and Schultz, C.L. 2013. Digital reconstruction of the otic region and inner ear of the non-mammalian cynodont *Brasilitherium riograndensis* (Late Triassic, Brazil) and its relevance to the evolution of the mammalian ear. Journal of Mammalian Evolution 20: 291-307. DOI: 10.1007/s10914-012-9221-2

Rodrigues, P.G., Ruf, I., and Schultz, C.L. 2014. Study of a digital cranial endocast of the non-mammaliaform cynodont *Brasilitherium riograndensis* (Later Triassic, Brazil) and its relevance to the evolution of the mammalian brain. Paläontologische zeitschrift 88: 329-352.

Rodrigues, P.G., Martinelli, A.G., Schultz, C.L., Corfe, I.J., Gill, P.G., Soares, M.B., and Rayfield, E.J. 2018. Digital cranial endocast of *Riograndia guaibensis* (Late Triassic, Brazil) sheds light on the evolution of the brain in non-mammalian cynodonts. Historical Biology, 1-18. Available from: https://doi.org/10.1080/08912963.2018.1427742 DOI: 10.1080/08912963.2018.1427742

Rowe, T.B. 1986. Osteological diagnosis of *Mammalia*, L. 1758, and its relationships to extinct Synapsida [dissertation]. Berkeley, CA: University of California, Berkeley.

Rowe, T.B. 1988. Definition, diagnosis and origin of Mammalia. Journal of Vertebrate Paleontology 8: 241-264.

Rowe, T.B. 1993. Phylogenetic systematics and the early history of mammals. In F. S. Szalay, M. J. Novacek, and M. C. McKenna (Eds.), Mammalian Phylogeny (pp. 129-145). New York, NY: Springer-Verlag.

Rowe, T.B. 1996a. Coevolution of the mammalian middle ear and neocortex. Science 273: 651-654.

Rowe, T.B. 1996b. Brain heterochrony and evolution of the mammalian middle ear. In M. Ghiselin and G. Pinna (Eds.), New Perspectives on the History of Life (pp. 71-96). San Francisco, CA: California Academy of Sciences, Memoir 20.

Rowe, T.B. 2017. The emergence of mammals. In: J. Kaas (Ed.), Evolution of Nervous Systems 2e. vol. 2 (pp. 1-52). Amsterdam, Netherlands: Elsevier.

Rowe, T.B. In press A. Mammalia. In P. Cantino, K. de Queiroz, and J.A. Gauthier (Eds.), Phylonyms, the Companion Volume to the Phylocode (14 pp.). Yale Peabody Museum of Natural History.

Rowe, T.B. In press B. Mammaliaformes. In P. Cantino, K. de Queiroz, and J.A. Gauthier (Eds.), Phylonyms, the Companion Volume to the Phylocode (13 pp.). Yale Peabody Museum of Natural History.

Rowe, T.B. In press C. Mammaliamorpha. In P. Cantino, K. de Queiroz, and J.A. Gauthier, (Eds.), *Phylonyms, the Companion Volume to the Phylocode* (13 pp.). Yale Peabody Museum of Natural History.

Rowe, T.B. In press D. Cynodontia. In P. Cantino, K. de Queiroz, and J.A. Gauthier (Eds.), *Phylonyms, the Companion Volume to the Phylocode* (24 pp.). Yale Peabody Museum of Natural History.

Rowe, T.B. In press E. Therapsida. In P. Cantino, K. de Queiroz, and J.A. Gauthier, (Eds), Phylonyms, the Companion Volume to the Phylocode (21 pp.). Yale Peabody Museum of Natural History.

Rowe, T.B. In press F. Pan-Mammalia. In P. Cantino, K. de Queiroz, and J. A. Gauthier (Eds.), Phylonyms, the Companion Volume to the Phylocode (19 pp.). Yale Peabody Museum of Natural History.

Rowe, T.B., and Gauthier, J.A. 1992. Ancestry, paleontology, and definition of the name Mammalia. Systematic Biology 41: 372-378.

Rowe, T.B., Carlson, W.A., and Bottorff, W. 1995. *Thrinaxodon*: Digital Atlas of the Skull. CD-ROM (Second Edition, for Windows and Macintosh platforms), University of Texas Press, 547 megabytes

Rowe, T.B., Kappelman, J.A., Carlson, W.D., Ketcham, R.A., and Denison, C.A. 1997. High-resolution computed tomography: a breakthrough technology for earth scientists. Geotimes 42: 23-27.

Rowe, T.B., Eiting, T.P., Macrini, T.E. and Ketcham, R.A. 2005. Organization of the olfactory and respiratory skeleton in the nose of the gray short-tailed opossum *Monodelphis domestica*. Journal of Mammalian Evolution 12: 303-336.

Rowe, T.B., Macrini, T.E., and Luo, Z.-X. 2011. Fossil evidence on origin of the mammalian brain. Science 332: 955-957.

Rowe, T. and Frank, L.R. 2011. The disappearing third dimension. Science 331: 712-714. DOI: 10.1126/science.1202828

Rowe, T.B., and Shepherd, G.M. 2016. The role of ortho-retronasal olfaction in mammalian cortical evolution. Journal of Comparative Neurology 524: 471-495. DOI:10.1002/cne.23802

Rowe, T.B., Luo, Z.-X., Ketcham, R.A., Maisano, J.A., and Colbert, M.W. 2016. X-Ray computed tomography datasets for forensic analysis of vertebrate fossils. Scientific Data 3: 160040. Available from: https://www.nature.com/articles/sdata201640 DOI: 10.1038/sdata.2016.40

Rubidge, B.S., and Sidor, C.A. 2001. Evolutionary patterns among Permo-Triassic therapsids. Annual Review of Ecology and Systematics 32: 449–480.

Ruf, I., Maier, W., Rodriguez, P.G., and Schultz, C.L. 2014. Nasal anatomy of the non-mammaliaform cynodont *Brasilitherium riograndensis* (Euynodontia, Therapsida) reveals new insight into mammalian evolution. Anatomical Record 297: 2018-2030.

Ruta, M., Botha-Brink, J., Mitchell, S.A., and Benton, M.J. 2013. The radiation of cynodonts and the ground plan of mammalian morphological diversity. Proceedings of the Royal Society B 280: 20131865.

Schieber, M.A. 2007. Chapter 2: Comparative anatomy and physiology of the corticospinal system. In, A.A. Eisen and P.J. Shaw (Eds.), Handbook of Clinical Neurology (vol. 82, 3rd series, p. 15-37). New York, NY: Elsevier.

Sereno, P.C. 2007. Logical basis for morphological characters in phylogenetics. Cladistics 23: 565-587.

Shepherd, G.M., and Rowe, T.B. 2017. Neocortical lamination: insights from neuron types and evolutionary precursors. Frontiers in Neuroanatomy 11:100. DOI: 10.3389/fnana.2017.00100

Shubin, N.H., Crompton, A.W., Sues, H.-D., and Olsen, P.E. 1991. New fossil evidence on the sister-group of mammals and early Mesozoic faunal distributions. Science 251: 1063-1065.

Sidor, C.A., and Smith, R.M. 2004. A new galesaurid (Therapsida: Cynodontia) from the lower Triassic of South Africa. Palaeontology 47: 535-556.

Sidor, C.A., and Hancox, P.J. 2006. *Elliotherium kersteni*, a new tritheledontid from the Lower Elliot Formation (Upper Triassic) of South Africa. Journal of Paleontology 80: 333-342.

Sigurdsen, T., Huttenlocker, A.K., Modesto, S.P., Rowe, T.B. and Damiani, R. 2012. Reassessment of the morphology and paleobiology of the therocephalian *Tetracynodon*

darti (Therapsida), and the phylogenetic relationships of Baurioidea. Journal of Vertebrate Paleontology 32: 1113-1134.

Simon, R.V. 2013. Cranial osteology of the long-beaked echidna, and the definition, diagnosis, and origin of Monotremata and its major subclades [M.S. Thesis]. Austin: University of Texas.

Simpson, G.G. 1927. Mesozoic Mammalia, IX; the brain of Jurassic mammals. American Journal of Science 82: 259-268.

Simpson, G.G. 1931. A new classification of mammals. Bulletin of the American Museum of Natural History 59: 259-293.

Soares, M.B., Schultz, C.L., and Horn, B.D. 2011. New information on *Riograndia guaibensis* Bonaparte, Ferigolo & Ribeiro, 2001 (Eucynodontia, Tritheledontidae) from the Late Triassic of southern Brazil: anatomical and biostratigraphic implications. Anais da Academia Brasileira de Ciências 83: 329-354.

Soares MB, Martinelli AG, Oliveira TV. 2014. A new prozostrodontian cynodont (Therapsida), from the Late Triassic *Riograndia* Asseblage Zone (Santa Maria Supersequence) of Southern Brazil. Anais da Academia Brasileira de Ciências 86: 1673-1691.

Stensiö, E.A., 1927. The Downtonian and Devonian vertebrates of Spitsbergen. I, Family Cephalaspidae.

Striedter, G.F. 2005. Principles of brain evolution. Sunderland, MA: Sinauer Associates, Inc. p. 436.

Striedter, G.F. 2006. Précis of principles of brain evolution. Behavioral and Brain Sciences 29: 1-36.

Striedter, G.F. and Charvet, C.J. 2008. Developmental origins of species differences in telecephalon and tectum size: morphometric comparisonsbetween a parakeet (*Mellopsittacus undulates*) and a quail (*Colinus virginianus*). Journal of Comparative Neurology 507: 1667-1675.

Sues, H.-D. 1986. The skull and dentition of two tritylodontid synapsids from the Lower Jurassic of western North America. Bulletin of the Museum of Comparative Zoology 151: 217-268.

Sues, H.-D. 2001. On *Microconodon*, a Late Triassic cynodont from the Newark Supergroup of eastern North America. Bulletin of the Museum of Comparative Zoology 156: 37-48.

Swofford, D.L. 2006. Paup*: phylogenetic analysis using parsimony, version 4.0b10.

Tatarinov, L.P. 1963. New Late Permian therocephalian. Paleontologicheskiy Zhurnal 4: 46-94.

Turner, E.L. 1924. The pyramidal tract of the Virginian opossum (*Didelphis virginiana*). Journal of Comparative Neurology 36: 387.

Van Bemmelen, J.F. 1901. Der Schadelbau der Monotremen. Denksch Med- Naturwis Ges Jena, [Semons Zool. Forsch.-reis., 3t' Bd., II, IV Lieferung]. VI: 729-98.

Van Dongen, P.A.M. 1998. Brain size in vertebrates. In The Central Nervous System of Vertebrates (pp. 2099-2134). Springer, Berlin, Heidelberg.

Voogd, J., Schraa-Tam, C.K.L., van der Geest, J.N., and De Zeeuw, C.I. 2012. Visuomotor cerebellum in human and non-human primates. Cerebellum 11: 392-410. DOI: 10.1007/s12311-010-0204-7

Wang, Y., Hu, Y., Meng, J., and Li, C. 2001. An ossified Meckel's cartilage in two Cretaceous mammals and origin of the mammalian middle ear. Science 294: 357-361.

Wible, J.R. 1991. Origin of Mammalia: the craniodental evidence reexamined. Journal of Vertebrate Paleontology 11: 1-28.

Wild, J.M. and Williams, M.N. 2000. Rostral Wulst in passerine birds. I. Origin, course, and terminations of an avian pyramidal tract. Journal of Comparative Neurology 416: 429-450.

Yopak, K.E., Lisney, T.J., Darlington, R.B., Collin, S.P., Montgomery, J.C., and Finlay, B.L. 2010. A conserved pattern of brain scaling from sharks to primates. Proceedings of the National Academy of Sciences 107: 12946-12951.Zander, R. 2004. Minimal values for reliability of bootstrap and jacknife proportions, Decay Index, and Bayesian posterior probability. Phyloinformatics 2: 1-13.

Zee, D.S., Yamazaki, A., Butler, P.H., and Gucer, G. 1981. Effects of ablation of flocculus and paraflocculus of eye movements in Primates. Journal of Neurophysiology 46: 878-899.

Zelená, J. 1994. Nerves and Mechanoreceptors: the Role of Innervation in the Development and Maintenance of Mammalian Mechanoreceptors. London, U.K.: Chapman & Hall.